Optogenetic Gene Therapy for Vision Restoration

Light-sensitive proteins, viral vectors and bipolar cell adaptation to a diseased state



Doron Hickey

Merton College

A thesis submitted for the degree of

Doctor of Philosophy

Michaelmas 2015

Declaration

The results in this thesis are my own work, except where indicated.

Fluorescence-activated cell sorting was completed with the technical assistance of Mr Andrew Worth, Flow Sorting Facility Manager, Jenner Institute, University of Oxford.

The microarray analysis and preliminary data analysis was performed by Cambridge Genomic Services (University of Cambridge) using samples that I prepared.

Dr Mandeep Singh performed the intraocular injections reported in chapter three.



Doron Hickey
January 2016

Abstract

Inherited retinal dystrophies are a heterogeneous group of retinal diseases that often lead to blindness. The diverse range of causative gene mutations poses great challenges to developing therapies to improve the vision of affected people. One technique being investigated is optogenetics for vision restoration, a technique that aims to deliver light-sensitising molecules to the affected retina. This research project provides data on a range of variables that need to be optimised in order to successfully restore vision using an optogenetic gene therapy approach.

Fifteen wild type, chimeric and fusion constructs based on human opsins were compared by *in vitro* and *in vivo* tests to select the optimal light-sensitising construct. Of these, wild type rhodopsin, melanopsin and melanopsin–Gα subunit fusion constructs show the most promise for future studies.

For delivery of the light-sensitising construct, the adeno-associated virus (AAV) serotype AAV2/2(7m8) was shown to perform best compared to two other AAV serotypes when tested in degenerate mouse eyes and macaque and human retinal explants. The importance of the delivery route to the eye, the use of a targeted versus non-targeted approach and the AAV vector concentration were all tested in *in vivo* experiments.

In addition to testing such variables, the gene expression changes in target retinal bipolar cells in late-stage retinal degeneration were examined by microarray analysis of bipolar cell enriched samples isolated by fluorescence-activated cell sorting. Genes important for G protein signalling were generally expressed at a similar level in the degenerate state, while genes associated with oxidative stress and metabolism were differentially expressed.

Collectively, these data will inform the choice of construct, delivery method and target cell in future research into optogenetic strategies for vision restoration.

Acknowledgments

Alone we can do so little; together we can do so much

– Helen Keller

I have been fortunate to be supported by many generous, skilled and professional people and I would like to use this opportunity to express to them my sincere gratitude.

I am deeply grateful for the support I received from Nigel Evans and the Woolf Fisher Trust, without whom none of this would have been possible. It is an immense privilege to be a Woolf Fisher Scholar.

To my supervisors, Professors Mark Hankins and Robert MacLaren, I thank you both greatly for providing me with the opportunity to make my contribution and for your wise and insightful support and advice throughout.

For teaching me the skills I needed to undertake this project I would like to thank Sher Aslam, Alun Barnard, Camiel Boon, Laurence Brown, Alona Cramer, Dany Dauletbekov, Wayne Davies, Sam de Silva, Dominik Fischer, Maria Inês Rodrigues, Aarti Jagannath, Michelle McClements, Carrie Pothecary and Mandeep Singh. Thanks to Tom Edwards for his help and enthusiasm with the human retinal explant work. Thank you to the people who donated their retinal tissue for this work.

To the staff at the JR BMS, thank you for your help and support managing the mice. Your professionalism and dedication was appreciated. Thank you to David Farningham and the staff at the MRC Centre for Macaques for providing the macaque tissue and an enlightening tour of the facility.

To Jess Rodgers: your moral support and practical help with the plate reader, injections and pupillometry work was much appreciated.

Special thanks to Steve Hughes for his perpetual enthusiasm and willingness to help, teach and feed me.

To my Fernhollow friends, thank you for keeping me alert and challenged during the long days of writing.

To Mum and Dad: the freedom that you gave me to explore my world instilled in me the curiosity that drove this research; your hard work and sacrifice gave me the opportunities to make it a reality — thank you. I know you warned me against following you into science, but you are role models worth following.

For enabling this journey to have been as professionally and personally fulfilling as it has been, I am forever indebted to my partner, Claire. With you I am a better scientist and a better person. Grazzi ħafna Claire.

Finally, to the people whose lives have been touched by the diseases we seek to treat: thank you for the inspiration you provide for this work.

Table of contents

Declaration ii
Abstract iii
Acknowledgments iv
List of figures ix
List of tables xi
Abbreviations xii
Glossary xiv
1 General Introduction 1
1.1 The prevalence and diversity of inherited retinal dystrophies 1
1.2 The spectrum of therapies for inherited retinal dystrophies 2
1.2.1 Ocular gene therapy 5
1.2.2 Mutation-independent therapeutic strategies 7
1.3 Optogenetics for vision restoration 11
1.4 Aims 15
1.4.1 Light-sensitive molecules — comparison of wild type and engineered human opsins 15
1.4.2 Target cells for optogenetic gene therapy 18
1.4.3 AAV vectors for optogenetic gene therapy 19
1.4.4 Injection route 21
1.4.5 AAV concentration 22
2 Materials and Methods 24
2.1 Molecular biology 24
2.1.1 Plasmids 24
2.1.2 Cloning of chimeric opsin constructs 25
2.1.3 Cloning of opsin–G protein fusion constructs 26
2.1.4 Cloning of floxed melanopsin and rhodopsin constructs 27
2.1.5 Polymerase chain reactions 27
2.1.6 Genotyping 28
2.1.7 Agarose gel electrophoresis 29
2.1.8 Gel extraction 29
2.1.9 Restriction digest 29
2.1.10 Ligation 29
2.1.11 Transformation 30
2.1.12 Bacterial culture and plasmid purification 30
2.1.13 DNA quantification 30
2.1.14 DNA sequencing 30
2.1.15 DNase treatment and denaturation of AAV for titering 30
2.1.16 Quantitative PCR 31
2.1.17 Collection of RNA from a cell monolayer 32
2.1.18 RNA extraction 33
2.1.19 First-strand cDNA synthesis and RNase H digest 34
2.1.20 Bioanalyzer assessment of RNA quality and quantity 34
2.1.21 Illumina MouseWG-6 microarray 35
2.1.22 Western blotting 36
2.1.23 SDS-PAGE of AAV 37

2.1.24 Protein purification and absorbance spectroscopy 37
2.2 Animal material 39
2.2.1 Ethical review 39
2.2.2 Animal housing 40
2.2.3 Mouse strains 40
2.2.4 Mice used for a microarray study of retinal bipolar cells adaptation to retinal degeneration 40
2.3 Cell culture 42
2.3.1 Subculturing cell lines 42
2.3.2 *In vitro* plasmid transfection 42
2.3.3 *In vitro* knockdown of endogenous gene expression using siRNA 43
2.3.4 Live cell cAMP assay 43
2.3.5 Live cell calcium assays — sample preparation 45
2.3.6 Plate reader quantification of live cell calcium indicators 46
2.3.7 Microscope imaging of live cell calcium indicators 47
2.3.8 Image analysis of microscope imaging of live cell calcium imaging 47
2.3.9 Adeno-associated virus production 47
2.3.10 Poly(ethylene glycol) precipitation of AAV 51
2.3.11 Secondary concentration of AAV solutions 52
2.3.12 Macaque retinal explants 53
2.3.13 Human retinal explants 55
2.3.14 AAV transduction of primate retinal explants 55
2.3.15 AAV transduction of cell lines 56
2.3.16 Retina dissociation 56
2.3.17 Fluorescence-activated cell sorting 57
2.4 *In vivo* 59
2.4.1 Randomisation 59
2.4.2 General anaesthesia 59
2.4.3 Intraocular injections 59
2.4.4 Scanning laser ophthalmoscopy 61
2.4.5 Quantification of SLO images 61
2.4.6 Pupillometry 62
2.4.7 Optomotor response 63
2.4.8 Fos induction protocol 64
2.5 Tissue 65
2.5.1 Fixation of retinal explants 65
2.5.2 Immunocytochemistry 65
2.5.3 Tissue collection 67
2.5.4 Embedding and sectioning of eyes and explants 67
2.5.5 Immunohistochemistry — sections 68
2.5.6 Immunohistochemistry — flat mounts 69
2.5.7 Image acquisition 71
2.5.8 Confocal — standard image acquisition for AAV tropism studies 71
2.5.9 Statistical analysis and graphing 72
2.5.10 Network analysis of differentially expressed genes 73
3 Adeno-Associated Virus Tropism for Optogenetic Gene Therapy ... 74
3.1 Introduction 74
3.2 Results 80
3.2.1 *In vitro* testing of three serotypes of AAV-GFP 80
3.2.2 AAV tropism in a mouse model of retinal degeneration 81
3.2.3 AAV tropism in non-degenerate macaque retina 95
3.2.4 AAV tropism in human retinal explants 100

3.3 Discussion 103
3.3.1 Retinal tropism differences across species 103
3.3.2 AAV2/2(7m8) as a reliable serotype for optogenetic gene therapy 106
3.3.3 Retinal bipolar cells remain a challenging target cell 107
3.3.4 Limitations of experimental design 109

4 Chimeric Opsins as Potential Light Sensitisers 111

4.1 Introduction 111
4.2 Results 116
4.2.1 Rhodopsin/melanopsin chimeric opsins 116
4.2.2 Long-wave-sensitive opsin/melanopsin chimeric opsins 129
4.3 Discussion 135
4.3.1 Rhodopsin/melanopsin chimeric opsins are able to couple to two G protein pathways 135
4.3.2 Distinct chromophore requirements of wild type and chimeric opsins 138
4.3.3 Human chimeric opsins display advantages as optogenetic tools over other chimeric opsins 139
4.3.4 Challenges of obtaining G protein functional data for LWS opsin 139
4.3.5 Chimeric opsins as candidate optogenetic tools for vision restoration 141

5 Opsin–G protein Fusion Proteins as Optogenetic Tools for Vision Restoration 145

5.1 Introduction 145
5.2 Results 148
5.2.1 *In vitro* testing of melanopsin– and rhodopsin–G protein fusion proteins 148
5.2.2 *In vivo* assessment of a melanopsin–G protein fusion AAV vector 157
5.3 Discussion 166
5.3.1 Opsin–G protein fusion proteins are able to utilise the fused Gα subunit 166
5.3.2 *In vivo* assessment of melanopsin–G protein fusion protein efficacy was impaired by inefficient gene delivery 168
5.3.3 Fused G_q and G_{11} Gα subunits are inefficient at changing the signalling pathway of an opsin 171

6 Bipolar Cell-Targeted and Non-Targeted Opsin Expression ... 174

6.1 Introduction 174
6.2 Results 179
6.2.1 *In vitro* testing of floxed and non-floxed human opsins 179
6.2.2 A pilot *in vivo* study of floxed and non-floxed opsins in a mouse model of retinal degeneration 182
6.3 Discussion 190
6.3.1 Targeted versus non-targeted expression of melanopsin in the degenerate retina 190
6.3.2 Transduction efficiency improved with higher concentration AAV vectors ... 191
6.3.3 Comparison of floxed rhodopsin and floxed melanopsin AAV vectors 192

7 Bipolar Cell Gene Expression in Retinal Degeneration 196

7.1 Introduction 196
7.1.1 Bipolar cells as a target for optogenetic gene therapy for vision restoration 196
7.1.2 Pathophysiology of retinal bipolar cells in retinal degeneration 198

7.1.3 A study of bipolar cell-specific gene expression changes in a mouse model of retinal degeneration 201
7.2 Results 203
7.2.1 FACS isolation of retinal bipolar cells from *L7*-Cre-positive retinas 204
7.2.2 Microarray study of bipolar cell gene expression changes in retinal degeneration 207
7.3 Discussion 218
7.3.1 Analysis of G protein signalling-related genes in the degenerate retina informs the choice of optogenetic gene therapy 218
7.3.2 Non-G protein signalling related gene expression changes in the degenerate retina 220
7.3.3 Quality of data from a microarray study of retinal bipolar cell adaptation to retinal degeneration 224
8 General Discussion 230
8.1 Selecting a light-sensitive molecule for optogenetic gene therapy 230
8.1.1 Potential benefits of G_o-coupled opsins for vision restoration 235
8.1.2 Challenges of melanopsin AAV vectors 236
8.2 Appropriate choice of animal model of retinal degeneration 237
8.3 Appropriate vision tests for optogenetic vision restoration 239
8.4 Selecting target cells for optogenetic gene therapy 239
8.5 Variables to maximise transduction efficiency in the degenerate retina 242
8.5.1 Choice of AAV vector 242
8.5.2 Vector concentration 244
8.5.3 Quality control of AAV vectors 245
8.5.4 Injection delivery route 246
8.6 Heading towards the optogenetically sensed light 248
Appendices 252
Appendix I – Reagents 252
Appendix II – Primers and small interfering RNA 254
Appendix III – Kits 256
Appendix IV – Hardware 257
Appendix V – Software 257
Appendix VI – AAV vectors 258
Appendix VII – Microarray report 259
Appendix VIII – Solutions 273
References 274

List of figures

1.1 Therapeutic options for inherited retinal dystrophies 3
1.2 Variables tested to optimise an optogenetic gene therapy strategy 16

2.1 AAV production by triple transfection and iodixanol gradients 38
2.2 Creation of macaque retinal explants 54

3.1 *In vitro* testing of three serotypes of AAV-GFP 75
3.2 SLO of degenerate retinas intravitreally injected with AAV-GFP 82
3.3 SLO of degenerate retinas subretinally injected with AAV-GFP 84
3.4 Comparison of intravitreal and subretinal SLO quantification 86
3.5 GFP expression by retinal layer in retinas injected intravitreally with AAV-GFP .. 87
3.6 GFP expression by retinal layer in retinas injected subretinally with AAV-GFP 89
3.7 Comparison of intravitreal and subretinal GFP quantification 91
3.8 Colocalisation of GFP with retinal cell markers 92
3.9 Macaque foveal explants transduced with three serotypes of AAV-GFP 96
3.10 Macaque retinal explants labelled for GFP and rhodopsin 97
3.11 Macaque retinal explants labelled for GFP and retinal cell markers 99
3.12 Human retinal explants — whole retina 101
3.13 Human retinal explants — vertical section colocalisation 102

4.1 Human rhodopsin/melanopsin chimeric opsins 113
4.2 Human rhodopsin/melanopsin chimeric opsins primary sequences 118
4.3 Immunocytochemistry of rhodopsin/melanopsin chimeric opsins 119
4.4 Functional testing of rhodopsin/melanopsin chimeric opsins 122
4.5 Statistical comparison of rhodopsin/melanopsin functional tests 124
4.6 Effect of exogenous 9-*cis* retinal on rhodopsin/melanopsin chimeric opsins 126
4.7 Human rhodopsin/melanopsin chimeric opsins compared to Opto-α_1AR 128
4.8 Human LWS/melanopsin chimeric opsins 130
4.9 Immunocytochemistry of LWS/melanopsin chimeric opsins 131
4.10 Functional testing of LWS/melanopsin chimeric opsins 133
4.11 Absorption spectra of LWS and a LWS/melanopsin chimeric opsin 136

5.1 Heterologous expression of melanopsin and melanopsin fusion proteins 149
5.2 $G_{q/11}$ activity of opsin–G protein fusion proteins 151
5.3 Effects of G protein knockdown on melanopsin–G protein fusion proteins 153
5.4 G_i activity of opsin–G protein fusion proteins 156

5.5 *In vitro* testing of melanopsin and melanopsin–*GNA11* AAV vectors 158
5.6 Melanopsin and melanopsin–*GNA11* AAV vectors injected in C3H/HeH mice ... 160
5.7 Pupillometry and optomotor response of mice injected with melanopsin and melanopsin–*GNA11* AAV vectors 162
5.8 Fos expression in mice injected with melanopsin and melanopsin–*GNA11* AAV vectors 165

6.1 *L7*-Cre EYFP transgenic mice and floxed and non-floxed opsin AAV vectors 177
6.2 *In vitro* expression of floxed and non-floxed melanopsin AAV vectors 180
6.3 *In vitro* function of floxed and non-floxed opsins 181
6.4 Immunolabelled *L7*-Cre eyes injected with floxed and non-floxed opsins — low magnification 185
6.5 Immunolabelled *L7*-Cre eyes injected with floxed and non-floxed opsins — high magnification 186
6.6 Colocalisation of opsin with retinal cell markers 187
6.7 Pupillometry and optomotor response of mice injected with floxed and non-floxed opsins AAV vectors 189

7.1 FACS protocol for isolating *L7*-Cre-positive cells 203
7.2 Validation of FACS techniques 205
7.3 Immunocytochemistry of FAC-sorted cells from *L7*-Cre retina 206
7.4 Quantitative PCR of FACS populations 208
7.5 FACS dot plots of samples used for a microarray study comparing bipolar cells from degenerate and non-degenerate retinas 209
7.6 Heat map and volcano plot comparing gene expression in bipolar cells from degenerate and non-degenerate retinas 212
7.7 Network of differentially expressed genes from a microarray study 214
7.8 Expression levels of G protein signalling genes 217
7.9 Potential sources of rod RNA contamination 226

8.1 Optimisation of variables for an optogenetics for vision restoration strategy 231

List of tables

2.1 Primary and secondary antibodies 66

3.1 Summary of transduction pattern of three AAV serotypes in mouse retina 93

6.1 Intraocular injections of floxed and non-floxed opsin AAV vectors..... 183

7.1 YFP-positive FACS samples used for a microarray study of retinal degeneration 211
7.2 Statistically significantly differentially expressed gene probes..... 213
7.3 Differential expression of G protein signalling genes 215

Abbreviations

AAV	adeno-associated virus
ANOVA	analysis of variance
AUC	area under the curve
bp	base pairs
BSS	balanced salt solution
cAMP	cyclic adenosine monophosphate
cDNA	complementary deoxyribonucleic acid
CAG	cytomegalovirus early enhancer, chicken beta actin, rabbit beta globin
CRISPR	clustered regularly-interspaced short palindromic repeats
DMEM	Dulbecco's modified Eagle's medium
EC_{50}	light intensity for half maximal pupillary reflex
EYFP	enhanced yellow fluorescent protein
FACS	fluorescence-activated cell sorting
FDR	false discovery rate
G	gauge (Stubs iron wire gauge system)
GCL	ganglion cell layer
GDP	guanosine-5′-diphosphate
GFAP	glial fibrillary acidic protein
GNA11	guanine nucleotide binding protein (G protein), alpha 11 (Gq class)
GNAQ	guanine nucleotide binding protein (G protein), q polypeptide
GPCR	G protein-coupled receptor
GTP	guanosine-5′-triphosphate
HBSS	Hank's balanced salt solution
ICL	intracellular loop
INL	inner nuclear layer
ITR	inverted terminal repeat
kb	kilobase
kDa	kilodalton
LB	lysogeny broth
LWS	long-wave-sensitive
M	molar
mGluR6	metabotropic glutamate receptor 6
mRNA	messenger ribonucleic acid
OCT	optimum cutting temperature
ONL	outer nuclear layer
OPN1LW	opsin 1 (cone pigments), long-wave-sensitive
OPN4	melanopsin
Pχ	postnatal day χ

PBS	phosphate buffered saline
PEG	poly(ethylene glycol)
PEI	polyethylenimine
PI	propidium iodide
PKCα	protein kinase C, alpha
pRGC	photosensitive retinal ganglion cell
qPCR	quantitative polymerase chain reaction
RGC	retinal ganglion cell
RHO	rhodopsin
RIN	RNA integrity number
RPE	retinal pigment epithelium
RPMI	Roswell Park Memorial Institute
s.e.m.	standard error of the mean
siRNA	small interfering ribonucleic acid
SLO	scanning laser ophthalmoscopy
Tris	2-amino-2-hydroxymethyl-propane-1,3-diol; $(HOCH_2)_3CNH_2$
vg	vector genome(s)
WPRE	woodchuck hepatitis virus posttranscriptional regulatory element

Glossary

Apoprotein	The polypeptide part of a conjugated protein.
Apoptosis	Programmed cell death.
Bistable	Having two stable and light-interconvertible states.
Bleb	The area of detached retina created by a subretinal injection.
Centre-surround	A feature of retinal physiology whereby a receptive field centre is surrounded by an antagonistic area.
Chromophore	The part of a molecule that absorbs visible light.
Dominant negative	A dominant mutation whose product acts in opposition to normal gene function.
Fovea	Small, central pit in the macula. Responsible for high-acuity vision.
Foveola	The centre of the fovea.
G proteins	Guanine nucleotide-binding proteins. Often function as heterotrimeric G protein complexes with α, β and γ subunits.
Kinetics	The rate at which a reaction proceeds
Macula	Pigmented, central, cone-rich region of the primate retina.
Metazoa	Multicellular, eukaryotic organisms of the kingdom Animalia
Minute of arc	A unit of angular measurement. Equal to one sixtieth of a degree.
OFF	A cell that is stimulated in response to a decrease in light.
ON	A cell that is stimulated in response to an increase in light.
Optogenetics	The use of light-sensitive molecules, typically genetically encoded, to light-sensitise cells.
Pattern vision	The innate ability of the visual system to recognize a set of stimuli arranged in a pattern. Normally dependent upon photoreceptor light detection.
Photopigment	A light-sensitive molecule
Pixel value	A number that represents the brightness of a pixel.
Retinectomy	The excision of retinal tissue.
Serotype	Distinct variations within a species.
Spike	A short-lasting rise and fall of a cell's electrical membrane potential. Also known as an action potential.
Transduce	The use of viral methods to introduce nucleic acids into cells.
Transfect	The use of non-viral methods to introduce nucleic acids into cells.
Tropism	The specificity of a virus for a particular host cell or tissue.
Z-score	The number of standard deviations an observation is above the mean.

1

General Introduction

1.1 The prevalence and diversity of inherited retinal dystrophies

Our ability to perceive the world through the detection of light is a fundamental property shared with nearly all forms of life (Spudich et al., 2000). From archaea to bacteria, plants and animals; a plethora of biological systems have evolved light-sensing capabilities to adapt to, and compete in, their light environment. It is vision that enables humans to interact with the world beyond our fingertips, to sense and plan for the challenges around us, to gather information vital to maintaining social connections and developing skills.

Tragically, the joy and pleasures of vision are not shared by all. In 2010 there were an estimated 32 to 39 million blind (defined as Snellen visual acuity less than 3/60) people in the world and a further 191 to 246 million people with moderate to severe visual impairment (visual acuity between 6/18 and 3/60) (Pascolini and Mariotti, 2012; Stevens et al., 2013). It is estimated that 65 to 75% of blindness is avoidable — largely due to untreated cataract and refractive error (Pascolini and Mariotti, 2012; Stevens et al., 2013). Globally it is estimated that 1 in 3,000, or more than 2 million people, have a form of inherited retinal degeneration (Boughman et al., 1980; Haim, 2002; Wright et

al., 2010) — a collective term for a group of chronic and progressive diseases of the retina caused by mutation to a single gene. While this constitutes a small fraction of the global burden of vision impairment, inherited retinal dystrophies account for a significant proportion of vision loss in countries that effectively prevent avoidable blindness. For example, in England and Wales, inherited retinal dystrophies were the leading cause of blindness certifications in people aged 16 to 64 years in 2009 to 2010 (Liew et al., 2014).

The challenge of diagnosing and treating inherited retinal dystrophies stems from the clinical and genetic heterogeneity of such conditions. Two hundred and forty different genes are known to cause a form of inherited retinal disease (Daiger et al., 2015). Mutations of different genes can cause similar clinical phenotypes; for example, at least 58 different genes cause a retinitis pigmentosa phenotype (Daiger et al., 2015). Conversely, different mutations of a single gene can cause different clinical phenotypes — for example, *ABCA4* mutations can lead to multiple phenotypes including juvenile macular degeneration and retinitis pigmentosa (Klevering et al., 2004; Michaelides et al., 2006). In people with a clinical diagnosis of non-syndromic retinal dystrophy the causative mutation is found in approximately 50 to 60% of cases (Chiang and Trzupek, 2015).

1.2 The spectrum of therapies for inherited retinal dystrophies

Such diversity of disease within the inherited retinal dystrophy category has led to research into a wide range of potential therapies, many of which are undergoing clinical trials. These treatments fit into a hierarchy that address the disease at different stages (Figure 1.1).

For diseases where the causative genetic mutations are known and the parents are affected or known carriers, pre-implantation genetic diagnosis can be utilised to select

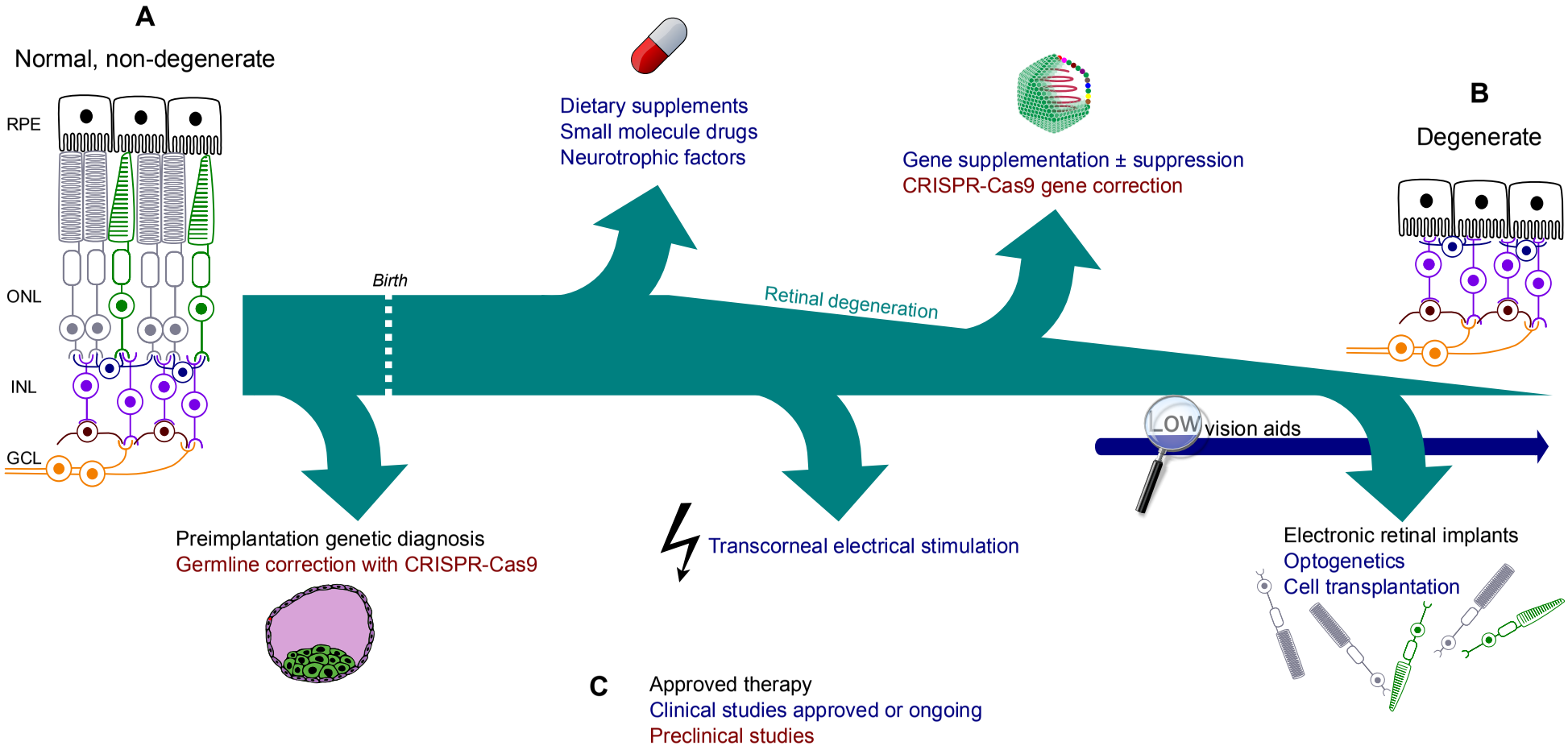


Figure 1.1. Therapeutic options for inherited retinal dystrophies — approved and under investigation
(**A**) Normal retinal function can be impaired by mutations in over two hundred genes. (**B**) Many different mutations associated with inherited retinal dystrophies cause the progressive loss of photoreceptors of the outer nuclear layer (ONL), while the inner nuclear layer (INL) and ganglion cell layer (GCL) remain relatively well preserved, even in the degenerate state. (**C**) A number of therapeutic options are approved or under investigation to slow, halt or reverse the vision loss associated with retinal degeneration. Low vision aids are the current standard of treatment in the late stage of retinal degeneration (blue arrow). The approximate time that the therapy would be applied is indicated by its position along the horizontal. RPE, retinal pigment epithelium.

only unaffected and/or non-carrier embryos for implantation. Germ line correction of mutations using technologies such as CRISPR-Cas9 are a future possibility — current technology works with limited efficiency and specificity and is not approved for clinical use (Wu et al., 2013; Long et al., 2014; Liang et al., 2015).

Following diagnosis with inherited retinal dystrophy there are a number of therapies that are under investigation for slowing the rate of disease progression without replacing the defective gene. Transcorneal electrical stimulation is one technique under clinical evaluation for patients with retinitis pigmentosa (Schatz et al., 2011). By periodically providing low current pulses to the eye it is hypothesised that the increased release of growth and neurotrophic factors will slow the rate of programmed cell death (also known as apoptosis) in the retina (Ni et al., 2009). Alternative methods to increasing the levels of intraocular neurotrophic factors include administering neurotrophic factor-expressing gene therapy (Buch et al., 2006; Byrne et al., 2015; Lipinski et al., 2015) or encapsulated cell technologies that secrete such factors (Tao, 2006). Clinical trials have suggested that these therapies may be able to slow the rate of vision loss (Zhang et al., 2011) or, in some cases, cause short-term vision gains (Sieving et al., 2006). Dietary supplementation is another therapeutic option presently in clinical trial. Use of synthetic chromophore shows sustained benefits for a small fraction of people with *RPE65* and *LRAT* mutations (Koenekoop et al., 2014) and the use of dietary deuterated vitamin A slows the rate of degeneration in *Abca4* knockout mice (Charbel Issa et al., 2015). Dietary supplementation with vitamin A or vitamin E showed a slower rate of electroretinogram decline in the vitamin A group and a greater rate of function loss in the vitamin E group, compared to the placebo group (Berson et al., 1993).

Dietary supplementation with the ω-3 polyunsaturated fatty acid docosahexaenoic acid (DHA) is another dietary treatment that has been tested for retinitis pigmentosa. In a

four-year study of high-dose DHA in X-linked retinitis pigmentosa patients the treatment was found to be safe, but with no benefit to rod or cone electroretinogram function (Hoffman et al., 2014).

Antisense oligonucleotides, which are short synthetic nucleic acids (16 – 20 nucleotides) that are able to bind to mRNA and modify their functionality, have been applied to treat specific forms of inherited retinal dystrophies (Collin et al., 2012). A significant advantage of this approach is that the size of the mutated gene does not create any barrier to therapy. However, using this approach requires a customised product to be developed for each mutation. Splice-switching oligonucleotides have been applied to allow skipping of a mutant cryptic splice site that is created in a disease-causing mutation in the *CEP290* gene; a mutation that manifests as Leber congenital amaurosis (Gérard et al., 2015).

Translational read-through inducing drugs are under investigation as a treatment option for in-frame nonsense mutations in choroideremia (Moosajee et al., 2008), Usher syndrome type 1C (Goldmann et al., 2011), dominant rhodopsin disease and RPE65 mutations (Guerin et al., 2008). It is estimated that one third of all genetic diseases are caused by in-frame nonsense mutations, so a significant number of patients may benefit from these drugs, which function independent of the size of the mutated gene.

1.2.1 Ocular gene therapy

Gene supplementation is one of the therapeutic approaches relatively advanced in its translation to clinical application. In this approach, wild type copies of the mutant gene are delivered to the cells of the eye that normally express the gene. By providing the cell with a normal copy of the affected gene this approach aims to return treated cells to a normal functional state and therefore restore vision, or slow the rate of vision loss. The gene supplementation approach is most suitable for loss-of-function recessive and X-

linked disease, as well as dominant disease caused by haploinsufficiency, where the presence of a single wild type allele is not sufficient for normal cellular function (Cai et al., 2010). In combination with a method to suppress the mutant allele, gene supplementation is also being used to treat dominant negative and toxic gain-of-function disease (Millington-Ward et al., 2011). The use of CRISPR-Cas9 to correct somatic cell mutations by *in vivo* gene therapy is an alternative to gene supplementation and is in the early phases of development (Yin et al., 2014; Ran et al., 2015).

Techniques that aim to provide a normal copy of a gene to cells of the eye can be divided into viral and non-viral techniques. Some of the non-viral techniques that have been utilised include naked plasmids (Dezawa et al., 2002), naked oligonucleotides (Hangai et al., 1998) as well as DNA complexed in liposomes (Fattal et al., 2004), in nanoparticles (Bourges et al., 2003; Cai et al., 2010) or with polyethylenimine (Gomes dos Santos et al., 2006). These techniques have not been widely adopted for translational research due to their low transfection rates and short duration of transgene expression (Andrieu-Soler et al., 2006).

The different viral vectors used to treat inherited retinal dystrophies include adenovirus (Vollrath et al., 2001), lentivirus (Tschernutter et al., 2005; Yáñez-Muñoz et al., 2006) and adeno-associated virus (AAV). Due to its greater ability to efficiently transduce a wide range of cells and lower risk of genomic integration and inflammatory response (Bennett, 2003), AAV has become the most commonly used viral vector for ocular gene therapy studies. However, due to its larger packaging capacity (8 – 10 kb (Balaggan and Ali, 2012)) lentivirus vectors are being tested to treat diseases caused by genes that are beyond the packaging capacity of a single AAV vector, such as *ABCA4* (Kong et al., 2008), *CEP290* (Burnight et al., 2014) and *MYO7A* (Zallocchi et al., 2014). Clinical trials using *ABCA4*- and *MYO7A*-expressing lentivirus vectors are ongoing (NCT01367444 and NCT01505062; clinicaltrials.gov).

Clinical trials using AAV gene therapy to treat a number of inherited retinal dystrophies using gene supplementation are underway. The first clinical studies were completed on patients with *RPE65* mutations (Maguire et al. 2008; Bainbridge et al. 2008; Hauswirth et al. 2008). Data from at least three years of follow-up in two of the three trials has shown that the observed short-term benefit for some patients was not sustained in the long-term (Bainbridge et al., 2015; Jacobson et al., 2015). A gene therapy trial for choroideremia has shown encouraging early signs of benefit for some patients (MacLaren et al. 2014). Additionally, there are ongoing AAV gene therapy trials assessing the safety and efficacy of *MERTK* (NCT01482195) and *MT-ND4* (NCT02161380) gene supplementation therapies for causes of retinitis pigmentosa and Leber hereditary optic neuropathy, respectively.

Preclinical studies of AAV gene supplementation gene therapy are underway for inherited retinal dystrophies caused by a wide range of other causative mutations, including *ABCA4* (Trapani et al., 2015), *BEST1* (Guziewicz et al., 2013), *CNGA3* (Pang et al., 2012), *CNGB3* (Komáromy et al., 2013), *CRB1* (Pellissier et al., 2015), *MYO7A* (Colella et al., 2013), *PDE6A* (Wert et al., 2013), *PDE6B* (Nishiguchi et al., 2015), *RHO* (Mao et al., 2011), *RPGR* (Wu et al., 2015), *RPGRIP1* (Lhériteau et al., 2014) and *RS1* (Byrne et al., 2014).

1.2.2 Mutation-independent therapeutic strategies

Understanding the pathophysiology and developing clinically approved treatments for the hundreds of causative mutations implicated in inherited retinal dystrophies is a large undertaking for the biomedical research and pharmaceutical communities. For rare mutations, it may be economically difficult to justify investment in a bespoke treatment. Therefore, developing therapies that are effective regardless of the causative mutation

would have great benefits. Therapies that fit into this category include cell therapies, electronic retinal implants and optogenetics.

1.2.2.a Cell transplantation therapy

Although the causative mutations of inherited retinal dystrophies are widely varied, the end-stage phenotype is predictable. In end-stage rod-cone dystrophy, cone-rod dystrophy, macular dystrophy and Leber congenital amaurosis, the retina is largely devoid of an outer nuclear layer and there is variable reduction in the density of retinal pigment epithelium (Milam et al., 1998; Bramall et al., 2010). Cell-based therapies aim to replace the lost cells with normally functioning cells of the same class. Preclinical studies that aim to replace photoreceptors have transplanted photoreceptor precursor cells from early postnatal wild type mice into retinally degenerate adult mice (MacLaren et al., 2006; Singh et al., 2013), wild type adult mice (MacLaren et al., 2006; West et al., 2008) and knockout mice (Lamba et al., 2009; Pearson et al., 2012). Photoreceptor donor cells have also been grown from three-dimensional embryonic stem cell cultures (Gonzalez-Cordero et al., 2013). Human embryonic stem cells have been transplanted into clinical trial patients with *ABCA4*-retinopathy and advanced age-related macular degeneration (Schwartz et al. 2015). Results after 22 months suggested that transplantation was safe, led to an increase in retinal pigmentation in the injected area and was associated with visual acuity improvement in some recipients. Ideally a person's own stem cells will be used for cell-replacement therapy, but this comes with the added challenge of *ex vivo* correction of the causative mutation (Hanna et al., 2007; Cramer and MacLaren, 2013).

1.2.2.b Electronic retinal implants

Electronic retinal implants are a method to electrically stimulate the remaining cells in the degenerate retina to mimic the electrical changes that would normally occur following the detection of light by photoreceptors. Devices that are positioned on the

inner layer of the retina (so-called epiretinal implants) and subretinally have both been tested in clinical trials and have shown restoration of rudimentary vision (detection of large, high contrast objects) in the majority of patients (Humayun et al. 2012; Stingl et al. 2015). The spacing of the electrodes (corresponding to 15 minutes of arc in the subretinal implant (Zrenner et al., 2011)) and the fact that an electrode electrically stimulates all cell types in a relatively large area of retina limits an electronic retinal implant's maximum achievable visual acuity. A further limitation of these devices is that they have a limited working life before they fail and require explantation.

1.2.2.c Optogenetics

Optogenetics is another approach that holds promise for restoring vision to the blind retina. It is this technique that is investigated in this research project. The background and important features of this technique will be presented, followed by a discussion of how this project's experiments aim to contribute to the field.

Optogenetics is the use of light-sensitive molecules, typically genetically encoded, to light-sensitise cells. By light-sensitising a cell, its physiology can be manipulated by a light stimulus. In some circumstances a chemical means of cellular stimulation can match the spatial and temporal resolution of optogenetics (Steigert, 2010), but optogenetics has the advantages of greater scalability and a less invasive means of stimulus delivery (Yizhar et al., 2011).

The field of optogenetics began when Zemelman and colleagues (2002) co-expressed *Drosophila* rhodopsin, its native G protein partner, G_q, and arrestin in neurons and demonstrated that this enabled the selective firing of action potentials in illuminated neurons. The field expanded greatly with the realisation that the expression of three metazoan genes could be replaced with the expression of a single gene that encoded channelrhodopsin-2 — a microbial-type opsin from the unicellular green alga

Chlamydomonas reinhardtii — that is a light-activated (λ_{max} 470 nm) cation-selective channel (Nagel et al., 2003). The absorption of a photon by all-*trans* retinal, the chromophore of channelrhodopsin-2, causes a conformational change leading to the opening of an intrinsic cation pore (Lórenz-Fonfría and Heberle, 2014). While channelrhodopsin-2 causes a cell to depolarise, halorhodopsin, a light-activated chloride pump from the archaebacterium *Natronomonas pharaonis,* causes light-induced hyperpolarisation (Zhang et al., 2007).

Since wild type microbial opsins were cloned, numerous variants have been engineered to have different spectral properties, greater photocurrent amplitudes and different kinetic responses (Nagel et al., 2005; Zhang et al., 2008; Lin et al., 2009; Gunaydin et al., 2010; Kleinlogel et al., 2011). Attempts to improve the light sensitivity of channelrhodopsin-2 have had the unintended consequences of shortening the duration and size of the light-induced current (see §1.4.1 for a discussion of comparative light sensitivities; Berndt et al., 2009; Lin et al., 2009). Together, channelrhodopsin-2, halorhodopsin and their variants have been used as tools to interrogate neural circuits involved in addiction (Witten et al., 2010), memory (Goshen et al., 2011), eye movements (Jazayeri et al., 2012) and sleep (Adamantidis et al., 2007). Microbial opsins have also been used to manipulate cardiac and skeletal muscle physiology (Arrenberg et al., 2010; Bruegmann et al., 2010).

Microbial-type opsins, or type 1 opsins, are light-sensitive receptor and effector proteins expressed by eubacteria, archaea, fungi and algae that typically use all-*trans* retinal as a chromophore to absorb light (Sharma et al., 2006). Animal opsins, or type 2 opsins, are G protein-coupled receptors (GPCRs) that also detect light through a vitamin A-derived retinal co-factor (typically 11-*cis* retinal) but signal their effects through protein-protein interactions. This leads to a signal amplification that can allow a single photon of light

to have a substantial effect on cell physiology (Baylor et al., 1979). Both type 1 and 2 opsins are integral membrane proteins with seven transmembrane domains, but their shared sequence homology is minimal (Fenno et al., 2011).

In parallel with the work on microbial opsins, advances have occurred in the field of mammalian opsins. Melanopsin, an opsin originally isolated from dermal melanophores of *Xenopus laevis* (Provencio et al., 1998), can light-sensitise mammalian neuronal-like cells (Melyan et al., 2005; Qiu et al., 2005). Melanopsin is expressed in approximately 1% of mammalian retinal ganglion cells, rendering them intrinsically photosensitive (Hattar et al., 2002). These photosensitive retinal ganglion cells act as irradiance detectors and play an important role in circadian entrainment, the pupillary-light reflex and light adaptation (Güler et al., 2008; Hatori et al., 2008; Allen et al., 2014). Melanopsin couples to the $G_{q/11}$ pathway, a property shared with invertebrate visual opsins (Graham et al., 2008; Bailes and Lucas, 2013). This gives melanopsin an advantage as an optogenetic tool as the Gα subunits of the $G_{q/11}$ family are widely expressed (Strathmann and Simon, 1990; Wilkie et al., 1991). In contrast, the native Gα subunits of visual opsins are only expressed in their respective photoreceptors (Lerea et al., 1986).

1.3 Optogenetics for vision restoration

By ectopically expressing opsins in remaining neuronal cells of the degenerate retina, optogenetics for vision aims to restore retinal function by enabling these opsin-expressing cells to take over the light-sensing role from the photoreceptors that have undergone apoptosis. Both type 1 and type 2 opsins have been explored as optogenetic tools for vision restoration in preclinical studies. Channelrhodopsin-2 and its variants are the most widely studied optogenetic tools for vision. Channelrhodopsin-2 has been expressed in a non-targeted manner (Bi et al., 2006; Farah et al., 2007; Tomita et al.,

2007; Ivanova and Pan, 2009) and has been targeted to ON retinal bipolar cells (Lagali et al., 2008; Doroudchi et al., 2011; Macé et al., 2014). Expression is well-tolerated and can be sustained for up to 18 months post-injection in non-degenerate retinas (Ivanova and Pan, 2009; Doroudchi et al., 2011). Channelrhodopsin-2 expression enables light-induced spike activity in ganglion cells (Bi et al., 2006; Lagali et al., 2008; Ivanova and Pan, 2009; Doroudchi et al., 2011; Macé et al., 2014) and in vision centres of the brain (Bi et al., 2006; Tomita et al., 2007; Macé et al., 2014). Performance improvements in visually-guided behavioural tests have been demonstrated following channelrhodopsin-2 expression in multiple mouse models of retinal degeneration (Lagali et al., 2008; Doroudchi et al., 2011; Macé et al., 2014).

In an alternative approach, halorhodopsin expression was targeted to residual cone cells of two mouse models of retinal degeneration (Busskamp et al., 2010). This treatment was effective at increasing ganglion cells' spike firing, with some evidence of directional selectivity. Visually guided behaviours were also improved, relative to the control group. Zhang and colleagues (2009) injected a ubiquitously-expressing halorhodopsin AAV vector into retinally degenerate mice. Patch-clamp recordings demonstrated light-induced hyperpolarisation, similar to a normal OFF ganglion cell response. In one set of experiments, Zhang and colleagues co-injected channelrhodopsin-2 and halorhodopsin-expressing AAV vectors and were able to record ON and OFF type responses using different wavelength light stimuli.

The next step to recapitulate the centre-surround receptive field was taken by Greenberg and colleagues (2011). By including subcellular localisation sequences in expression cassettes for humanised channelrhodopsin-2 and enhanced halorhodopsin, this group engineered retinal ganglion cells to express both opsins at either the soma (centre) or in the dendrites (surround). This approach was effective in creating a centre-surround receptive field. Behavioural effects were not reported.

Melanopsin was first applied as an optogenetic tool for vision by Lin and colleagues (2008). Using an AAV vector with a ubiquitous promoter, mouse melanopsin delivered by intravitreal injection resulted in ectopic expression predominantly in ganglion cells. Melanopsin gene therapy was associated with increased retinal light sensitivity, with improvements in the pupillary light reflex and gains in visually-guided behavioural tests. A chimeric opsin consisting of the extracellular and transmembrane domains of mouse melanopsin and the intracellular surface of mouse metabotropic glutamate receptor 6 (mGluR6) has also been tested in a mouse model of retinal degeneration (van Wyk et al., 2015). Using gene therapy and a transgenic mouse line, van Wyk and colleagues demonstrated improved light sensitivity at the retinal and cortical levels, as well as in a visual reflex test and visually guided behavioural test. Beyond its application to retinal disease, melanopsin has also been used as an optogenetic tool in the study of cardiac pacemaking (Beiert et al., 2014) and glucose metabolism (Ye et al., 2011).

Mammalian rhodopsin has also been investigated as an optogenetic tool for vision restoration with rat (Gaub et al., 2015) and human (Cehajic-Kapetanovic et al., 2015) rhodopsin expression targeted to ON bipolar cells leading to signs of enhanced light sensitivity at the retinal, brain and behavioural level.

Alternative methods to light-sensitise cells include the use of a genetically and chemically engineered light-gated ionotropic glutamate receptor, known as LiGluR (Caporale et al., 2011; Gaub et al., 2014), or small molecule photoswitches (Polosukhina et al., 2012; Tochitsky et al., 2014). Targeting LiGluR to retinal ganglion cells or ON bipolar cells led to the restoration of functional vision in mouse and dog models of retinal degeneration. Acrylamide-azobenzene-quaternary ammonium (AAQ), a small molecule that interacts with and photosensitises potassium channels, has been shown to light-sensitise retinal ganglion cells, bipolar and amacrine cells with

functional benefits to visual function (Polosukhina et al., 2012). DENAQ, a diethylamino derivative of AAQ, is another chemical photoswitch that has shown functional benefits in a mouse model of retinal degeneration (Tochitsky et al., 2014). The main disadvantage of these approaches is that they require repeated intraocular dosing of a chemical substrate.

Optogenetic gene therapy has not yet been tested in humans. However, a phase I/II clinical trial to test channelrhodopsin-2 in people with retinitis pigmentosa was approved in 2015 and is currently recruiting patients (NCT02556736, clinicaltrials.gov). Arguably, the proof of concept for optogenetics in humans is provided by electronic retina implant trials. Just as optogenetics aims to recapitulate light-dependent ganglion cell spiking activity using biological tools, electronic retina implants achieve this with electronic hardware. The evidence that electronic retina implants are able to restore some vision provides reassurance that residual cells in the degenerate retina are still able to subserve vision, given appropriate stimuli.

An ideal optogenetic therapy for vision restoration would have the following properties: highly light-sensitive, fast onset and offset of response, relatively high visual acuity, colour vision, non-toxic and delivered in a single dose. Current strategies fall short of a number of these goals. Achieving such aims depend not only on the choice of light-sensitive molecule, but also on having a high level of expression of the light-sensitive protein in the target cell(s). To maximise the outcomes of an optogenetic gene therapy for vision strategy a coordinated approach optimising all of the components needs to be taken.

1.4 Aims

The objective of this research project was to investigate a number of the challenges that must be met in order to restore vision using an optogenetics approach. Specifically, the experiments in this research project aimed to provide data on:

a) the choice of light-sensitive optogenetic tool (chapters four, five and six),

b) the choice of target cell(s) for gene therapy (chapters six and seven),

c) the optimal way in which the light-sensitive molecule should be delivered to the eye (chapters three and six), and

d) the gene expression changes seen in one particular target cell type, the retinal bipolar cell, during retinal degeneration (chapter seven).

The variables tested are summarised in Figure 1.2. The following sections briefly explain each variable and how it will be experimentally addressed.

1.4.1 Light-sensitive molecules — comparison of wild type and engineered human opsins

This research project utilises human proteins due to their potential benefits for translational research. Using human proteins should have the benefits of increased light sensitivity and lower risk of immune responses over alternative light-sensitive molecules.

The sensitivity differences between type 1 and type 2 opsins were apparent in a direct comparison by Gaub and colleagues (2015). Multielectrode array retinal ganglion cell recordings demonstrated that similar responses were induced at light levels more than two orders of magnitude lower in degenerate retinas transduced with rat rhodopsin, compared to channelrhodopsin-2. Van Wyk and colleagues (2015) also generated an irradiance response curve from extracellular recordings of ON retinal ganglion cells in

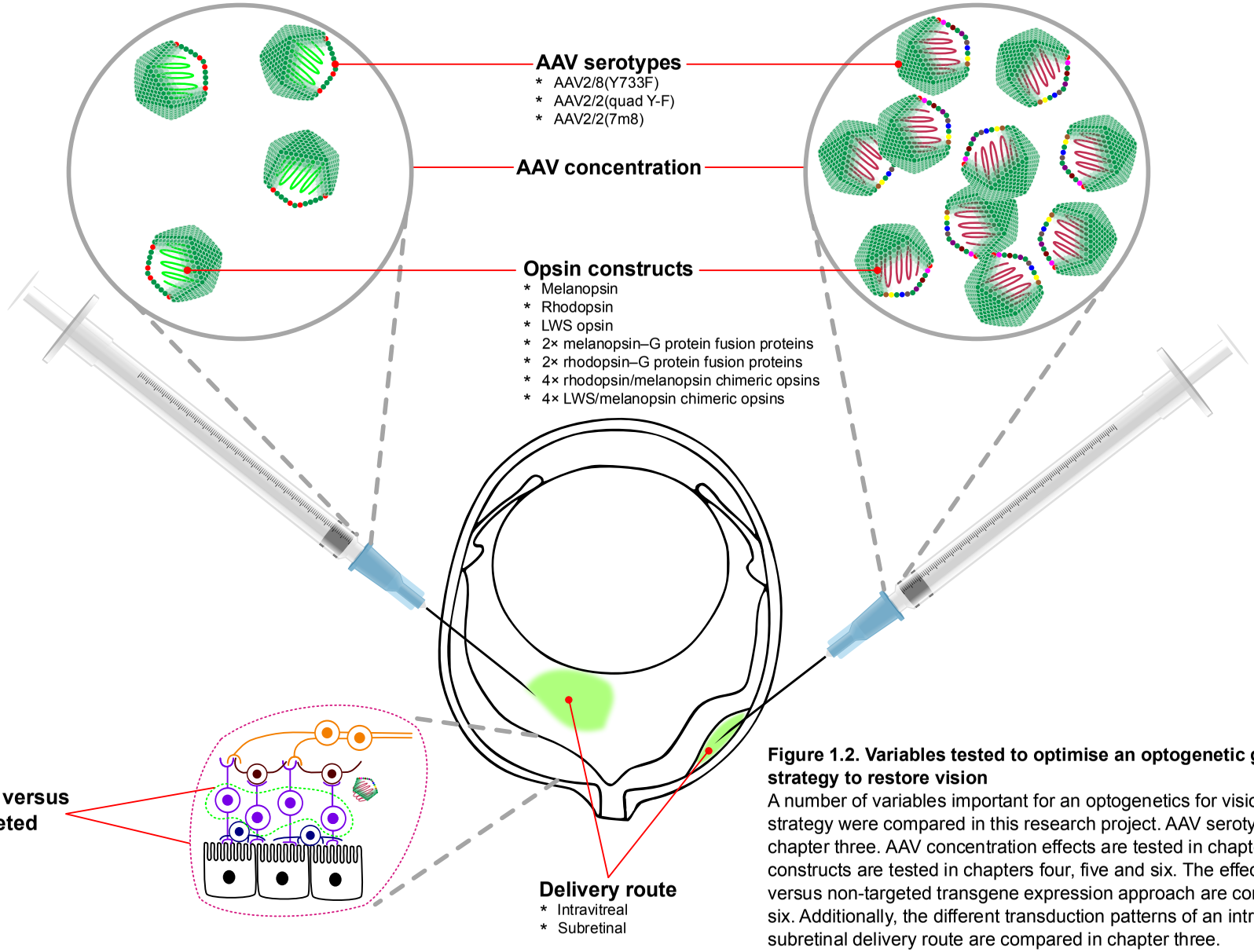


Figure 1.2. Variables tested to optimise an optogenetic gene therapy strategy to restore vision
A number of variables important for an optogenetics for vision gene therapy strategy were compared in this research project. AAV serotypes are compared in chapter three. AAV concentration effects are tested in chapter six. Different opsin constructs are tested in chapters four, five and six. The effects of a targeted versus non-targeted transgene expression approach are compared in chapter six. Additionally, the different transduction patterns of an intravitreal versus subretinal delivery route are compared in chapter three.

transgenic mice expressing Opto-mGluR6, a chimeric type 2 opsin. Their data showed that these cells were responding similarly to ganglion cells in retinas expressing channelrhodopsin-2, but at light intensities 2 – 3 orders of magnitude lower (channelrhodopsin-2 data was derived from: Lagali et al. 2008; Doroudchi et al. 2011). Using microbial opsins for a clinical treatment would require amplified light levels from modified spectacles, whereas additional hardware would be unnecessary if a type 2 opsin was used. Additionally, the light intensities required to achieve substantial responses in channelrhodopsin-2 transduced eyes ($>10^{16}$ photons cm^{-2} s^{-1} (Bi et al., 2006; Lagali et al., 2008; Ivanova and Pan, 2009; Zhang et al., 2009; Doroudchi et al., 2011)) — equivalent to bright daylight (Doroudchi et al., 2011) — cause retinal toxicity (Grimm et al., 2001; Joly et al., 2009).

The use of human proteins, or in the case of chimeric and fusion proteins (see below), amino acid sequences from human proteins, also lowers the risk of an immune response should this work be translated to a human application.

In this research project a total of 15 proteins were tested as potential optogenetic tools for restoring vision. Three of the 15 were wild type human opsins: melanopsin, rhodopsin and long-wave-sensitive (LWS) opsin. Eight proteins were chimeric opsins. By replacing the intracellular surface of rhodopsin and LWS opsin with the corresponding sequence from melanopsin it was hypothesised that the intracellular signalling properties of rhodopsin and LWS opsin could be modified, while retaining the rapid and sensitive properties of the visual opsins. Rhodopsin-based chimeric opsins showed an enhanced ability to signal via the G protein pathway normally activated by melanopsin, but the response magnitude and kinetics were inferior to melanopsin. Chapter four presents the results of these *in vitro* studies.

A further four were fusion proteins that had either wild type melanopsin or rhodopsin fused to either G_q or G_{11}, which are the Gα subunits that melanopsin activates upon absorbing light. By covalently fusing one of these Gα subunits to an opsin it was hypothesised that the light-response characteristics could be enhanced. In chapter five these four fusion constructs were compared to their non-fused wild type counterparts *in vitro*. Melanopsin–G protein fusion proteins showed potential as optogenetics tools and so were compared with wild type melanopsin and a sham treatment in an *in vivo* study in a mouse model of retinal degeneration.

Chapter six reports the results of a pilot study comparing subretinal injections of AAV vectors containing floxed melanopsin or floxed rhodopsin into *L7*-Cre retinally degenerate mice. By using the Cre-lox system the expression of these wild type opsins was limited to Cre-expressing cells, which in the *L7*-Cre mouse are principally ON bipolar cells. The small numbers of mice in this study meant that statistically significant differences in behavioural tests were not achieved. However, immunohistochemistry suggested higher levels of rhodopsin expression were obtained.

1.4.2 Target cells for optogenetic gene therapy

A critical factor for an effective optogenetic gene therapy strategy is the choice of cell(s) that the therapy targets. The optimal cellular light response will only be achieved by an optogenetic strategy if the target cell expresses signalling proteins that the optogenetic protein is able to activate. The retina is estimated to have more than 60 functional cell types (Masland, 2011), each of which will have a unique transcriptome. Expressing a light sensitive protein in an inappropriate cell type may be not only ineffective but also counterproductive due to the multiple parallel pathways that carry visual information to the brain (Wässle, 2004); light sensitising antagonistic or inhibitory pathways with an optogenetic gene therapy could diminish the net effect at

the cortical level and limit the potential gain in vision. For these reasons it is prudent to select and accurately target an appropriate cell type(s) for optogenetic gene therapy.

This research project addressed the issue of cell targeting by studying gene expression in one target cell type, by empirically comparing the efficacy of two different targeting strategies and comparing the targeting abilities of three AAV serotypes. Chapter seven presents the results of a microarray study that compared the gene expression changes in retinal bipolar cells from a mouse model of retinal degeneration to age-matched non-degenerate controls. The aim of this study was to better understand how bipolar cells adapt to the loss of photoreceptors and what the implications of these changes could be for optimising an optogenetics gene therapy strategy. Genes involved in metabolism and oxidative stress are differentially expressed, while genes encoding proteins important for intracellular signalling are largely unchanged in their expression levels. The comparative levels of gene expression also give an indication as to which opsins might work efficiently when expressed in ON bipolar cells.

Chapter six presents pilot data comparing a targeted versus non-targeted opsin expression approach. Floxed and non-floxed melanopsin AAV vectors were injected subretinally into *L7*-Cre retinally degenerate mice. At the concentrations injected the level of melanopsin expression was higher in mice that received the non-targeted (that is, non-floxed) AAV vector. However, the small number of animals means that it is difficult to draw conclusions from the behavioural tests.

1.4.3 AAV vectors for optogenetic gene therapy

AAV vectors were compared with the aim of establishing which serotype offered the broadest range of tropism and, particularly, which was best at transducing ON bipolar cells. AAV was selected as the vector for *in vivo* studies in this project due to its established record of long-term stable transgene expression (Lebherz et al., 2005;

Rivera et al., 2005) and safety in clinical trials (Maguire et al., 2008; Jacobson et al., 2012; MacLaren et al., 2014), including after repeat administration (Amado et al., 2010; Bennett et al., 2012). Outstanding concerns relating to insertional mutagenesis (Hacein-Bey-Abina et al., 2003; Boztug et al., 2010; Winslow et al., 2011), tissue toxicity (Lipinski et al., 2014) and immune responses (Hoffman et al., 1997; Reichel et al., 1998; Seiler et al., 2007) were the primary reasons for not using lentivirus and adenovirus vectors.

Apart from an early study that used electroporation to transfer DNA (Lagali et al., 2008), all other optogenetics for vision studies requiring the transfer of DNA have used AAV vectors. Early studies used wild type AAV2 (Bi et al., 2006; Lin et al., 2008; Ivanova and Pan, 2009; Zhang et al., 2009), but subsequent published studies have used AAV serotypes with targeted mutations (Doroudchi et al., 2011; Gaub et al., 2015; van Wyk et al., 2015) and a serotype selected from a process of directed evolution (Macé et al., 2014).

In chapter three, three AAV serotypes that have been used in other optogenetics for vision studies were compared in a mouse model of retinal degeneration and *ex vivo* cultures of macaque and human retina. Two of the serotypes were created by targeted mutations to modify surface tyrosine (Y) amino acid residues to phenylalanine (F) residues: AAV2/8(Y733F) and AAV2/2(quad Y-F) (Petrs-Silva et al., 2009, 2011). The third serotype was the product of a directed evolution process designed to select a serotype effective at transducing photoreceptors following intravitreal injection: AAV2/2(7m8) (Dalkara et al., 2013). No published study compares these three AAV serotypes in retinally degenerate mice. All three serotypes performed effectively following subretinal injection, but AAV2/2(quad Y-F) and AAV2/2(7m8) transduced the mouse retina more efficiently following intravitreal injection, compared to AAV2/8(Y733F). Results from the mouse and primate studies suggested that

AAV2/2(7m8) performed most effectively and so this serotype was selected for subsequent *in vivo* studies.

1.4.4 Injection route

The route by which a vector is delivered to the eye can have an important effect on the outcome. Injecting vector into the vitreous chamber (the so-called intravitreal route) allows vector to spread over a larger area and provides greater access to the inner retina, but this comes at the cost of a dilutional effect and a potentially greater inflammatory effect compared to subretinal injections (Bennett, 2003). In contrast, a subretinal injection delivers vector to the potential space between the retinal pigment epithelium and the photoreceptors (or inner nuclear layer in the degenerate retina). The subretinal approach therefore puts a high concentration of vector in close proximity to the outer retina and contains the vector in the bleb created by the injection. Disadvantages to this approach are that the transduced area can be limited and the more technical surgery increases the risk of retinal damage.

Both intravitreal and subretinal delivery routes are under assessment in ongoing clinical trials (each trial uses just one of the routes). Some research groups have suggested that detachment of the macula for subretinal injection can have negative effects on anatomical and functional outcomes (Jacobson et al., 2006, 2012; Bainbridge et al., 2015); however, this has not been a consistent finding in all clinical studies that have involved detachment of the macula (MacLaren et al., 2014). Intravitreal and subretinal approaches have also been used for preclinical optogenetics for vision studies, but none has compared the two directly.

In this research project the optimal route of AAV delivery was assessed using data from chapters three, five and six. In these experiments AAV vector was delivered by intravitreal or subretinal injection and transgene expression was assessed by *in vivo*

imaging and immunohistochemistry. GFP-expressing AAV2/2(7m8) performed similarly following either route of injection. However, the greatest opsin expression was achieved using the subretinal route.

1.4.5 AAV concentration

A final variable that needs to be considered in optimising a strategy for optogenetic gene therapy for vision is the concentration of the vector delivered to the eye. Achieving the optimal concentration is a balance between a concentration high enough to achieve the desired therapeutic effect, but not so high as to lead to an unacceptable risk of vector toxicity or a harmful immune response (Jacobson et al. 2006; Bainbridge et al. 2015; Barker et al. 2009).

One of the first AAV gene supplementation clinical trials had both low and high dose arms and this group reported a dose-response in their safety and efficacy data (Bainbridge et al., 2015). Preclinical studies have also shown a clear relationship between AAV vector dose and transduction efficiency (Ivanova and Pan, 2009; Petrs-Silva et al., 2009).

The range of concentrations reported in the optogenetics for vision literature is wide: from 1×10^{11} genomic particles/ml (Bi et al., 2006) to 1.8×10^{14} particles/ml (Macé et al., 2014). One of the difficulties in confidently comparing the concentrations used in other studies is that the terminology is inconsistent. Some studies report concentrations in terms of “particles”, which suggests the number of viral capsids, and others “genomic counts”, implying the number of genome copies. A significant fraction of viral particles can be empty, so a given vector could have accurate “particle” and “genomic counts” results that differ by an order of magnitude (Sommer et al., 2003).

In this research project AAV vectors were injected at two approximate concentrations. In chapters three and five and a subgroup of mice in chapter six, each eye received

approximately $1.5 \times 10^9 – 3 \times 10^9$ vector genomes (vg), corresponding to a concentration of approximately $1 \times 10^{12} – 2 \times 10^{12}$ vg/ml. In chapter six a subgroup received approximately 2×10^{10} vg (1.3×10^{13} vg/ml). The levels of transgene expression were notably greater using the higher concentration vector, without obvious adverse effects, suggesting that this dose at a minimum is appropriate.

By testing this range of variables it is hoped that useful data can be gathered to identify the optimal optogenetics strategy to restore vision to the degenerate retina.

2

Materials and Methods

2.1 Molecular biology

2.1.1 Plasmids

The UF6.1 plasmid containing humanised GFP (GenBank accession number U50963.1) driven by a ubiquitous **C**MV enhancer, chicken beta-**a**ctin, rabbit beta-**g**lobin (CAG) promoter was a gift from Professor Bill Hauswirth, University of Florida (Zolotukhin et al., 1996).

Plasmids containing the *rep-cap* genes to make AAV2/8(Y733F) and AAV2/2(quad Y-F) AAV serotypes were gifts from Dr Samantha de Silva, University of Oxford, who had created them by site-directed mutagenesis, based on published effective mutation sites (Zhong et al., 2008; de Silva et al., 2015). The *rep-cap* plasmid to produce AAV2/2(7m8) was a gift from Professor John Flannery, University of California, Berkeley (Dalkara et al., 2013).

A mammalian expression plasmid with inverted terminal repeats (ITRs), suitable for AAV production, was obtained from a commercial source (Vector BioLabs, Malvern, PA). The genetically encoded calcium sensor, GCaMP6f, was obtained from a plasmid

repository (Addgene, Cambridge, MA). The cAMP biosensor GloSensor was purchased (Promega, Fitchburg, WI — see Appendix I for full reagent details).

The pAAV-Ef1a-DIO-hChR2(H134R)-EYFP-WPRE-pA plasmid was a gift from Professor Karl Deisseroth, Stanford University.

2.1.2 Cloning of chimeric opsin constructs

Clones of human rhodopsin (*RHO*, RefSeq accession number NM_000539.3), human melanopsin transcript variant 1 (*OPN4*, NM_033282.3) and human long wavelength sensitive (*LWS*, NM_020061.4) opsin cDNA, each in pMT4 plasmids, were gifts from Dr Wayne Davies (University of Oxford).

Intracellular/transmembrane boundaries were based on previously published rhodopsin boundaries (Davies et al., 2007b). Primers were designed to allow the SPLICE technique (Davies et al., 2007a) to be used to amplify the separate component sequences of each chimera and then combine them into a single chimeric DNA sequence (Appendix II).

The primers used to create the 5′ end included an EcoRI site upstream of the start codon. The 3′ primers mutated the stop codon to create an alanine residue allowing the reading frame to continue to a downstream sequence coding for the 1D4 bovine rhodopsin epitope. Downstream of the mutated stop codon, the 3′ primers contained a SalI restriction site. Full-length chimeric opsin amplicons were double digested using EcoRI and SalI restriction endonucleases (New England Biolabs, Ipswich, MA). Empty pMT4 vector (a gift from Dr Wayne Davies) was double digested with EcoRI and SalI for ligation.

2.1.3 Cloning of opsin–G protein fusion constructs

Human *GNAQ* (RefSeq accession number NM_002072.3) and *GNA11* (NM_002067.2) DNA sequences were amplified from a cDNA library created from human SH-SY5Y cells (a gift from Dr Laurence Brown, University of Oxford). Silent point mutation of the EcoRI and SalI sites within *GNAQ* was undertaken using the SPLICE technique.

Using the SPLICE technique, primers were designed such that the 3′ ends of melanopsin and rhodopsin amplicons had an overlap with the 5′ ends of *GNAQ* and *GNA11* amplicons. Overlapping PCR was undertaken on opsin amplicons combined with G protein amplicons, resulting in a single open reading frame of the wild type opsin and wild type G protein DNA sequence. The primers used to create the overlapping fragment replaced the stop codon of the opsin and the start codon of the G protein sequence with a short linker sequence. This sequence consists of the NotI restriction site and an additional base to maintain the frame. This linker inserted three alanine residues. A range of linkers sequences have been used by other research groups, including an enterokinase (Molinari et al., 2003) and thrombin (Seifert et al., 1999a) cleavage site or a hexahistidine tag (Seifert et al., 1998a). The 5′ opsin primer created an EcoRI restriction site upstream of the start codon and the 3′ G protein primer created a SalI site downstream of the stop codon. Opsin–G protein amplicons were EcoRI/SalI double digested and ligated into pMT4.

Following *in vitro* testing, wild type melanopsin and melanopsin–*GNA11* were subcloned into a plasmid appropriate for AAV production. Primers were designed to create a 5′ HindIII restriction site and a 3′ AvrII site at the ends of the cDNA sequences. Using pMT4 plasmids as templates, PCR reactions using these primers created amplicons with these terminal restriction sites. Following double digest reactions, each sticky-ended cDNA was inserted into an AvrII/HindIII digested plasmid with a CAG promoter and AAV2 ITRs (Vector BioLabs).

2.1.4 Cloning of floxed melanopsin and rhodopsin constructs

To create floxed melanopsin and floxed rhodopsin clones, primers were designed to add a 5′ NheI restriction site and a 3′ AscI restriction site to the cDNA sequence. Following KOD PCR (§2.1.5) with these primers an AscI/NheI double digest was performed and the resulting sticky ended sequence ligated into an AscI/NheI double digested pAAV-Ef1a-DIO-hChR2(H134R)-EYFP-WPRE-pA plasmid. In the recipient plasmid the NheI site was in the 3′ position and the AscI site was in the 5′ position, therefore, in the act of ligating, the cDNA was inverted. Using these restriction sites preserved the four lox sequences.

To create a non-floxed human melanopsin plasmid to compare with the floxed version, melanopsin was subcloned into the pAAV-Ef1a-DIO-hChR2(H134R)-EYFP-WPRE-pA plasmid in the correct orientation. Primers were designed to add a 5′ XbaI restriction site and a 3′ EcoRI restriction site to the melanopsin cDNA sequence. Following a EcoRI/XbaI double digest of insert and pAAV-Ef1a-DIO-hChR2(H134R)-EYFP-WPRE-pA plasmid, the two were ligated and cloned. Using these restriction sites ensured that the four lox sequences were removed.

The template for these cloning experiments was pMT4 containing rhodopsin or melanopsin with a 1D4 tag. Primers were designed to keep the 1D4 sequence in the final clones.

2.1.5 Polymerase chain reactions

Cloning PCRs used a *Thermococcus kodakaraensis* (KOD) Hot Start DNA Polymerase kit (Toyobo, Osaka, Japan — see Appendix III for full kit details). Each 50 µl reaction consisted of: 1 µl of template DNA, 1 µl of KOD Hot Start DNA polymerase, 5 µl of 10× KOD buffer, 5 µl of deoxynucleotides (dNTPs; 2 mM each), 3 µl of 25 mM magnesium sulphate ($MgSO_4$), 1.5 µl of 10 µM forward primer, 1.5 µl of 10 µM reverse

primer and 32 µl of molecular grade water. Reactions were mixed and centrifuged briefly.

The following thermal cycler settings were applied: 95 °C for two minutes as a polymerase activation step followed by 40 cycles of: 95 °C for 30 seconds, 60 °C (typically) for 30 seconds and 70 °C for 40 seconds. Annealing temperature was 60 °C, or was determined empirically using a temperature gradient if 60 °C was not initially successful.

Genotyping PCR reactions used Immomix Red (Bioline, London, UK). Each 12.5 µl reaction consisted of 1 µl of genomic DNA, 6.25 µl of 2× Immomix Red, 0.5 µl of each primer (10 µM) and made up to 12.5 µl with molecular grade water. Reactions were mixed in nuclease-free 200 µl PCR tubes (STARLAB, Hamburg, Germany — see Appendix IV for full hardware details), centrifuged briefly and run in a thermal cycler (Bio-Rad, Hercules, CA).

2.1.6 Genotyping

Ear notches were collected by the investigator and animal husbandry staff using an ear punch tool. The tissue was transferred to a nuclease-free tube and stored at -20 °C.

100 µl of 50 mM sodium hydroxide was added to each ear notch and to an empty tube (negative control) and incubated at 95 °C for one hour. After a brief vortex, tubes were centrifuged at 16,200 g for two minutes. 10 µl of 1 M Tris hydrochloride (pH 6.0) was added, the tubes were vortexed and centrifuged again at 16,200 g for two minutes. Finally, 500 µl of AnalaR water (VWR International, Radnor, PA) was added. One microlitre of solution was used for each genotyping PCR. Extracted DNA was stored at -20 °C.

Mice were genotyped for the presence of: a) Cre recombinase, b) *Gpr179* (a naturally occurring mutation in a number of strains of *rd1* mice (Balmer et al., 2013; Chang, 2015); mutations of this gene are known to cause congenital stationary night blindness in humans (Audo et al., 2012), c) *Rd1* (a naturally-occurring, recessive nonsense mutation of rod-specific phosphodiesterase 6B (*Pde6b*) that causes a rapid retinal degeneration in mice) and d) EYFP using primers in Appendix II. For example gel results see Figure 5.6.

2.1.7 Agarose gel electrophoresis

PCR products were run on a 2% agarose (Geneflow, Lichfield, UK) gel in Tris/acetate/EDTA buffer and visualised with ethidium bromide (Sigma-Aldrich, St. Louis, MO) under ultraviolet illumination.

2.1.8 Gel extraction

PCR amplicons were purified from PCR mixtures or from agarose gel using a PCR purification kit (Qiagen, Hilden, Germany) or a gel extraction kit (Qiagen), respectively, as per the manufacturer's instructions. DNA was eluted using 30 µl of Buffer EB. If not for immediate use, DNA was stored at -20 °C.

2.1.9 Restriction digest

Restriction digest reactions were performed using a range of restriction enzymes (all New England Biolabs) according to the manufacturer's instructions.

2.1.10 Ligation

Sticky ended insert and plasmid were combined in a reaction with T4 DNA ligase and accompanying buffer (New England Biolabs). The volumes of insert and plasmid were varied to achieve a (3 – 5):1 insert:plasmid molar ratio. The reaction was mixed and left

room temperature for at least one hour before proceeding to transformation. Reactions were stored at 4 °C.

2.1.11 Transformation

5 µl ligation products were transformed into a mixture of XL10-Gold ultracompetent *Escherichia coli* cells (Agilent Technologies, Santa Clara, CA) and 2-mercaptoethanol (Sigma-Aldrich) according to the manufacturer's instructions.

Transformed *E. coli* were spread on agar plates containing the appropriate antibiotic and left to grow for 12 to 16 hours at 37 °C.

2.1.12 Bacterial culture and plasmid purification

Individual colonies from agar plates were picked and grown in 4 ml of lysogeny broth (LB) nutrient media and antibiotic for 6 to 10 hours before 500 µl of growth culture was transferred to sterile LB with antibiotic. This was incubated for 12 to 16 hours at 37 °C, 225 rpm on an orbital shaker. Cells were pelleted, frozen and purified using a column-based mini (Sigma-Aldrich), maxi (Invitrogen, Waltham, MA) or mega prep (Qiagen) protocol, according to manufacturer's instructions.

2.1.13 DNA quantification

DNA concentrations were quantified using a NanoDrop 1000 spectrophotometer (Thermo Scientific, Waltham, MA).

2.1.14 DNA sequencing

Source BioScience (Nottingham, UK) provided Sanger sequencing services. Samples and primers were provided according to their requirements.

2.1.15 DNase treatment and denaturation of AAV for titering

AAV samples were DNAase treated and heat denatured for use in quantitative PCR (qPCR) titering. One microlitre of AAV solution was combined with 1 µl of DNase I, 1

µl of DNase I buffer (both New England Biolabs) and 7 µl of molecular grade water in a nuclease-free microcentrifuge tube. The tube was placed at 37 °C for one hour. To this 90 µl of molecular grade water was added and the mixture incubated at 90 °C for 15 minutes. The sample was left on ice until being used for qPCR.

2.1.16 Quantitative PCR

Quantitative PCR (qPCR) was performed using iTaq Universal SYBR Green Supermix kit (Bio-Rad). Each 10 µl reaction consisted of 5 µl of 2× iTaq Universal SYBR Green Supermix, 1 µl of cDNA, 1 µl of forward and 1 µl of reverse primers (2 µM initial concentration) and 2 µl of molecular grade water with in a white walled 96-well plate supplied in the kit.

Reactions were run in triplicate in a CFX Connect machine (Bio-Rad). The annealing temperature was the temperature at which fluorescence readings were taken. Annealing temperatures are available in Appendix II. Each reaction ran for 40 cycles.

Primers were designed such that, where possible, they spanned at least one exon-exon boundary. Primer efficiencies were determined using a 1:10 serial dilution of a plasmid of known concentration that contained the target sequence.

Ct values were determined using the default settings of the CFX Manager software (version 3.0, Bio-Rad — see Appendix V for full software details). Data was exported to Excel (Microsoft, Redmond, WA) for analysis.

The delta delta Ct method was used for comparative gene expression calculations. Ct values were converted to initial copy numbers (R_o) using the formula: 2^{-Ct}. Plotting the housekeeper gene R_o values checked whether the results were consistent between housekeeper genes. For human samples *ACTB* and *RPLP0* were used as housekeeping genes, while in mouse samples *Gapdh* and *Rplp0* were the housekeeping genes. Gene expression was normalised by dividing R_o value of the gene of interest by the R_o value

of the geometric mean of the housekeeping genes. Sample gene of interest values were then divided by the control values to achieve the value of the relative gene expression in the sample, relative to the control sample, normalised to housekeeper gene expression.

Where absolute copy number was to be determined for AAV titering, a standard curve was run on the same plate as the DNase and denatured AAV samples. A standard curve was created by at least four 1:10 serial dilutions of a plasmid of known concentration that contained the target sequence. By programming the CFX Manager software with the copy numbers of the known standard curve samples, the software computed the copy numbers of the AAV samples. Plasmid mass was converted to copy number using web-based software (http://cels.uri.edu/gsc/cndna.html). Technical replicates were averaged. To adjust the copy number to vector genomes (vg)/ml, the qPCR-derived value was: (1) multiplied by 100 to adjust for the 1:100 dilution during the DNase and denaturation protocol; (2) doubled, because the plasmid used for the standard curve was double-stranded DNA, whereas an AAV genome is single-stranded, so twice as many AAV genome copies are required to produce an equal fluorescence signal; and (3) multiplied by 1,000 to convert from vg/µl to vg/ml (see Appendix VI for AAV concentrations).

2.1.17 Collection of RNA from a cell monolayer

To collect RNA from a cultured cell monolayer growing in a 6-well plate, media was removed and the cells were washed with PBS. 600 µl of lysis buffer (PureLink RNA Mini Kit, Ambion, Waltham, MA) mixed with 6 µl of 2-mercaptoethanol (Sigma-Aldrich) was added to the well and repeatedly washed over the cells. Lysed cell solution was then transferred to a 1.5 ml RNase-free microcentrifuge tube. Homogenisation and the remainder of the PureLink RNA Mini Kit protocol was completed as described in the following section.

2.1.18 RNA extraction

Total RNA was extracted from cells and tissues for qPCR and microarray. Different kits were used depending on the scale of the process: a RNeasy Micro Kit (Qiagen) for <500,000 cells (all FACS samples) and a PureLink RNA Mini Kit (Ambion) for ≥500,000 cells. The manufacturers' instructions were followed for both, except where modifications are noted below.

In preparation of handling RNA samples, the laboratory bench, tube rack and pipettes were cleaned using DNAZap PCR degradation solutions and RNaseZap wipes (both Ambion), as per the manufacturer's instructions. The microcentrifuge was wiped with RNaseZap wipes. Pipettes were also irradiated in a UV steriliser (UVP, Upland, CA). New nuclease-free pipette tips were used and gloves were frequently changed.

During FACS, cells were sorted directly into RLT (lysis) buffer with 2-mercaptoethanol and transported from the FACS facility to the investigator's laboratory on wet ice.

The protocols for both kits were based on the same chemical principles. A guanidinium isothiocynate-based lysis buffer mixed with 1% (vol%) 2-mercaptoethanol (Sigma-Aldrich) was used to lyse cells and inhibit RNase and DNase activity. Tissue was disrupted in lysis buffer using RNase-free pestles. Homogenisation was achieved by passing the solution through a 21 G needle (Becton Dickinson and Company, Franklin Lakes, NJ) connected to a 1 ml syringe (Henke-Sass, Wolf GmbH; Tuttlingen, Germany) twelve times.

For samples processed using the PureLink RNA Mini Kit, an equal volume of 70% (vol%) ethanol (Sigma-Aldrich) was added to precipitate nucleic acids. Samples containing FAC-sorted cells received an equal volume of 100% ethanol to account for dilution from sheath fluid (Tighe and Held, 2010). Precipitated nucleic acids were bound to a silica membrane. Wash buffers were passed over the membrane by

centrifugation. Finally, passing RNase-free water over the membrane by centrifugation eluted the remaining nucleic acids. Eluted RNA was stored at -80 °C (U570 Premium, New Brunswick Scientific, Hamburg, Germany).

Samples processed using the PureLink RNA Mini Kit were eluted once with 30 µl of RNase-free water. For samples processed with the RNeasy Micro Kit, a first elution using 14 µl of RNase-free water was followed by a second aliquot of 14 µl of RNase-free water with elution into the same tube.

A small aliquot (1 – 3 µl) was taken from the eluted volume and stored in a fresh RNase-free microcentrifuge tube to be used for quality control assays (§2.1.20).

For samples processed using the RNeasy Micro Kit an on-column DNase step was performed using an RNase-free DNase Set (Qiagen), as per the manufacturer's instructions. The DNase I and buffer RDD solutions were mixed fresh each time. Samples processed using the PureLink RNA Mini Kit underwent off-column DNase I digest (Invitrogen), as per the manufacturer's instructions.

2.1.19 First-strand cDNA synthesis and RNase H digest

RNA was converted to cDNA for downstream applications using a SuperScript III reverse transcriptase kit (Invitrogen), oligo$(dT)_{20}$ primers (Sigma-Aldrich) and RNaseOUT (Invitrogen), as per the manufacturer's instructions. RNase H (New England Biolabs) was used to degrade RNA. DNA was stored at -20 °C.

2.1.20 Bioanalyzer assessment of RNA quality and quantity

RNA quality and quantity was assessed using a 2100 Bioanalyzer (Agilent Technologies) and an RNA 6000 Pico Kit (Agilent Technologies), as per the manufacturer's instructions. The Bioanalyzer was connected to a computer running 2100 Expert software (Agilent Technologies).

To avoid unnecessary freeze-thaw cycles, a 1 – 3 µl aliquot from the RNA extraction process was used for Bioanalyzer analysis. The aliquot was thawed on wet ice and 1 µl was used for the Bioanalyzer run.

RNA from non-degenerate retina had an average concentration of 608 ± 263 pg/µl and a RIN value of 9.4 ± 0.2. Degenerate retinas yielded 364 ± 143 pg/µl of RNA with a RIN value of 9.5 ± 0.1 (Table 7.1).

2.1.21 Illumina MouseWG-6 microarray

A microarray study using RNA extracted from the YFP-positive fraction from degenerate and non-degenerate *L7*-Cre EYFP mouse retinas was conducted by Cambridge Genomic Services (CGS). See Appendix VII for the complete report from CGS.

Briefly, RNA samples were transported to CGS on dry ice. RNA quantity and purity was assessed using a SpectroStar (BMG Labtech) and a 2100 Bioanalyzer. Total RNA was amplified using an Ovation Pico WTA v2 kit (NuGEN Technologies, San Carlos, CA). Amplified cDNA was biotinylated using a BiotinIL kit (NuGEN Technologies) before being hybridised to a MouseWG-6 v2 Expression BeadChip (Illumina, San Diego, CA). The BeadChip was read with a Bead Array Reader (Illumina) and the data imported to GenomeStudio (Illumina). Lumi and limma packages for R were used to process the data. Probes with fluorescence values not significantly different ($P > 0.01$) from negative controls were excluded. Quantile normalisation was used to remove technical variation between arrays. Results were corrected for multiple testing using False Discovery Rate (FDR) testing (Benjamini and Hochberg, 1995). Probes were considered to be statistically significantly differentially expressed when adjusted $P < 0.05$.

Quality controls integrated into the arrays included hybridisation controls, mismatch and perfect match probes for stringency, labelling controls and negative controls. One sample from the degenerate group was removed from the final analysis due to failing multiple quality control measures.

2.1.22 Western blotting

293T cells from three wells of a 6-well plate that had been transfected two days prior with melanopsin, melanopsin–*GNAQ*, melanopsin–*GNA11* and no opsin were harvested, pelleted and temporarily stored at -80 °C. Samples were thawed on ice before being resuspended in 200 µl of Tris lysis buffer with protease inhibitor cocktail (F. Hoffman-La Roche). Samples were homogenised by sonication and stored on ice. Following centrifugation at 25,000 g at 4 °C for 30 minutes the supernatant was transferred to a fresh microcentrifuge tube.

Sample (1 – 1.2 µg/µl) and 2× Laemmli buffer (Sigma-Aldrich) were combined in equal volume (15 µl) and left at room temperature for 30 minutes. All 30 µl of sample/Laemmli and 7 µl of protein ladder (Geneflow) was loaded into a 10% Tris HCl precast gel (Bio-Rad) and run in Tris/glycine/SDS running buffer (National Diagnostics, Atlanta, GA) at 100 V for two hours.

Protein was transferred to a polyvinylidene fluoride (PVDF) membrane (Bio-Rad) using a Trans-Blot Turbo Transfer System (Bio-Rad; seven minutes on mixed molecular weight setting). The membrane was cut to allow the lower molecular weight section to be stained for GAPDH and the higher molecular weight section for OPN4.

Each membrane was placed protein side down into separate cassettes of a SNAP i.d. Protein Detection System (Merck Millipore, Billerica, MA). Membranes were blocked with 1% bovine serum albumin (BSA) in Tris-buffered saline with 0.1% Tween 20 (TBS-T) for ten minutes before being vacuumed through, according to the

manufacturer's instructions. Membranes were covered with 3 ml of primary antibody for ten minutes: rabbit anti-human melanopsin diluted 1:100 (Santa Cruz, Dallas, TX) and mouse anti-GAPDH diluted 1:10,000 in 1% BSA in TBS-T. Membranes were each washed thrice with 30 ml of TBS-T. Secondary antibodies (3 ml each) were applied: donkey anti-rabbit 1:10,000 to the melanopsin membrane and donkey anti-mouse 1:10,000 to the GAPDH membrane. Antibodies were diluted in 1% BSA in TBS-T and were incubated for ten minutes. Three further washes with TBS-T were applied.

Membranes were removed and placed protein side up in a tray and covered with 3 ml of enhanced chemiluminescence (ECL) substrate (Merck Millipore) for two minutes. Excess ECL substrate was removed and the membranes assembled in plastic wrap. In a dark room film was exposed to the membrane for one minute before being developed.

2.1.23 SDS-PAGE of AAV

The purity of AAV samples was determined by sodium dodecyl sulphate-polyacrylamide gel electrophoresis (SDS-PAGE). Ten microliters of concentrated or 20 µl of wash AAV solution were made up to 25 µl with 5 µl of 5× Laemmli buffer. Samples were placed at 95 °C for 15 minutes, then stored on ice. Denatured AAV proteins were then run on a 10% Tris-HCl gel (Bio-Rad) at 100 V for two hours. The gel was washed thrice with water on an orbital shaker for at least ten minutes each wash. Water was replaced with EZBlue (Sigma-Aldrich) and left shaking for at least 30 minutes. After rinsing with water for at least 30 minutes three bands representing VP1 (87 kDa), VP2 (72 kDa) and VP3 (62 kDa) could be visualised (Figure 2.1 C).

2.1.24 Protein purification and absorbance spectroscopy

Using a sepharose column with bound anti-1D4 antibody (gift from Jill Cowing), opsins were purified from 12× 140 mm plates of transfected 293T cells that had been incubated

A

Iodixanol fraction	OptiPrep (ml)	5 M NaCl (ml)	PBS-MK, 5× (ml)	H_2O, molecular biology grade (ml)	Phenol red (µl)
15%	2	1.6	1.6	2.8	-
25%	2.5	-	1.2	2.3	10
40%	3.35	-	1	0.65	-
60%	5	-	-	-	10

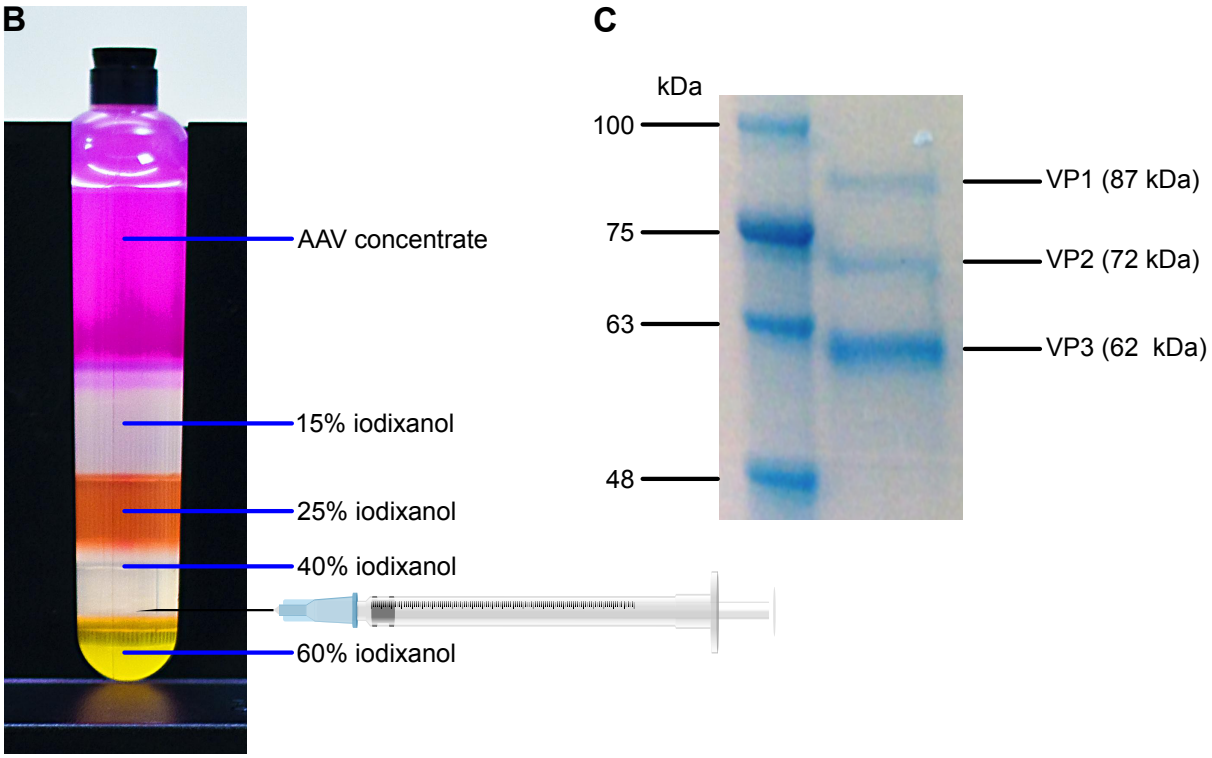


Figure 2.1. AAV production by triple transfection and iodixanol gradients
(**A**) Following the pelleting and lysis of triple-transfected 293T cells, AAV was purified by centrifugation through an iodixanol gradient. The table provides the volume of components required to make up an iodixanol gradient for AAV purification. (**B**) An iodixanol gradient. With the four layers of iodixanol in place AAV concentrate was layered on top. Following centrifugation the AAV-containing 40% fraction was removed by aspirating from the 40%–60% interface (Photo credit: Daniyar Dauletbekov). (**C**) Following AAV purification and concentration, the AAV capsid proteins, VP1, VP2 and VP3, were identified by SDS-PAGE.

with *11-cis* retinal in the dark. After washing the column, the sample was eluted by passing 1D4 peptide through the column.

A dark spectrum of the eluted opsin was obtained using a UV-visible spectrophotometer (Shimadzu, Kyoto, Japan). The sample was bleached by exposure to white light for an hour before another spectrum was obtained. In some cases, hydrochloric acid was applied to the sample to denature protein before another spectrophotometric reading was taken.

Spectral data was exported to Excel, where the bleached spectrum was subtracted from the dark spectrum. The difference spectrum was then fitted to a Govardovskii rhodopsin/vitamin-A1 template (Govardovskii et al., 2000) and the λ_{max} value determined.

2.2 Animal material

2.2.1 Ethical review

Animal experiments were performed in accordance with the United Kingdom's Animals (Scientific Procedures) Act 1986. Experiments were performed at a Home Office approved site (code: 30/2306) and under the purview of a project licence (30/2808) that was approved and periodically reviewed by the University of Oxford's Clinical Medicine Animal Welfare and Ethical Review Body and the Home Office. The candidate was appropriately trained to perform the procedures described and was assigned the personal licence code I58FB83B3 following Home Office-approved training.

The acquisition of human retina tissue from patients with retinal detachment and its subsequent culturing was approved by the Berkshire Research Ethics Committee, part of the National Health Service's National Research Ethics Service. The study was assigned the REC Code 10/H0505/8.

2.2.2 Animal housing

Mice were housed in individually ventilated cages under a 12-hour light (<100 lux)/dark cycle with the cage temperature set to 21 ± 3 °C and 55 ± 10% relative humidity. Pellets of RM3 diet (Special Diets Services, Witham, UK) and water were available *ad libitum*. Mice were weaned at approximately 21 days old. Cages were lined with sawdust. Paper strips and a red plastic tube provided cover and bedding material. Cages were cleaned every one to two weeks, depending on the number of mice present and whether it was a breeding cage.

2.2.3 Mouse strains

Tg(Pcp2-cre)756Mro/0 (referred to as *L7*-Cre) mice (Marino et al., 2002) were a gift from Professor Sebastian Brandner, University College London (via Professor Simon Fisher, Max Planck Institute for Psycholinguistics). *L7*-Cre mice had a mixed FVB/N and C57BL/6JOlaHsd background before being crossed with C3H/HeNCrl and EYFP mice (details below). Gt(ROSA)26Sor$^{tm1(EYFP)Cos}$ mice (Srinivas et al., 2001) were a gift from Dr Elizabeth Slee, University of Oxford. All experimental mice were homozygous for this allele (referred to as EYFP mice). C3H/HeNCrl mice used for AAV tropism studies and crossing with *L7*-Cre mice were purchased from Charles River (Wilmington, MA). C3H/HeH mice used for melanopsin–G protein fusion *in vivo* experiments were purchased MRC Harwell. Non-degenerate C3H/HeN *Pde6b*$^{+/+}$ were a gift from Professor Russell Foster, University of Oxford.

2.2.4 Mice used for a microarray study of retinal bipolar cells adaptation to retinal degeneration

The target age for undertaking FACS and extracting RNA from the retinas of transgenic mice expressing EYFP in a subset of their bipolar cells was 90-days-old. This age was judged to be relatively late in the degeneration process, when most photoreceptors had undergone apoptosis, and would therefore be a time at which physiologically important

gene expression changes would be occurring. In mice that are homozygous for the *rd1* mutation in the phosphodiesterase 6B gene, rods are absent from the posterior retina by 36 days old and absent from the far periphery by 65 days old (Carter-Dawson et al., 1978). Therefore, for most of the retina, bipolar cells were without rod photoreceptor inputs for at least two months. Other studies looking at changes in degenerate bipolar cells have examined retinas from mice aged 90 days or less (Strettoi and Pignatelli, 2000; Strettoi et al., 2003; Punzo and Cepko, 2007; Holt et al., 2015). These studies have shown that patterns of gene expression changes can vary significantly with age, indicating dynamic changes in gene expression from the beginning of the degeneration process (Hackam et al., 2004; Armata et al., 2006). Defining the age and stage of degeneration in a given model is therefore critical for study reproducibility and relevance.

An equal number of male and female samples in both degenerate and non-degenerate groups were used to ensure any findings were robust and applicable, regardless of gender.

The mice used for this study were not highly inbred for two reasons. Firstly, it was not possible to have a congenic line for this study because both degenerate ($Pde6b^{rd1/rd1}$) and non-degenerate ($Pde6b^{+/+}$) mice were required and due to wanting to avoid the potentially negative consequences of homozygosity for the *L7*-Cre transgene allele (insertion location unknown). Secondly, by using mice that were not highly inbred it was hypothesised that the results would be more applicable to a wider range of strains.

Although mice that are heterozygous for the *rd1* mutation have an anatomically normal retina and do not have a degeneration phenotype, it has been found that these retinas have lower levels of cGMP and an abnormal electroretinogram (Ferrendelli and Cohen, 1974; Doshi et al., 1985; Low, 1987; Voaden and Willmott, 1990). To avoid the

possibility that such abnormal photoreceptor biochemistry could have downstream effects for the gene expression of bipolar cells, mice that were heterozygous for the *rd1* mutation were not included for this study.

2.3 Cell culture

2.3.1 Subculturing cell lines

293T cells were cultured in Dulbecco's Modified Eagle's Medium (DMEM), complete with L-glutamine (2 mM), penicillin (100 units/ml), streptomycin (100 µg/ml) and 10% fetal bovine serum (all Sigma-Aldrich; see Appendix VIII for full solution details). Flasks (T75, Sarstedt, Nümbrecht, Germany) were kept at 37 °C in a 5% CO_2 humidified environment (HERA Cell 150, Thermo Electron, Waltham, MA). Cells were subcultured every three to five days, prior to becoming confluent.

To subculture the cells, the media was removed and the cells were washed with PBS. Enough trypsin (5 mg/ml, Sigma-Aldrich) was applied to cover the cells (2 ml for a T75 flask) and the flask incubated at 37 °C for approximately 5 minutes. An equal volume of complete DMEM was added to the trypsin and the flask surface thoroughly washed. The cell solution was pipetted into a 15 ml conical centrifuge tube and centrifuged at 1,200 g for five minutes at room temperature. The supernatant was poured off and the pellet resuspended in complete DMEM. A fraction of the resuspended volume (typically one tenth to one sixth) was transferred to a T75 flask containing 10 ml of complete DMEM and the flask was placed in a 37 °C, 5% CO_2, humidified incubator.

2.3.2 *In vitro* plasmid transfection

Cultured cells were transfected using GeneJuice transfection reagent (Merck Millipore). For every 1 µg of DNA, 100 µl of RPMI-1640 medium (Sigma-Aldrich) and 3 µl of GeneJuice were combined, according to the manufacturer's instructions. The

transfection mixture was added to cell culture medium that was complete with serum and antibiotics.

For double and triple transfections, double or triple the amount of GeneJuice was mixed with a given volume of RPMI. Plasmids for co-transfections were mixed before being added to the RPMI/GeneJuice solution.

2.3.3 *In vitro* knockdown of endogenous gene expression using siRNA

Cells were seeded at 200,000 cells per 35 mm dish in complete DMEM and the following day the media was changed to RPMI with 10% fetal bovine serum and 1% L-glutamine. For each 35 mm dish, 400 µl of RPMI was combined with 6 µl of Lipofectamine RNAiMAX (Invitrogen) and briefly vortexed. After 5 minutes a total of 6 µl of 20 µM siRNA was added. For co-transfections, 3 µl of each siRNA solution was mixed together prior to adding the RPMI/Lipofectamine mix. The transfection mixture was left at room temperature for at least 15 minutes, flicking to mix occasionally, before being added to the cell media (final total siRNA concentration in dish 50 nM). The day after transfection, media was changed back to complete DMEM with antibiotics.

The efficacy of siRNAs was assessed using qPCR to quantify relative gene expression changes (§2.1.16).

Negative control siRNA (Ambion) was not complementary to any sequence in the vertebrate transcriptome. See Appendix II for anti-*GNAQ* and anti-*GNA11* siRNA details.

2.3.4 Live cell cAMP assay

Intracellular cyclic adenosine monophosphate (cAMP) concentrations were assayed by pGloSensor-22F plasmid (Promega) co-transfection of 293T cells. GloSensor-22F encodes for cAMP binding domains fused to a mutant form of *Photinus pyralis*

luciferase. The binding of cAMP activates luciferase and catalyses the two-step reaction of luciferin, oxygen and ATP into oxyluciferin, AMP and light and therefore leads to increased bioluminescent light emission (Fan et al., 2008; Binkowski et al., 2009).

15,000 293T cells in complete CO_2-independent media (Gibco, Waltham, MA) were seeded into each well of a white-walled, clear-bottomed 96-well plate (Sarstedt) and kept in a humidified incubator at 37 °C, 5% CO_2. The day after seeding, cells were transfected with GloSensor-22F plasmid only (no opsin control) or in combination with a plasmid encoding an opsin. For each well the equivalent of 5 µl of RPMI, 0.3 µl of GeneJuice and 50 ng of each plasmid was used for a standard GeneJuice transfection.

On the second day after transfection, cells were loaded with 9-*cis* retinal (Sigma-Aldrich) and beetle luciferin (Promega). Under room lights 100 µl of media was removed from each well, leaving approximately 50 µl. In a darkened room using a red LED headlight, 50 µl of loading mixture was added. Loading mixture contained 20 µM 9-*cis* retinal and 4 mM beetle luciferin in complete CO_2-independent media. Each well therefore contained 10 µM 9-*cis* retinal and 2 mM luciferin. The loaded plate was wrapped in foil and incubated for at least two hours at room temperature.

Under dim red light a loaded plate was placed in a plate reader (FLUOStar Omega, BMG Labtech, Ortenberg, Germany) with a fluorescence optic, connected to a computer running Omega software (BMG Labtech). Plate temperature was monitored, but not controlled (typically 25 – 27 °C). A script was written to automate the following protocol:

1) Baseline: 5 cycles

2) Plate ejected for 35 seconds. Under dim red light 11 µl of forskolin (20 µM) added to each well (final concentration 2 µM). Forskolin is a small molecule

drug that activates adenylate cyclase, which in turn catalyses the conversion of ATP to cAMP. It was used to elevate cAMP levels.

3) Forskolin response: 14 cycles

4) Light stimulus: 100 Hz flashes for two seconds from internal xenon flashlamp through either a 485 nm or 544 nm bandpass filter (10 nm bandwidth; BMG Labtech).

5) Light response: 35 cycles

Steps 1, 3 and 5 were set in luminescence mode, while step 4 was set in fluorescence intensity mode. Each cycle had the following settings: gain 3,200, collection time 1 second, repeated every 30 seconds. For each time point, wells were imaged sequentially.

Data was exported from MARS data analysis software (BMG Labtech) to Excel. Data for each well was normalised to the first value of the 'Light response' phase of the protocol. Data from the four wells in each plate that received the same plasmid(s) transfection were averaged.

2.3.5 Live cell calcium assays — sample preparation

Intracellular calcium concentration was assayed using either Fluo-4, AM or Rhod-2, AM (Invitrogen) fluorescent dye or a genetically encoded calcium indicator, GCaMP6f (Chen et al., 2013).

Cells were seeded into 35 mm dishes (100,000 cells) or 96-well plates (15,000) in complete DMEM and CO_2-independent medium, respectively. Transfection was performed the following day. If the genetically encoded calcium indicator was to be used, then a double transfection with opsin and GCaMP6f plasmids was performed. Two days after transfection the cells were imaged.

On the day of imaging, 18 µl of 10% Pluronic F-127 in DMSO (diluted from 20% solution; Invitrogen) and 72 µl of 270 mM probenecid (Invitrogen) solution in HBSS (Gibco) were added to 50 µg of fluorescent dye. The dye solution was wrapped in metal foil and left at room temperature for at least 15 minutes.

Under dim red light, transfected cells were loaded with fluorescent calcium indicator dye (final concentration 5 µM) and 9-*cis* retinal (20 µM) and left to incubate at 37 °C for 40 to 50 minutes while wrapped in foil. Cells were washed with complete DMEM or CO_2-independent medium with probenecid (1.25 mM) for 10 minutes before imaging and subsequently kept at room temperature.

For cells transfected with GCaMP6f, 9-*cis* retinal was added to a final concentration of 20 µM when the effect of exogenous chromophore was being tested. Plates were left at room temperature in foil for at least ten minutes before placing in a plate reader. All plate preparation was conducted under dim red light.

2.3.6 Plate reader quantification of live cell calcium indicators

To quantify cell calcium, the 96-well plate was placed in the plate reader and left for 5 minutes. The plate reader internal temperature was monitored, but not controlled (typically 25 – 27 °C). A fluorescence optic was used with three spacers below it. Using a computer running Omega software a script was written to automate the following protocol:

1) Wells in odd numbered columns: 200 flashes (100 Hz) for 122 recordings (two minutes); 485 nm excitation filter, 520 nm emission filter.

2) Wells in even numbered columns: as above.

Each well was imaged for two minutes before the next well was imaged. Data was exported from MARS data analysis software to Excel. Data for each well was

normalised to the first value from that well. Data from the four wells in each plate that received the same plasmid(s) transfection were averaged (technical replicates).

2.3.7 Microscope imaging of live cell calcium indicators

Light from a xenon arc lamp (Cairn Research, Faversham, UK) was passed through a monochomator (Cairn Research) to an inverted microscope rig (Olympus, Tokyo, Japan) where it stimulated opsins and the fluorescent dyes (535 – 565 nm excitation bandwidth for Rhod-2, AM).

A suitable area of cells was selected by viewing under infrared light. An infrared image was captured before a series of images were taken under direct illumination. The chimeric opsin-transfected cells were imaged every two seconds for 20 seconds, followed by every five seconds for 40 seconds. Fusion protein-transfected cells were imaged every two seconds for two minutes. Two or three areas per dish were imaged (technical replicates).

2.3.8 Image analysis of microscope imaging of live cell calcium imaging

Calcium response and infrared images were imported into ImageJ (Schneider et al., 2012). Using the freehand draw tool, cells that responded to the light impulse were circumscribed. A cell was deemed responsive if its peak fluorescence was greater than 5% above the starting fluorescence (F_o) and within the first minute the fluorescence signal began to decrease. Using the Time Series Analyzer plugin (UCLA, Los Angeles, CA) the average pixel value at each time point was extracted and copied into Excel. The total number of cells in the image was counted to calculate the response rate (number of responsive cells/total cell number).

2.3.9 Adeno-associated virus production

Recombinant adeno-associated virus (AAV) was produced by a triple transfection of 293T cells followed by iodixanol purification, buffer exchange and concentration.

All steps that involved exposing cells or AAV-containing solutions to the open air were conducted in a laminar flow cabinet to minimise the risk of infection and contamination.

2.3.9.a Cell culture

293T cells were grown to approximately 80% confluency in a T175 flask (Greiner Bio-One, Kremsmünster, Austria) before being resuspended, trypsinised, centrifuged and resuspended in DMEM (§2.3.1). Cell density was determined using a hemocytometer (Hausser Scientific, Horsham, PA). Approximately 35 million 293T cells were seeded into a hyperflask (Sigma-Aldrich) filled with complete DMEM. Two hyperflasks were seeded for each AAV preparation. Hyperflasks were incubated at 37 °C in a 5% CO_2 humidified environment for two to three days, until cells were 60 – 80% confluent.

2.3.9.b Triple transfection of 293T cells

Cells were triple transfected with a total of 500 µg of DNA per hyperflask using polyethylenimine (PEI; Polysciences, Warrington, PA) transfection agent. The three plasmids mixed in a 1:1:1 molar ratio were a helper plasmid (pAdΔF6) containing essential adenovirus helper genes required for AAV production (Xiao et al., 1998), a *rep-cap* plasmid containing the AAV replication and capsid encoding genes, and an expression cassette plasmid with AAV2 ITRs. (The ITRs are the only components of the AAV genome that must be provided in cis, while the *rep* and *cap* genes can be provided in trans.)

The three plasmids were mixed in a 50 ml conical centrifuge tube and the volume made up to 10 ml with 150 mM sodium chloride (NaCl). In a separate 50 ml tube, 1.125 ml of 1 mg/ml PEI (pH 7.0) was made up to 10 ml with 150 mM NaCl. Drop by drop, the PEI mixture was added to the plasmid mixture using a P1000 pipette. Every 2 ml the solution was swirled. The complete mixture was incubated at room temperature for approximately 20 minutes.

Transfection mixture was poured into a 500 ml bottle of DMEM made up with 2% fetal bovine serum, 2 mM L-glutamine, 100 units/ml penicillin and 100 µg/ml streptomycin. This media was used to replace the hyperflask media. The hyperflask was returned to a 37 °C, 5% CO_2 incubator for three days.

2.3.9.c Harvesting of transfected 293T cells

When the transfected cells were confluent, approximately 200 ml of media was poured out of the hyperflask (see §2.3.10 for modified protocol utilising media). The hyperflask was vigorously shaken to detach the cells. The hyperflask was emptied into a sterile 500 ml bottle (Nalgene PPCO centrifuge bottle, Thermo Scientific) and centrifuged at 180 g for 10 minutes at 20 °C (Heraeus Megafuge 16R, Thermo Scientific). Most of the supernatant was poured off, leaving a poorly defined cell pellet and approximately 30 ml of media, which was transferred to a 50 ml conical centrifuge tube. Centrifuging this at 180 g for 10 minutes at 20 °C produced a well-defined cell pellet. The media was poured off and the pellet resuspended in 15 ml of lysis buffer (see Appendix VIII) and 500 µl of protease inhibitor solution (one protease inhibitor cocktail tablet (F. Hoffman-La Roche, Basel, Switzerland) dissolved in 1 ml of lysis buffer). The lysed cell pellet was stored at -80 °C.

2.3.9.d Purification of AAV

Lysed cell pellet was thawed in a 37 °C water bath for 15 minutes and returned to -80 °C for at least an hour. This freeze-thaw cycle was repeated three times. After the final thaw, benzonase nuclease (Merck Millipore) was added to a final concentration of 50 U/ml and incubated in a 37 °C water bath for 45 minutes, mixing every 15 minutes. Centrifugation at 3,700 g for 20 minutes at 20 °C enabled separation of AAV-containing supernatant from the pellet of cell debris.

Iodixanol gradients were made in ultracentrifuge tubes (Optiseal, Beckman Coulter, Brea, CA) by layering 15%, 25%, 40% and lastly 60% iodixanol fractions below one

another. The components of each iodixanol fraction are listed in Figure 2.1 A. Firstly, 7.2 ml of 15% iodixanol fraction was pipetted into an ultracentrifuge tube. Secondly, 4.8 ml of 25% iodixanol fraction was pipetted into a 15 ml conical centrifuge tube. Using a UV-sterilised 3.5 ml transfer pipette (Sarstedt) approximately half of the 4.8 ml was aspirated, the tip positioned at the bottom of the ultracentrifuge tube, below the 15% iodixanol mixture, and slowly ejected. Taking care not to disturb the layers, the transfer pipette was slowly removed from the tube and filled with the remaining volume of 25% iodixanol fraction. The tip was returned to the bottom of the ultracentrifuge tube and the remaining volume was carefully ejected. This process was repeated to place 4 ml of 40% iodixanol and 4 ml of 60% iodixanol fraction at the bottom of the ultracentrifuge tube. See Figure 2.1 B for the final appearance of an iodixanol gradient.

Using a transfer pipette the AAV-containing supernatant was transferred to the top of an iodixanol gradient, filling the ultracentrifuge tube entirely. The tube cap was inserted so as to ensure there was no air in the tube. Three iodixanol gradients were required for each AAV preparation. Full ultracentrifuge tubes were carefully transferred into an ultracentrifuge rotor (Type 70Ti, Beckman Coulter) and spun at 358,300 g for 90 minutes at 20 °C (Optima XE-90 Ultracentrifuge, Beckman Coulter). Acceleration and deceleration were set to maximum.

Ultracentrifuge tubes were carefully removed from the rotor and the cap removed. Using an 18 G needle (BD Microlance 3, Becton, Dickinson and Company) attached to a 10 ml syringe (BD Plastipak, Becton, Dickinson and Company) the ultracentrifuge tube was punctured at the junction of the 40% and 60% fractions (Figure 2.1 B). With the bevel up the AAV-containing 40% fraction was slowly aspirated. Care was taken to minimise the amount of 25% and 60% fraction that was aspirated. Aspirated 40% fraction from all gradients containing the same AAV preparation were ejected into a 50 ml conical centrifuge tube and stored at 4 °C overnight.

2.3.9.e Buffer exchange and concentration of AAV

In the final stage of the AAV production protocol, iodixanol was replaced with a saline buffer and AAV was concentrated by reducing the final volume. AAV loss was minimised by use of a centrifuge tube containing a removable cellulose filter that binds proteins with a molecular weight greater than 100 kDa (Amicon Ultra-15, Merck Millipore). First, the filter was washed by adding 5 ml of saline (PBS or BSS with 0.001% Pluronic F-68 (PF68; Gibco)) and centrifuging at 3,000 g for 15 minutes at 20 °C. The AAV-containing iodixanol was thoroughly mixed with 5 ml of saline and transferred to the washed filter. Centrifuging at 3,000 g at 20 °C continued until the volume was reduced to approximately 1 ml. A further 15 ml of saline was mixed with the residual volume and centrifuged at 3,000 g at 20 °C until the volume was again reduced to approximately 1 ml. The addition of 15 ml of saline was repeated twice more. For the final centrifuge step the volume was reduced to 250 – 500 µl to concentrate AAV particles in a small volume. Using a P200 pipette the filter was washed by passing the remaining AAV solution over the filter at least 20 times. Concentrated AAV was aliquoted in 10 and 20 µl volumes into 500 µl nuclease-free tubes. The filter was then washed another 20 times with 500 µl of fresh saline and 50 and 100 µl aliquots were made of 'wash AAV'. Aliquots were stored at -80 °C. When necessary, AAV solutions were diluted using the same saline used for purification.

AAV titre was determined by qPCR (§2.1.16) and capsid proteins were visualised by SDS-PAGE (§2.1.23).

2.3.10 Poly(ethylene glycol) precipitation of AAV

In a modification of the AAV production protocol, all media (excluding the cell pellet) from a hyperflask was combined with poly(ethylene glycol) (PEG; Sigma-Aldrich) to precipitate AAV and allow the collection of AAV that was otherwise discarded.

Instead of being discarded, media that was initially removed from a hyperflask and supernatant from cell pelleting centrifugation steps was set-aside in centrifuge bottles. A volume of 0.22 µm-filtered (Merck Millipore) 40% PEG (w/v in 2.5 M NaCl) was added to have a final concentration of 8% PEG (w/v). After mixing thoroughly, the bottles were covered in wet ice for at least two hours to allow precipitation to occur.

To pellet the precipitate, bottles were centrifuged at 2,500 g for 30 minutes at 4 °C. After discarding most of the supernatant the pellet was washed off the sides of the bottle and transferred to a 50 ml conical centrifuge tube. To create a well-formed pellet, PEG-precipitate was again centrifuged at 2,500 g for 30 minutes at 4 °C. All the supernatant was poured off and the pellet was resuspended with 10 ml of lysis buffer and 333 µl of protease inhibitor solution. The PEG-precipitated AAV in lysis buffer was stored at -80 °C.

Instead of undergoing multiple freeze-thaw cycles (§2.3.9.d), prior to the addition of benzonase, the tube containing PEG-precipitated AAV in lysis buffer was placed in a rotating drum inside a 37 °C hybridisation incubator (Techne, Stone, UK) for at least two hours to solubilise the AAV particles. Following the addition of benzonase the PEG-precipitated AAV solution was treated identically to the cell pellet AAV solution (§2.3.9.d).

2.3.11 Secondary concentration of AAV solutions

The concentration of AAV from the protocol described was suboptimal for *in vivo* use from preparations of CAG-*OPN4* and CAG-*OPN4*-*GNA11* (both packaged in AAV2/2(7m8)). Concentrated and wash AAV aliquots were therefore combined and concentrated further to increase AAV titre.

Aliquots that had been stored at -80 °C were thawed on ice. A 2 ml cellulose filter (Amicon Ultra-2, Merck Millipore) was pre-rinsed with 2 ml of 0.22 µm filter-sterilised

0.001% PF68 in BSS by centrifuging at 3,000 g for two minutes. The membrane was covered with 0.001% PF68 in BSS and the filter unit filled with AAV solution. Centrifugation at 3,000 g for two minutes reduced the volume to approximately 50 µl. If necessary, the filter unit was filled with any remaining AAV solution and the centrifugation repeated. The aliquot tubes that were filled with AAV solution were rinsed with fresh 0.001% PF68 in BSS and this was loaded into the filter unit for a final centrifugation. As per the manufacturer's instructions, once the final volume reduced to 30 – 50 µl the filter unit was inverted and centrifuged at 1,000 g for two minutes to recover the concentrated solution. The solution was transferred to a UV-sterilised injection tube and stored at -80 °C.

2.3.12 Macaque retinal explants

Rhesus macaque (*Macaca mullata*) eyes were obtained from the MRC Centre for Macaques (Porton Down, UK). Tissue was collected post-mortem from male and female macaques ranging in age from five to 19 years old (mean: 14.8 years old) undergoing planned euthanasia. After sedation with 10 mg/kg intramuscular ketamine and a lethal overdose of 200 – 300 mg/kg intravenous pentobarbitone (carried out by staff at the MRC Centre), the eyes were immediately enucleated. In a dish of complete neurobasal A (see below) the cornea and lens were removed and radial incisions made to flatten the retina (Figure 2.2 A). A 3 mm diameter biopsy tool was used to take discs of neuroretina from the fovea and from around the vascular arcades (referred to as peripheral samples; Figure 2.2 B). Using a transfer pipette (Sarstedt) each retinal disc explant was transferred to a tube containing chilled complete neurobasal A, which was stored in a cooled polystyrene box for transport to the laboratory (a period of 2 – 6 hours).

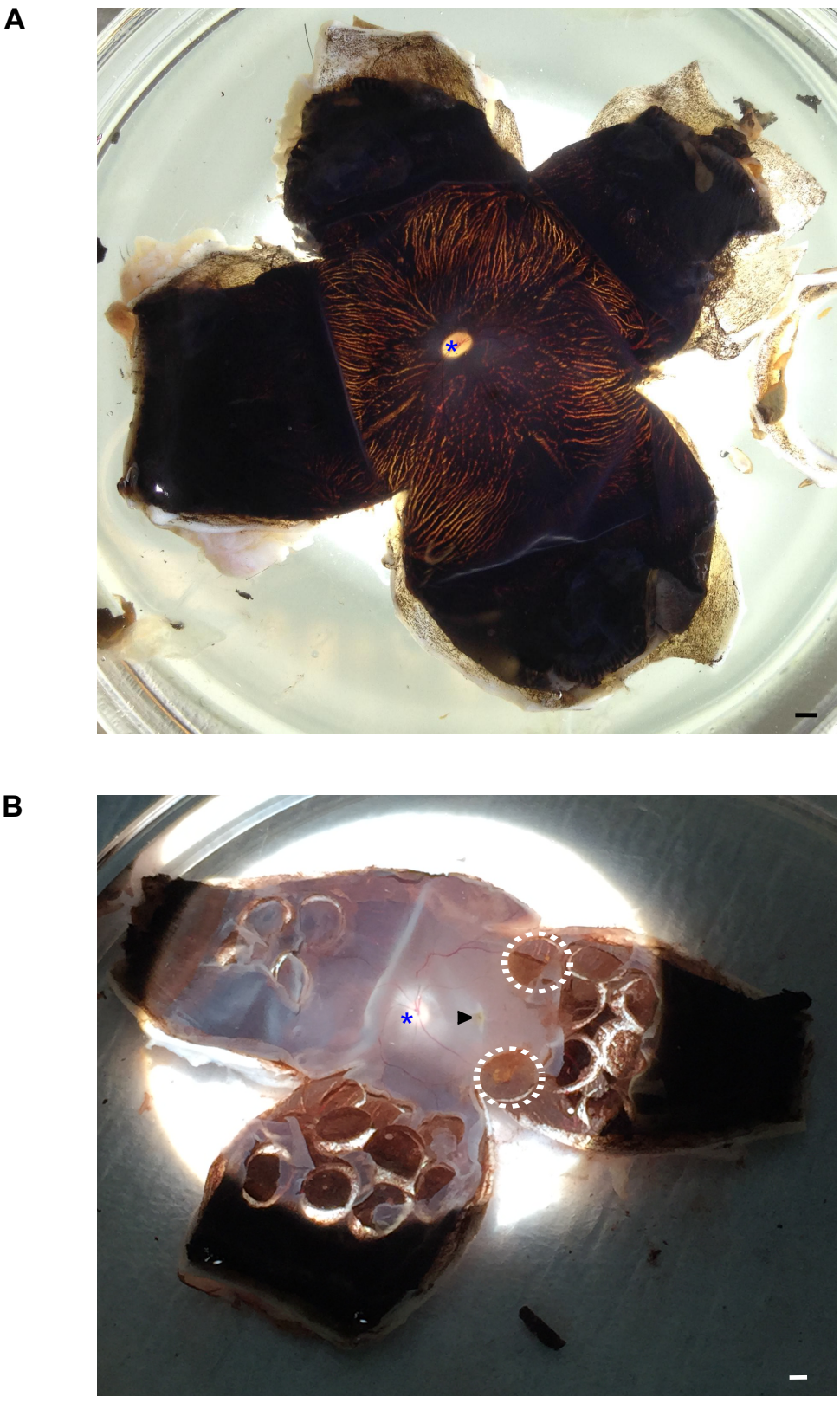


Figure 2.2. Creation of macaque retinal explants
(**A**) The retina of each macaque eye was flattened by radial cuts centred around the optic nerve head (*). (**B**) Using a 3 mm diameter biopsy tool discs of neuroretina were taken from around the vascular arcades (dashed circles; referred to as peripheral retina) and centred on the fovea (arrowhead). Retinal explants were cultured *ex vivo* in the presence of AAV vectors and their transduction patterns examined. Scale bar represents approximately 1 mm.

In the laboratory a transfer pipette was used to place each retinal disc into a tissue culture insert (0.4 µm pore size, VWR International) placed in a well of a 24-well plate. 500 µl of complete neurobasal A was placed in each well below the insert and 200 µl placed in the insert. Explants were cultured at 34 °C, 5% CO_2.

Complete neurobasal A was made of penicillin (final concentration: 100 units/ml), streptomycin (100 µg/ml; Sigma-Aldrich), L-glutamine (800 µM; Sigma-Aldrich), B-27 supplement (2%; Gibco) and N-2 supplement (1%; Gibco) in neurobasal A (Gibco).

2.3.13 Human retinal explants

Human retina samples were obtained from consented patients who underwent retinectomy for retinal detachment at the Oxford Eye Hospital. Patients were aged 39, 60 and 83 years old. Depending on the surgical requirements the retinectomy was performed by the vitreoretinal surgeons with ophthalmic surgical scissors or with a 20 G or 23 G vitrector. Samples were removed from the eye using a backflush flute needle and ejected into a sterile sample bottle containing balanced salt solution (BSS).

As soon as possible, samples were brought to the laboratory where a transfer pipette and/or a pipette tip was used to place each retinal fragment into a tissue culture insert (0.4 µm pore size) placed in a well of a 24-well plate. 400 µl of complete neurobasal A was placed in each well below the insert and 300 µl placed in the insert. Explants were cultured at 34 °C, 5% CO_2.

2.3.14 AAV transduction of primate retinal explants

Approximately 24 hours after retina explant cultures began, AAV was applied. The media below the insert was replaced with 400 µl of complete neurobasal A and the media above the insert was removed and a volume of complete neurobasal A was applied such that when the volume of AAV solution was applied the total volume was

200 µl. A volume of AAV containing 10^{10} vg was applied. Explants were incubated at 34 °C, 5% CO_2. Media below the insert was replaced every two days.

2.3.15 AAV transduction of cell lines

Approximately 24 hours after plating 10,000 293T cells in wells of a 96-well plate (Sarstedt) the complete DMEM media was replaced with 200 µl of fresh media per well. AAV was pipetted into the well and mixed by gentle horizontal shaking. Typically, 1 µl of concentrated or 5 µl of wash AAV solution was applied per well. The plate was incubated at 37 °C, 5% CO_2 for up to seven days.

2.3.16 Retina dissociation

A papain dissociation system (Worthington Biochemical Corporation, Lakewood, NJ) was used to dissociate mouse retinas for FACS. Component solutions were made up as per the manufacturer's instructions. A fresh papain solution was made for each day on which FACS occurred. After making up 5.25 ml of papain solution of approximately 20 units/ml papain and 0.005% DNase, 250 µl of papain solution was aliquoted into microcentrifuge tubes and placed on ice.

Dissection steps were completed on a lab bench that had been cleaned with RNaseZap wipes (Ambion) according to the manufacturer's instructions and with forceps cleaned with DNAZap PCR DNA degradation solutions (Ambion) according to the manufacturer's instructions. Between mice instruments were cleaned with DNAZap PCR DNA degradation solutions.

Tg(Pcp2-cre)756Mro; Gt(ROSA)26Sor$^{tm1(EYFP)Cos}$; *Pde6b*$^{rd1/rd1}$ (*L7*-Cre EYFP *rd1*) and Tg(Pcp2-cre)756Mro; Gt(ROSA)26Sor$^{tm1(EYFP)Cos}$; *Pde6b*$^{+/+}$ (*L7*-Cre EYFP, non-degenerate) mice aged 89 to 91 days that had been on a 12:12 light:dark cycle were killed by cervical dislocation at five to six hours into their light phase and their eyes promptly removed with forceps. In 0.22 µm-filtered PBS the retinas were dissected as

completely as possible, with minimal attached retinal pigment epithelium and placed in papain solution. Both retinas from each mouse were placed in a single tube and promptly placed in a 37 °C water bath for a 40-minute incubation. Approximately every ten minutes the tube was flicked to encourage the break-up of tissue. Tubes were transferred to a laminar flow cabinet where the samples were triturated 12 times each with a 5 ml pipette, a P1000 pipette and a P200 pipette.

Tubes were centrifuged at 300 g for five minutes at room temperature. Supernatant was discarded and cells resuspended in 315 µl of DNase/albumin-inhibitor solution made with ratios according to the manufacturer's instructions. In a fresh microcentrifuge tube 500 µl of albumin-inhibitor solution was added before the complete volume of resuspended cell solution was carefully layered on the top. Samples were centrifuged at 70 g for six minutes at room temperature. Supernatant was discarded and cells were resuspended in 1 ml of cell dissociation Hank's balanced salt solution (HBSS; Gibco).

2.3.17 Fluorescence-activated cell sorting

A MoFlo Legacy (Beckman Coulter) FACS with a 70 µm nozzle was utilised to isolate YFP-positive cells. Dissociated retinas were transported on ice to the FACS facility at the Jenner Institute (Old Road Campus Research Building, University of Oxford). The time between completing the dissociation protocol and starting FACS was typically 45 minutes. If clumps were seen, then the sample was passed through a 35 µm cell filter (BD Falcon). Before each sample the system was flushed with 100% industrial methylated spirits (Fisher Scientific, Waltham, MA) and PBS containing a 50 units/ml RiboLock RNase inhibitor (Fisher Scientific).

Approximately five minutes before sorting started 1 µl of 1 mg/ml of propidium iodide (Enzo Life Sciences, Farmingdale, NY) was added to the sample (final concentration 1 µg/ml) to act as a dead cell stain.

A 488 nm laser (Sapphire 488-200, Coherent, Santa Clara, CA) set to 100 mW was used to excite EYFP and propidium iodide fluorophores. Fluorescence compensation was achieved by using compensation control samples to estimate the spectral overlap as a percentage of the signal of one fluorophore in its primary channel and subtract that value from the signal in the other channel.

Settings were optimised to exclude cell fragments (low forward and side scatter values), multiplets of cells (based on pulse width) and cells with high-compensated propidium iodide fluorescence. By passing YFP-positive and YFP-negative samples through FACS, a YFP-positive population was clearly identified. Based on compensated YFP-fluorescence, gating settings were set to isolate YFP-positive and YFP-negative cell fractions, which were sorted into separate microcentrifuge tubes. Settings were adjusted for each sample to include a similar distribution of YFP-positive cells. The event rate depended on cell density, but was kept below 3,000 events/second.

Summit software (Beckman Coulter) was used to control the MoFlo Legacy and to analyse and present FACS sort profiles, which were presented as logicle displays.

Cells were sorted into 1.5 ml microcentrifuge tubes, each containing 500 µl of RLT (lysis) buffer (Qiagen) and 5 µl of 2-mercaptoethanol (Sigma-Aldrich). Every five minutes sorting was stopped and the tubes of sorted cells were manually flicked to ensure mixing. A tube received up to 500,000 cells before a new tube was used. Once collection was complete the tube of sorted cells in lysis buffer was placed in ice and returned to the John Radcliffe Hospital laboratory for RNA extraction. The delay from first sorted cells until the start of RNA extraction was typically less than 2.5 hours.

2.4 In vivo

2.4.1 Randomisation

A third party made up and labelled AAV injection tubes in a way that de-identified the contents. Unmasking was done once experiments and analyses were complete.

2.4.2 General anaesthesia

Mice were anaesthetised using 80 µg/g of body mass of ketamine (Vetalar, Zoetis, Florham Park, NJ) and 10 µg/g xylazine (Rompun, Bayer AG, Leverkusen, Germany) administered via intraperitoneal injection using a 1 ml insulin syringe and 29 G needle (Terumo, Tokyo, Japan). Ketamine and xylazine were mixed together with the appropriate volume of sterile water.

Anaesthestic reversal was achieved by intraperitoneal injection of 2 µg/g of body mass of atipamezole (Antisedan, Orion Corporation, Espoo, Finland), made up with sterile water.

2.4.3 Intraocular injections

After the induction of general anaesthesia, 1% (w/v) tropicamide and 2.5% (w/v) phenylephrine (Bausch & Lomb, Bridgewater, NJ) were applied to dilate the pupils. Once adequate depth of anaesthesia had been achieved and the pupils dilated, carbomer gel (Viscotears; Alcon, Hünenberg, Switzerland) was applied to both eyes and a 6 mm diameter cover glass (VWR International) placed on the gel to enable visualisation of the fundus.

AAV solution was thawed on ice and transferred to a plastic injection tube. The solution was diluted to the appropriate concentration with saline, when necessary. Using a 5 µl syringe (65 RN, Hamilton Company, Reno, NV) and a 34 G, 10 mm long, point style 2 needle (Hamilton Company), 1 – 1.5 µl of AAV solution was aspirated with a 0.5 µl air

bubble between the solution and the distal tip of the plunger. The air bubble aided visualisation of the injection site.

If a subretinal injection was to be performed, a 1 ml insulin syringe with a 29 G needle was used to create a small, full-thickness corneal wound — a so-called anterior chamber tap. This reduced ocular pressure to aid globe manipulation and intraocular injection. The eye was held in position by grasping the superior rectus muscle with forceps. Under the visualisation of an operating microscope (Leica Microsystems, Wetzlar, Germany) the needle was advanced through the sclera, choroid and retinal pigment epithelium, into the subretinal space. The injection site was posterior to the equator and typically superotemporal in the left eye and superonasal in the right eye. When the needle tip was visualised as being subretinal the AAV solution was injected. The appearance of air bubbles under the retina confirmed a subretinal injection.

The procedure for an intravitreal injection was simpler as it did not include an anterior chamber tap. Stabilising the eye by grasping the superior rectus with forceps, the needle was passed through the sclera, choroid and retina and into the vitreous chamber, where the solution was injected. Seeing an air bubble against the posterior surface of the lens confirmed the injection was intravitreal. The rise in intraocular pressure caused by the injection typically caused the cornea to become opaque. The needle was left *in situ* for at least 30 seconds to allow the opacity to lessen.

All injection wounds were allowed to self-seal. Following intraocular injection, drops of 0.5% (w/v) chloramphenicol and 0.5% (w/v) proxymetacaine hydrochloride (Bausch & Lomb) were applied to both eyes. Mice were placed in a chamber warmed to approximately 35 °C for the duration of their recovery from anaesthesia. Mice were monitored for signs of ocular or systemic health issues in the hours and days after an injection.

Between injections with the same AAV solution the needle and syringe were flushed at least ten times with sterile saline solution. Between different AAV solutions the needles and syringe was flushed at least 20 times.

2.4.4 Scanning laser ophthalmoscopy

Scanning laser ophthalmoscopy was performed as an *in vivo* method to visualise the distribution and intensity of GFP expression. Mice were imaged using a Spectralis HRA (Heidelberg Engineering, Heidelberg, Germany) with general anaesthesia.

Pupillary dilation was achieved by the application of a 1:1 mixture of 1% (w/v) tropicamide and 2.5% (w/v) phenylephrine (Bausch & Lomb, Bridgewater, NJ) at least five minutes prior to imaging. A drop of hypromellose BPC 0.3% (w/v) (Martindale Pharma, Romford, UK) followed by a custom-made contact lens was applied to each cornea to prevent dehydration and cataract formation (Issa et al., 2012).

When images were to be compared between animals a set protocol was followed to minimise systematic error. In near-infrared (NIR) mode (820 nm laser) with a 55° lens, the focal plane was adjusted to the layer of maximum reflectance and an image acquired. Changing to autofluorescence mode (488 nm excitation laser, 500 – 700 nm emission detection) a series of images were acquired at sensitivity settings 40, 50, 60, 70, 80 and 90. The automated real time feature, without normalisation, was used to improve image quality. In NIR mode the focal plane was moved to the inner retina to acquire images of the ganglion cell layer in NIR and autofluorescence modes. Images of other areas of interest were acquired, but not using standardised settings.

2.4.5 Quantification of SLO images

Images were exported from Eye Explorer software (Heidelberg Engineering) as 1,536 × 1,536 pixel TIFF images. Images acquired at a sensitivity setting of 70 were compared. Using ImageJ the images were converted to 8-bit. A circular region of interest outlining

the whole 55° field of view was overlaid on each image. A minimum pixel value threshold was set to 30. This value was chosen as it included all areas that were subjectively judged to be transduced. The minimum threshold value was kept constant across all images. The measure function was used to calculate the percentage of the area within the region of interest that was above the threshold and the mean pixel value of the area above the threshold. These data were copied into Excel for analysis.

2.4.6 Pupillometry

Mice were dark-adapted in a custom-made light-tight chamber for at least one hour. During the dark adaptation period, under dim red light, 1% (w/v) tropicamide was applied to the left eye and wiped away to ensure the right eye was not pharmacologically dilated. Pupillometry recordings were undertaken during zeitgeber time four to eight (i.e. starting from four hours after lights on).

Under dim red light the mouse was scruffed and its left eye placed at the opening of a Ganzfeld dome (Pro-Lite Technology, Cranfield, UK). The head was position to ensure that the right eye was adequately illuminated by an infrared LED (850 nm, 10 nm half-bandwidth) and was in focus for the camera (BRSL, Newbury, UK). Custom-programmed software recorded the right eye for two seconds prior to the light pulse, opened the shutter for two seconds and continued to record images at approximately five frames per second for a further 20 seconds after the shutter closed. Full-spectrum light from a xenon arc light source (L.O.T. Oriel, Darmstadt, Germany) was passed through a neutral density filter (log 1 – 4 units, L.O.T. Oriel) and a light guide before entering the Ganzfeld dome. Monochromatic filters were not used. Irradiance was measured at the opening of the Ganzfeld dome with a radiometrically-calibrated spectrometer (Ocean Optics, Dunedin, FL).

Each mouse was imaged twice on a given day with the same light intensity. At the time of imaging the investigator was masked to the treatment, but not masked to mice that had not received an intraocular injection. Images were imported into ImageJ for analysis. The technical replicate that had the greater constrict was selected for analysis.

Pupil area was manually measured at baseline (0 – 2 seconds), the end of the light pulse (4 seconds), and six further time points (6, 8, 10, 14, 18 and 22 seconds) using the elliptical tool. These data were copied into Excel. Pupil area at the four second time point (end of light pulse) at the four different light intensities were inputted to a custom-programmed Excel template that adjusted the slope and EC_{50} values of an irradiance response fitted curve to minimise the sum of the squared residuals. The EC_{50} output from this process was used to calculate the average light intensity required for half maximal response (EC_{50}) for each treatment group.

2.4.7 Optomotor response

As a reflexive test of pattern vision, the optomotor response was conducted. A custom-made rotating drum apparatus was used to provide a rotating visual stimulus. A plastic cylinder 55 cm tall and 30 cm in diameter rotated at two revolutions per minute, a speed established as effective by other groups (Abdeljalil et al., 2005; Busskamp et al., 2010). The cylinder was lined by a cardboard sheet, covered with 100% contrast black and white vertical stripes that subtended 0.1 cycles/degree when viewed from the platform on which the mouse was placed. This spatial frequency has been shown to be an effective stimulus for recording the optomotor response and optokinetic nystagmus in normal mice (Abdeljalil et al., 2005; Cahill and Nathans, 2008; van Alphen et al., 2009) and optogenetically treated mice (Busskamp et al., 2010; van Wyk et al., 2015). The platform was 20 cm above the base. A webcam (Logitech, Romanel-sur-Morges, Switzerland) connected to a computer was placed in the centre of the drum,

approximately ten centimetres above the top edge of the drum. Videos were recorded using the webcam's software. Custom software was used to control the direction and speed of the drum's rotation.

Mice under a 12:12 light:dark cycle were tested between 4 and 12 hours into their light cycle. Each mouse was placed on the platform under ambient room lighting (approximately 20 – 30 lux at the platform). After being left for two minutes to habituate to the platform the cylinder rotation programme began. The cylinder was programmed to alternate between rotating clockwise and anti-clockwise rotation in 30-second intervals for a total of two minutes. At the completion of the first test period a fluorescent white light placed approximately five centimetres above the top edge of the drum was switched on to increase the brightness to approximately 400 – 500 lux at the platform. With the overhead light on, the same two-minute protocol with clockwise and anti-clockwise rotation alternating in 30-second intervals was repeated. By testing the mice at two light levels it was hoped there would be a greater chance of detecting reflexive head turns.

The investigator manually scored recorded videos. A head turn was scored if the mouse's head rotated smoothly in sync with the speed and direction of the drum for at least 20 degrees before moving in the opposite direction. At the time of testing and analysis the investigator was masked to the treatment that each mouse had received, but not masked to which were the no-injection control mice.

2.4.8 Fos induction protocol

Mice that had been on a 12 hours light, 12 hours dark cycle were transferred under dim red light from their home cages to open top cages in light-tight chambers approximately one hour into their dark period.

At zeitgeber time 16 (four hours in to the dark phase) light-pulse mice were exposed to approximately 400 lux of white light for 30 minutes. No-light-pulse mice were handled identically, but were not exposed to a light pulse. Thirty minutes after the end of the light pulse the mice were sacrificed by cervical dislocation under dim red light and their eyes fixed with 4% formaldehyde. Eyes were treated identically for sectioning and anti-Fos immunohistochemistry protocols (§2.5.5).

Using standardised acquisition settings confocal images were obtained (Carl Zeiss, Oberkochen, Germany). Confocal images were imported to ImageJ where a maximum image projection was created from each Z stack. A minimum pixel value threshold was set to just above the background fluorescence level. Using the 'Measure' tool the area above the threshold was determined for each image. At least three images were obtained from each eye (technical replicates) and averaged to compare between different animals (biological replicates).

2.5 Tissue

2.5.1 Fixation of retinal explants

Seven days after AAV was applied, explants were fixed. Using a transfer pipette explants were washed in PBS and then fixed in 4% formaldehyde (Thermo Fisher Scientific) in PBS for two hours at room temperature. Following another wash in PBS, explants were placed in 30% sucrose (w/v in PBS; Sigma-Aldrich) and stored at 4 °C.

2.5.2 Immunocytochemistry

Cultured cells were washed with PBS prior to fixation with 4% formaldehyde for ten minutes. Cells were washed three times with 0.05% Tween 20 (Sigma-Aldrich) in PBS and permeabilised by covering with 0.2% Triton X-100 for five minutes. For 30 minutes cells were incubated at room temperature in 5% donkey serum (Sigma-Aldrich) with 0.05% Tween 20 in PBS. Primary antibodies (Table 2.1) were diluted in 1%

Primary antibodies

Staining	Immunogen	Host species	Source (product code)	Clonality	Dilution
Brn3a	Epitope mapping near the N-terminus of Brn3a of human origin	Goat	Santa Cruz (sc-31984)	Polyclonal	1:1,000
Calbindin	Full length native protein corresponding 28 kDa calbindin-D protein purified from rat kidney	Rabbit	Abcam (ab11426)	Polyclonal	1:5,000
Calbindin	[CB-955]. Purified bovine kidney calbindin-D-28K	Mouse	Abcam (ab82812)	Monoclonal	1:1,000
Fos	Synthetic peptide corresponding to the sequence of human c-Fos	Rabbit	Cell Signalling Technology (9F6)	Monoclonal	1:200
GAD67	[1G10.2]. Recombinant GAD67 protein	Mouse	Millipore (MAB5406)	Monoclonal	1:500
GFAP	GFAP isolated from cow spinal cord	Rabbit	Abcam (ab7779)	Polyclonal	1:1,000
GFP (and EYFP)	Recombinant full length protein	Chicken	(1) Aves (GFP-1010); (2) Abcam (ab13970)	Polyclonal	1:1,000
GlyT1	Synthetic peptide from the carboxy-terminus as predicted from the cloned rat GLYT1	Goat	Millipore (AB1770)	Polyclonal	1:1,000
OPN4 (human)	Amino acids 379 – 478 mapping to the C-terminus of melanopsin of human origin (H-300)	Rabbit	Santa Cruz (sc-32870)	Polyclonal	1:250
OPN4 (mouse)	Amino acids 1 – 15 mapping to the N-terminus of melanopsin of mouse origin (UF006)	Rabbit	Advanced Targeting Systems (AB-N38)	Polyclonal	1:2,500
PKCα	[133]. Recognises the sequence PQFVHPILQSAV at the C-terminus of PKCα	Mouse	Abcam (ab11723)	Monoclonal	1:500
PKCα	[Y124]. Synthetic peptide corresponding to residues in C-terminus of human PKCα	Rabbit	Abcam (ab32376)	Monoclonal	1:1,000
Red/green opsin	Recombinant human red/green opsin	Rabbit	Millipore (AB5405)	Polyclonal	1:1,000
Rhodopsin	Synthetic peptide corresponding to bovine rhodopsin amino acids 338 – 348	Rabbit	Abcam (ab3424)	Polyclonal	1:1,000
Rhodopsin (1D4)	C-terminal 9 amino acids of mammalian rhodopsin (TETSQVAPA)	Mouse	Gift from Dr Jill Cowing	Monoclonal	1:1,000

Secondary antibodies

Target species	Host species	Fluorophore	Source (product code)
Chicken	Donkey	Alexa Fluor 488	Jackson ImmunoResearch (703-545-155)
Goat	Donkey	Alexa Fluor 488	Invitrogen (A11055)
Goat	Donkey	Alexa Fluor 568	Invitrogen (A11057)
Goat	Donkey	Alexa Fluor 633	Invitrogen (A21082)
Mouse	Donkey	Alexa Fluor 488	Invitrogen (A21202)
Mouse	Donkey	Alexa Fluor 568	Invitrogen (A10037)
Mouse	Donkey	Alexa Fluor 647	Invitrogen (A31571)
Rabbit	Donkey	Alexa Fluor 488	Invitrogen (A21206)
Rabbit	Donkey	Alexa Fluor 555	Invitrogen (A31572)
Rabbit	Donkey	Alexa Fluor 568	Invitrogen (A10042)
Rabbit	Donkey	Alexa Fluor 647	Invitrogen (A31573)

Table 2.1. Details of primary and secondary antibodies

donkey serum with 0.05% Tween 20 in PBS and incubated at room temperature for at least one hour.

Fresh 0.05% Tween 20 in PBS was used to wash the cells five times. Secondary antibodies (Table 2.1) were diluted 1 in 200 with 1% donkey serum and 0.05% Tween 20 in PBS. Cells were incubated with secondary antibodies in the dark for at least 30 minutes at room temperature.

A final series of five washes with PBS were completed. Included in the fourth wash was the nuclear stain Hoechst 33342 (Molecular Probes, Waltham, MA), which was diluted 1 in 5,000 (final concentration: 2 µg/ml) in PBS. For storage, cells were immersed in PBS, and kept dark with metal foil at 4 °C.

2.5.3 Tissue collection

Mice were culled by cervical dislocation. Immediately following the confirmation of death the eyes were enucleated using forceps to grasp behind the eye and pull outwards. The cornea was punctured using a 29 G needle connected to a 1 ml insulin syringe (Terumo, Tokyo, Japan) and the eye immersed in 4% formaldehyde in PBS at 4 °C overnight. After 16 – 24 hours the eye was rinsed in PBS for approximately one minute before being immersed in 30% sucrose for at least the time required for it to become negatively buoyant.

2.5.4 Embedding and sectioning of eyes and explants

Tissue that had been formaldehyde fixed and immersed in 30% sucrose was briefly washed in PBS and transferred to a mould containing Optimum Cutting Temperature (OCT; Tissue Tek, Sakura Finetek, Tokyo, Japan). After five minutes the tissue was arranged into the desired position and placed on pellets of dry ice. Once the OCT had frozen the sample was stored at -80 °C.

If an eye was being embedded, the cornea and lens were removed prior to immersion in OCT. Eyes were oriented so that the equator was vertical, thus producing 'C'-shaped sections that typically included peripheral and central retina in each section.

Because retinal explants had a tendency to curl up, care was taken when embedding them. By placing a plastic mould containing an explant in OCT onto a pellet of dry ice a localised area of OCT was frozen. Visualised under a dissecting microscope (Leica Microsystems) a corner of the explant was frozen onto an area of frozen OCT. With an end fixed in place, the explant was then uncurled and the dry ice used to freeze the remainder of the OCT.

Samples were sectioned using a cryostat (LM1850, Leica Biosystems, Wetzlar, Germany). Cryostat temperature was adjusted to achieve flat sections and was typically between -20 °C and -25 °C. Sections were 20 µm thick and were applied to Polysine slides (Menzel-Gläser, Braunschweig, Germany).

Sections were left to dry at room temperature under metal foil for at least one hour before being stored at -20 °C.

2.5.5 Immunohistochemistry — sections

Slides that had been stored at -20 °C were dried at room temperature for at least one hour. Sections were circumscribed with a barrier pen (Vector Laboratories, Burlingame, CA). Tissue was permeabilised with 0.2% Triton X-100 (Sigma-Aldrich) in PBS for at least 20 minutes at room temperature. Sections were rinsed with PBS for at least one minute. Sections were blocked with 10% donkey serum in 0.2% Triton X-100 in PBS for at least one hour at room temperature. Primary antibodies were diluted (Table 2.1) in 2.5% donkey serum and 0.2% Triton X-100 in PBS. Slides were placed in a humidified box and placed at 4 °C overnight (or room temperature for at least two hours when labelling for GFP). When double or triple labelling the two or three, respectively,

primary antibodies were mixed together and applied in a single solution, unless otherwise stated.

Sections were washed by covering in 0.05% Tween 20 in PBS for at least ten minutes. This was repeated four times. Secondary antibodies were diluted 1:200 in 2.5% donkey serum and 0.2% Triton X-100 in PBS. Slides covered with secondary antibody solution were placed in a humidified dark box and incubated at room temperature for two hours. When double or triple labelling the two or three, respectively, secondary antibodies were mixed together and applied in a single solution. Care was taken to use secondary antibodies that had been cross-adsorbed against IgG immunoglobulins from other species being used for a multi-labelling experiment.

Sections again underwent four washes with 0.05% Tween 20 in PBS for at least ten minutes for each wash. One final wash was completed with water. Excess water was removed from the slide and ProLong Gold with DAPI mountant (Invitrogen) was applied to each section. A coverslip was lowered on to the sections and air bubbles displaced. Slides were placed in a dark box at room temperature overnight. After the mountant had set, the slides were stored at 4 °C.

2.5.6 Immunohistochemistry — flat mounts

Eyes that had been fixed and immersed in sucrose, as described in §2.5.3, were also used for flat mount immunohistochemistry. Visualised through a dissecting microscope the retina was removed from the eyecup and transferred to 30% sucrose in a microcentrifuge tube.

To facilitate antibody penetration, the retina was freeze-fractured using liquid nitrogen. The sample was placed in a mortar containing liquid nitrogen and left to freeze. The tube was removed and thawed at room temperature. Degenerate retinas underwent one freeze-thaw cycle, while non-degenerate retinas had two cycles.

Retinas were permeabilised by immersion in 1% Triton X-100 for ten minutes, repeated three times. Retinas were blocked by immersion in 10% donkey serum for at least two hours (typically overnight). Primary antibodies were diluted in 2.5% donkey serum and 1% Triton X-100 in PBS. Retinas were incubated in primary antibody solution for up to three days at 4 °C.

Retinas were washed with 0.2% Triton X-100 in PBS three times, with each step lasting at least 30 minutes on an orbital shaker. Secondary antibodies were diluted 1 in 200 with 2.5% donkey serum and 1% Triton X-100 in PBS and incubated in the dark overnight at 4 °C.

Retinas were washed with 0.2% Triton X-100 in PBS four times, each step lasting at least 40 minutes on an orbital shaker. During the fourth wash step Hoechst 33342, diluted 1 in 5,000 in PBS, was added. A final wash was done with water. Visualised under a dissecting microscope the retina was cleaned of debris and cuts were made to enable it to be flattened. The retina was transferred to a Polysine slide, with the ganglion cell layer facing up. The retina was dried before applying ProLong Gold mountant. A coverslip was lowered onto the retina and bubbles displaced. The slide was left in the dark at room temperature overnight for the mountant to set before being stored in the dark at 4 °C.

As with the immunohistochemistry protocol for sections, when there were multiple antibody targets in a given tissue the primary antibodies were mixed together and applied simultaneously, as were the secondary antibodies. Care was taken to use secondary antibodies that had been cross-adsorbed against IgG immunoglobulins from other species being used for a multi-labelling experiment.

2.5.7 Image acquisition

Micrograph images were acquired using an inverted epifluorescence (Leica Microsystems) or an inverted confocal (Carl Zeiss) microscope. Settings were optimised to minimise signal interference and avoid image saturation. Where quantitative or semi-quantitative comparisons between samples were to be made, the acquisition settings were kept constant.

Using ImageJ a noise filter was applied to some images and minimum and maximum pixel values of the whole image were adjusted to aid visualisation of relevant features in figures.

2.5.8 Confocal — standard image acquisition for AAV tropism studies

Slides that had undergone the slide immunohistochemistry protocol in parallel were imaged on an inverted confocal microscope under standardised conditions. Using a 40× oil immersion lens two sections from each slide were imaged. Two slides per eye were imaged, providing representative coverage across the eye. Images were acquired from areas of high fluorescence that were not at the extreme periphery of the retina, adjacent to optic nerve or at an obvious injection site. Within the section the imaging plane was set to that which gave the greatest total fluorescence, as judged subjectively. The pinhole was set to 1 Airy unit for the green channel. For image snaps that were to be compared laser power, gain, speed (7), averaging (1) and image resolution (1024 x 1024) were kept constant after being set to minimise pixel saturation.

Using ImageJ each image was manually segmented into the inner nuclear layer, inner plexiform layer and ganglion cell layer using the polygon selection tool. A threshold minimum pixel value was set and the measure tool used to calculate the percentage area and mean pixel value of each of the three regions of interest of each image. These data were copied into Excel. The mean of the percentage area and pixel value from the

multiple images of a given eye (technical replicates) was used as the value to compare between eyes of different animals (biological replicates).

2.5.9 Statistical analysis and graphing

Statistical analysis and chart preparation was completed using Prism (GraphPad, San Diego, CA).

The area under curve (AUC) function was used to calculate AUC and the time at which the peak relative fluorescence value was reached. Due to the drifting baseline in data from microscope-based calcium imaging, peaks that occurred at 40 seconds or later were excluded.

Response rates following siRNA knockdown were compared using unpaired two-tailed *t* tests. When comparing one independent variable with more than two conditions and a single dependent variable, an ordinary one-way analysis of variance (ANOVA) test was applied. When comparing two independent variables, with at least two conditions and a single dependent variable, an ordinary two-way ANOVA was used. Post hoc tests were conducted with Bonferroni's multiple comparisons tests. When available, sample groups were all compared to a single control group. When not available, all groups were compared to each other. $\alpha = 0.05$ for all tests.

As a representation of the effectiveness of each chimeric opsin at activating the $G_{q/11}$ and G_i pathways, representative values were derived (Figure 4.4 E). For the $G_{q/11}$ assay, the peak relative fluorescence value was calculated from plate reader data. For the G_i assay, the peak residual (difference between sample and GloSensor only) between 10.5- and 14.5-minute time points was calculated. Values from both assays were calculated for each biological replicate, averaged and normalised to positive controls (melanopsin for the $G_{q/11}$ assay and rhodopsin for the G_i assay).

For cell culture experiments, a technical replicate was a different area of a 35 mm dish, or a different well within a 96-well plate that had been transfected and imaged in parallel. Biological replicates were transfected and imaged on different days to each other.

Graphical data is presented as mean ± standard error of the mean (s.e.m.).

2.5.10 Network analysis of differentially expressed genes

To investigate commonalities between genes that found to be differentially expressed in a statistically significant manner in the microarray study, network analysis software was utilised. Known photoreceptor genes were excluded from the analysis. To exclude a potential bias in the selection of photoreceptor genes a Gene Ontology (GO) list was used (AmiGO 2 version 2.2.0, http://amigo.geneontology.org, accessed August 17th 2015). Using the taxon filter 'Mus musculus', a list of 173 genes annotated with 'photoreceptor cell' (CL:0000210) was generated. This list was imported to Excel and those statistically significantly differentially expressed genes that were on the GO list were removed.

The list of 60 genes that were differentially expressed but not on the GO photoreceptor list were inputted to GeneMANIA (http://genemania.org, accessed August 17th 2015) with the settings: species, 'M. musculus'; related genes, zero; related attributes, zero.

(Viral) tropism

The specificity of a virus for a particular host cell or tissue.

late 19th cent.: from Greek *tropos* **'turning'** (from *trepein* **'to turn'**) + -ism.

3

Adeno-Associated Virus Tropism for Optogenetic Gene Therapy

3.1 Introduction

The use of a highly effective vector is critical to the success of an optogenetic gene therapy strategy. The efficacy of a vector is measured by both the efficiency with which the genetic cargo is delivered and its specificity for the target cell type (its tropism). In the retina, AAV is the gene therapy vector of choice for most research groups and gene therapy companies due to its established record of safety and efficacy in preclinical studies and clinical trials (Bennett, 2003; Maguire et al., 2008; Jacobson et al., 2012; MacLaren et al., 2014). This research project therefore utilised AAV vectors.

AAV is a species of non-enveloped virus from the genus *Dependoparvovirus*, first described in 1965 from a sample of simian adenovirus (Atchison et al., 1965). Dependoviruses require co-infection with a 'helper virus' to replicate. Each AAV virion contains a single-stranded DNA genome of approximately 4.7 kb (group II, Baltimore classification) surrounded by an icosahedral capsid of 20 to 25 nm in diameter (see Figure 3.1 for a schematic; Srivastava et al. 1983; Gerry et al. 1973; Melnick et al. 1965). A capsid consists of 60 protein subunits of three capsid proteins — VP1, VP2

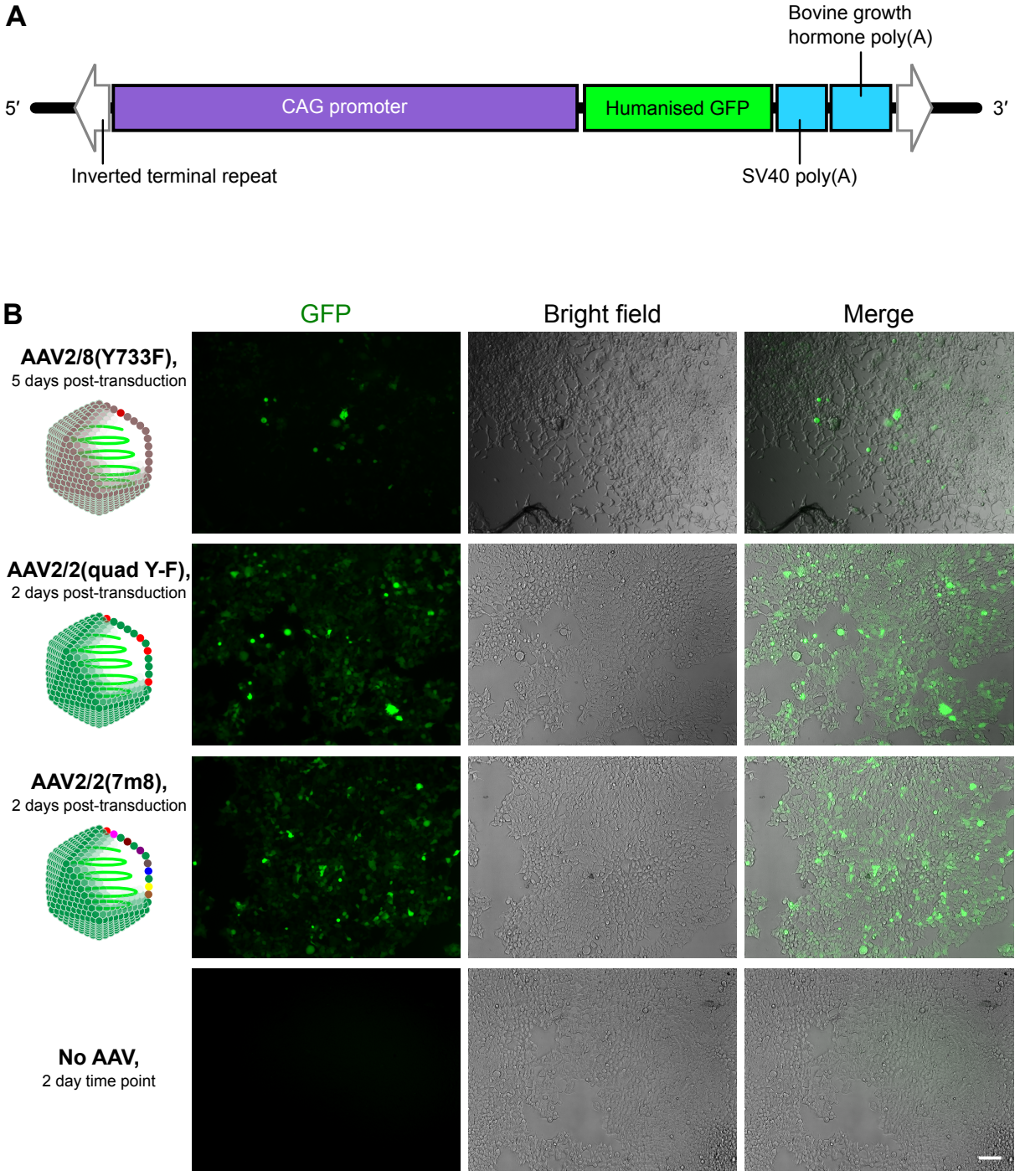


Figure 3.1. Live 293T cells transduced with three serotypes of GFP-expressing adeno-associated virus (AAV) (**A**) DNA expression cassette used to produce three serotypes of AAV-GFP. A ubiquitous CAG promoter drove GFP expression. (**B**) 293T cells were transduced with the three serotypes of AAV-GFP. Cells transduced with AAV2/8 (Y733F)-GFP showed a moderate level of GFP expression five days after the application of virus. In contrast, cells transduced with AAV2/2(quad Y-F) or AAV2/2(7m8) expressed relatively high levels of GFP by two days after virus application. Cells that had not been transduced with AAV-GFP had very low levels of green fluorescence at the two day time point. All epifluorescence images were acquired with the same acquisition settings. Scale bar represents 100 µm. Schematic of icosahedral AAV virions of three serotypes are provided (not to scale, capsid subunits are indicative only).

and VP3 in an approximate 1:1:10 ratio — that are encoded by alternative splicing of the *cap* gene (Becerra et al., 1988; Horowitz et al., 2013).

Twelve naturally occurring AAV serotypes have hitherto been documented (Schmidt et al., 2008). Each serotype has distinct biochemical properties, including cell tropism and response to circulating antibodies (Xiao et al., 1999; Rabinowitz and Samulski, 2000; Schmidt et al., 2008). Without empirical testing, it is not possible to predict the tropism characteristics of an AAV serotype once injected into the eye.

Recombinant AAV pseudotypes are created by combining genomic elements from one serotype (typically AAV2) with the capsid of another serotype. This allows a single expression cassette containing AAV2 inverted terminal repeats (ITRs) to be packaged into a variety of capsids, thereby displaying a range of tropism characteristics and avoiding any pre-existing immunity to a particular serotype (Xiao et al., 1998; Auricchio, 2003).

A greater understanding of AAV biology has led to the creation of a range of rationally designed recombinant AAV serotypes. A significant insight came from the finding that the phosphorylation of tyrosine residues of AAV2 impairs nuclear trafficking of the vector (Zhong et al., 2007). Phosphorylation is followed by capsid ubiquitination, which marks the AAV virion for proteasome-mediated degradation. By analysing the crystal structure of AAV2 (Xie et al., 2002), Zhong and colleagues (2008) identified seven surface tyrosine residues of VP3 that could be phosphorylated. Mutation of these tyrosine residues (abbreviated to ‘Y’) to phenylalanine (F) led to significant increases in transgene expression *in vitro* and *in vivo*, allowing a comparable transgene expression level to be achieved with an approximately 10-fold lower AAV dose.

Having established that single tyrosine to phenylalanine (Y-F) capsid mutations increase transduction efficiency, multiple capsid mutants were created by Petrs-Silva

and colleagues (2011) and tested by intravitreal and subretinal injection into non-degenerate mouse retinas. By mutating two to seven surface tyrosine residues the transduction efficiency was increased, tropism was extended to cell types not previously transduced and some mutants were noted to show earlier onset of transgene expression relative to wild type AAV2.

AAV8, a serotype originally isolated from rhesus monkeys (Gao et al., 2002), is effective at transducing photoreceptors and retinal pigment epithelium more efficiently than AAV2 and AAV5 (Natkunarajah et al., 2008). Building on the findings from AAV2 site-directed tyrosine to phenylalanine mutations, Petrs-Silva and colleagues (2009) created a capsid-mutant AAV8 serotype termed AAV2/8(Y733F). When delivered by intravitreal injection, AAV2/8(Y733F) transduced more cells and demonstrated significantly higher transgene expression compared to wild type AAV2/8. Subretinal injections of AAV2/8(Y733F) led to stronger and more widespread GFP signal, as detected by *in vivo* imaging, compared to wild type and mutant AAV2, AAV8 and AAV9 variants from as early as ten days post-injection.

In contrast to the targeted mutation approach, a directed evolution approach has been employed to generate AAV serotypes with novel tropism characteristics (Maheshri et al., 2006; Klimczak et al., 2009). Dalkara and colleagues (2013) used an *in vivo* directed evolution strategy to create novel AAV serotypes that are more efficient at transducing photoreceptors after being injected intravitreally. From a large (~3×10^7) library of diverse AAV variants, only those virions that were endocytosed into photoreceptors following an intravitreal injection were selected for another round of evolution. One of the variants ultimately obtained, AAV2/2(7m8), was selected for *in vivo* studies in mice and macaque and showed strong expression across the retina and in all retinal layers (Dalkara et al., 2013).

This research project aimed to build on the published studies by testing three AAV serotypes in retinally degenerate mice as well as macaque and human explants.

The three serotypes selected for this study were: AAV2/8(Y733F), AAV2/2(Y272, 444, 500, 730F) (abbreviated to 'quad Y-F') and AAV2/2(7m8) (Figure 3.1). AAV2/8(Y733F) was selected as Petrs-Silva and colleagues (2009) showed this to be the best performing of the AAV2, AAV8 and AAV9 serotypes they tested. Additionally, this was the serotype of choice for a previous *in vivo* study testing human melanopsin as an optogenetic gene therapy tool for restoring sight to retinally degenerate mice in our laboratory (Dr Samantha de Silva, manuscript in preparation).

Of the AAV2 capsid mutants, AAV2(quad Y-F) was chosen for further assessment in the degenerate mouse retina. AAV2(quad Y-F) has been found to transduce photoreceptors following intravitreal injection, but also to occasionally transduce retinal bipolar cell when injected subretinally (Petrs-Silva et al., 2011). Given the potential benefits of transducing bipolar cells for optogenetic vision restoration (see chapter seven), this was a serotype that warranted further investigation.

Finally, AAV2/2(7m8) was selected as it represented a completely different approach to AAV development and demonstrated potent transduction across the retina in non-degenerate mice and macaque retinas (Dalkara et al., 2013).

To compare the transduction profiles in a range of species, the three recombinant AAV serotypes were tested in mice, macaque and human retinas. To date, *in vivo* murine tropism studies of these AAV serotypes have been limited to non-degenerate mice (Petrs-Silva et al., 2009, 2011; Dalkara et al., 2013). The remodelling that occurs during retinal degeneration can cause changes in AAV spread and transduction efficiency (Kolstad et al., 2010). As the target tissue for optogenetic gene therapy will be degenerate retina, it is most appropriate to use a model of degenerate retinal disease to

study which AAV serotype is most suitable for optogenetic gene therapy. We therefore wanted to compare the transduction profile of three recombinant AAV serotypes in a model of retinal degeneration, the *rd1* mouse. The *rd1* mutation is a naturally occurring nonsense mutation of the rod-specific cGMP phosphodiesterase 6B (*Pde6b*) gene (Bowes et al., 1990; Pittler and Baehr, 1991). The truncation of PDE6B renders it non-functional, leading to elevated cGMP and apoptosis (Lolley et al., 1994). The result is a rapid death of rods starting in the second postnatal week and secondary loss of cones continuing for many months (Carter-Dawson et al., 1978). Photosensitive retinal ganglion cells persist and mediate non-visual functions (Foster et al., 1991; Hattar et al., 2003). Mutation of the human homolog of the same name can cause retinitis pigmentosa (McLaughlin et al., 1993; Bayes et al., 1995) and congenital stationary night blindness (Gal et al., 1994; Bayes et al., 1995). As well as facilitating testing on a diseased model, the use of a mouse model allowed a comparison of intravitreal and subretinal injection of AAV vectors.

The last common ancestor of humans and macaques (*Macaca mulatta*) dates to approximately 29.1 million years ago, while the evolutionary branch point for humans and the house mouse (*Mus musculus*) is approximately 90.9 million years ago (Hedges et al., 2015). With its greater shared ancestry, the macaque retina shares features with the human retina that the mouse retina does not have, such as a cone-rich fovea, cones that express three, rather than two, spectrally distinct opsins and a similar vasculature network (Schein, 1988; Jacobs, 1996). Given that this translational research project aims to develop knowledge towards treating humans with retinal degeneration, any information that could be gathered on the performance of the three selected AAV serotypes in primate tissue was highly valuable.

Aims

- Compare the tropism of three AAV serotypes in retinally degenerate mice and primate retina, in terms of the extent and specificity of the cell types transduced.
- Compare the relative efficacy of intravitreal and subretinal injection routes in retinally degenerate mice.

3.2 Results

3.2.1 *In vitro* testing of three serotypes of AAV-GFP

Three recombinant AAV vectors were produced, all containing humanised GFP (Zolotukhin et al., 1996) driven by a ubiquitous CAG synthetic promoter (Figure 3.1 A) to achieve strong expression in all transduced cells. The 3.23 kb single stranded sequence was packaged into three different AAV capsids: AAV2/8(Y733F), AAV2/2(quad Y-F) and AAV2/2(7m8).

As a qualitative assessment of the *in vitro* function of the AAV-GFP vectors, approximately 3×10^9 vg, 1×10^9 vg and 6×10^8 vg of AAV2/8(Y733F), AAV2/2(quad Y-F) and AAV2/2(7m8), respectively, were added to each well of 293T cells. After two days extensive GFP expression was seen in wells that had been transduced with AAV2/2(quad Y-F) or AAV2/2(7m8) (Figure 3.1 B). Despite a greater number of vector genomes being applied, GFP fluorescence from 293T cells transduced with AAV2/8(Y733F) was slower to appear and even five days after transduction the level of GFP fluorescence was notably lower than that from the other two viruses (Figure 3.1 B). Low *in vitro* transduction efficiency of AAV2/8 compared to AAV2/2 has been previously documented (Klein et al., 2006) and does not correlate with *in vivo* performance (Harding et al., 2006; Klein et al., 2008).

3.2.2 AAV tropism in a mouse model of retinal degeneration

Under general anaesthesia, each eye of female 13 to 14 week old C3H/HeN mice was injected with approximately 3×10^9 vg of one of three different serotypes of AAV-GFP. One eye received an intravitreal injection, the other a subretinal injection. Four eyes were injected for each combination of AAV serotype and delivery route.

3.2.2.a Scanning laser ophthalmoscopy *in vivo* fundus imaging

Three weeks after injection the mice were anaesthetised and underwent *in vivo* scanning laser ophthalmoscopy (SLO). SLO enabled the distribution and intensity of GFP expression in the retina to be quantified across the groups.

3.2.2.a.i Intravitreal injection

In all three groups the area around the optic disc showed the most fluorescence (Figure 3.2 A – C). In eyes injected with AAV2/2(quad Y-F) or AAV2/2(7m8) the fluorescence extended beyond the central 55° to the peripheral retina where it was strongest adjacent to blood vessels. Fluorescence was mostly speckled, with small, highly fluorescent foci.

The fluorescence signal from retinas injected intravitreally with AAV2/8(Y733F) was generally sparse and low, but in one eye a peripheral area of high fluorescence enclosing an area of absent signal was found (Figure 3.2 D). From this area, trails of fluorescence, from what are presumed to be GFP-expressing retinal ganglion cell axons, led to the optic disc. This is thought to be the injection site, the abnormal transduction pattern being due to the disturbance of tissue integrity. More widespread areas of fluorescent retinal ganglion cells were seen in other injected eyes (Figure 3.2 E).

Of those mice that received an intravitreal injection of AAV-GFP, those in the AAV2/2(7m8) group had the greatest area above a threshold of GFP intensity, with 91 ± 2.2% (mean ± s.e.m.; n = 3) of the fundus area above the threshold (Figure 3.2 F). This compares to 51 ± 17% (n = 4) for those that received AAV2/2(quad Y-F) and 3.4 ±

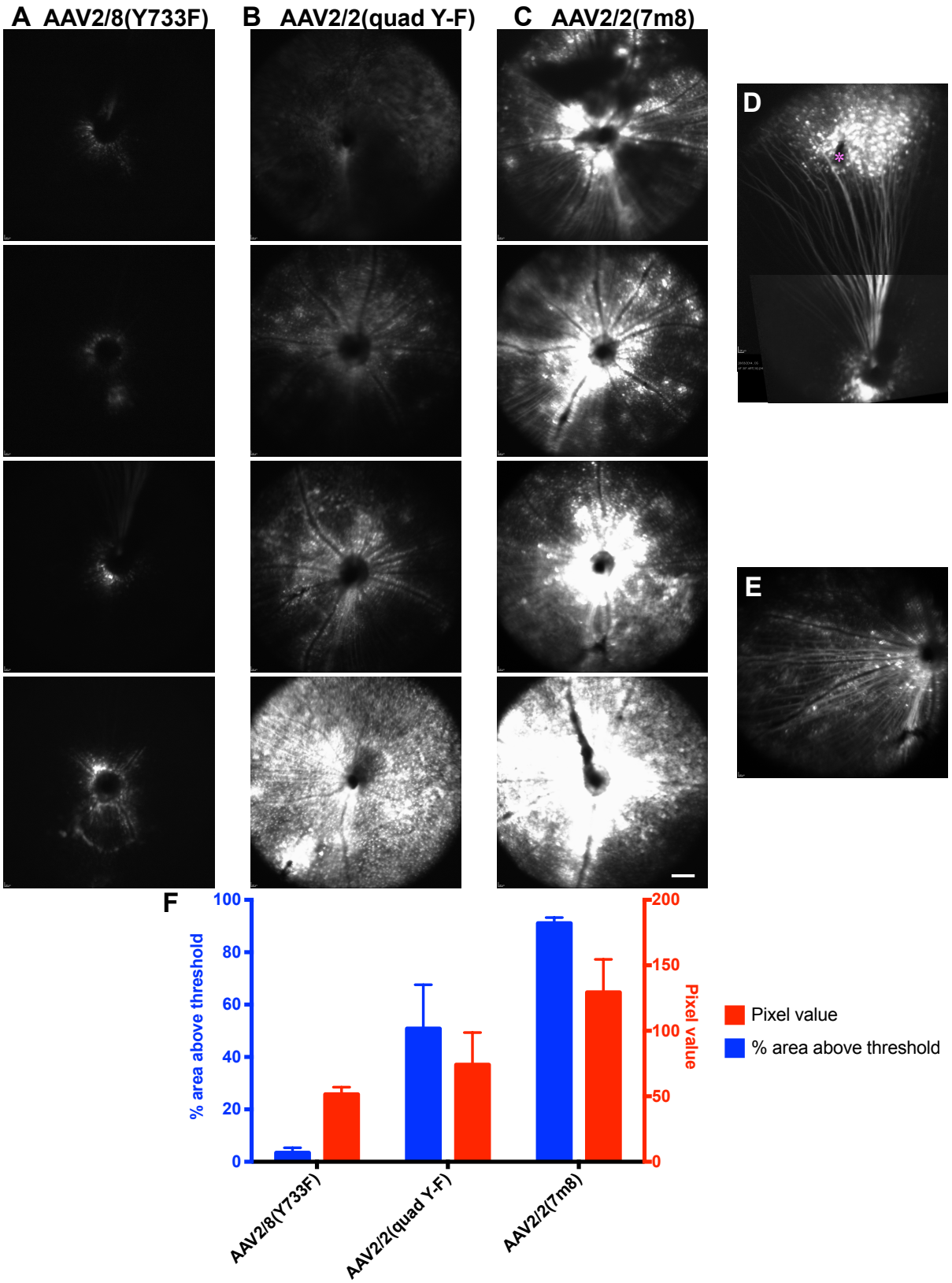


Figure 3.2. Scanning laser ophthalmoscopy of degenerate mouse retinas injected intravitreally with three GFP-expressing AAV serotypes

(**A** – **E**) Mice were injected at 13 – 14 weeks of age and assessed three weeks post-injection by SLO. Images centered on the optic disc were acquired from each of the four eyes injected with each of the following serotypes: (**A**) AAV2/8(Y733F), (**B**) AAV2/2(quad Y-F) and (**C**) AAV2/2(7m8). The same autofluorescence settings were used. (**D**) High levels of GFP fluorescence were seen around the presumed injection site (*) of an eye injected with AAV2/8 (Y733F), with retinal ganglion cell axons projecting from the injection site to the optic nerve head. (**E**) GFP-expressing ganglion cell axons were also noted in eyes injected with the other two serotypes. This example is from the AAV2/2(7m8) group. (**F**) SLO images were quantified by setting a threshold pixel value and determining the area of each image above this threshold and the intensity of the signal ('Pixel value') in the area above the threshold (mean ± s.e.m.; n = 4, AAV2/8(Y733F) and AAV2/2(quad Y-F); n = 3, AAV2/2(7m8)). Scale bar represents 1 mm.

1.9% (n = 4) for the AAV2/8(Y733F) group. Within the area that was above the threshold, retinas in the AAV2/2(7m8) group had the brightest GFP signal, with a mean pixel value of 129 ± 25, compared to 74 ± 24 for AAV2/2(quad Y-F) and 52 ± 5.4 for the AAV2/8(Y733F) group (see below for statistical comparisons).

3.2.2.a.ii Subretinal injection

The bleb created to deliver AAV vector between the neuroretina and the retinal pigment epithelium detached approximately 40% of the retina; however, the fluorescence did not appear to be limited to the boundary of the bleb. In most eyes fluorescence was seen at all angles around the optic disc (Figure 3.3 A –C).

Despite the AAV vector being delivered subretinally to this group of eyes, lines of fluorescence from the periphery to the optic disc were notable in some eyes, indicating the AAV had traversed the retina and transduced retinal ganglion cells in the innermost retinal layer (Figure 3.3 D).

The pattern of GFP expression in the subretinally injected group was notably different from the intravitreally injected group. Of those eyes that received a subretinal injection, the AAV2/8(Y733F) capsid gave the greatest area above threshold transduced: 81 ± 10% (n = 4) (Figure 3.3 F). The AAV2/2(7m8) group was slightly less with 75 ± 13% and the AAV2/2(quad Y-F) group had a mean area above threshold of 55 ± 18% (n = 4, both groups). Within the area above threshold AAV2/8(Y733F) and AAV2/2(7m8) had a similar GFP intensity signal — 114 ± 22 and 110 ± 33, respectively — while AAV2/2(quad Y-F) was the least intense with a mean pixel value of 78 ± 18.

3.2.2.a.iii Statistical comparison of SLO data

An ordinary two-way ANOVA examining the effect of delivery route (intravitreal or subretinal) and AAV serotype on the area above threshold showed a statistically significant interaction between AAV serotype and area above threshold, F (2, 17) = 5.1,

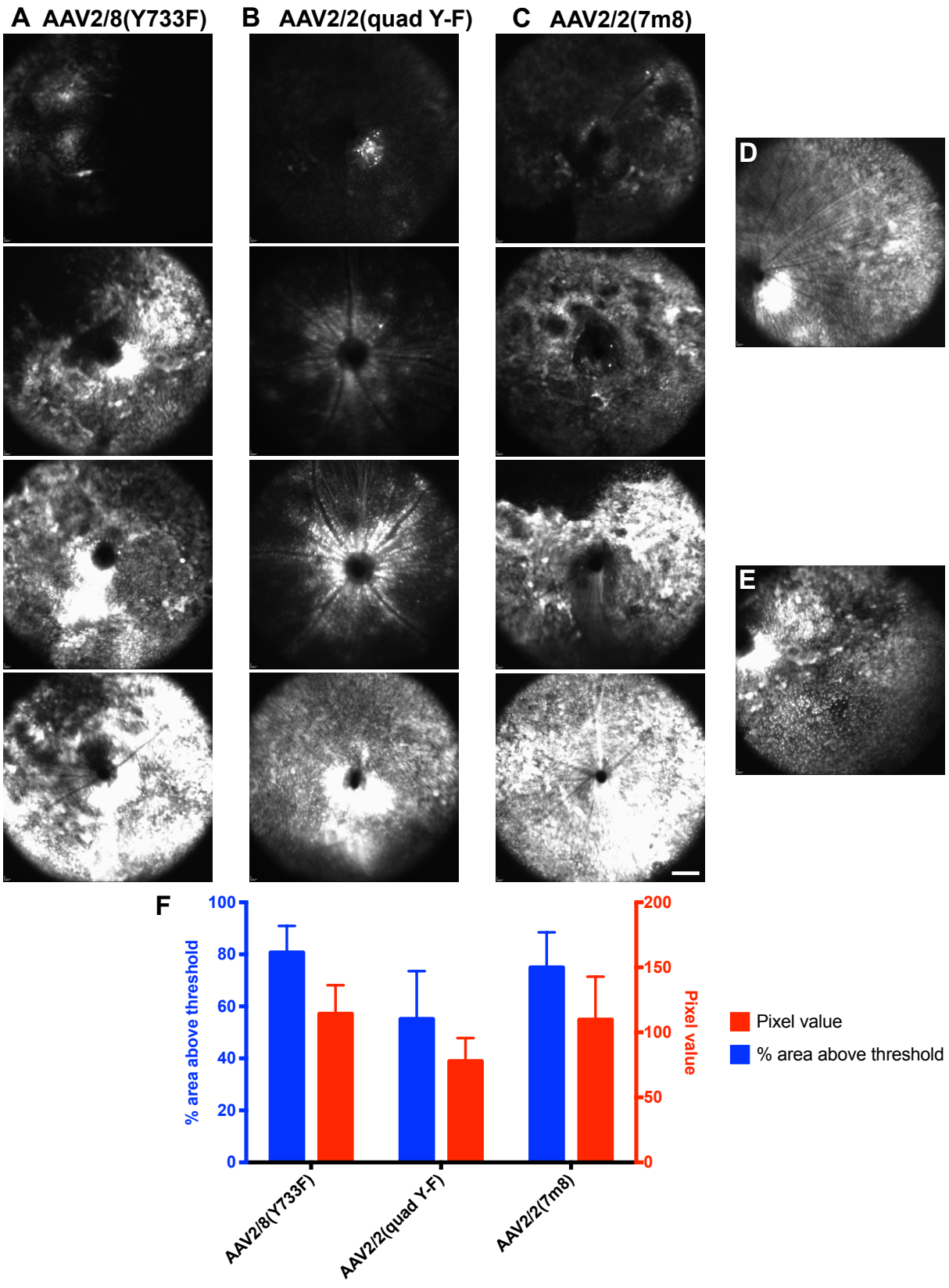


Figure 3.3. Scanning laser ophthalmoscopy of degenerate mouse retinas injected subretinally with three GFP-expressing AAV serotypes

(**A** – **E**) Mice were injected at 13 – 14 weeks of age and assessed three weeks post-injection by SLO. Images centered on the optic disc were acquired from each of the four eyes injected with each of the following serotypes: (**A**) AAV2/8(Y733F), (**B**) AAV2/2(quad Y-F) and (**C**) AAV2/2(7m8). The same autofluorescence settings were used. (**D**) In the inner layer of the retina, fluorescing retinal ganglion cell axons were identified, in this case in an eye injected with AAV2/2(quad Y-F)-GFP. (**E**) GFP fluorescence was often noted to be a speckled pattern, as in this eye injected with AAV2/8(Y733F)-GFP. (**F**) SLO images were quantified by setting a threshold pixel value and determining the area of each image above this threshold and the intensity of the signal ('Pixel value') in the area above the threshold (mean ± s.e.m.; n = 4). Scale bar represents 1 mm.

$P = 0.019$ (Figure 3.4 A; n = 4, all groups except intravitreal AAV2/2(7m8) (n = 3)). Simple effects analysis with Bonferroni correction showed that the area above threshold from an intravitreal injection with AAV2/8(Y733F) (3.4 ± 1.9%) was significantly lower than each of subretinal AAV2/8(Y733F) (81 ± 10%; $P < 0.01$), intravitreal AAV2/2(7m8) (91 ± 2.2%; $P < 0.01$) and subretinal AAV2/2(7m8) (75 ± 13%; $P < 0.05$). An ordinary two-way ANOVA examining the effect of delivery route and AAV serotype on pixel value showed no statistically significant interactions (Figure 3.4 B).

3.2.2.b GFP quantification from immunohistochemistry

To compare the level of GFP expression across retinal layers, vertical sections of the C3H/HeN eyes that had received injections of three serotypes of AAV-GFP were prepared.

The penetration and transgene expression efficiency was quantified by dividing the retina into the three remaining layers (inner nuclear layer, inner plexiform layer and ganglion cell layer) and calculating the percentage area above a threshold and the mean pixel value within the area above threshold.

3.2.2.b.i Intravitreal injection

Of those eyes that received an intravitreal injection, AAV2/2(7m8) produced the greatest area above threshold in all three layers of the degenerate retina, with 39 ± 4.1%, 30 ± 7.6% and 10 ± 5.7% of the ganglion cell layer, inner plexiform layer and inner nuclear layer, respectively, above the threshold (Figure 3.5 B). The area transduced by AAV2/2(7m8) in the ganglion cell layer and inner plexiform layer was notably higher than the transduced areas from AAV2/8(Y733F) (11 ± 5.7% and 3.9 ± 3.2%, respectively) and AAV2/2(quad Y-F) (21 ± 8.4% and 12 ± 6.2%, respectively) intravitreal injections.

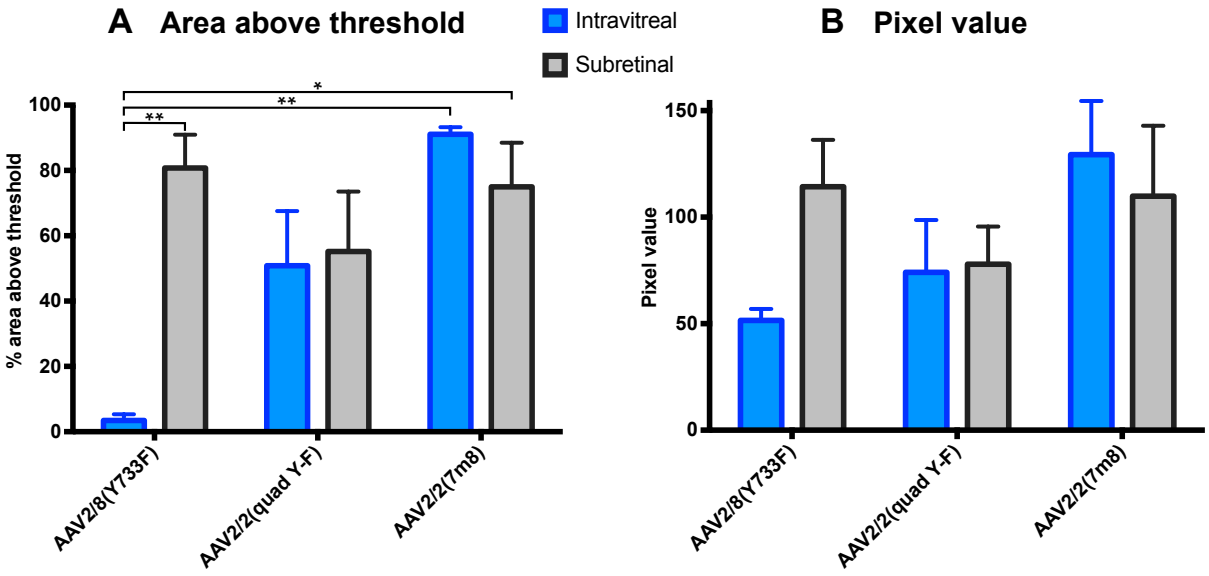


Figure 3.4. Statistical analysis of scanning laser ophthalmoscopy data comparing delivery routes and AAV serotypes in retinally degenerate mice
(**A**) An ordinary two-way ANOVA examining the effect of delivery route (intravitreal or subretinal) and AAV serotype on the area above threshold showed a statistically significant interaction between AAV serotype and area above threshold, F (2, 17) = 5.1, P = 0.019 (n = 4, all groups except intravitreal AAV2/2(7m8) (n = 3)). Simple effects analysis showed that the area above threshold from an intravitreal injection with AAV2/8(Y733F) was significantly lower than each of the following groups: subretinal AAV2/8(Y733F), intravitreal AAV2/2(7m8) and subretinal AAV2/2 (7m8). (**B**) An ordinary two-way ANOVA examining the effect of delivery route and AAV serotype on pixel value showed no statistically significant interactions. * P < 0.05, ** P < 0.01.

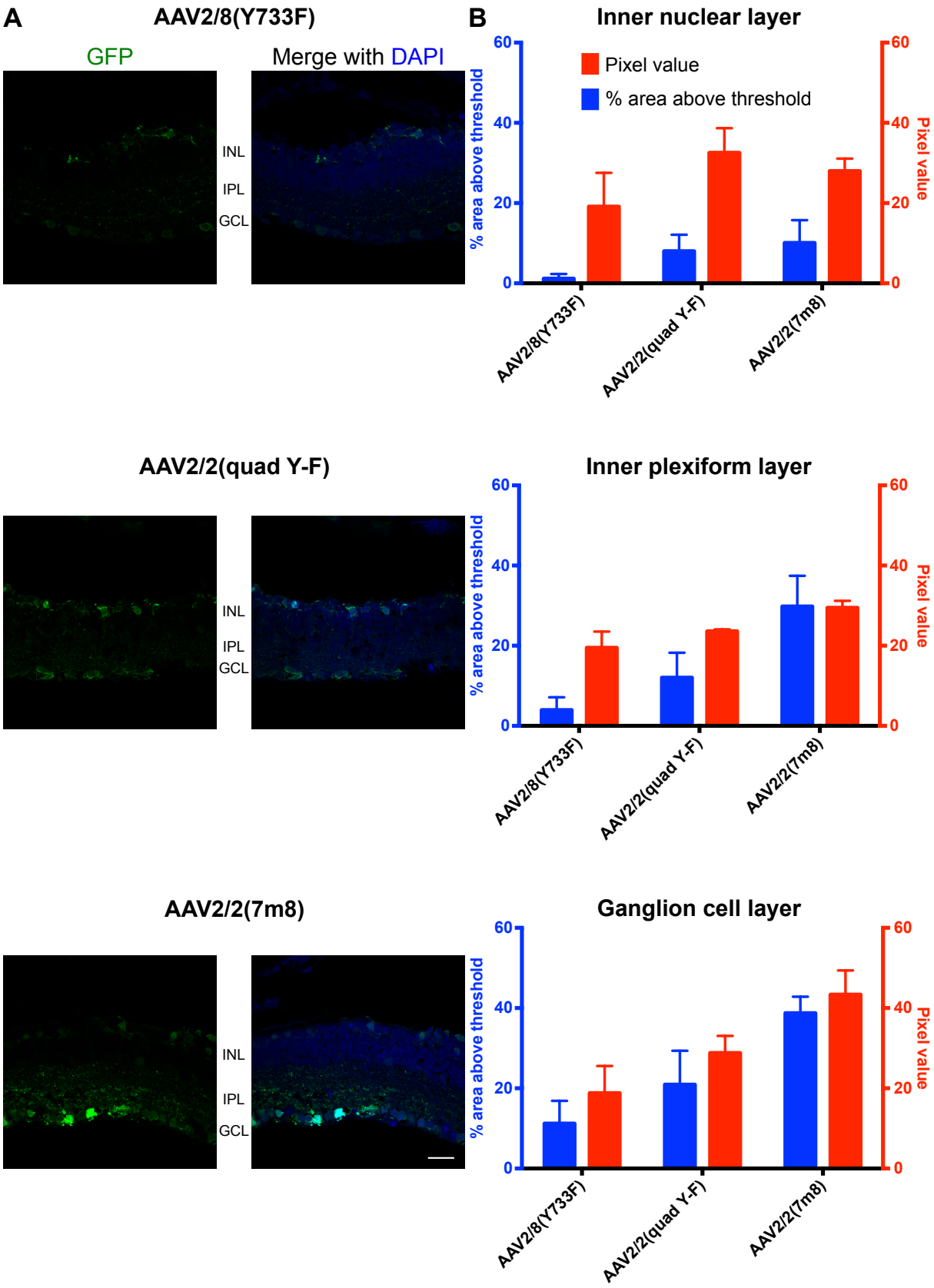


Figure 3.5. GFP expression in layers of degenerate retinas intravitreally injected with three serotypes AAV-GFP
(**A**) Confocal fluorescence micrographs of retinas that were injected intravitreally with three different AAV serotypes, each expressing GFP driven by a ubiquitous promoter. Images were acquired on the same settings to enable comparison of GFP distribution and intensity. (**B**) The retina was segmented into three layers and the percentage of each layer above a set threshold value and the mean pixel value within the area above the threshold was determined (mean ± s.e.m.; n = 3). GCL, ganglion cell layer; IPL, inner plexiform layer; INL, inner nuclear layer. Scale bar represents 20 µm.

In the inner nuclear layer, AAV2/2(quad Y-F) and AAV2/2(7m8) groups had comparable areas transduced with 8.0 ± 4.1% and 10 ± 5.7%, respectively, above threshold. The AAV2/8(Y733F) group in contrast had 1.1 ± 1.1% of its inner nuclear layer above threshold.

Consistent with the scanning laser ophthalmoscopy results, an intravitreal injection with AAV2/8(Y733F) was not as effective as the other two serotypes, with the least area transduced in all layers of the degenerate retina.

When the pixel value of the area above threshold was compared there was less spread between the groups (Figure 3.5 B). The ganglion cell layer of retinas that had received an intravitreal injection of AAV2/2(7m8) was an outlier with a pixel value in the area above threshold of 43 ± 6.0, while other layers of retinas transduced with AAV2/2(7m8) or AAV2/2(quad Y-F) had pixel values between 23 and 33. Pixel values in the AAV2/8(Y733F) were between 18 and 20 in all three retinal layers (see below for statistical comparisons).

3.2.2.b.ii Subretinal injection

When the AAV vector was delivered subretinally a different pattern of GFP expression was evident. Generally, subretinal injections resulted in a smaller area of the ganglion cell and inner plexiform layers being above threshold and more of the inner nuclear layer being above threshold, compared to retinas that had received the same AAV by the intravitreal route (Figure 3.6). The one exception to this pattern was that the area of the ganglion cell layer above threshold was higher when AAV2/2(quad Y-F) was delivered subretinally (25 ± 6.6%), compared to intravitreally (21 ± 8.4%; Figure 3.7 A).

Injection with AAV2/2(quad Y-F) resulted in a slightly greater area of the inner nuclear layer having GFP expression above threshold (13 ± 5.2%) compared to

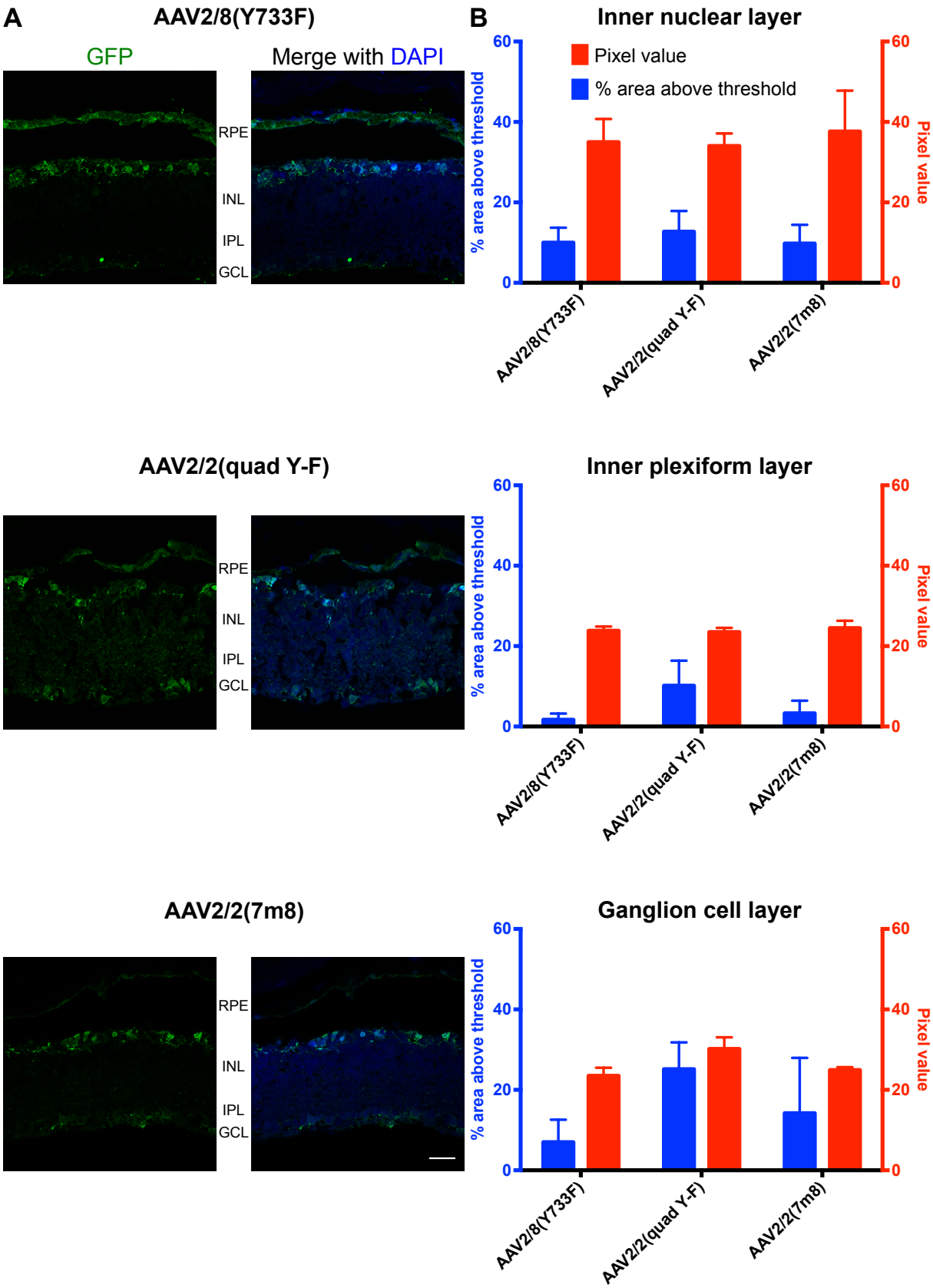


Figure 3.6. GFP expression in layers of degenerate retinas subretinally injected with three serotypes of AAV-GFP
(**A**) Confocal fluorescence micrographs of retinas injected subretinally with three different AAV serotypes, each expressing GFP driven by a ubiquitous promoter. Images were acquired on the same settings to enable comparison of GFP distribution and intensity. (**B**) The retina was segmented into three layers and the percentage of each layer above a set threshold value and the mean pixel value within the area above the threshold was determined (mean ± s.e.m.; n = 3, AAV2/8(Y733F) and AAV2/2(quad Y-F); n = 2, AAV2/2(7m8)). GCL, ganglion cell layer; IPL, inner plexiform layer; INL, inner nuclear layer; RPE, retinal pigment epithelium. Scale bar represents 20 µm.

AAV2/8(Y733F) (10 ± 3.7%) and AAV2/2(7m8) (9.8 ± 4.6%) (Figure 3.6 B). For all three serotypes, the pixel values in the areas above threshold in the inner nuclear layer were higher compared to both the ganglion cell and inner plexiform layer (Figure 3.6 B).

Although it was not quantified, the retinal pigment epithelium was clearly transduced in all three groups that received AAV via the subretinal route (Figure 3.6 A).

3.2.2.b.iii Statistical comparison of GFP quantification data

Ordinary two-way ANOVA tests were used to examine the effect of delivery route (intravitreal or subretinal) and AAV serotype on the area above threshold for each of the three layers of the retina (Figure 3.7 A). There was a statistically significant interaction between delivery route and area above threshold in the inner plexiform layer, F (1, 11) = 5.2, P = 0.043 (n = 3, all groups except intravitreal AAV2/2(7m8) (n = 2)). Simple effects analysis showed that the area above threshold in the inner plexiform layer from a subretinal injection with AAV2/8(Y733F) (1.7 ± 1.5%) was significantly ($P < 0.05$, Bonferroni correction) lower than the area above threshold due to an intravitreal injection with AAV2/2(7m8) (29.8 ± 7.6%). Ordinary two-way ANOVA tests examining the effect of delivery route and AAV serotype on the pixel value in each of the three layers of the retina showed no statistically significant interactions (Figure 3.7 B).

3.2.2.c Colocalisation of GFP with retinal cell markers

To determine which cell types of *rd1* degenerate mouse retinas were being transduced by intravitreal or subretinal injection of three serotypes of AAV-GFP, vertical sections were co-labelled with a range of antibody retinal cell markers (Figure 3.8). The relative transduction efficiency of the different serotypes did not differ greatly — the same cell types were transduced in all cases (Table 3.1). The route of delivery also did not influence which cell types were transduced; however, there were differences in the level

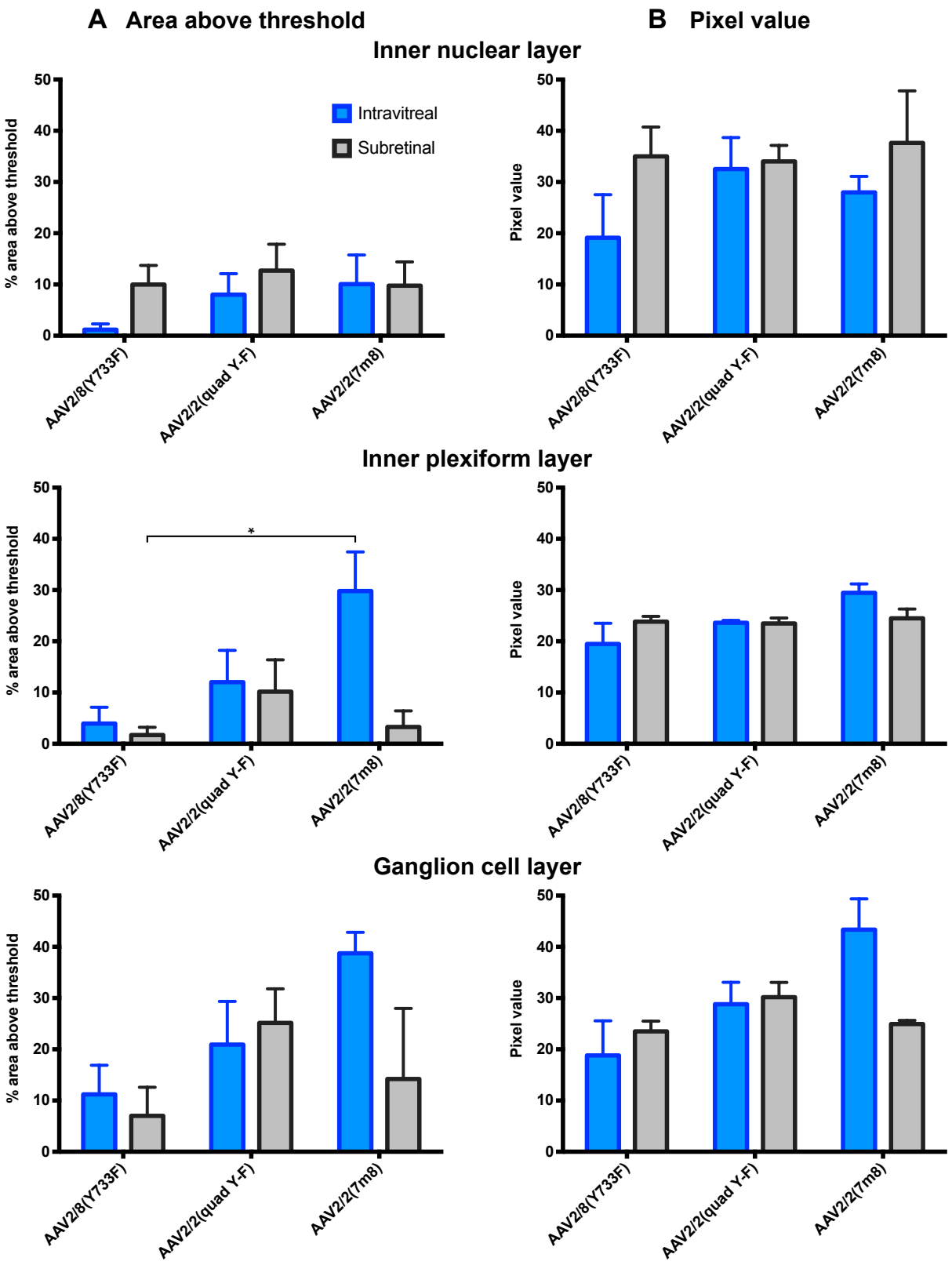


Figure 3.7. Statistical analysis of immunohistochemistry data comparing delivery routes and AAV serotypes in retinally degenerate mice

(**A**) Ordinary two-way ANOVA tests examining the effect of delivery route (intravitreal or subretinal) and AAV serotype on the area above threshold for each of the three layers of the retina were examined. Only the effect of delivery route and AAV serotype on the area above threshold in the inner plexiform layer showed a statistically significant interaction between delivery route and area above threshold, F (1, 11) = 5.2, P = 0.043 (n = 3, all groups except intravitreal AAV2/2(7m8) (n = 2)). Simple effects analysis showed that the area above threshold in the inner plexiform layer from a subretinal injection with AAV2/8(Y733F) was significantly lower than the area associated with an intravitreal injection with AAV2/2(7m8). (**B**) Ordinary two-way ANOVA tests examining the effect of delivery route and AAV serotype on the pixel value in each of the three layers of the retina showed no statistically significant interactions. * $P < 0.05$

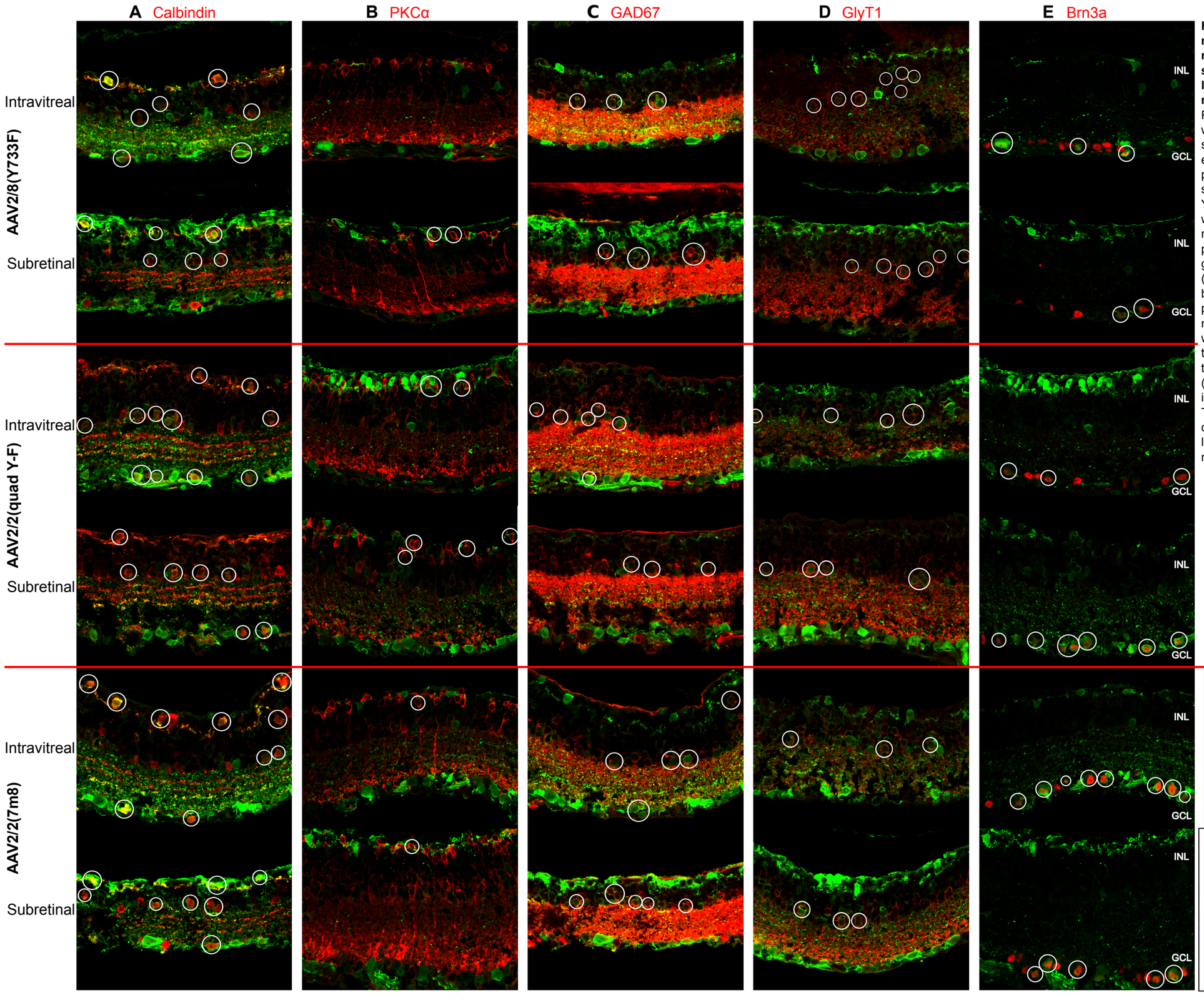


Figure 3.8. Confocal fluorescence micrographs of retinally degenerate mouse retinas injected with three serotypes of AAV-GFP and double labelled for GFP and retinal cell markers
Retinally degenerate *rd1* mouse retinas were injected either intravitreally or subretinally with an AAV vector expressing GFP driven by a ubiquitous promoter, with one of three AAV serotypes: AAV2/8(Y733F), AAV2/2(quad Y-F) or AAV2/2(7m8). Vertical sections were double immunolabelled for GFP and retinal cell markers: (**A**) calbindin; (**B**) protein kinase C alpha (PKCα); (**C**) glutamate decarboxylase 67 (GAD67); (**D**) glycine transporter 1 (GlyT1); (**E**) brain-specific homeobox/POU domain protein 3a (Brn3a) or (**F**) mouse melanopsin (mOPN4). Cell bodies that were immunopositive for both GFP and the cell marker are encircled. (**G**) A retina that was injected subretinally with AAV2/2 (7m8) was flat mounted and immunolabelled for GFP and PKCα. See Table 3.1 for a summary of the colocalisation results. GCL, ganglion cell layer; INL, inner nuclear layer. Scale bar represents 20 µm.

Degenerate mouse retinas

	Retinal pigment epithelium	Horizontal cells (calbindin)	Rod bipolar cells (PKCα)	Amacrine cells (calbindin, GAD67, GlyT1)	Retinal ganglion cells (Brn3a)	Photosensitive retinal ganglion cells (mOPN4)
AAV2/8(Y733F) Intravitreal	++	++	+/-	+	++	
AAV2/8(Y733F) Subretinal	++	+++	+/-	+	++	
AAV2/2(quad Y-F) Intravitreal	++	++	+/-	+	++	
AAV2/2(quad Y-F) Subretinal	++	+++	+/-	+	++	
AAV2/2(7m8) Intravitreal	++	++	+/-	+	++	+
AAV2/2(7m8) Subretinal	++	+++	+/-	+	++	

Non-degenerate macaque retinal explants

	Rod bipolar cells (PKCα)	Amacrine cells (calbindin, GlyT1)	Retinal ganglion cells (Brn3a)	Rods (rhodopsin)	Cones (calbindin)
AAV2/8(Y733F)	+/-	+	+	+/-	+
AAV2/2(quad Y-F)	+/-	+	+	+/-	++
AAV2/2(7m8)	+/-	+	++	+/-	+++

Human retinal explants

	Rod bipolar cells (PKCα)	Rods (rhodopsin)	Cones (calbindin)	Müller cells (GFAP)
AAV2/8(Y733F)	-	-	-	
AAV2/2(quad Y-F)	-	+	-	++
AAV2/2(7m8)	-	+	-	++

Table 3.1. Semi-quantitative summary of transduction patterns of three AAV serotypes delivered intravitreally and subretinally to degenerate mouse retinas and to macaque and human retinal explants
The cell marker antibody used to identify the cell type is indicated in parentheses. +/-, occasional transduction; +, consistent, weak transduction; ++, strong, consistent transduction; +++, very strong transduction.

of expression of GFP in the transduced cells depending on the delivery route. The cell types transduced in the different retinal layers will now be outlined.

3.2.2.c.i Inner nuclear layer

The cell type most strongly transduced in the inner nuclear layer was horizontal cells. Horizontal cells were identified by their position in the outer part of the inner nuclear layer and their positive staining with an anti-calbindin antibody (Figure 3.8 A). Calbindin-positive GFP-expressing cells were observed following intravitreal and subretinal injection of AAV2/8(Y733F), AAV2/2(quad Y-F) or AAV2/2(7m8).

Protein kinase C alpha (PKCα) was immunolabelled to identify rod bipolar cells (Figure 3.8 B). In retinas injected intravitreally or subretinally PKCα- and GFP-positive cells were sparse. When transduced PKCα-positive cells were seen, their level of GFP expression was very low compared to horizontal cells.

A population of amacrine cells were identified by immunolabelling with antibodies against calbindin, glutamate decarboxylase 67 (GAD67) and glycine transporter 1 (GlyT1) (Figure 3.8 A, C and D). Retinas from each of the viral serotypes and delivery routes had amacrine cell marker-positive GFP-expressing cells in the inner half of the inner nuclear layer. Some GFP-positive amacrine cells were co-labelled with antibodies against both calbindin and GAD67. Generally, cells that were immunolabelled with an amacrine cell marker were weakly GFP-positive, compared to the GFP levels expressed in horizontal and ganglion cells.

3.2.2.c.ii Ganglion cell layer

Transduced cells in the ganglion cell layer included photosensitive retinal ganglion cells, Brn3a-positive retinal ganglion cells and amacrine cells. The majority of the GFP-positive cells in the ganglion cell layer were Brn3a-positive retinal ganglion cells, which generally had a high level of GFP expression compared to other cell types (Figure 3.8

E). Brn3a-positive retinal ganglion cells were observed irrespective of whether the AAV-GFP was injected subretinally or intravitreally.

A small number of GFP-positive cells that co-labelled for calbindin or GAD67 were present in the ganglion cell layer, suggesting that some displaced amacrine cells were transduced (Figure 3.8 A and C).

Sections from a retina that had received an intravitreal injection of AAV2/2(7m8)-GFP were immunolabelled with an anti-mouse melanopsin antibody, demonstrating that AAV2/2(7m8) transduced melanopsin-positive photosensitive retinal ganglion cells (Figure 3.8 F).

3.2.2.c.iii Retinal pigment epithelium

All AAV-GFP vectors regardless of serotype and delivery route showed strong GFP expression in retinal pigment epithelial cells (for subretinal injection see Figure 3.6 A).

3.2.3 AAV tropism in non-degenerate macaque retina

To compare the transduction pattern in mice to that of a primate, the three serotypes of AAV-GFP were applied to explants of foveal and peripheral retina from rhesus macaques (*Macaca mullata*). Eight days after adding 10^{10} vg to each explant, GFP expression was evident in immunolabelled explants (Figure 3.9). GFP expression was strongest in the periphery of the foveal explants. The AAV2/2(7m8) transduced foveal explant featured higher levels of GFP expression that extended more centrally towards the foveola (Figure 3.9 C).

Vertical sections of foveal and peripheral retina explants were immunolabelled for GFP and rhodopsin (anti-1D4 antibody). Foveal explants were found to have significantly more widespread and higher levels of GFP expression than peripheral retina explants transduced with the same AAV serotype (Figure 3.10). The outer nuclear layer contained the highest number of GFP-positive cells. Some explants had a cluster of

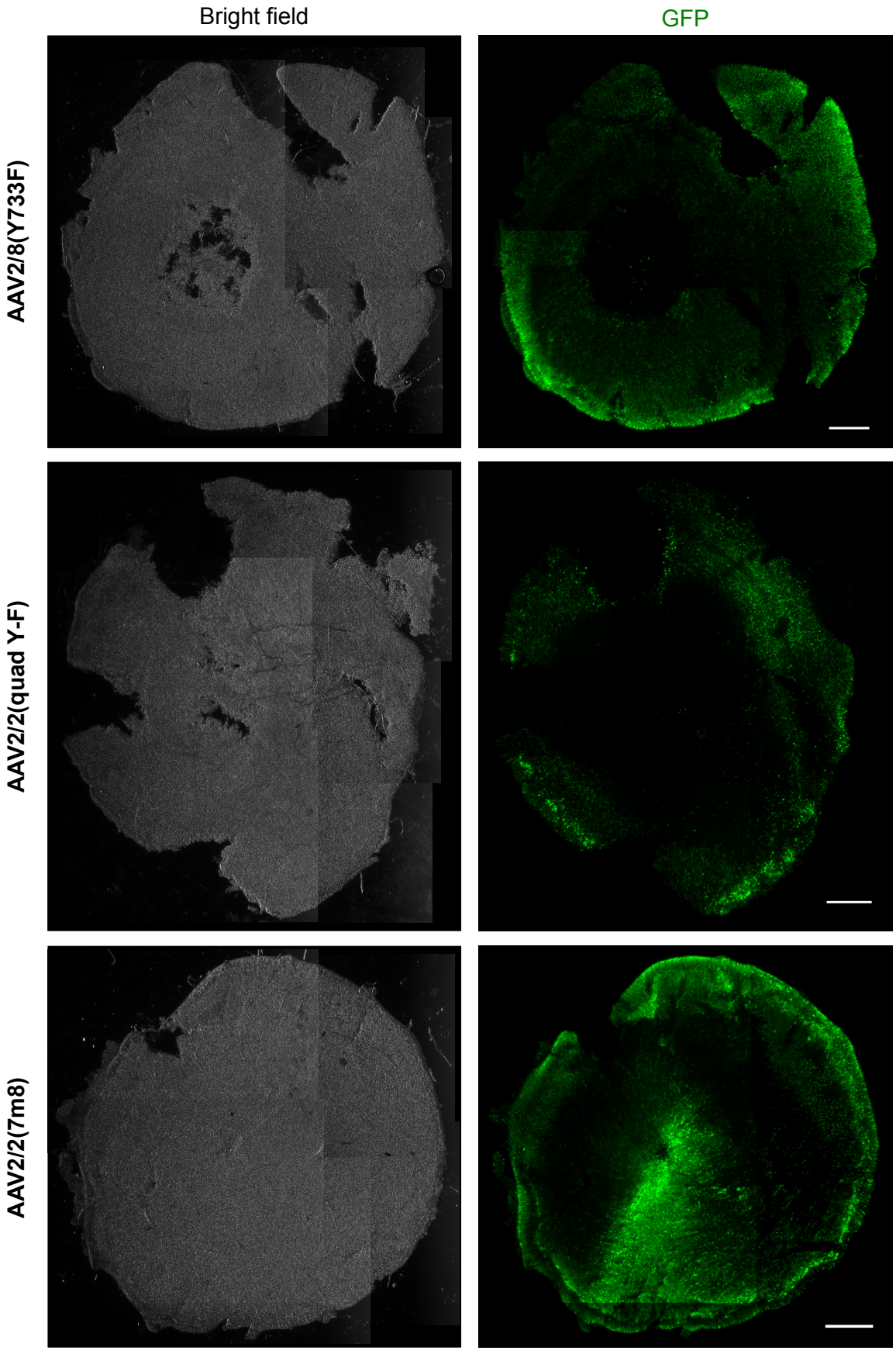


Figure 3.9. Macaque fovea explants transduced with three serotypes of AAV-GFP
Three millimetre diameter discs of macaque retina centered on the fovea were cultured for eight days in AAV-GFP solution before being fixed and immunolabelled with anti-GFP antibody. Three different AAV serotypes were used to transduce different explants: AAV2/8(Y733F), AAV2/2(quad Y-F) and AAV2/2(7m8). Images were acquired using the same settings. The outer nuclear layer is nearest the camera in all images. Scale bar represents 500 µm.

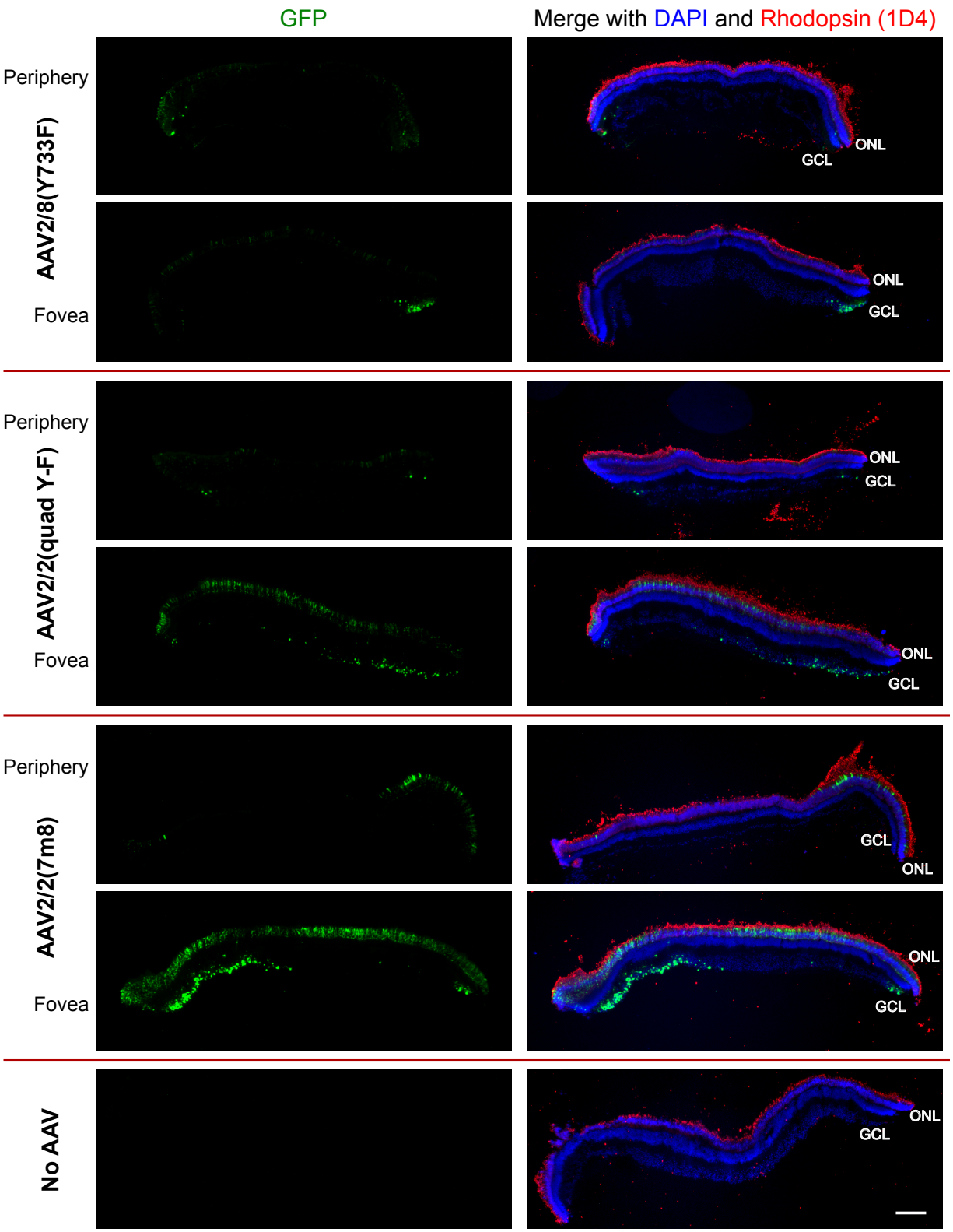


Figure 3.10. Fluorescence micrographs of peripheral and foveal macaque retina explants transduced with three serotypes of AAV-GFP and double labelled for GFP and rhodopsin
Macaque explants from the fovea and around the vascular arcades ('Periphery') were transduced with AAV-GFP with one of three serotypes — AAV2/8(Y733F), AAV2/2(quad Y-F) or AAV2/2(7m8) — or no AAV. Explants were fixed, sectioned and double immunolabelled with antibodies against GFP and rhodopsin (1D4) to show the distribution of GFP in the retinal layers. All sections are oriented with photoreceptors up. GCL, ganglion cell layer; INL, inner nuclear layer; ONL, outer nuclear layer. Scale bar represents 200 µm.

GFP-positive cells in the ganglion cell layer, but only towards an edge of the section (Figure 3.10).

Vertical sections of macaque retinal explants were also immunolabelled with retinal cell marker antibodies to identify the cells that were transduced by the three AAV-GFP viruses. The vast majority of GFP-positive cells were cones (Figure 3.11 A) — regardless of the serotype of the AAV-GFP vector, calbindin colocalised (Chiquet et al., 2002) with almost all of the GFP-positive cells in the outer nuclear layer. In addition to being calbindin-positive, most of the GFP-positive cells in the outer nuclear layer were cone arrestin-positive (data not shown), rhodopsin-negative (Figure 3.11 C) and their nucleus was in the outer part of the outer nuclear layer — features consistent with cones. Only a small number of GFP-positive, calbindin-negative cells in the inner part of the outer nuclear layer were identified (Figure 3.11 A). These are likely to be rods.

GFP-positive cells in the ganglion cell layer were restricted to the edge of the explants, where significant tissue damage was caused when the explant disc was cut from the retina. Because of the traumatic conditions associated with GFP-expression in this retinal layer, it is unlikely that these cells would be transduced in normal circumstances. Some of the GFP-positive cells in the ganglion cell layer were noted to be Brn3a positive (data not shown), while others were calbindin-positive (Figure 3.11 A). Also at the periphery of a foveal section, a GFP-positive cell in the inner nuclear layer was found to co-label for PKCα (Figure 3.11 B).

The pattern of cell types transduced was similar across the three AAV serotypes, but AAV2/2(7m8) transduced explants had higher levels of GFP expression spread over a larger area of retina (Table 3.1).

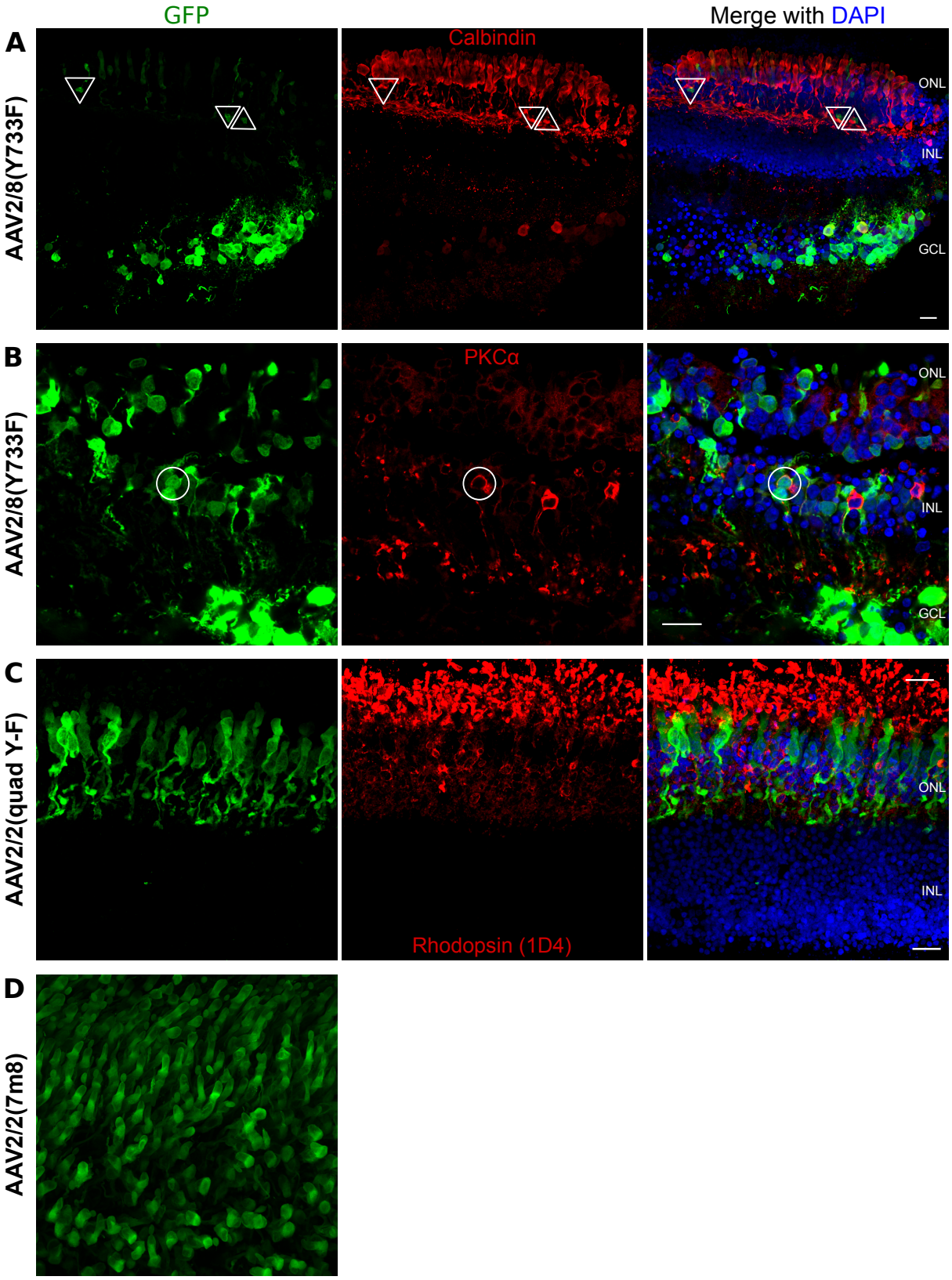


Figure 3.11. Confocal fluorescence micrographs of macaque retina transduced with three serotypes of AAV-GFP, co-labelled for retinal cell markers

(**A**) Vertical section of a AAV2/8(Y733F)-GFP transduced macaque foveal explant. Most GFP-positive photoreceptors were also calbindin-positive, indicating they were cones. Only a small number of GFP-positive photoreceptors were calbindin-negative (triangle enclosed cells). (**B**) AAV2/8(Y733F)-GFP transduced macaque foveal explant immunolabelled with anti-GFP and anti-protein kinase C alpha (PKCα). At the very periphery of the flat mounted explant, a PKCα-positive cell was noted (encircled). (**C**) Section from a AAV2/2(quad Y-F)-GFP transduced foveal macaque explant. GFP-positive photoreceptors were rhodopsin-negative, as determined by 1D4 immunolabelling. (**D**) Flat mount macaque foveal explant transduced with AAV2/2(7m8)-GFP showing a high proportion of GFP-positive photoreceptors. ONL, outer nuclear layer; INL, inner nuclear layer; GCL, ganglion cell layer. Scale bar 20μm.

3.2.4 AAV tropism in human retinal explants

Explants of human retina were also transduced with three different AAV-GFP serotypes. Human retina was acquired from patients undergoing retinectomy. Seven days after applying 10^{10} vg of the AAV serotypes, the human retina samples were fixed and immunolabelled for GFP and retinal cell markers.

Immunolabelling of transduced human retina samples showed GFP-expression across the width of each of the samples transduced with an AAV-GFP vector (Figure 3.12). A human retinal explant that was not transduced with an AAV-GFP vector did not show any signal in the GFP channel (Figure 3.13 A). While the human retinal explant transduced with AAV2/8(Y733F) showed GFP-expression limited to cells largely in the inner nuclear layer (Figure 3.12 A), explants transduced with AAV2/2(quad Y-F) and AAV2/2(7m8) showed extensive GFP expression in all layers of the retina (Figure 3.12 B and C).

Rod bipolar cells were identified by immunolabelling PKCα (Figure 3.13 A). No GFP-positive cells were found to be PKCα-positive, suggesting very few rod bipolar cells were transduced in these human retinal explants.

Rod photoreceptors were transduced, as shown by co-labelling with an anti-1D4 antibody that binds to rhodopsin (Figure 3.13 B). Transduced cones were not identified (red/green opsin and cone arrestin staining; data not shown), but this may be due to the low number of cones in the peripheral retina, which is where these retina samples were taken from.

The extensive GFP expression in human retinal explants transduced with AAV2/2(quad Y-F) and AAV2/2(7m8) had an unusual pattern, which was not stereotypical of a particular cell type in a normal retina. However, some of the areas of GFP expression that spanned the full thickness of the retina colocalised with glial fibrillary acidic

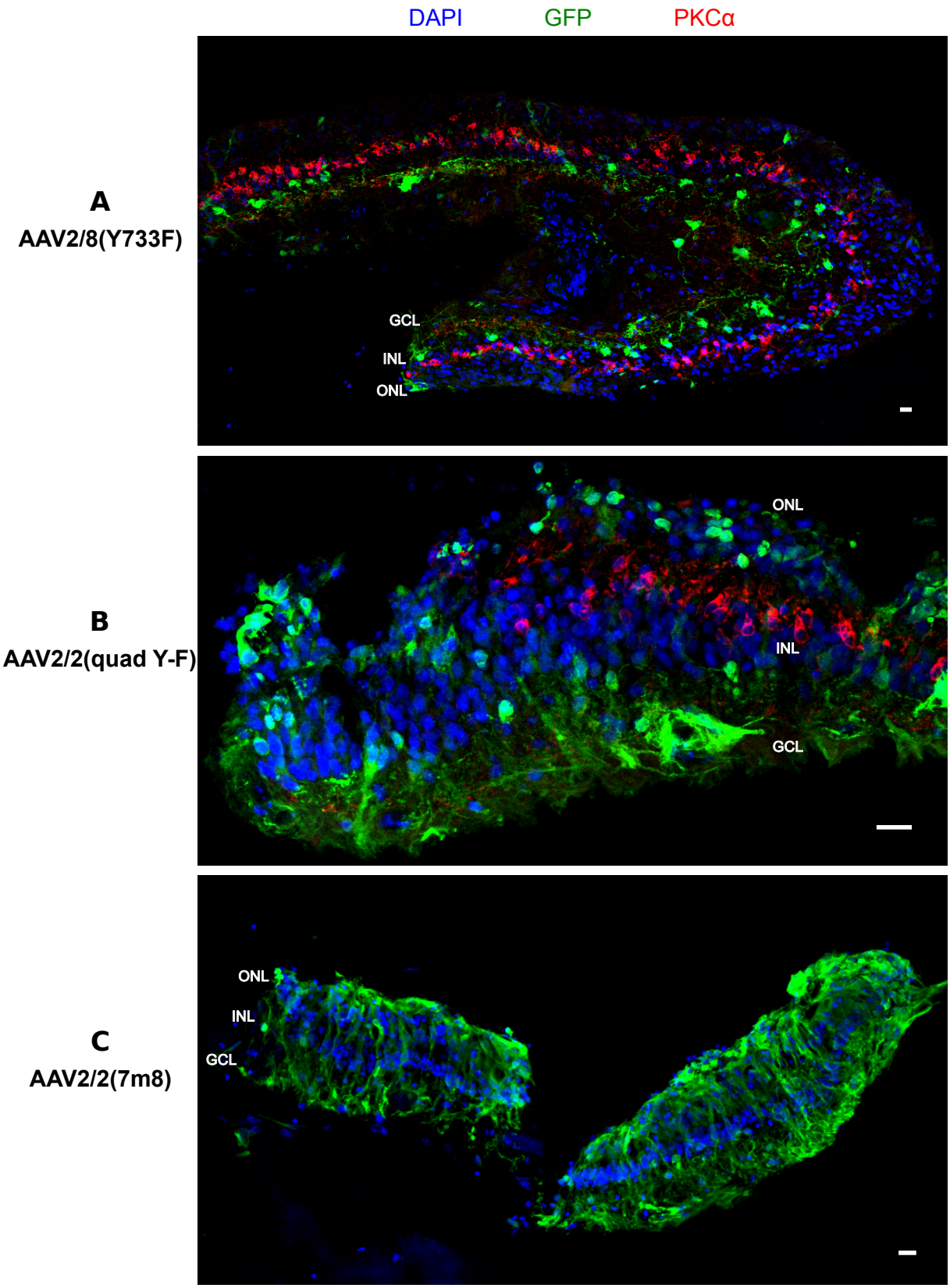


Figure 3.12. Fluorescence micrographs of human retina explants transduced with three serotypes of AAV-GFP

Retina from patients requiring retinectomy was cultured for one week in the presence of AAV-GFP of three different serotypes: (**A**) AAV2/8(Y733F), (**B**) AAV2/2(quad Y-F) or (**C**) AAV2/2(7m8). Explants were sectioned and immunolabelled for GFP and cell markers, such as protein kinase C alpha (PKCα, used in (**A**) and (**B**) only). GFP was largely limited to the inner nuclear layer (INL) of AAV2/8(Y733F) transduced retina, but extended throughout all retinal layers in retina transduced with AAV2/2(quad Y-F) and AAV2/2 (7m8). GCL, ganglion cell layer; ONL, outer nuclear layer. Scale bar represents 20 μm.

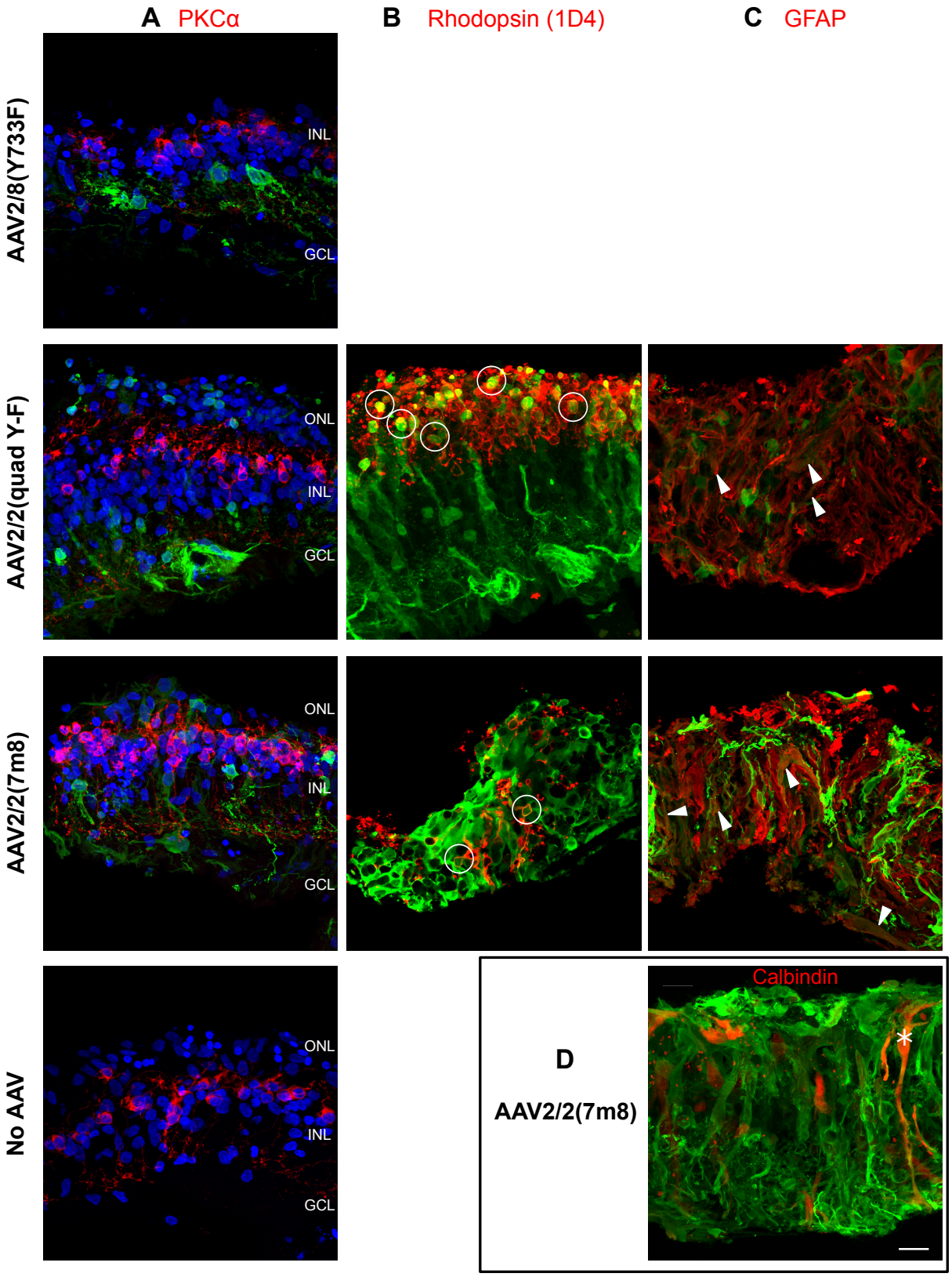


Figure 3.13. Fluorescence micrographs of human retina transduced with three serotypes of AAV-GFP, immunloabelled with retinal cell markers

Human retina explants transduced with either AAV2/8(Y733F)-, AAV2/2(quad Y-F)- or AAV2/2(7m8)-GFP, co-labelled for GFP and (**A**) protein kinase C alpha (PKCα), (**B**) rhodopsin, (**C**) glial fibrillary acidic protein (GFAP) or (**D**) calbindin. (**A**) No cells were clearly double labelled for GFP and PKCα. (**B**) Explants transduced with both AAV2/2 (quad Y-F)-GFP and AAV2/2(7m8)-GFP were identified as co-labelled for GFP and rhodopsin, suggesting transduced rods (examples encircled). (**C**) AAV2/2(quad Y-F)-GFP and AAV2/2(7m8)-GFP transduced retinas showed GFP co-localisation with GFAP (arrowheads). (**D**) Sections of AAV2/2(7m8)-GFP transduced retina were noted to have cells that were both GFP and calbindin positive (*). All sections are oriented with the photoreceptors up. ONL, outer nuclear layer; INL, inner nuclear layer; GCL, ganglion cell layer. Scale bar represents 20 μm.

protein (GFAP) (and calbindin), suggesting some of these cells were Müller cells (Figure 3.13 C and D).

3.3 Discussion

By packaging an expression cassette containing GFP driven by a ubiquitous promoter into three different AAV capsids and using these to transduce mouse, macaque and human retinas, this study aimed to deepen our understanding of the relative transduction efficiencies and transduction patterns of three AAV serotypes. This study guided the choice of AAV serotype and delivery route for subsequent experiments that aimed to maximise transgene expression across the degenerate mouse retina (chapters five and six).

3.3.1 Retinal tropism differences across species

The general pattern of GFP expression varied greatly between mouse, macaque and human retinas. This may be due to species-specific tropism factors, the health status of the tissue and/or the experimental procedure.

In degenerate mouse retina, horizontal cells, retinal ganglion cells and retinal pigment epithelium were the cell types that had the greatest levels of GFP expression, regardless of the AAV serotype injected (Table 3.1). In general, intravitreal injections resulted in retinal ganglion cells having the highest GFP levels, while subretinal injections led to horizontal cells having the highest GFP fluorescence. Amacrine cells were consistently transduced, but had low levels of GFP fluorescence compared to horizontal or retinal ganglion cells. Watanabe and colleagues (2013) performed subretinal injections of AAV2/2 and AAV2/8 (no capsid mutations) into non-degenerate retinas and also found that horizontal and ganglion cells were efficiently transduced while amacrine cells were less commonly transduced and bipolar cells were rarely transduced.

The AAV serotypes tested in this research project show good ability to penetrate the degenerate mouse retina. When injected intravitreally, transduction of horizontal cells and retinal pigment epithelium at the outer most layer of the degenerate retina were observed. Conversely, AAV-GFP vectors injected subretinally were noted to transduce cells in the ganglion cell layer, the innermost layer of the retina. AAV2/2(quad Y-F) and AAV2/2(7m8) were particularly effective at traversing the retina. These observations therefore demonstrate that the AAV virions are travelling through the retina and are still at concentrations sufficient to transduce cells and cause a detectable level of GFP to be expressed. Good penetration laterally across the retina was also observed, with GFP expression visible outside of the bleb created during the subretinal injection.

Due to the restricted availability of macaque retinal tissue, only *ex vivo* studies using wild type retinal explants were completed. While the retinal tissue was acquired from non-degenerate macaques, making it less relevant to modelling the transduction pattern in retinally degenerate humans, by cutting the explants from the retina the inner limiting membrane was no longer a significant barrier to AAV at the edges of the retina. Additionally, the variable health status of different cell types in culture may have influenced their probability of being transduced.

The predominant cell type transduced in the macaque retinal explants was cone photoreceptors (Table 3.1). GFP expression was high in cones across the retina in samples that received AAV2/2(7m8)-GFP, while GFP expression was limited to the outer edges of explants that received AAV2/8(Y733F)-GFP or AAV2/2(quad Y-F)-GFP. Yin and colleagues (2011) reported that wild type AAV2 intravitreally injected into macaque eyes led to a ring of fluorescence, centred on the fovea — suggesting a common mechanism leading to poor transduction of the central fovea. GFP expression was also seen in the ganglion cell layer, but this was often at the extreme periphery of

the explants. It was, therefore, unclear as to whether this transduction was facilitated by the absence of the inner limiting membrane as a barrier to diffusion, or whether the trauma of cutting the explant had disrupted the explant integrity and/or health in ways that enabled transduction at the periphery. It is possible that the periphery of each explant replicated a degenerate retina that has a more permeable inner limiting membrane (Kolstad et al., 2010).

The level of GFP expression was greater in retinal explants taken from the fovea than from the periphery (typically from around the vascular arcades). This is consistent with the fact that cones were the most common cell type transduced; cones are highly concentrated in the fovea but not in the periphery of the retina. The absence of photoreceptors in a degenerate retina would mean that AAV virions that would otherwise bind to and transduce cones would be available to transduce other cell types. This may increase the transduction of cell types that were not transduced in these experiments, such as bipolar cells.

The results of this experiment compare well with those reported by Dalkara and colleagues (2013). In their study, AAV2/2(quad Y-F)-GFP and AAV2/2(7m8)-GFP were injected intravitreally into one eye each of a *Macaca fascicularis* monkey. By three weeks after the injection, GFP expression was evident at the fovea, with the AAV2/2(7m8)-GFP eye showing higher levels of GFP expression. Patches of peripheral transduction were present, but these were mainly outside the vascular arcades. Although the current study used *ex vivo* explants rather than *in vivo* injections into a different species, and used a CAG promoter rather than the cytomegalovirus promoter used by Dalkara and colleagues, it is interesting to note the consistent finding of greater GFP transduction by AAV2/2(7m8) compared to AAV2/2(quad Y-F).

Given the diseased nature of the human retina samples, the variable extraction techniques and variable sizes, it is difficult to draw definitive conclusions from the differences seen between the different serotypes (Table 3.1). Despite being qualitative, it is significant to note that all three AAV serotypes transduced human retina relatively efficiently. Given that these retina samples typically came from patients who had chronic retinal detachments, these transduced areas of retina are likely to have quite abnormal physiology and this may explain the unusual patterns of GFP expression in some of the samples. Activated Müller cells, for example, appeared to be a strongly transduced cell type in samples transduced with AAV2/2(7m8) and AAV2/2(quad Y-F). Such a pattern of GFP expression was not seen in degenerate mouse or non-degenerate macaque transduced retinal samples.

Rods appeared to be more commonly transduced than cones in the human retina samples. This is likely to be due to the human samples being from peripheral retina where rods far outnumber cones, whereas in the macaque foveal samples cones are the dominant photoreceptor type.

3.3.2 AAV2/2(7m8) as a reliable serotype for optogenetic gene therapy

Across the three species tested, it was judged that the AAV2/2(7m8) serotype was the most efficient at transducing a wide area of a given retina and a diverse range of cell types. In the degenerate mouse retina, AAV2/2(7m8) injected either intravitreally or subretinally led to retinas having a large area expressing GFP, as detected by scanning laser ophthalmoscopy, and a range of cell types transduced across the full thickness of the retina, as identified on vertical sections.

When applied to macaque retina explants, AAV2/2(7m8) produced the greatest amount and intensity of GFP fluorescence in foveal samples, compared to AAV2/8(Y733F) and AAV2/2(quad Y-F). Predominantly cones were transduced, but cells in the ganglion cell

layer were also found to be GFP-positive. In contrast, when applied to human retinal explants, AAV2/2(7m8) transduced rods but few cones were identified as being transduced. Large cells that spanned the retina, presumed to be Müller cells, were also transduced strongly.

Given its consistently good tropism efficacy *in vitro* and across three species, AAV2/2(7m8) was selected to be the serotype used for subsequent experiments in this research project (chapters five and six).

3.3.3 Retinal bipolar cells remain a challenging target cell

Consistent with other published studies, it was found that bipolar cells had very low rates of transduction (van Wyk et al., 2015). The outer half of the inner nuclear layer, where bipolar cell bodies are found, was notably devoid of fluorescence in the vast majority of retinal sections that were examined. Colocalisation of GFP fluorescence with a marker of rod bipolar cells, protein kinase C alpha, showed that rod bipolar cells were only sparsely transduced in mouse and macaque retinas and, when they were transduced, they only expressed relatively low levels of GFP. Given that retinal bipolar cells are an ideal target for optogenetic gene therapy (§7.1; Dalkara et al., 2015), these low rates of bipolar cell transduction are disappointing.

It is likely that the concentration of AAV required to effectively transduce retinal bipolar and amacrine cells is relatively high. This conclusion can be drawn from the observation that the GFP expression in horizontal cells and retinal ganglion cells at the extreme outer and inner aspects of the degenerate mouse retina were often high, while the GFP expression in the rest of the inner nuclear layer was often very low. The gradient of AAV concentration from the injection site means that bipolar and amacrine cells must be exposed to a higher concentration than the retinal layer furthest from the injection site (horizontal cells for an intravitreal injection and retinal ganglion cells for a

subretinal injection), yet this layer typically had higher GFP expression than either the bipolar or amacrine cells. Effective bipolar cell transduction using these AAV serotypes may therefore require higher AAV concentrations than tested in this set of experiments (see chapter six for the use of higher concentration AAV vectors).

AAV serotypes with greater bipolar cell specificity would improve bipolar cell transduction, while reducing off-target transduction. AAV2/2(quad Y-F+T-V) is a serotype that was rationally designed by Scalabrino and colleagues (2015) to target bipolar cells. In addition to targeted mutations of four surface tyrosine residues, this capsid also has a threonine to valine mutation. AAV2/2(quad Y-F+T-V) showed a reasonably good rate of bipolar cell transduction in a non-degenerate mouse model at concentrations greater than 10^{13} vg/ml, while AAV2/8(Y733F) capsid failed to transduce bipolar cells (Scalabrino et al., 2015). Cronin and colleagues (2014) also developed a synthetic AAV capsid that transduced mouse bipolar cells more efficiently than its derivative wild type capsid.

It remains unclear what factors contribute to poor bipolar cell transduction. Successful transduction requires AAV virions to travel to the inner nuclear layer where they need to be endocytosed, transported to the nucleus and read by the cell's transcriptional and translational machinery. Ineffective AAV interactions with bipolar cell receptors at any of these steps could limit AAV activity in bipolar cells. These inefficiencies have been partially overcome by using high AAV concentrations (Cronin et al., 2014; Gaub et al., 2014; Macé et al., 2014; van Wyk et al., 2015), but this comes with a higher risk of off-target effects and an immune response (Willett and Bennett, 2013).

Despite the limited bipolar cell transduction, the three AAV serotypes tested demonstrated strong GFP expression in a wide range of cells, particularly horizontal cells, retinal ganglion cells and retinal pigment epithelium.

3.3.4 Limitations of experimental design

One of the limitations of this experiment was that all of the data was gathered at a single time point — three weeks after injection for the mouse studies and approximately one week for macaque and human explant studies. As seen in *in vitro* tests, different serotypes can have different rates of expression. This is understood to be related to the different ways in which AAV capsids interact with cell surface receptors and the rate at which the vector genome is uncoated (Thomas et al., 2004). Other studies have assessed outcomes in non-degenerate mice at four weeks (Petrs-Silva et al., 2011), while Natkunarajah and colleagues (2008) found that i*n vivo* fluorescence from AAV2/8 (no capsid mutations) did not reach a plateau until seven weeks post-injection. Given that optogenetic gene therapy aims to provide long-term treatment, it would be appropriate to investigate whether the differences observed between these serotypes is sustained over a longer time period.

A further limitation of this study was that only one concentration of AAV vector was investigated. Studies have shown that the number of vector genomes injected can have an important influence on the transduction efficiency and pattern (Ivanova and Pan, 2009; Petrs-Silva et al., 2009). The number of vector genomes injected was limited by the lowest concentration of the AAV preparations that were produced. So although the highest concentration of AAV vectors available and a large volume was injected, more transduction could have been achieved with higher concentrations of AAV. Perhaps if higher concentrations of vector were injected a critical threshold for bipolar cell transduction may have been crossed and a significant increase in bipolar cell GFP expression may have resulted. The concentration of AAV-GFP vectors used in this study were similar to those used in further *in vivo* studies in this research project, so these data are a useful reference for the transduction that was expected in further studies

(chapters five and six). In addition to the vector quantity, it is desirable to better characterise the quality of each vector solution to ensure comparability (§8.5.3).

In summary, the experiments detailed in this chapter met the primary aim of comparing the tropism of three AAV serotypes in a mouse model of retinal degeneration and primate tissue. The results suggest that AAV2/2(7m8) performed consistently superiorly to AAV2/8(Y733F) and AAV2/2(quad Y-F) following intravitreal and subretinal injections in *rd1* mice as well as when exposed to macaque and human retinal explants. A secondary aim, to compare the transduction patterns following intravitreal and subretinal injections, was also achieved by comparing the GFP expression patterns in *rd1* mice that received the same AAV-GFP vector via the two injection routes. AAV2/8(Y733F) did not perform as well when delivered by intravitreal injection, while AAV2/2(quad Y-F) and AAV2/2(7m8) had a similar extent and area of retinal transduction, regardless of the delivery route. These results contribute valuable data towards the discussion of the relative merits of intravitreal versus subretinal injections for clinical therapy (Boye et al., 2013). While these data suggest an intravitreal injection may be as efficacious without the potentially harmful effects of retinal detachment, further studies in large animal models (and humans) are required to take into account the differences in eye anatomy, which is likely to have an important effect on transduction outcome (see §8.5.4 for further discussion).

Chimera

1. (Biology) a DNA molecule with sequences derived from two or more different organisms, formed by laboratory manipulation.
2. (in Greek mythology) a fire-breathing female monster with a lion's head, a goat's body, and a serpent's tail.

late Middle English: via Latin from Greek *khimaira* **'she-goat or chimera'**.

4

Chimeric Opsins as Potential Light Sensitisers

4.1 Introduction

The selection of a light-sensitive molecule for optogenetic gene therapy for vision is challenging due to the wide range of properties desired for such a molecule. Ideally the molecule will have high light sensitivity, be non-toxic, have rapid and strong biological signalling, be capable of delivery in a single dose and cause no immune response. Currently, all available options are a compromise on one or more of these properties.

Arguably, the current light-sensitive molecules of choice are human opsins, a family of light-sensitive proteins. A gene therapy strategy using human opsins has a number of advantages over other strategies. First, patients will have immune tolerance to therapeutic human opsins, having been exposed to the protein from very early in life. Second, by acting through second messenger systems the activation of one opsin can amplify to a large downstream effect, making opsin-expressing cells highly light sensitive.

The human genome has nine opsin genes, which belong to six different classes: four visual opsins (rhodopsin and three cone opsin genes); opsin-3 (*OPN3*, alternatively known as panopsin or encephalopsin); melanopsin (*OPN4*); opsin-5 (*OPN5*, neuropsin);

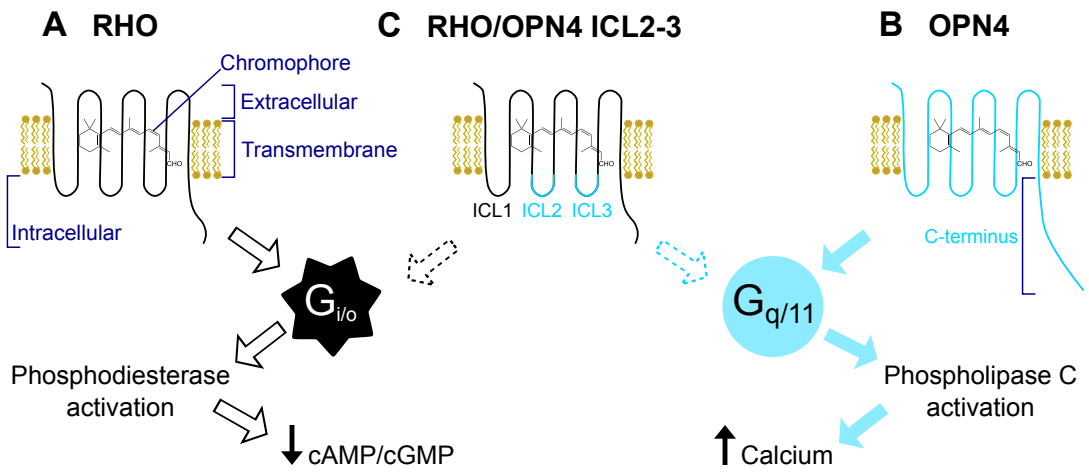
retinal pigment epithelium-derived **r**hodopsin **h**omolog (*RRH*, peropsin); and **r**etinal **G** protein coupled **r**eceptor (*RGR*) (Terakita, 2005).

Opsins are members of the **g**uanine nucleotide-binding **p**rotein (**G** protein)-**c**oupled **r**eceptor (GPCR) superfamily, a group of more than 1,000 proteins encoded in the human genome that act as sensors for a wide variety of extracellular stimuli and signal their effect by activating G proteins inside a cell (Wettschureck and Offermanns, 2005).

G proteins are heterotrimeric proteins consisting of three subunits: α, β and γ. It is the α subunit that largely defines the properties of each G protein (Arshavsky et al., 2002). Based on structural and functional similarities α subunits are divided into four classes: $G_{i/o}$, G_s, $G_{q/11}$ and $G_{12/13}$ (Wilkie et al., 1992). The activation of a G protein by a GPCR leads to a cascade of biochemical changes that can have a range of effects on a cell's physiology.

All GPCRs share a common structure that includes seven transmembrane α helices, an extracellular amino (N)-terminus, and an intracellular carboxy (C)-terminus (Figure 4.1). Crystal structures of a number of GPCRs (Rasmussen et al., 2007; Granier et al., 2012; Manglik et al., 2012; Shukla et al., 2013), including bovine (Palczewski, 2000) and squid (Murakami and Kouyama, 2008) rhodopsin, have provided insights into their structure/function relationships. The structural homology of GPCRs can allow sequences from one GPCR to be substituted into the corresponding location of another, conferring some of the functional properties of the donor sequence.

Such chimeric GPCRs have previously been created by combining the transmembrane and extracellular domains of bovine or human rhodopsin with the intracellular loops of adrenergic receptor GPCRs (Kim et al., 2005; Airan et al., 2009; Bailes et al., 2012). These studies showed that replacing the intracellular surface can cause rhodopsin to lose signalling efficiency for its native signalling pathway and gain the ability to signal via



D

Opsin	Single photon response	Rate of onset and offset	Spontaneous activity	Requires continuous supply of chromophore	Availability of second messenger	Wavelength of maximum absorbance (nm)	Immune tolerance
Melanopsin	Large	Slow	Moderate	No	Very common ($G_{q/11}$)	480	Yes
Rhodopsin	Moderate	Moderately fast	Very low	Yes	Uncommon ($G_{t\text{-}r}$)	500	Yes
Cone opsins	Small	Fast	Low	Yes	Uncommon ($G_{t\text{-}c}$)	430 (blue), 530 (green), 555 (red, LWS)	Yes
Channelrhodopsin-2	Very small	Very fast	Very low	Yes/No*	n/a	470	No

Figure 4.1. Human rhodopsin/melanopsin chimeric opsins
(**A**) Human rhodopsin (RHO) activates G protein partners of the $G_{i/o}$ family, including transducin, which activates phosphodiesterase enzymes, resulting in a reduction in cyclic nucleotide second messenger concentration. (**B**) The activation of human melanopsin (OPN4) leads to the activation of its G protein partners G_q and G_{11}, which activate phospholipase C and lead to an increase in intracellular calcium. (**C**) Chimeric opsins were created and their G protein coupling properties were tested. A schematic of rhodopsin with the second and third intracellular loops (ICL) replaced with the corresponding sequence from melanopsin (RHO/OPN4 ICL2-3) is shown. (**D**) A comparison of the properties of cells normally expressing melanopsin (photosensitive retinal ganglion cells), rhodopsin (rod cells) and cone opsins (cone cells). By creating chimeric opsins it was hypothesised that the fast response characteristics of visual opsins could be combined with the ubiquitous signalling ability of melanopsin. The properties of the microbial opsin channelrhodopsin-2 are also provided for comparison. * Some variants of channelrhodopsin-2 are bistable and do not require a continuous supply of chromophore.

non-native pathways. The studies also highlighted the importance of the second and third intracellular loops in specifying the relative efficacy for different G protein pathways.

A further example of a chimeric opsin consists of mouse melanopsin with the second and third intracellular loops and C-terminus sequences substituted with the corresponding sequence of mouse metabotropic glutamate receptor 6 (mGluR6) (van Wyk et al., 2015). The authors of this study hypothesised that this chimera, Opto-mGluR6, would have the bistable properties of melanopsin and couple to the $G_{i/o}$ pathway of mGluR6 receptors in ON bipolar cells. Indeed, by targeting Opto-mGluR6 expression to ON bipolar cells in *rd1* mice, van Wyk and colleagues were able to demonstrate an improvement in light sensitivity at the level of the retina, brain and through behavioural tests.

Photoreceptors and melanopsin-expressing photosensitive retinal ganglion cells have contrasting physiological properties that make them well adapted to their different roles in the retina (Figure 4.1 D). By creating chimeras of visual opsins and melanopsin, this project aimed to develop optogenetic tools that combined the desirable properties from both groups.

Rods and photosensitive retinal ganglion cells are highly light-sensitive at the molecular level — both cell types have a detectable response to a single photon of light (Baylor et al., 1979; Do et al., 2009). The effective duration of a photosensitive retinal ganglion cell's response to a light stimulus is 20 times greater than that of mouse rods and more than 100 times greater than mouse cones (Raport et al., 1994; Nikonov et al., 2006; Do et al., 2009). Photosensitive retinal ganglion cells have been found to spontaneously spike at a rate of approximately 2 hertz in the dark (Do et al., 2009), but the greater thermal stability of rhodopsin means that spontaneous activity in rods is much lower

(measured as 0.00031 per second, per cell; Luo et al., 2011). Rhodopsin's native G protein partner, rod transducin ($G_{t\text{-}r}$), is exclusively expressed in rods (Lerea et al., 1986). Rod transducin plays a critical role in the activation and deactivation a rod's light response (Sagoo and Lagnado, 1997; Calvert et al., 2000). Rhodopsin can couple to other Gα subunits of the $G_{i/o}$ family *in vitro* (Kanaho et al., 1984; Terakita et al., 2002; Bailes and Lucas, 2013) and *in vivo* (Figure 4.1 A; Cao et al. 2012; Gutierrez et al. 2011a; Li et al. 2005). Mammalian rhodopsin does not activate the $G_{q/11}$ pathway (Terakita et al., 1998).

By contrast, melanopsin couples to the $G_{q/11}$ pathway (Figure 4.1 B; Graham et al., 2008; Bailes and Lucas, 2013). The $G_{q/11}$ second messenger pathways are ubiquitous in the retina (Hughes et al., 2014) and throughout the body, with at least one of G_q and G_{11} found in every cell type screened (Strathmann and Simon, 1990; Wilkie et al., 1991; Hubbard and Hepler, 2006; Hughes et al., 2014).

Although these cellular characteristics are emergent properties of a complex of intracellular processes, this research project aimed to investigate the contribution of the opsins to these cellular properties. Chimeric opsins that combined the transmembrane and extracellular domains of human rhodopsin with a variable amount of human melanopsin substituted into the intracellular surface were compared to wild type rhodopsin and melanopsin as optogenetic tools. It was hypothesised that such chimeric opsins would have the greater thermal stability and speed of response of visual opsins, but couple to the ubiquitous G protein pathway of melanopsin. In addition to rhodopsin/melanopsin chimeras, long-wave-sensitive (LWS)/melanopsin chimeric opsins were also tested. LWS opsin natively couples to a cone-specific form of transducin, $G_{t\text{-}c}$, but can couple to rod transducin *in vitro* (Lerea et al., 1986; Imamoto et al., 2013). Coupling of cone opsins to other Gα subunits of the $G_{i/o}$ family has not been reported. Cone cells and cone opsins have faster onset and offset kinetics and are more

bleach resistant than rods and rhodopsin, respectively (Nikonov et al., 2006; Imamoto et al., 2013). The importance of transducin function in defining a cell's light response characteristics was highlighted in a study by Tachibanaki and colleagues (2001). Using carp rod and cone cells they reported that transducin activation by opsin is 30 times less effective and that the phosphorylation rates is 20 times faster, in cones compared to rods. These properties are likely to contribute to the fast response, but lower light sensitivity of cones compared to rods.

Such fast kinetics make cone opsins appealing as optogenetic tools for vision. However, cone opsins' apparent greater specificity for transducin makes it necessary to modify their signalling pathway. LWS/melanopsin chimeras were created to explore the hypothesis that replacing the intracellular surface of a cone opsin could maintain the relatively fast kinetics while signalling via the $G_{q/11}$ pathway.

Aims

- Clone and functionally test chimeric opsins based on human rhodopsin, LWS opsin and melanopsin to determine if any such chimeric opsins have properties making them useful as optogenetic tools for vision restoration.
- Develop an understanding of structure/function relationships of rhodopsin, LWS opsin and melanopsin through the functional testing of chimeric opsins based on these human opsins.

4.2 Results

4.2.1 Rhodopsin/melanopsin chimeric opsins

4.2.1.a Immunocytochemistry

Four human rhodopsin/human melanopsin chimeric opsins were cloned. The rhodopsin DNA sequence for the transmembrane and extracellular domains was retained with the DNA sequences that make up the intracellular surface replaced to a variable extent with

the corresponding sequence from melanopsin (Figure 4.1 C). The four rhodopsin/melanopsin chimeric opsins were: (1) rhodopsin (*RHO*) with the third intracellular loop (ICL) from melanopsin (*OPN4*), designated as *RHO*/*OPN4* ICL3; (2) rhodopsin with the second and third intracellular loops from melanopsin, *RHO*/*OPN4* ICL2-3; (3) rhodopsin with the first, second and third intracellular loops from melanopsin, *RHO*/*OPN4* ICL1-3, and (4) rhodopsin with the entire intracellular surface (ICS; that is, the three intracellular loops and the intracellular C-terminal sequence) from melanopsin, *RHO*/*OPN4* ICS (Figure 4.2).

Each of the coding sequences was tagged with the 1D4 sequence at the 3′ end.

293T cells transfected with rhodopsin and rhodopsin/melanopsin chimeric opsin plasmids were immunolabelled with polyclonal and monoclonal antibodies against rhodopsin and assessed by confocal microscopy (Figure 4.3). Cells transfected with *RHO* and *RHO*/*OPN4* ICL 3 had a high degree of signal colocalisation from the polyclonal and monoclonal (anti-1D4) rhodopsin antibodies. Signal was strongest at the plasma membrane. However, in cells transfected with *RHO*/*OPN4* ICL 2-3, *RHO*/*OPN4* ICL 1-3 and *RHO*/*OPN4* ICS there was a notable separation of the signal from the two antibodies. The monoclonal antibody immunofluorescence was most intense at the plasma membrane of transfected cells, whereas the signal from the polyclonal antibody was relatively weak at the plasma membrane and strong at focal points within the cytoplasm. In most transfected cells the presence of immunofluorescence signal from cell processes suggested the opsin was being trafficked to distant parts of the cell.

4.2.1.b Functional assessment of rhodopsin/melanopsin chimeric opsins

The function of the rhodopsin/melanopsin chimeric opsins was assessed using *in vitro* assays of G_i and $G_{q/11}$ function, for which wild type rhodopsin and melanopsin served as positive controls, respectively.

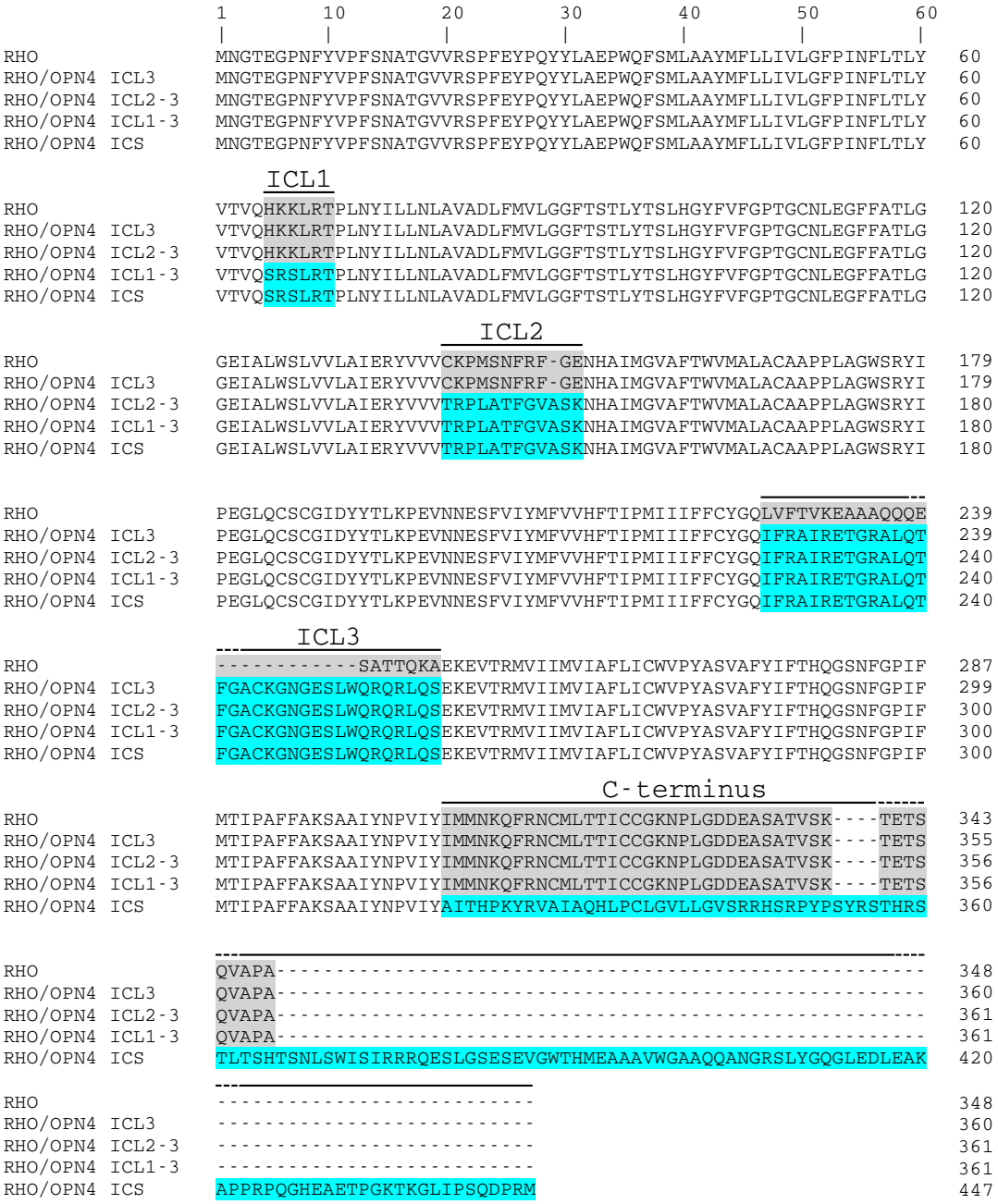


Figure 4.2. Human rhodopsin/melanopsin chimeric opsins primary sequences
The intracellular loops (ICL) and the C-terminus of rhodopsin (RHO; grey) were replaced with the corresponding sequence from melanopsin (OPN4; blue) to create rhodopsin/melanopsin chimeric opsins. All coding sequences featured a 3′ 1D4 tag when cloned into a pMT4 plasmid. This has been omitted for clarity. ICS, intracellular surface.

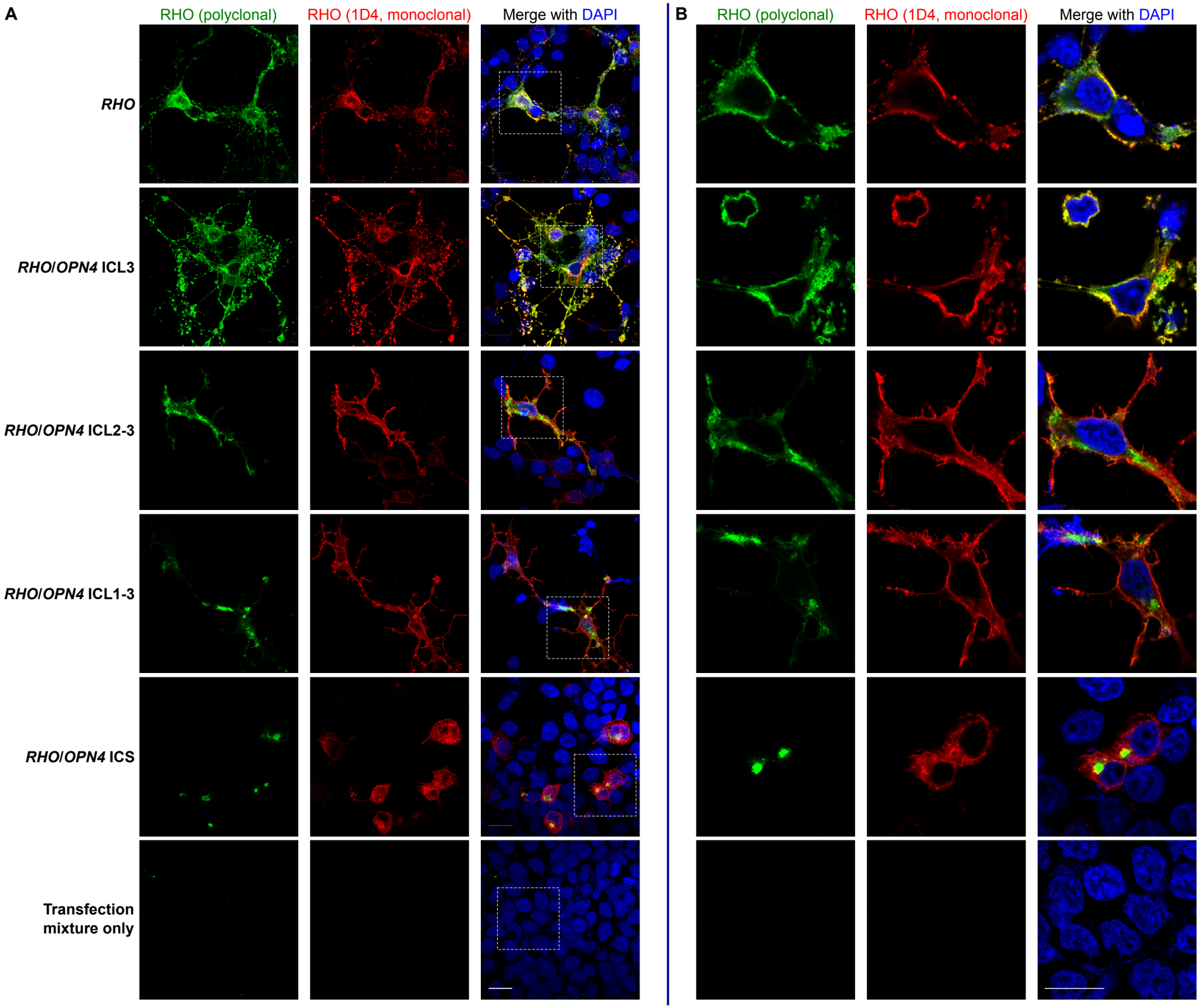


Figure 4.3. Immunocytochemistry of 293T cells expressing rhodopsin/ melanopsin chimeric opsins and wild type rhodopsin
Two days after transfecting cells with wild type rhodopsin and rhodopsin/melanopsin chimeric opsin plasmids (all 1D4 tagged), the cells were fixed and immunloabelled with a polyclonal (green) and monoclonal (red) antibodies against the 1D4 amino acid sequence. Representative cells were imaged at (**A**) low (Z stack) and (**B**) high (single slice) magnification. A high degree of co-localisation was seen between the polyclonal and monoclonal antibody channels in cells transfected with wild type rhodopsin and rhodopsin (RHO) with the third intracellular loop (ICL) replaced with the corresponding sequence from melanopsin (OPN4), *RHO*/*OPN4* ICL3. In other chimeric opsins the signal from the monoclonal antibody was most concentrated at the plasma membrane (with the exception of *RHO*/*OPN4* ICS) and the signal from the polyclonal antibody was relatively weak at the plasma membrane and strong from foci in the cytoplasm. ICS, intracellular surface. Scale bar represents 20 μm.

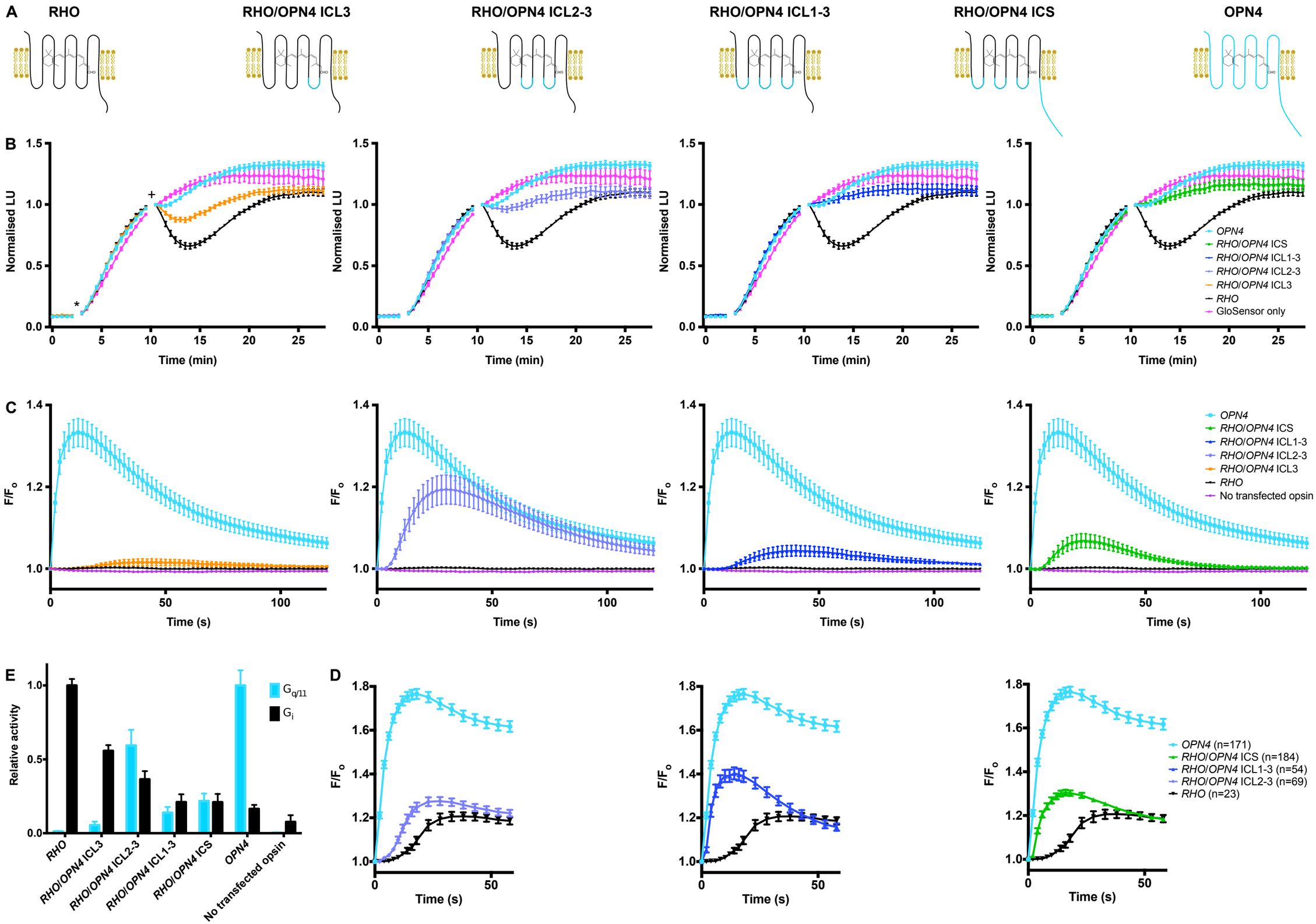
Human rhodopsin expressed in 293T cells showed a clear, relatively large, light-dependent reduction in cAMP-dependent bioluminescence, while human melanopsin produced a small decrease in bioluminescence relative to a no-opsin control (Figure 4.4 B).

$G_{q/11}$ activation was assessed using fluorescent calcium dyes. When loaded with Fluo-4 dye and recorded in a plate reader, melanopsin transfected cells produced a rapid increase in relative fluorescence signal following illumination with 485 nm light (Figure 4.4 C). Similarly, when loaded with Rhod-2 dye and stimulated with 535 – 565 nm light, responsive cells produced a rapid, large increase in fluorescence signal (Figure 4.4 D).

Rhodopsin/melanopsin chimeric opsins displayed properties that were intermediate between that of rhodopsin and melanopsin. *RHO*/*OPN4* ICL3 produced a cAMP effect that was the largest of all the chimeric opsins, but this was still only approximately 50% as large as the response produced by wild type rhodopsin (Figure 4.4 B and E). In the calcium assay, *RHO*/*OPN4* ICL3 produced a small and slow increase in signal relative to rhodopsin and the no-opsin control (Figure 4.4 C). Of the chimeric opsins, this was the smallest calcium rise that was documented.

RHO/*OPN4* ICL2-3, with both the second and third intracellular loops substituted, had moderate function in both cAMP and calcium assays. In the cAMP assay *RHO*/*OPN4* ICL2-3 produced a drop in cAMP-dependent bioluminescence that was notably greater and more sustained than that of melanopsin, but less than that of *RHO*/*OPN4* ICL3 (Figure 4.4 B). In the plate reader assay of calcium kinetics *RHO*/*OPN4* ICL2-3 produced the largest mean peak signal of the four chimeric opsins (Figure 4.4 C). When only responsive cells (those cells that showed a greater than a 5% rise in fluorescence compared to baseline fluorescence) were analysed the kinetics followed a similar

Figure 4.4. *In vitro* G_i and $G_{q/11}$ function of rhodopsin/melanopsin chimeric opsins and wild type rhodopsin and melanopsin
(**A**) Schematics of rhodopsin (RHO, black), rhodopsin/melanopsin chimeric opsins and melanopsin (OPN4, cyan) with 11-*cis* retinal *in situ* in a plasma membrane. (**B**) The ability of rhodopsin/melanopsin chimeric opsins, wild type rhodopsin and melanopsin to couple to the G_i G protein pathway was assayed using GloSensor, a cAMP biosensor. The baseline bioluminescence level was measured before forskolin was added (*) to raise the baseline level of cAMP. The transfected 293T cells were then illuminated with 485 nm light (+) and the response measured. The response was normalised to the first reading after the light stimulation (mean ± s.e.m.; n = 8). (**C**) $G_{q/11}$ activity was tested using fluorescent calcium dyes. In a plate reader-based assay, transfected 293T cells were loaded with Fluo-4 dye before being illuminated with 485 nm light (520 nm emission filter). The relative fluorescence units value (F) was normalised to the value of the first reading (F_o) (n = 11). (**D**) To further understand the calcium response kinetics, transfected 293T cells were loaded with Rhod-2 fluorescent dye and stimulated with 535 – 565 nm light in a microscope-based assay. Only the fluorescence data from cells that responded to the light stimulus with a greater than 5% increase in fluorescence contributed to these traces. Each light-responsive cell was treated as an independent biological replicate (see panel for n values). (**E**) The maximum $G_{q/11}$ and G_i activity of each chimeric opsin, normalised to melanopsin and rhodopsin, respectively, was calculated. $G_{q/11}$ values were derived from the plate reader-based assay. The same control data is used for each kinetic graph. ICL, intracellular loop; ICS, intracellular surface; LU, luminescence units.


A
RHO
RHO/OPN4 ICL3
RHO/OPN4 ICL2-3
RHO/OPN4 ICL1-3
RHO/OPN4 ICS
OPN4
B
Normalised LU
Time (min)
OPN4
RHO/OPN4 ICS
RHO/OPN4 ICL1-3
RHO/OPN4 ICL2-3
RHO/OPN4 ICL3
RHO
GloSensor only
C
F/F0
Time (s)
OPN4
RHO/OPN4 ICS
RHO/OPN4 ICL1-3
RHO/OPN4 ICL2-3
RHO/OPN4 ICL3
RHO
No transfected opsin
E
Relative activity
Gq/11
Gi
RHO
RHO/OPN4 ICL3
RHO/OPN4 ICL2-3
RHO/OPN4 ICL1-3
RHO/OPN4 ICS
OPN4
No transfected opsin
D
F/F0
Time (s)
OPN4 (n=171)
RHO/OPN4 ICS (n=184)
RHO/OPN4 ICL1-3 (n=54)
RHO/OPN4 ICL2-3 (n=69)
RHO (n=23)

pattern to the plate reader data, with a delayed rise to peak signal compared to melanopsin (Figure 4.4 D). The peak signal of *RHO*/*OPN4* ICL2-3 responsive cells was lower than that from *RHO*/*OPN4* ICL1-3 and *RHO*/*OPN4* ICS transfected cells (Figure 4.4 D).

RHO/*OPN4* ICL1-3 and *RHO*/*OPN4* ICS produced similar results on the cAMP and calcium assays. Both slightly reduced intracellular cAMP following illumination with 485 nm light (Figure 4.4 B). There was a difference between the traces of these two chimeric opsins and those of the GloSensor only and wild type melanopsin controls, but the reduction was not as great as for *RHO*/*OPN4* ICL3 and *RHO*/*OPN4* ICL2-3.

RHO/*OPN4* ICL1-3 and *RHO*/*OPN4* ICS both produced calcium signal increases substantially greater than those from no-opsin and rhodopsin controls, but the kinetics of their responses differed based on the nature of the assessment. In the plate reader assay (Figure 4.4 C) both produced moderate signal increases intermediate between those of *RHO*/*OPN4* ICL3 and *RHO*/*OPN4* ICL2-3, with a five to ten second delay from light onset until the signal rose from the baseline (similar to the *RHO*/*OPN4* ICL2-3 data). However, when only the responsive cells were analysed there was no such delay, with the signal increasing immediately after the first period of illumination (Figure 4.4 D).

The area under the curve following light stimulus in the cAMP assay was used for a statistical analysis (Figure 4.5 A). There was a statistically significant difference between rhodopsin/melanopsin chimeric opsins, rhodopsin, melanopsin and the GloSensor only group (F (6, 49) = 11.8, $P < 0.0001$; ordinary one-way ANOVA). Post hoc testing, with Bonferroni correction, found a statistically significant smaller area under the curve for the following groups, relative to the GloSensor only group (20.3 ±

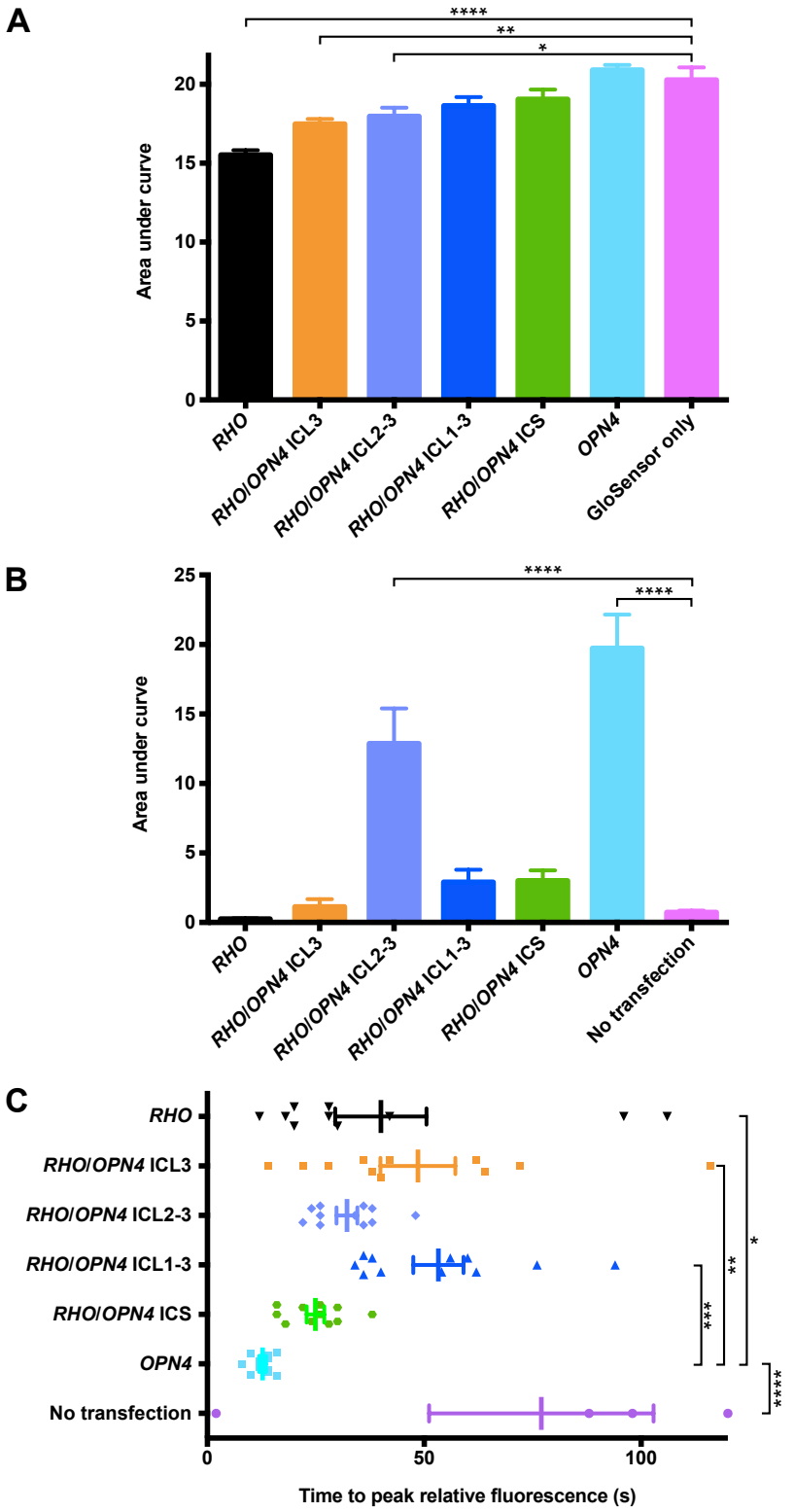


Figure 4.5. Statistical analysis of cAMP and calcium imaging data comparing rhodopsin/melanopsin chimeric opsins

(**A**) Analysis of the area under the curve of cAMP assay data (Figure 4.4 B) showed statistically significant differences between the groups ($P < 0.0001$; ordinary one-way ANOVA). Post hoc testing found a statistically significant smaller area under the curve for the following groups, relative to the GloSensor only group: rhodopsin (*RHO*), *RHO*/*OPN4* ICL3 and *RHO*/*OPN4* ICL2-3. (**B**) Analysis of the area under the curve of the plate reader assay of intracellular calcium (Figure 4.4 C) showed a statistically significant difference between the groups ($P < 0.0001$; ordinary one-way ANOVA). Post hoc testing found a statistically significant greater area under the curve for the following groups, relative to the no transfection group: *RHO*/*OPN4* ICL2-3 and melanopsin (*OPN4*). (**C**) The time to peak relative fluorescence (Figure 4.4 C) did show statistically significant differences between the groups ($P < 0.0001$; ordinary one-way ANOVA; n = 11). Post hoc testing showed statistically significant greater time to peak in the following groups, compared to melanopsin: rhodopsin, *RHO*/*OPN4* ICL3, *RHO*/*OPN4* ICL1-3 and no opsin transfection. * $P < 0.05$, ** $P < 0.01$, *** $P < 0.001$, **** $P < 0.0001$.

0.8 arbitrary units): rhodopsin (15.5 ± 0.3; $P < 0.0001$), *RHO*/*OPN4* ICL3 (17.5 ± 0.3; $P < 0.01$) and *RHO*/*OPN4* ICL2-3 (18.0 ± 0.6; $P < 0.05$).

Analysis of the area under the curve of the plate reader assay of intracellular calcium showed a statistically significant difference between the groups (Figure 4.5 B; F (6, 70) = 28.2, $P < 0.0001$; ordinary one-way ANOVA). Post hoc testing, with Bonferroni correction, found a statistically significant greater area under the curve for the following groups, relative to the no transfection group (0.72 ± 0.13 arbitrary units): *RHO*/*OPN4* ICL2-3 (12.87 ± 4.19; $P < 0.0001$) and *OPN4* (19.72 ± 4.03; $P < 0.0001$).

The time to peak relative fluorescence did show statistically significant differences between the groups (Figure 4.5 C; F (6, 62) = 6.4, $P < 0.0001$; ordinary one-way ANOVA; n = 11). Post hoc testing, with Bonferroni correction, showed statistically significant greater time to peak in the following groups, compared to melanopsin (12.7 ± 0.8 seconds): rhodopsin (40.0 ± 10.5 seconds; $P < 0.05$), *RHO*/*OPN4* ICL3 (48.5 ± 8.6 seconds; $P < 0.01$), *RHO*/*OPN4* ICL1-3 (53.3 ± 5.8 seconds; $P < 0.001$) and no opsin transfection (77.0 ± 25.9 seconds; $P < 0.0001$).

In summary, as more of the intracellular rhodopsin protein sequence was substituted with the corresponding sequence of melanopsin, the $G_{q/11}$ function of the chimeric proteins generally increased, and their G_i function decreased (Figure 4.4 E). However, none of the chimeric opsins functioned as efficiently as the corresponding wild type protein.

4.2.1.c Rhodopsin/melanopsin chimeric opsins require exogenous chromophore

Rhodopsin and all rhodopsin/melanopsin chimeric opsins were dependent on exogenous 9-*cis* retinal for correct biological functioning.

In the absence of 9-*cis* retinal chromophore, transfected 293T cells did not display the characteristic drop in cAMP-dependent bioluminescence (Figure 4.6 A). However,

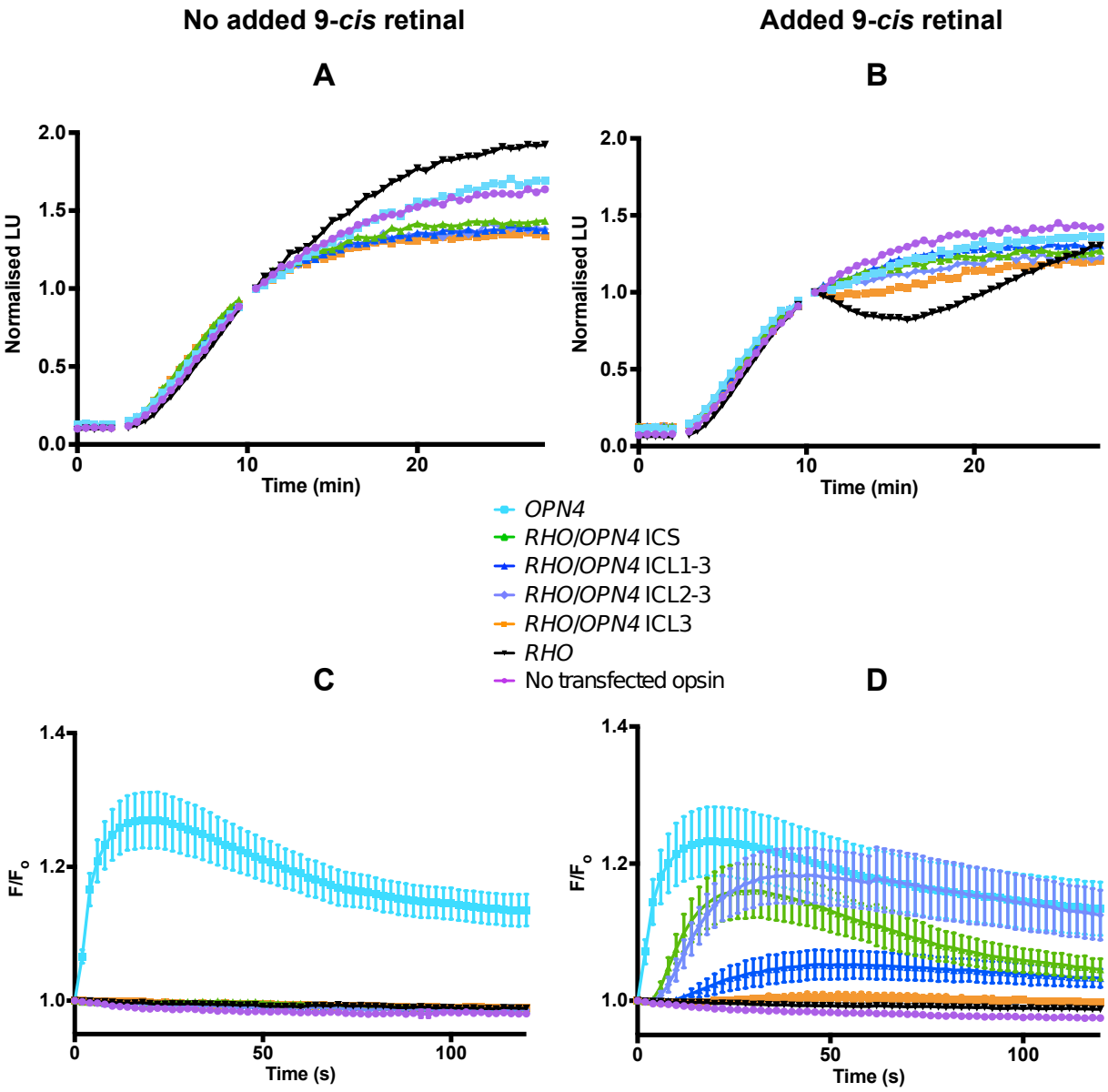


Figure 4.6. The effect of adding 9-*cis* retinal to rhodopsin/melanopsin chimeric opsins, rhodopsin and melanopsin

293T cells transfected with rhodopsin (*RHO*), melanopsin (*OPN4*) or chimeric combinations of these two wild type opsins, were assayed for their light-induced effects on cellular: (**A** and **B**) cyclic adenosine monophosphate using a GloSensor reporter (n = 1), and (**C** and **D**) calcium using a genetically encoded calcium indicator, GCaMP6f (mean ± s.e.m.; n = 6). The same wells were tested in a plate reader twice: (**A** and **C**) before adding 9-*cis* retinal, and (**B** and **D**) after adding 9-*cis* retinal to the cells. The addition of 9-*cis* retinal was required for rhodopsin and its derivative chimeric opsins to function, while melanopsin produced a calcium response in the absence of exogenous 9-*cis* retinal. F/F_o, fluorescence intensity relative to baseline fluorescence; ICL, intracellular loop; ICS, intracellular surface; LU, luninescence units.

adding 9-*cis* retinal to the cells led to the return of the rhodopsin and *RHO*/*OPN4* ICL3 light-induced drop in signal (Figure 4.6 B).

Similarly, in the calcium assay, no light-dependent increase in signal was detected from any of the rhodopsin/melanopsin chimeric opsins (Figure 4.6 C) unless cells were first incubated with 9-*cis* retinal (Figure 4.6 D).

In contrast, there was no distinguishable difference in the response characteristics of wild type melanopsin with or without added 9-*cis* retinal.

4.2.1.d Rhodopsin/melanopsin chimeras compared to Opto-α_1AR chimeric opsin

The function of the rhodopsin/melanopsin chimeric opsins was compared to that of another chimeric opsin: Opto-α_1AR. Opto-α_1AR consists of the transmembrane and extracellular domains of bovine rhodopsin and the intracellular surface (intracellular loops and C-terminus) from human α_{1a}-adrenergic receptor, and thus couples to the $G_{q/11}$ second messenger system (Airan et al., 2009).

Opto-α_1AR produced a moderate calcium response that was slower to rise to a lower peak than *RHO*/*OPN4* ICL2-3 and *RHO*/*OPN4* ICS (Figure 4.7 D). The response of cells transfected with Opto-α_1AR was greater than that of *RHO*/*OPN4* ICL3 and *RHO*/*OPN4* ICL1-3. The offset kinetics of the Opto-α_1AR calcium response were notably different than those of the rhodopsin/melanopsin chimeric proteins. During the two minutes of the calcium assay Opto-α_1AR transfected cells continued to increase in their signal, while responsive rhodopsin/melanopsin chimeric opsins reached a peak by approximately 45 seconds and then decreased in signal.

In the cAMP assay Opto-α_1AR transfected cells did not show any light-dependent change in bioluminescence, with a very similar result to that of cells not transfected with any opsin (Figure 4.7 B).

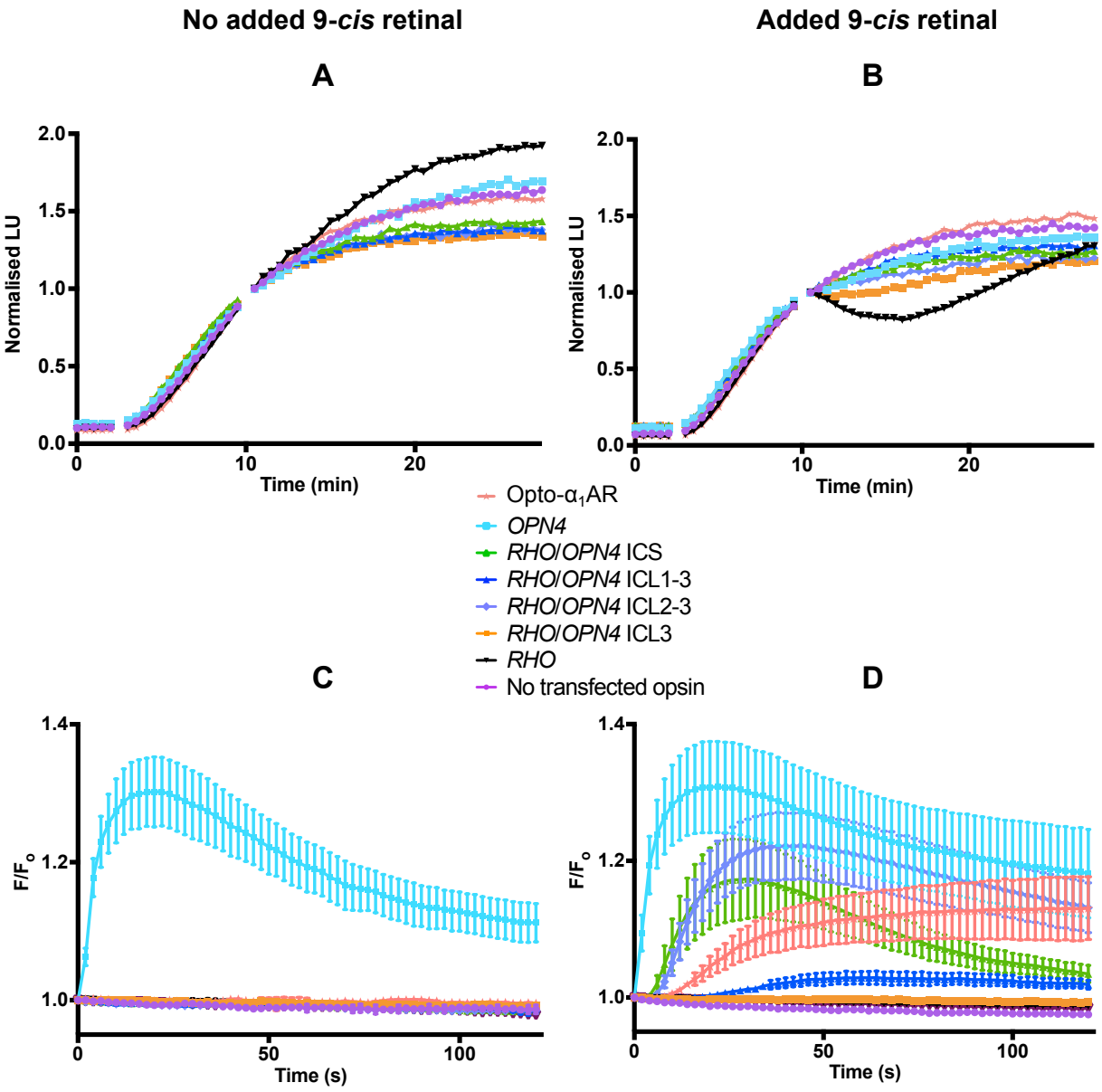


Figure 4.7. Opto-α_1AR compared to rhodopsin/melanopsin chimeric opsins, with and without exogenous 9-*cis* retinal

293T cells transfected with rhodopsin (*RHO*), melanopsin (*OPN4*), rhodopsin/melanopsin chimeric opsins or a bovine rhodopsin/human α_{1a}-adrenergic receptor chimeric opsin (Opto-α_1AR), were assayed for their light-induced effects on cellular: (**A** and **B**) cyclic adenosine monophosphate using a GloSensor reporter (n = 1), and (**C** and **D**) calcium using a genetically encoded calcium indicator, GCaMP6f (mean ± s.e.m.; n = 3). The same wells were tested in a plate reader twice: (**A** and **C**) before adding 9-*cis* retinal, and (**B** and **D**) after adding 9-*cis* retinal to the cells. Opto-α_1AR functioned similarly to rhodopsin/melanopsin chimeric opsins in requiring the addition of exogenous 9-*cis* retinal to effective produce a light-dependent calcium response. F/F_o, fluorescence intensity relative to baseline fluorescence; ICL, intracellular loop; ICS, intracellular surface; LU, luninescence units.

As with rhodopsin/melanopsin chimeric opsins, Opto-α_1AR required exogenous 9-*cis* retinal to function, as demonstrated by the observation that Opto-α_1AR only produced an observable rise in light-dependent calcium signal after the addition of 9-*cis* retinal (Figure 4.7 C and D).

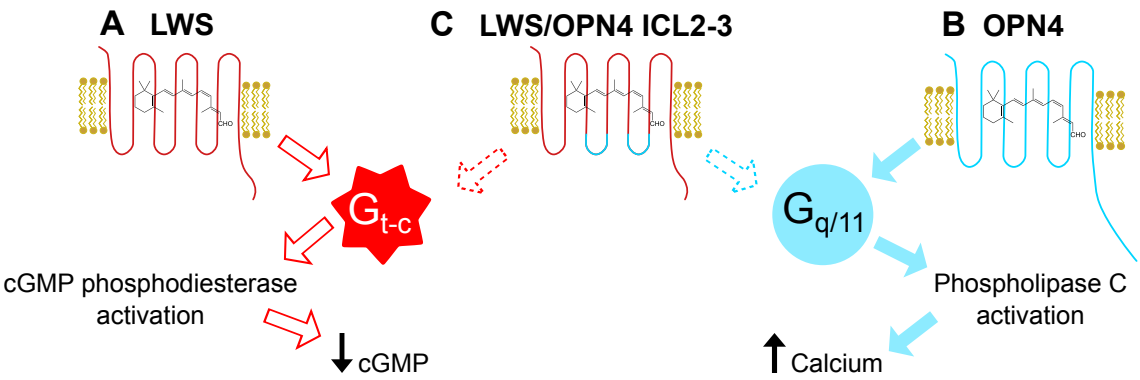
4.2.2 Long-wave-sensitive opsin/melanopsin chimeric opsins

4.2.2.a Immunocytochemistry

Four human long-wave-sensitive (*LWS*) opsin/human melanopsin chimeric opsins were cloned. The *LWS* opsin transmembrane and extracellular domain sequence was retained while the DNA sequences that make up the intracellular surface were replaced to a variable extent with the corresponding DNA sequence from melanopsin (Figure 4.8 C). The four *LWS*/melanopsin chimeras were: (1) *LWS* with the third intracellular loop sequence from melanopsin, designated as *LWS*/*OPN4* ICL3; (2) *LWS* with the second and third intracellular loop sequences from melanopsin, *LWS*/*OPN4* ICL2-3; (3) *LWS* with the first, second and third intracellular loop sequences from melanopsin, *LWS*/*OPN4* ICL1-3, and (4) *LWS* with the entire intracellular surface (ICS, the three intracellular loops and the intracellular C-terminal sequence) from melanopsin, *LWS*/*OPN4* ICS (Figures 4.8 D and 4.10 A).

Each of the coding sequences was tagged with the 1D4 sequence at the 3′ end.

Immunocytochemistry on 293T cells transfected with *LWS*/melanopsin chimeric opsins gave distinct patterns of immunoreactivity using polyclonal and monoclonal antibodies against the 1D4 tag (Figure 4.9). Cells transfected with *LWS*/*OPN4* ICL3, *LWS*/*OPN4* ICL2-3 and wild type *LWS* had their strongest signal from the monoclonal antibody (anti-1D4) at the plasma membrane of the cell. In contrast, signal from monoclonal antibody binding in *LWS*/*OPN4* ICL1-3 and *LWS*/*OPN4* ICS transfected cells appeared to be more evenly distributed throughout the cell.



D

```
                          1         10        20        30        40        50        60
                          |         |         |         |         |         |         |
LWS                       MAQQWSLQRLAGRHPQDSYEDSTQSSIFTYTNSNSTRGPFEGPNYHIAPRWVYHLTSVWM   60
LWS/OPN4 ICL3             MAQQWSLQRLAGRHPQDSYEDSTQSSIFTYTNSNSTRGPFEGPNYHIAPRWVYHLTSVWM   60
LWS/OPN4 ICL2-3           MAQQWSLQRLAGRHPQDSYEDSTQSSIFTYTNSNSTRGPFEGPNYHIAPRWVYHLTSVWM   60
LWS/OPN4 ICL1-3           MAQQWSLQRLAGRHPQDSYEDSTQSSIFTYTNSNSTRGPFEGPNYHIAPRWVYHLTSVWM   60
LWS/OPN4 ICS              MAQQWSLQRLAGRHPQDSYEDSTQSSIFTYTNSNSTRGPFEGPNYHIAPRWVYHLTSVWM   60

                                                ICL1
LWS                       IFVVTASVFTNGLVLAATMKFKKLRHPLNWILVNLAVADLAETVIASTISIVNQVSGYFV   120
LWS/OPN4 ICL3             IFVVTASVFTNGLVLAATMKFKKLRHPLNWILVNLAVADLAETVIASTISIVNQVSGYFV   120
LWS/OPN4 ICL2-3           IFVVTASVFTNGLVLAATMKFKKLRHPLNWILVNLAVADLAETVIASTISIVNQVSGYFV   120
LWS/OPN4 ICL1-3           IFVVTASVFTNGLVLAATMKSRSLRTPLNWILVNLAVADLAETVIASTISIVNQVSGYFV   120
LWS/OPN4 ICS              IFVVTASVFTNGLVLAATMKSRSLRTPLNWILVNLAVADLAETVIASTISIVNQVSGYFV   120

                                                                ICL2
LWS                       LGHPMCVLEGYTVSLCGITGLWSLAIISWERWMVVCKPFGNVRF-DAKLAIVGIAFSWIW   179
LWS/OPN4 ICL3             LGHPMCVLEGYTVSLCGITGLWSLAIISWERWLVVCKPFGNVRF-DAKLAIVGIAFSWIW   179
LWS/OPN4 ICL2-3           LGHPMCVLEGYTVSLCGITGLWSLAIISWERWLVVTRPLATFGVASKKLAIVGIAFSWIW   180
LWS/OPN4 ICL1-3           LGHPMCVLEGYTVSLCGITGLWSLAIISWERWLVVTRPLATFGVASKKLAIVGIAFSWIW   180
LWS/OPN4 ICS              LGHPMCVLEGYTVSLCGITGLWSLAIISWERWLVVTRPLATFGVASKKLAIVGIAFSWIW   180

LWS                       AAVWTAPPIFGWSRYWPHGLKTSCGPDVFSGSSYPGVQSYMIVLMVTCCIIPLAIIMLCY   239
LWS/OPN4 ICL3             SAVWTAPPIFGWSRYWPHGLKTSCGPDVFSGSSYPGVQSYMIVLMVTCCIIPLAIIMLCY   239
LWS/OPN4 ICL2-3           SAVWTAPPIFGWSRYWPHGLKTSCGPDVFSGSSYPGVQSYMIVLMVTCCIIPLAIIMLCY   240
LWS/OPN4 ICL1-3           SAVWTAPPIFGWSRYWPHGLKTSCGPDVFSGSSYPGVQSYMIVLMVTCCIIPLAIIMLCY   240
LWS/OPN4 ICS              SAVWTAPPIFGWSRYWPHGLKTSCGPDVFSGSSYPGVQSYMIVLMVTCCIIPLAIIMLCY   240

                                    ICL3
LWS                       LQVWLAIRAVAKQQKE------------SESTQKAEKEVTRMVVVMIFAYCVCWGPYTFF   287
LWS/OPN4 ICL3             LQIFRAIRETGRALQTFGACKGNGESLWQRQRLQSEKEVTRMVVVMIFAYCVCWGPYTFF   299
LWS/OPN4 ICL2-3           LQIFRAIRETGRALQTFGACKGNGESLWQRQRLQSEKEVTRMVVVMIFAYCVCWGPYTFF   300
LWS/OPN4 ICL1-3           LQIFRAIRETGRALQTFGACKGNGESLWQRQRLQSEKEVTRMVVVMIFAYCVCWGPYTFF   300
LWS/OPN4 ICS              LQIFRAIRETGRALQTFGACKGNGESLWQRQRLQSEKEVTRMVVVMIFAYCVCWGPYTFF   300

LWS                       ACFAAANPGYAFHPLMAALPAYFAKSATIYNPVIYVFMNRQFRNCILQL-------FGKK   340
LWS/OPN4 ICL3             ACFAAANPGYAFHPLMAALPAYFAKSATIYNPVIYVFMNRQFRNCILQL-------FGKK   352
LWS/OPN4 ICL2-3           ACFAAANPGYAFHPLMAALPAYFAKSATIYNPVIYVFMNRQFRNCILQL-------FGKK   353
LWS/OPN4 ICL1-3           ACFAAANPGYAFHPLMAALPAYFAKSATIYNPVIYVFMNRQFRNCILQL-------FGKK   353
LWS/OPN4 ICS              ACFAAANPGYAFHPLMAALPAYFAKSATIYNPVIYAITHPKYRVAIAQHLPCLGVLLGVS   360

                                  C-terminus
LWS                       VDDGSELSSASKTEVSSVSSVSPA-------------------------------------   364
LWS/OPN4 ICL3             VDDGSELSSASKTEVSSVSSVSPA-------------------------------------   376
LWS/OPN4 ICL2-3           VDDGSELSSASKTEVSSVSSVSPA-------------------------------------   377
LWS/OPN4 ICL1-3           VDDGSELSSASKTEVSSVSSVSPA-------------------------------------   377
LWS/OPN4 ICS              RRHSRPYPSYRSTHRSTLTSHTSNLSWISIRRRQESLGSESEVGWTHMEAAAVWGAAQQA   420

LWS                       -------------------------------------------                   364
LWS/OPN4 ICL3             -------------------------------------------                   376
LWS/OPN4 ICL2-3           -------------------------------------------                   377
LWS/OPN4 ICL1-3           -------------------------------------------                   377
LWS/OPN4 ICS              NGRSLYGQGLEDLEAKAPPRPQGHEAETPGKTKGLIPSQDPRM                   463
```

Figure 4.8. Human long-wave-sensitive/melanopsin chimeric opsins
(**A**) Human long-wave-sensitive (LWS) opsin activates transducin, $G_{t\text{-}c}$, which activates cGMP phosphodiesterase, resulting in a reduction in cyclic guanosine monophosphate (cGMP) second messenger concentration. (**B**) The activation of human melanopsin (OPN4) leads to the activation of its G protein partners G_q and G_{11}, which activate phospholipase C and lead to an increase in intracellular calcium. (**C**) Chimeric opsins were created and their G protein coupling properties were tested. A schematic of LWS opsin with the second and third intracellular loops (ICL) replaced with the corresponding sequence from melanopsin (LWS/OPN4 ICL2-3) is shown. (**D**) The intracellular loops and the C-terminus of LWS opsin (red) were replaced with the corresponding sequence from melanopsin (blue) to create four LWS/melanopsin chimeric opsins. All coding sequences featured a 3′ 1D4 tag when cloned into a pMT4 plasmid. This has been omitted for clarity. ICS, intracellular surface.

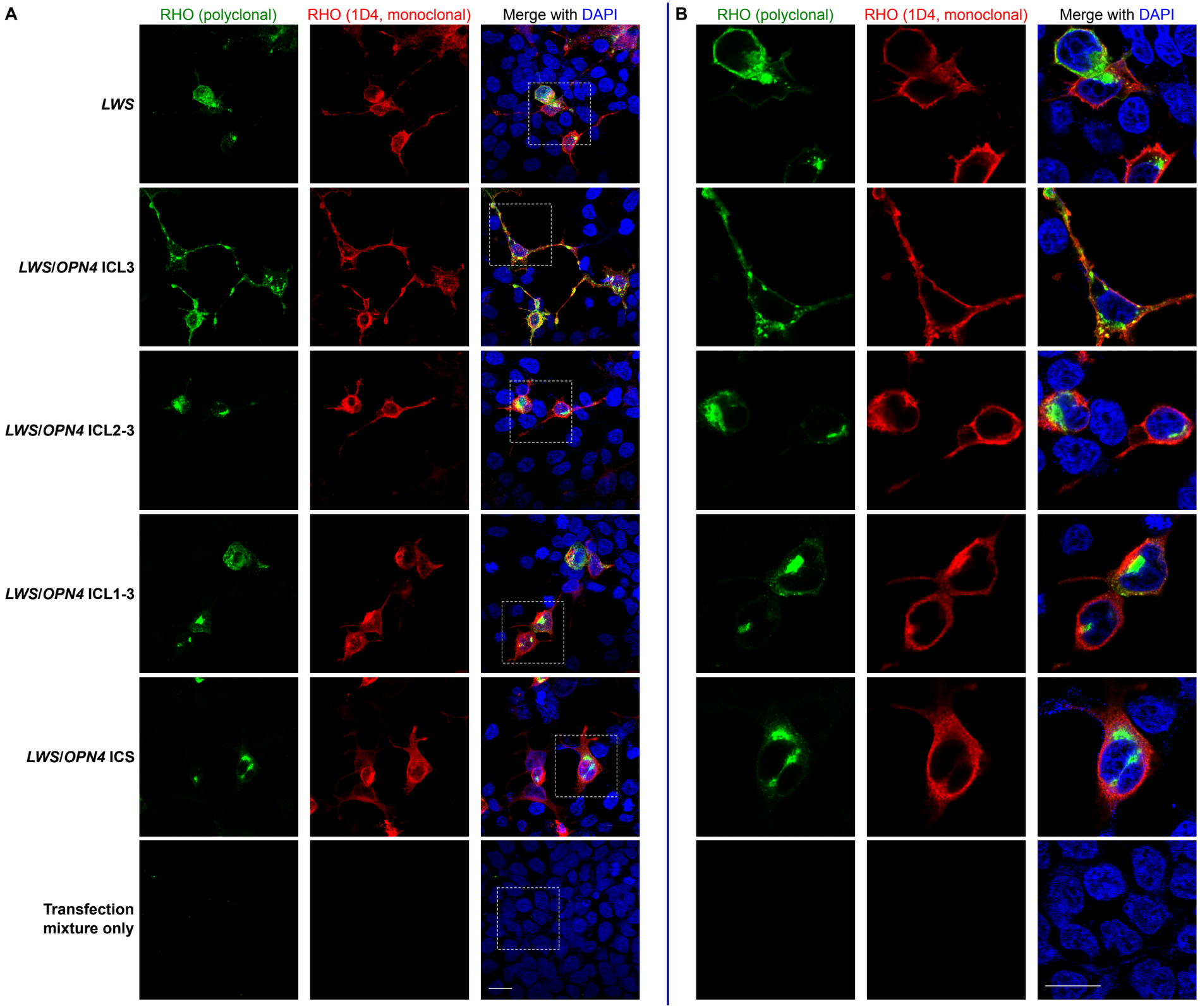
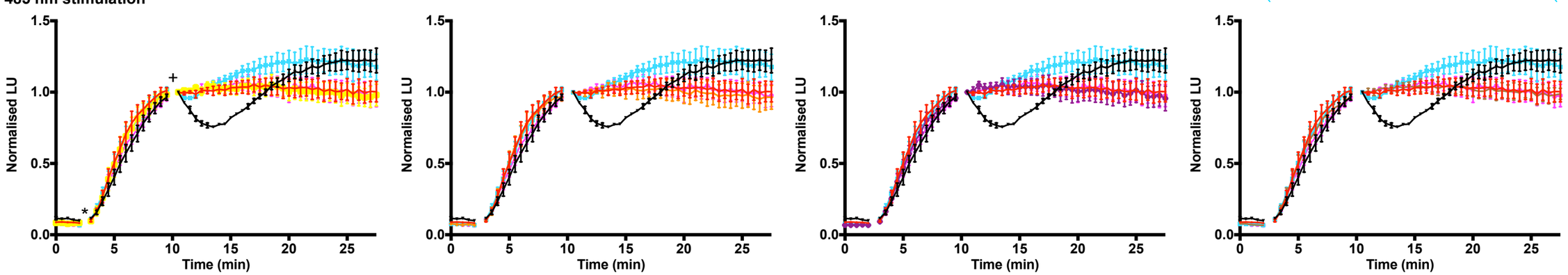
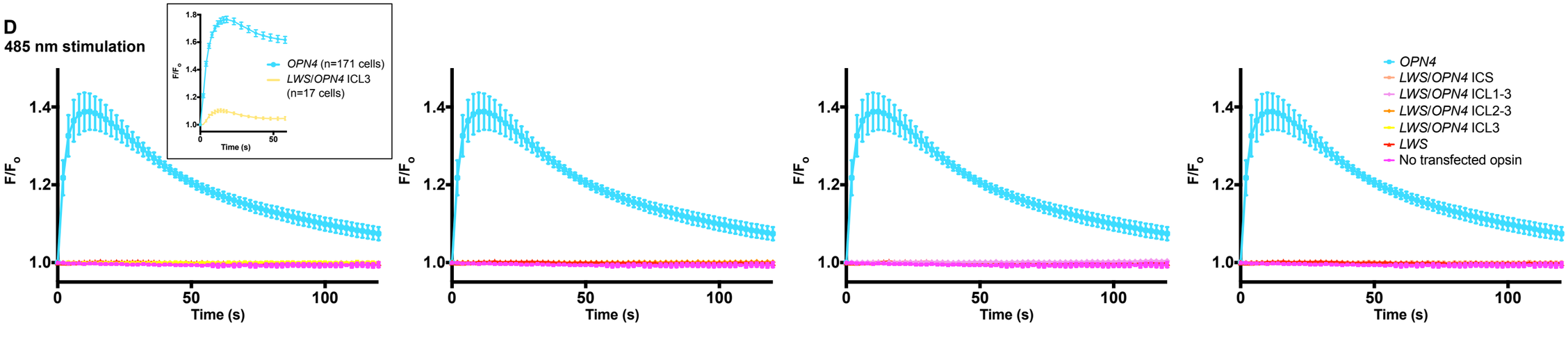


Figure 4.9. Immunocytochemistry of 293T cells expressing LWS/melanopsin chimeric opsins and wild type LWS opsin
Two days after transfecting with wild type long-wave sensitive (*LWS*) and *LWS*/melanopsin chimeric opsin plasmids (all 1D4 tagged), the cells were fixed and immunloabelled with a polyclonal (green) and monoclonal (red) antibodies against the 1D4 amino acid sequence of rhodopsin (RHO). Representative cells were imaged at (**A**) low (Z stack) and (**B**) high (single slice) magnification. The signal from the monoclonal antibody (red) was most concentrated at the plasma membrane in cells transfected with *LWS*, *LWS*/*OPN4* ICL3 and *LWS*/*OPN4* ICL2-3, but more evenly distributed in the cytoplasm in other transfected cells. The signal from the polyclonal antibody (green) was relatively weak at the plasma membrane and strong from foci in the cytoplasm in all chimeric opsin samples. ICS, intracellular surface. Scale bar represents 20 μm.

Figure 4.10. *In vitro* G_i and $G_{q/11}$ function of *LWS*/melanopsin chimeric opsins and wild type *LWS* opsin and melanopsin
(**A**) Schematic of long-wave-sensitive (LWS; red) opsin, LWS/melanopsin chimeric opsins and melanopsin (OPN4, cyan) with 11-*cis* retinal *in situ* in a plasma membrane. (**B**) The ability of LWS/melanopsin chimeric opsins, wild type LWS and melanopsin to couple to the G_i G protein pathway was assayed using GloSensor, a cAMP biosensor. The baseline bioluminescence level was measured before forskolin was added (*) to raise the baseline level of cAMP. The transfected 293T cells were then illuminated with 485 nm light (+) and the response measured. The response was normalised to the first reading after the light stimulation (mean ± s.e.m.; n = 4). (**C**) The same cAMP assay was run with a 544 nm light stimulus (n = 4). Neither assay caused *LWS* transfected cells to differ significantly from the response of cells transfected with only the GloSensor plasmid. (**D**) $G_{q/11}$ activity was tested using fluorescent calcium dyes. In a plate reader-based assay, transfected 293T cells were illuminated with 485 nm light. Data from the plate reader experiment suggested that none of the LWS/melanopsin chimeric opsins were capable of producing a calcium rise in response to light (n = 3). (**Inset**) However, when cells were stimulated with 535 – 565 nm light in a microscope-based assay, a small number of cells transfected with *LWS*/*OPN4* ICL3 responded with a small calcium rise. Only the fluorescence data from cells that responded to the light stimulus with a greater than 5% increase in fluorescence contributed to these traces. Each light-responsive cell was treated as an independent biological replicate (see panel for n values). F/F_o, fluorescence intensity relative to baseline fluorescence; ICL, intracellular loop; ICS, intracellular surface; LU, luninescence units.


A
LWS
LWS/OPN4 ICL3
LWS/OPN4 ICL2-3
LWS/OPN4 ICL1-3
LWS/OPN4 ICS
OPN4


B
485 nm stimulation
Normalised LU
Time (min)
C
544 nm stimulation
RHO
OPN4
LWS/OPN4 ICS
LWS/OPN4 ICL1-3
LWS/OPN4 ICL2-3
LWS/OPN4 ICL3
LWS
GloSensor only


D
485 nm stimulation
F/F0
Time (s)
OPN4 (n=171 cells)
LWS/OPN4 ICL3
(n=17 cells)
OPN4
LWS/OPN4 ICS
LWS/OPN4 ICL1-3
LWS/OPN4 ICL2-3
LWS/OPN4 ICL3
LWS
No transfected opsin

Signal from the polyclonal rhodopsin/1D4 antibody was notably different from that of the monoclonal antibody in cells transfected with each of the different *LWS*/melanopsin chimeras and wild type *LWS*. The signal from the polyclonal antibody was weaker at the plasma membrane and stronger at focal locations in the cytoplasm. The size of the bright focal areas of polyclonal antibody signal varied markedly.

4.2.2.b Functional assessment of *LWS*/melanopsin chimeric opsins

When expressed in cone photoreceptors, LWS opsin couples to cone α transducin, $G_{t\text{-}c}$, a member of the $G_{i/o}$ family of G proteins (Figure 4.8 A; Lerea et al. 1986). It was therefore hypothesised that LWS, like rhodopsin, would couple to 293T second messenger pathways and have a G_i-like effect on intracellular cAMP.

LWS-transfected 293T cells did not show light-induced changes in cAMP-dependent bioluminescence significantly different to negative control cells when stimulated with 485 nm or 544 nm filtered light from an internal plate reader xenon arc flash lamp (Figure 4.10 B and C). Stimulating *LWS* transfected cells with 544 nm light resulted in a pattern of signal that deviated slightly from that of the GloSensor-only control (Figure 4.10 C), but the amplitude of change was very small compared to that induced by rhodopsin stimulated with 485 nm light (Figure 4.10 B).

In an attempt to increase the extent of the light-induced LWS response, a number of variables were modified. Neither a brighter external xenon arc lamp filtered to emit 535 – 565 nm light nor a full-spectrum light notably increased the extent of the bioluminescence signal changes (data not shown). Adding 11-*cis* retinal, rather than 9-*cis* retinal, as the exogenous chromophore also failed to cause any change in the cAMP response characteristics to a light pulse (data not shown). Similarly, incubating transfected cells with 9-*cis* retinal for one day prior to imaging to provide a potential

chaperone (Noorwez et al., 2004; Insinna et al., 2012) also failed to change the nature of the cAMP response of light-stimulated *LWS*-transfected 293T cells (data not shown).

None of the *LWS*/melanopsin chimeric opsins were shown to produce a light-dependent calcium response in 293T cells when assayed using a plate reader. The traces of the four chimeric opsins and wild type LWS opsin were flat and indistinguishable from the no-opsin control (Figure 4.10 D). There was, however, a small number of responsive cells identified when the calcium assay was run on a fluorescence microscope. On two out of three days that independent experiments were run, responsive cells were identified following transfection with *LWS*/*OPN4* ICL3. From those two biological replicates a total of 17 cells were noted to be responsive out of a total of approximately 400 cells imaged. These responses were slower in their onset and much reduced in their intensity compared to the responses of melanopsin transfected cells (Figure 4.10 D, inset). No responses were seen in cells transfected with wild type *LWS* opsin or either of the other *LWS*/*OPN4* chimeric opsins.

Absorption spectroscopy was performed on *LWS*/*OPN4* ICS and *LWS* wild type-transfected 293T cells as an alternative assessment of photopigment function. Spectroscopy of LWS produced a maximum absorption of 558 nm, while LWS/OPN4 ICS did not form a functional photopigment (Figure 4.11).

4.3 Discussion

4.3.1 Rhodopsin/melanopsin chimeric opsins are able to couple to two G protein pathways

These experiments have demonstrated that substituting the intracellular surface of one opsin with that from another opsin can confer novel properties to the chimeric opsin. Combining rhodopsin extracellular and transmembrane sequences with melanopsin intracellular sequences created chimeric opsins that had some biological properties intermediate between the properties of the two wild type opsins.

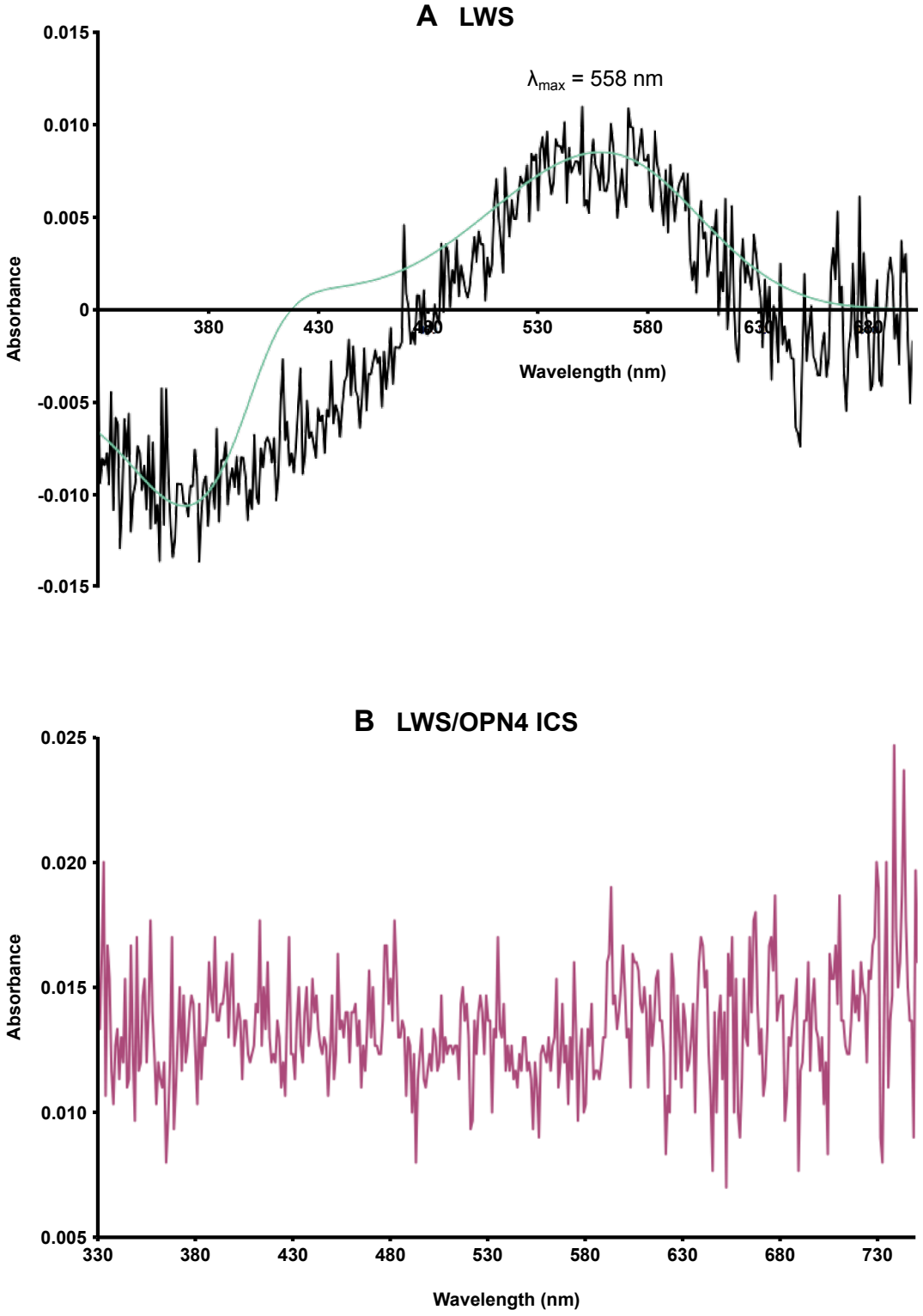


Figure 4.11. Absorption spectra of *in vitro* generated wild type LWS and a LWS/melanopsin chimeric opsin (**A**) Difference absorbance spectrum of wild type LWS opsin reconstituted with 11-*cis* retinal. A Govardovskii rhodopsin/vitamin-A_1 template (green line) allowed the wavelength of maximum absorption (λ_{max}) to be calculated as 558 nm. (**B**) Following the same procedure using 293T cells transfected with the *LWS*/*OPN4* ICS chimeric opsin (*LWS* with the intracellular sequences replaced with the corresponding sequences from melanopsin (*OPN4*)) failed to produce an interpretable difference absorbance spectrum. Difference spectra were calculated by subtracting the bleached spectrum from the dark spectrum.

Replacing just the third intracellular loop of rhodopsin with that from melanopsin was sufficient to produce responses in a calcium assay of $G_{q/11}$ function, when wild type rhodopsin had no apparent effect. This modification to rhodopsin came at the expense of reduced function in a cAMP assay of G_i activity, a result similar to that seen by Kim and colleagues (2005). Modifying the second and third loop changed the properties further, with greater $G_{q/11}$ activity and less G_i activity. Additional changes to rhodopsin led to chimeric opsins with minimal G_i activity and $G_{q/11}$ activity that had rapid onset but which was smaller in magnitude than melanopsin.

The difference in onset kinetics observed between the calcium response traces from the plate reader and the microscope-based imaging is likely due to the different techniques, rather than true biological differences. The plate reader assay served as an effective, high-throughput screening tool, but had the disadvantage of averaging the signal from a large number of responsive and non-responsive cells. In contrast, the fluorescence microscopy-based assay examined far fewer cells, but gathered cell-level data. Since the signal from the plate reader was proportional to the efficiency of the entire process — from transfection through to light-induced biochemical changes — it provided a valuable analogy for injecting a set amount of AAV vector and detecting changes in retinal light sensitivity. The use of different fluorescent calcium dyes for the two techniques is unlikely to be a critical factor.

The functional activity of the rhodopsin/melanopsin chimeric opsins correlate with the immunocytochemistry results. Wild type rhodopsin and all rhodopsin/melanopsin chimeric opsins, except RHO/OPN4 ICS, were concentrated at the plasma membrane when transfected into 293T cells. *RHO*/*OPN4* ICS transfected cells were notably more rounded with fewer processes than cells transfected with other chimeric opsins and opsin was more evenly distributed in the cytoplasm. Such a difference between the appearance of opsin-expressing cells has been seen by other groups when studying

mutant opsins (Sung et al., 1991; Davies et al., 2012). This data suggests that RHO/OPN4 ICS may not be effectively trafficked to the plasma membrane and could explain why the $G_{q/11}$ coupling efficiency of RHO/OPN4 ICS was similar to, and not better than, that of RHO/OPN4 ICL1-3.

Of significance was the discrepancy between the patterns of immunolabelling when the same opsin transfected cells were double labelled with polyclonal and monoclonal rhodopsin/1D4 antibodies. The peptide sequence that the two antibodies were raised against differs by only two amino acids, but their results were notably distinct in cells transfected with *RHO*/*OPN4* ICL2-3, *RHO*/*OPN4* ICL1-3 and *RHO*/*OPN4* ICS. In these samples, the polyclonal antibody predominantly labelled areas of the cytoplasm, with relatively little signal originating from the plasma membrane. It is thought that the monoclonal antibody may recognise an epitope that is specific to correctly folded opsin, while the polyclonal antibody recognises this epitope less efficiently and has greater relative affinity for other forms of the primary structure. The strongly labelled areas in the cytoplasm may therefore represent areas of immature or misfolded opsin. In the case of RHO/OPN4 ICS, the cytoplasmic areas immunolabelled by the polyclonal antibody appear similar to aggresomes of aggregated misfolded opsin documented by other groups studying rhodopsin mutants (Saliba et al., 2002). Further co-localisation studies using markers, such as vimentin or Hsc70 (Saliba et al., 2002), would be useful to confirm these areas as aggresomes.

4.3.2 Distinct chromophore requirements of wild type and chimeric opsins

The chromophore requirements of melanopsin differed from that of rhodopsin and the rhodopsin/melanopsin chimeric opsins. Wild type melanopsin transfected cells had a consistent calcium response whether or not exogenous 9-*cis* retinal was added. In contrast, no calcium or cAMP response was elicited from rhodopsin or

rhodopsin/melanopsin chimeric opsins without the addition of 9-*cis* retinal. These data lend support to the argument that melanopsin is bistable (Mure et al., 2009; Matsuyama et al., 2012) (or perhaps tristable (Emanuel and Do, 2015)) and is therefore able to utilise chromophore, such as all-*trans* retinal, that cannot form a stable association with visual opsins. To confirm this it would be of interest to perform liquid chromatography to detect which chromophores are present in the cell culture medium (Landers and Olson, 1988; Nöll, 1996).

4.3.3 Human chimeric opsins display advantages as optogenetic tools over other chimeric opsins

When compared to Opto-α_1AR, a bovine rhodopsin-based chimeric opsin developed by another research group (Airan et al., 2009), the human rhodopsin/melanopsin chimeric opsins displayed properties more suitable for use as optogenetic tools. The rhodopsin/melanopsin chimeric opsins showed faster onset and a greater magnitude of calcium rise. An additional difference was that Opto-α_1AR continued to increase in calcium signal during the imaging period, while rhodopsin/melanopsin chimeric opsins began to return to baseline. To improve temporal resolution a transient response is generally more desirable in optogenetics, making this a less appealing property of Opto-α_1AR.

4.3.4 Challenges of obtaining G protein functional data for LWS opsin

To have a $G_{q/11}$ signalling optogenetic tool with fast light-response kinetics and more red-shifted in its absorption properties, human LWS opsin was modified by substitution of its intracellular surface with the corresponding sequence from human melanopsin. LWS/melanopsin chimeric opsins proved far less successful than the rhodopsin/melanopsin chimeric opsins.

It was hypothesised that LWS opsin would, like rhodopsin, be able to couple to second messenger networks in 293T cells and produce a light-induced decrease in the signal from a cAMP-dependent bioluminescent biosensor. However, the data suggests that in our set of experimental conditions LWS-opsin did not couple to cAMP networks as efficiently as rhodopsin did. Changing experimental variables including the wavelength and intensity of the light stimulus, the chromophore applied and providing chromophore as a candidate chaperone, all failed to produce a light-dependent change in cAMP that was substantially different to negative control samples or resembled the response from rhodopsin-transfected cells. Without a cAMP response in *LWS* transfected cells, it was not possible to conclude how LWS/melanopsin chimeric opsins differed in their G protein signalling properties relative to wild type LWS opsin.

Data from absorption spectroscopy of wild type LWS opsin indicated that a functional photopigment was formed. The shape of the absorption spectrum was similar to that expected for an opsin (Govardovskii et al., 2000) and the maximum absorption of the LWS opsin sample, 558 nm, was similar to the results from other groups (552 – 562 nm; Merbs and Nathans, 1992, 1993; McClements et al., 2013). The failure to detect light-induced changes in cAMP levels in cells transfected with *LWS* may, therefore, be due to wild type LWS opsin not effectively coupling to the same 293T cell second messenger pathways that rhodopsin is able to, rather than due to not forming a functional, correctly folded opsin. These results suggest that LWS opsin may be more specific in its binding to G protein partners compared to rhodopsin; it may not be able to couple to G_i, as the more promiscuous rhodopsin does. Given the inefficiency with which cone opsin activates cone transducin, relative to rhodopsin activating rod transducin (Tachibanaki et al., 2001), it is perhaps not unexpected that LWS opsin would be even less effective at activating a non-native Gα subunit. LWS opsin's Gα specificity could be further tested by conducting a transducin activation assay (Terakita

et al., 2002; Ala-Laurila et al., 2009) or using real time fluorescence-based methods (Imamoto et al., 2013).

Aside from wild type LWS, only one of the LWS/melanopsin chimeric opsins produced responsive cells when assessed by calcium assays of $G_{q/11}$ function. Individual cells examined using fluorescence microscopy showed responsive 293T cells transfected with *LWS*/*OPN4* ICL3. Responsive cells were rare (<5% of cells) and their responses were small, and hence not detected by the plate reader assay, which averaged a relatively large area of responsive and non-responsive cells.

The pattern of immunolabelling in 293T cells transfected with *LWS* and *LWS*/melanopsin chimeric opsins provides some insight into why LWS/OPN4 ICL3 and wild type LWS may have been the only proteins of the group to produce any evidence of function. LWS/OPN4 ICL3 and wild type LWS were more concentrated at the plasma membrane and had smaller focal areas of signal from the cytoplasm, compared to the other LWS/melanopsin chimeric opsins. This suggests that LWS and LWS/OPN4 ICL3 are more efficiently trafficked to the plasma membrane than the other LWS/melanopsin chimeric opsins. Misfolding of the other LWS/melanopsin chimeric opsins may cause them to aggregate in the cytoplasm. It would be useful to complete absorption spectroscopy on all remaining chimeric opsins to confirm whether their function in the $G_{q/11}$ and G_i assays correlates with the ability of these chimeric opsins to form functional photopigments.

4.3.5 Chimeric opsins as candidate optogenetic tools for vision restoration

The aim of creating chimeric opsins was to have an optogenetic tool that combined the desirable functional properties of a visual opsin and melanopsin. While the rhodopsin/melanopsin chimeric opsins did show that changing the intracellular surface

to melanopsin sequence could increase signalling via the $G_{q/11}$ pathway, the fast onset and offset properties of rhodopsin were not evident in the $G_{q/11}$ assay.

This study also demonstrated that no chimeric opsin functioned as efficiently as the wild type opsins in either a $G_{q/11}$ or G_i assay, indicating that the wild type structure is well evolved to efficiently couple to its native pathways and that modification of this structure is unlikely to improve coupling to the native pathway or facilitate efficient coupling to a non-native second messenger system. The complex nature of the three dimensional structure of opsins (Palczewski, 2000) and their subsequent conformational changes upon activation (Scheerer et al., 2008) and release of chromophore (Park et al., 2008), means that prediction of the composition and functional role of the intracellular loops of opsins is challenging. Rhodopsin is the only opsin for which a crystal structure is available (Palczewski, 2000; Park et al., 2008), therefore predictions of the structure of other opsins must be based on assumptions of how other opsins relate to rhodopsin. Hydrophobicity-based predictions, as used in this study, go some way to mapping the structure of an opsin of unknown structure (Crasto, 2010), such as LWS opsin or melanopsin, onto that of rhodopsin. However, without a definitive high-resolution structural model of activated and inactivated melanopsin and LWS opsin the identity and role of different amino acid residues in the structure and function of these opsins will be subject to approximations. Therefore, the chimeric opsins created in these experiments are unlikely to represent the most optimal chimeric sequences as complete knowledge of the structure and functional role of each part of the opsin sequence is currently unavailable. As knowledge of the structure of opsins develops, it may be possible to rationally design chimeric opsins that are more effective at coupling to specific G protein intracellular pathways.

While these studies provided useful insights into the structure/function relationship of human opsins, the functional limitations of the chimeric opsins meant that none were

chosen for *in vivo* study. To definitively conclude that these chimeric opsins offer no unique advantages, these constructs should be tested in the target retinal neurons, whose light-response kinetics may differ significantly from 293T cells.

Compared to LWS opsin, rhodopsin is more suitable for the creation of chimeric opsins because (a) there is a reliable *in vitro* assay to assess its function and (b) this study suggests that the rhodopsin structure is more tolerant of modification.

However, ultimately, this study only tested a small set of chimeric opsins. Given the length of primary amino acid sequences of rhodopsin, LWS opsin and melanopsin, there are millions of potential chimeric opsin permutations. If a chimeric opsin is to be optimised for a particular property, subsequent studies could attempt a point mutation or directed evolution approach (Garriga et al., 1996; Pei et al., 2008; Dong et al., 2010).

In summary, the primary aim of this chapter was achieved by gaining functional data on the chimeric opsins that were created using the transmembrane and extracellular sequences of either human rhodopsin or LWS opsin and the intracellular sequences from human melanopsin. By achieving this aim, it was determined that none of the rhodopsin/melanopsin or LWS opsin/melanopsin chimeric opsins created through this approach had functional properties desirable of an optogenetic tool for vision restoration. In reaching this conclusion, the secondary aim of gaining a greater understanding of the structure/function relationships of the opsins tested was achieved.

A greater understanding of the function and structural stability of rhodopsin/melanopsin chimeric opsins was gained, relative to LWS opsin/melanopsin chimeric opsins. A cAMP assay was successful in quantifying the response to light of wild type rhodopsin and rhodopsin/melanopsin chimeric opsins, while the same assay did not produce an interpretable response from wild type LWS and LWS/melanopsin-expressing 293T cells, therefore limiting the data that could be gained from LWS opsin/melanopsin

chimeric opsins. Immunocytochemistry and absorption spectroscopy of 293T cells transfected with LWS opsin/melanopsin chimeric opsins suggested that aggresomes were formed even with minimal changes to the primary sequence, while rhodopsin/melanopsin chimeric opsins required more extensive modifications of the primary sequence before such aggresomes were identified on immunocytochemistry studies. This suggests that human rhodopsin is more amenable to the sequence modifications that this study produced.

In addition to the structural stability data, the calcium assay for $G_{q/11}$ function successfully demonstrated that by replacing the intracellular loops of rhodopsin with the corresponding sequence from melanopsin, the tendency of the chimeric opsin to signal via the $G_{q/11}$ pathway normally activated by melanopsin could be increased. As found for other GPCRs, the second and third intracellular loops were particularly important for defining which intracellular signaling pathway the opsin activated (Wess, 1997; Iiri et al., 1998; Terakita et al., 2002).

Fusion

The process or result of joining two or more things together to form a single entity.

mid 16th cent.: from Latin *fusio(n-)*, from *fundere* **'pour, melt'**.

5

Opsin–G protein Fusion Proteins as Optogenetic Tools for Vision Restoration

5.1 Introduction

A strategy that this research project explored to improve the efficacy of human opsins as optogenetic tools for restoring sight was to fuse human opsin apoproteins with human Gα subunits. It was hypothesised that opsin–G protein fusion proteins could be more effective than endogenous proteins at converting light into a biochemical response in target cells and that this would lead to improved visual outcomes.

Like all GPCRs, opsins activate heterotrimeric G proteins, which in turn activate intracellular effector molecules that change cellular function. Each G protein consists of α, β and γ subunits. The Gβ and Gγ subunits are usually found in close association with each other and is collectively termed the Gβγ subunit. It is the Gα subunit that largely determines the signalling specificity of a GPCR (Arshavsky et al., 2002). Gα subunits are activated by the exchange of bound GDP for GTP (Oldham and Hamm, 2008). The Gα and Gβγ subunits are mutually dependent on each other for correct plasma membrane localisation (Evanko et al., 2001; Michaelson et al., 2002; Takida and Wedegaertner, 2003). It is hypothesised that the increased expression of an opsin–Gα

fusion protein may induce increased synthesis and/or membrane localisation of the Gβ and Gγ subunits required for effective signalling.

G_q and G_{11} are the two endogenous Gα subunits that were selected for fusion to melanopsin and rhodopsin. Although G_q and G_{11} are ubiquitous throughout the retina (Hughes et al., 2014) and the body (Strathmann and Simon, 1990; Wilkie et al., 1991; Hubbard and Hepler, 2006), it was hypothesised that high levels of expression of $G_{q/11}$-coupled opsin in cells that do not normally express opsins could saturate the existing pathways and limit the potential for an optogenetic gene therapy to restore sight. The dissociation of GDP from the Gα subunit is usually the rate-limiting step in the G protein cycle (Ferguson et al., 1986).

The efficiency of GPCR signalling depends on the relative and absolute concentrations of GPCRs and G proteins (Seifert et al., 1999b). In rods, reducing the density of rhodopsin increases the rate of light response onset and recovery by enabling more frequent protein–protein contacts between phototransduction proteins (Calvert et al., 2001). Providing an opsin with a fused Gα subunit ensures that there is a 1:1 ratio of opsin to Gα subunit and that the opsin is in close proximity to a Gα subunit.

By creating melanopsin and rhodopsin $G_{q/11}$ fusion proteins, two separate hypotheses could be tested. The melanopsin–G protein fusion proteins tested whether covalently fusing an opsin to its native G protein partners could enhance the signalling characteristics of the opsin. This hypothesis is supported by the finding of previous studies which showed that fusion proteins have more efficient coupling with the fused G protein than the endogenous G protein (Bertin et al., 1994; Wenzel-Seifert et al., 1998). On the other hand, the rhodopsin–G protein fusion proteins tested whether fusing non-native G protein partners to the C-terminus of an opsin could increase the probability of an opsin signalling via the pathway of the fused G proteins.

GNAQ and *GNA11*, the genes that encode the Gα subunits G_q and G_{11}, respectively, were both used to create separate opsin–G protein fusion constructs. Although human *GNAQ* and *GNA11* are very similar, with 90% amino acid identity, both were tested in case there was a significant functional difference between them.

Although it is not yet known how G_q and G_{11} interact with melanopsin, evidence from other GPCRs and G proteins suggests that the C-terminus of Gα subunits is a critical region for determining specificity. The C-terminus of transducin has been found to interact with activated rhodopsin (Garcia et al., 1995; Janz and Farrens, 2004) and studies of chimeric G proteins have also demonstrated the importance of the C-terminus to GPCR interactions (Conklin et al., 1993). The opsin–G protein fusion proteins created for these experiments, like those of other GPCR–G protein fusion studies (Bertin et al., 1994; Seifert et al., 1998a; Grisshammer and Hermans, 2001), involved fusing the C-terminus of the opsin with the N-terminus of the Gα subunit. Such an arrangement should therefore allow the C-terminus of the Gα subunit to be free to interact with the intracellular surface of the opsin.

It is understood that this is the first study to investigate the properties of opsin–G protein fusion proteins. However, GPCR–Gα subunit fusions have been created by other research groups to study a number of properties of G proteins and GPCRs (Seifert et al., 1999b). The signalling efficiency of different G proteins was tested by fusing different G proteins to the same GPCR (Seifert et al., 1998b). Some G proteins that function in the unfused stated have been found to be ineffective when fused (Sautel and Milligan, 1998). It has also been found that GPCRs can interact with G proteins other than that which it is fused to (Burt et al., 1998).

In this series of experiments, four opsin–G protein fusion constructs were cloned by creating a single open reading frame of melanopsin or rhodopsin and G protein, q

polypeptide (*GNAQ*) and G protein, alpha 11 (*GNA11*; Figure 5.1 A and B). The fusion constructs were cloned and tested *in vitro* by immunocytochemistry and western blotting as well as functionally tested by $G_{q/11}$ and G_i assays. Based on encouraging *in vitro* results, melanopsin–*GNA11* and wild type melanopsin were packaged into AAV2/2(7m8) and delivered intravitreally into the eyes of retinally degenerate mice. Tests of light sensitivity at the cellular and retina level were not able to determine any functional differences between melanopsin or melanopsin–GNA11 fusion protein, but low expression levels made the results inconclusive.

Aims

- Clone and functionally test human opsin–Gα subunit fusions proteins to determine if any such fusion proteins have properties that make them useful as optogenetic tools for vision restoration.
- Develop an understanding of structure/function relationships of human opsin–Gα subunit fusions proteins through functional testing.

5.2 Results

5.2.1 *In vitro* testing of melanopsin– and rhodopsin–G protein fusion proteins

293T cells transfected with melanopsin–G protein plasmids were immunolabelled with an anti-human melanopsin antibody (Figure 5.1 C). A strong signal was visible for all constructs, even those with C-terminal fused G proteins despite the antibody's target epitope being the C-terminus of melanopsin. Immunofluorescence was most concentrated at the plasma membrane of a majority of cells, while in others it appeared to be more evenly distributed throughout the cytoplasm. This technique did not suggest that aggresomes were present (Saliba et al., 2002).

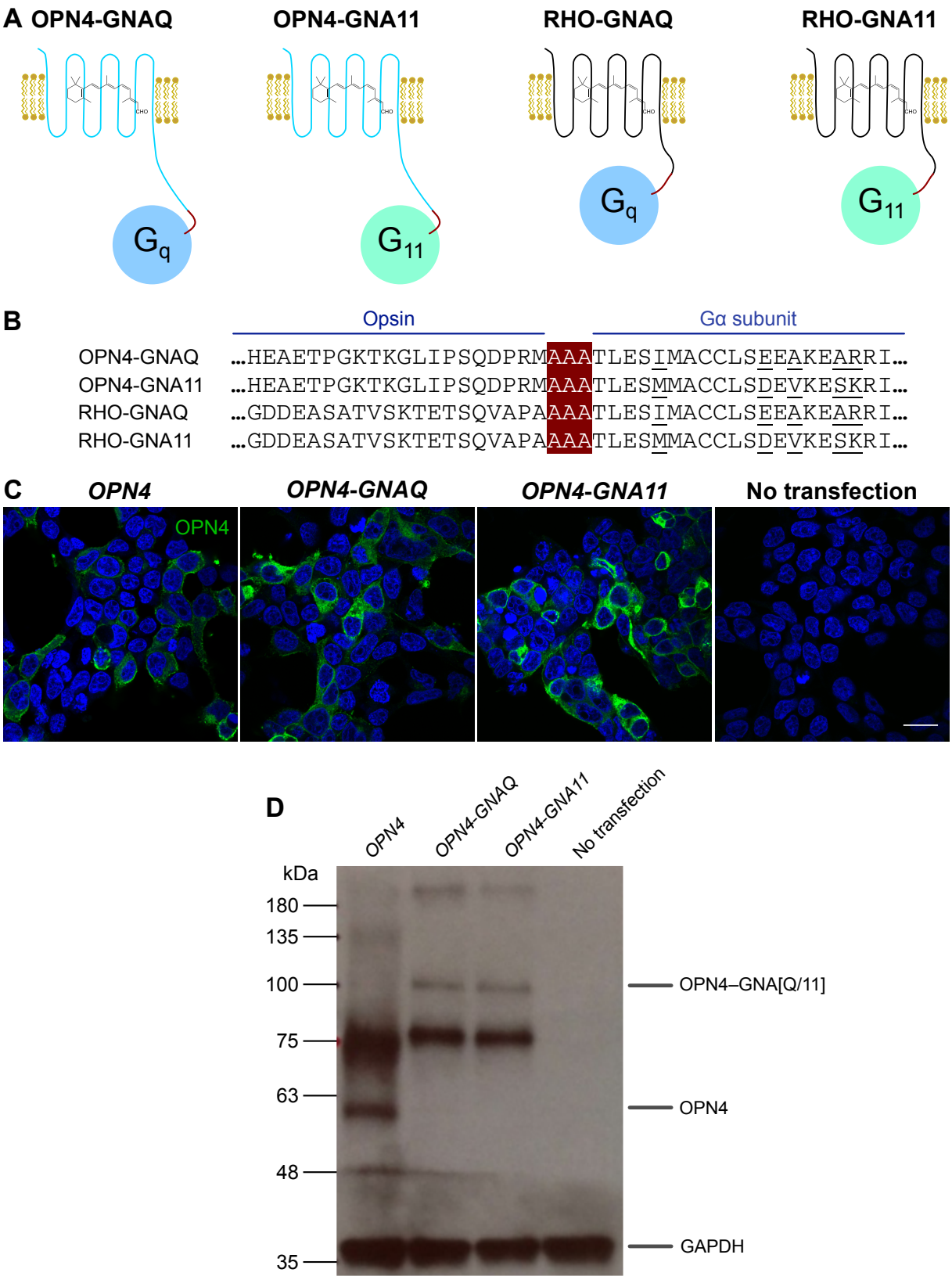


Figure 5.1. Heterologus expression of melanopsin and melanopsin fusion proteins in 293T cells
(**A**) Schematics of melanopsin– (OPN4) and rhodopsin– (RHO) G protein fusion proteins. By creating an open reading frame that included the opsin cDNA sequence and that of either *GNAQ* (G_q) or *GNA11* (G_{11}) fusion constructs were able to be cloned. (**B**) Between the primary structure of the opsin and the Gα subunit was a linker sequence of three alanine residues (highlighted in red). G_q and G_{11} share 90% of their primary structure. Differences are underlined. (**C**) 293T cells transfected with melanopsin and the melanopsin fusions showed a similar pattern of immunolabelling with an anti-human melanopsin antibody (green), with the strongest signal at the plasma membrane. Scale bar represents 20 μm. (**D**) Western blotting for human melanopsin (top half of blot) and GAPDH (bottom half) showed melanopsin and melanopsin fusion proteins to be of the expected size (53 and 95 kilodaltons (kDa)).

Western blot analysis was used to confirm that full-length melanopsin–G protein fusion proteins were being synthesised by 293T cells (Figure 5.1 D). Bands of approximately the predicted sizes of melanopsin and the two melanopsin–G protein fusion proteins (53 and 95 kDa, respectively) were identified. Protein bands at larger molecular weights (approximately 200 kDa) were present in the melanopsin–G protein lanes. These may represent oligomeric forms of the proteins (Suda et al., 2004).

The anti-melanopsin western blot also detected a band of approximately 75 kDa in size in samples from 293T cells transfected with melanopsin or melanopsin–G protein fusion proteins but not from the no-transfection control. The molecular identity of this band was not able to be confirmed. Performing a western blot using an alternative anti-melanopsin antibody did not produce an interpretable result (data not shown).

5.2.1.a $G_{q/11}$ activity of opsin–G protein fusion proteins

To determine whether fusing a G protein subunit to an opsin enhanced the opsin's G protein signalling capabilities, 293T cells were transfected with wild type melanopsin, rhodopsin and the four melanopsin– and rhodopsin–G protein fusion plasmids. Cells were tested for their $G_{q/11}$ signalling activity in a plate reader-based assay using fluorescent calcium dye.

Melanopsin–G protein fusion proteins produced light-induced calcium responses that were indistinguishable from those of wild type melanopsin in both the magnitude and kinetics of the responses (Figure 5.2 A). In contrast, the plate reader assay was not able to detect any significant light-induced calcium responses in cells transfected with rhodopsin–G protein fusion plasmids (Figure 5.2 A).

To study the effects of rhodopsin–G protein fusion proteins in more detail, transfected 293T cells were also examined for their light-induced calcium responses in a fluorescence microscopy-based assay to enable individual cells responses to be

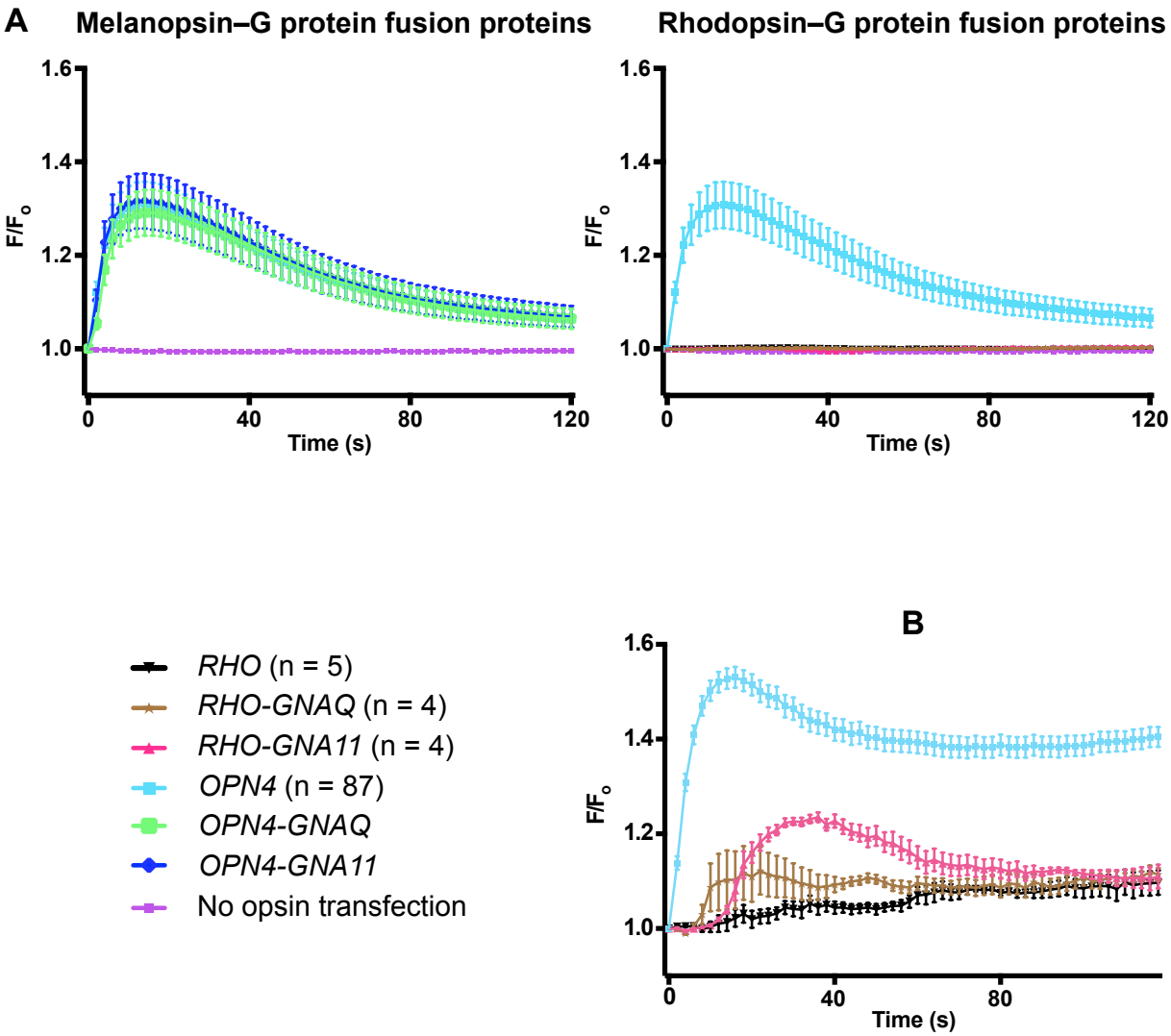


Figure 5.2. $G_{q/11}$ activity of melanopsin– and rhodopsin–G protein fusion proteins in 293T cells
(**A**) In this plate reader-based assay, melanopsin–G protein fusion transfected cells responded very similarly to cells transfected with wild type melanopsin (*OPN4*) with rapid inceases in light-induced fluorescence. Rhodopsin–G proteins behaved similarly to wild type rhodopsin (*RHO*) and did not induce any significant calcium response (mean ± s.e.m.; n = 6 experimental biological replicates). (**B**) To examine rhodopsin–G proteins more closely individual transfected cells were analysed for their light-induced calcium responses. A very small number of cells were identified as responding to the light stimulus (4 – 5 cells out of approximately 400 imaged cells). The kinetics of those responses were slow and of low magnitude (see key for number of cells treated as biological replicates). F/F_o, fluorescence intensity relative to baseline fluorescence.

recorded. By imaging approximately 400 cells, a very small number (four or five) transfected with rhodopsin or rhodopsin–G protein fusions were observed to have a greater than 5% increase in fluorescence during the imaging period. The calcium responses were slow and of small magnitude compared to those of melanopsin transfected cells (Figure 5.2 B).

5.2.1.b Small interfering RNA knockdown of 293T cell endogenous G proteins

293 cells are known to express relatively high levels of *GNAQ* (Atwood et al., 2011) raising the possibility that the levels of GNAQ and GNA11 in 293T cells could be much higher than those in retinal cells targeted for optogenetic gene therapy. This would mean that G protein availability would not be the rate limiting factor in 293T cells, as it might be in degenerate retinal cells.

To overcome this limitation in our *in vitro* model, small interfering RNA (siRNA) targeting the untranslated regions of the endogenous *GNAQ* and *GNA11* messenger RNA (mRNA) transcripts were utilised to lower the levels of GNAQ and GNA11 in the 293T cells used to assay $G_{q/11}$ activity.

By transfecting 293T cells with siRNAs that targeted the 3′ untranslated region of endogenous *GNAQ* and *GNA11* mRNA transcripts, the level of *GNAQ* and *GNA11* detected by quantitative PCR (qPCR) decreased to 10 to 20% of the levels detected in 293T cells transfected with a negative control siRNA (Figure 5.3 A). The level of transcript knockdown was similar whether the two siRNAs were used singly or in combination.

To assess the impact that reducing endogenous levels of GNAQ and GNA11 would have on $G_{q/11}$ signalling characteristics, 293T cells were cotransfected with anti-*GNAQ* and anti-*GNA11* siRNA and either melanopsin or one of the melanopsin–G protein plasmids. The percentage of cells transfected with wild type melanopsin that responded

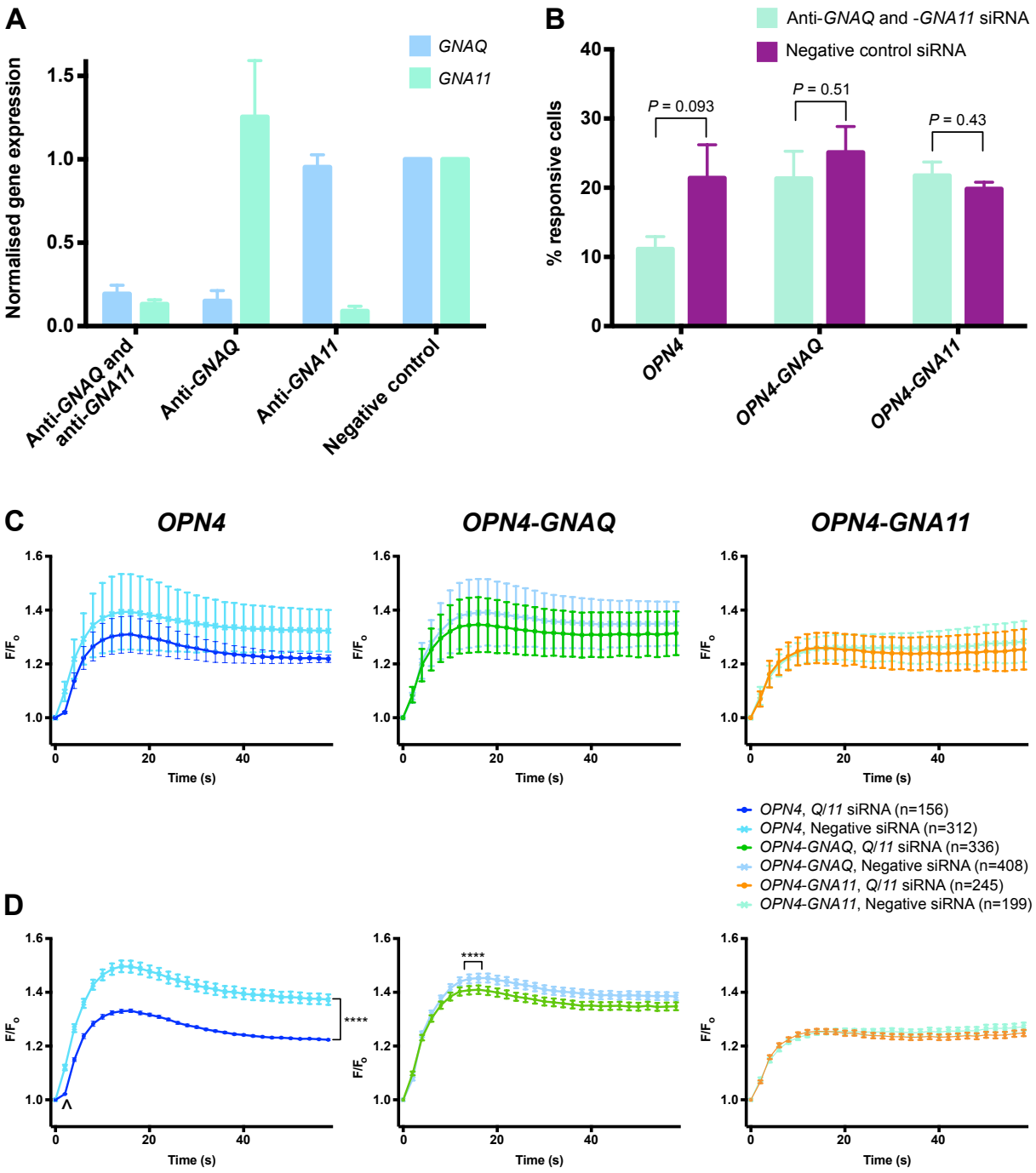


Figure 5.3. The effects of siRNA knockdown of endogenous G proteins on melanopsin and melanopsin–G protein calcium responses

(**A**) Anti-*GNAQ* and anti-*GNA11* siRNA reduced the level of endogenous Gα subunit mRNA in 293T cells to 10 – 20% of the level in cells transfected with negative control siRNA (mean ± s.e.m.; n = 2). (**B**) Cotransfection with anti-*GNAQ* and anti-*GNA11* siRNA and either melanopsin or melanopsin–G protein plasmids and loading with Rhod-2 fluorescent calcium dye enabled the response rate in conditions of lowered endogenous Gα subunits to be analysed. The percentage of cells that responded to a light stimulus was lower in cells cotransfected with melanopsin (*OPN4*) and anti-*GNAQ* and anti-*GNA11* siRNA than in cells cotransfected with melanopsin and negative control siRNA (unpaired *t* tests *P* values; n = 4, *OPN4* and *OPN4-GNAQ*; n = 3, *OPN4-GNA11*). (**C**) The kinetics of the light-responsive cells were similar for the melanopsin–G protein fusion groups, while melanopsin transfected cells showed a difference when endogenous Gα subunit transcripts were knocked down by siRNA (n = 4, *OPN4* and *OPN4-GNAQ*; n = 3, *OPN4-GNA11*). (**D**) When individual responsive cells were considered as independent experimental replicates, the difference between the response kinetics of melanopsin-transfected cells was more appreciable, while the similarities of the melanopsin–G protein fusions responses were maintained. Statistically significant ($P < 0.0001$) differences in area under the curve (*OPN4*: 72.5 ± 0.8, 81.2 ± 1.1 arbitrary units) and time to peak fluorescence (*OPN4-GNAQ*: 13.5 ± 0.3 s with anti-*GNAQ* and anti-*GNA11* siRNA, 16.2 ± 0.3 s with negative control siRNA) are denoted by ****. Note the slight onset delay in cells transfected with melanopsin and anti-*GNAQ* and anti-*GNA11* siRNA (^) (see key for number of cells treated as biological replicates). F/F_o, fluorescence intensity relative to baseline fluorescence; *Q/11* siRNA, anti-*GNAQ* and anti-*GNA11* siRNA.

to the light stimulus was lower in cells cotransfected with anti-*GNAQ* and anti-*GNA11* siRNA, compared to the negative control siRNA group (11 ± 1.8% and 21 ± 4.8%, respectively; $P = 0.093$, unpaired *t* test, two tailed, n = 4; Figure 5.3 B). In contrast, the response rates were similar for melanopsin–*GNAQ* (21 ± 3.9% with anti-*GNAQ* and anti-*GNA11* siRNA and 25 ± 3.7% with negative control siRNA; $P = 0.51$; n = 4) and melanopsin–*GNA11* (22 ± 2.0% and 20 ± 1.0%; $P = 0.43$; n = 3) regardless of whether G proteins were knocked down or not (Figure 5.3 B).

In the presence of anti-*GNAQ* and anti-*GNA11* siRNA the kinetics of the calcium response in 293T cells cotransfected with wild type melanopsin were attenuated relative to the response of cells that received negative control siRNA (Figure 5.3 C and D). When each complete repetition of the experiment is considered as a single biological replicate the difference between the areas under the curves of the responsive melanopsin transfected cells are not statistically significant ($P = 0.43$, unpaired *t* test, two tailed; n = 4; Figure 5.3 C). However, if each responsive cell is considered to be a biological replicate then the difference in areas under the curves are highly statistically significant (72.54 ± 0.80 and 81.17 ± 1.10 arbitrary units for melanopsin with anti-*GNAQ* and anti-*GNA11* siRNA (n = 156) and melanopsin with negative control siRNA (n = 312), respectively; $P < 0.0001$, unpaired *t* test, two tailed; Figure 5.3 D).

Cells transfected with either of the melanopsin–G protein fusion plasmids produced very similar calcium kinetics regardless of whether or not anti-*GNAQ* and-*GNA11* siRNA was applied — the rate of onset and the maximum fluorescence were both similar (Figure 5.3 C and D). Treating each responsive cell as a biological replicate, the area under the curves of cells transfected with melanopsin–*GNAQ* was slightly lower in the anti-*GNAQ* and anti-*GNA11* siRNA group compared to the negative control siRNA group (78.04 ± 0.78 and 80.17 ± 0.81 arbitrary units, respectively; $P = 0.061$, unpaired *t* test, two tailed; n = 336, anti-*GNAQ* and anti-*GNA11* siRNA; n = 408, negative control

siRNA). The melanopsin–*GNAQ* groups did have a statistically significant difference in their times to peak relative fluorescence ($P < 0.0001$, unpaired *t* test, two tailed), with the anti-*GNAQ* and anti-*GNA11* siRNA group reaching a lower peak slightly earlier (13.47 ± 0.26 s, n = 248) compared to the negative control siRNA group (16.18 ± 0.34 s, n = 273). Neither the area under the curve ($P = 0.48$, unpaired *t* test, two tailed) nor the time to peak ($P = 1.0$, unpaired *t* test, two tailed) significantly differed between the melanopsin–*GNA11* groups when individual cells were treated as biological replicates.

5.2.1.c G_i activity of opsin–G protein fusion proteins

To determine if the fused G protein subunit modified the G_i response characteristics of the opsins, a cAMP-based assay of G_i function was performed on the melanopsin– and rhodopsin–G protein fusion proteins.

Rhodopsin–G protein fusion proteins produced very different light-induced cAMP responses to wild type rhodopsin. After raising the cAMP level using forskolin, rhodopsin-transfected cells showed a decrease in cAMP-dependent bioluminescence. However, in cells transfected with rhodopsin–G protein fusion plasmids the bioluminescence signal continued to increase after the 485 nm light stimulation. Similarly, the small decrease in signal seen in cells transfected with wild type melanopsin was not as clear in cells transfected with melanopsin–G protein fusion plasmids (Figure 5.4 A).

Most striking was the absolute values of the bioluminescence signal that was produced by cells transfected with opsin–G protein fusion constructs. Cells transfected with melanopsin–G protein fusions reached values of 5,500 to 5,900 luminescence units, while cells transfected with either of the rhodopsin–G protein fusion plasmids reached a mean of 8,500 luminescence units (Figure 5.4 B). This is in contrast to cells transfected with melanopsin, rhodopsin or just the GloSensor reporter plasmid, which had a mean

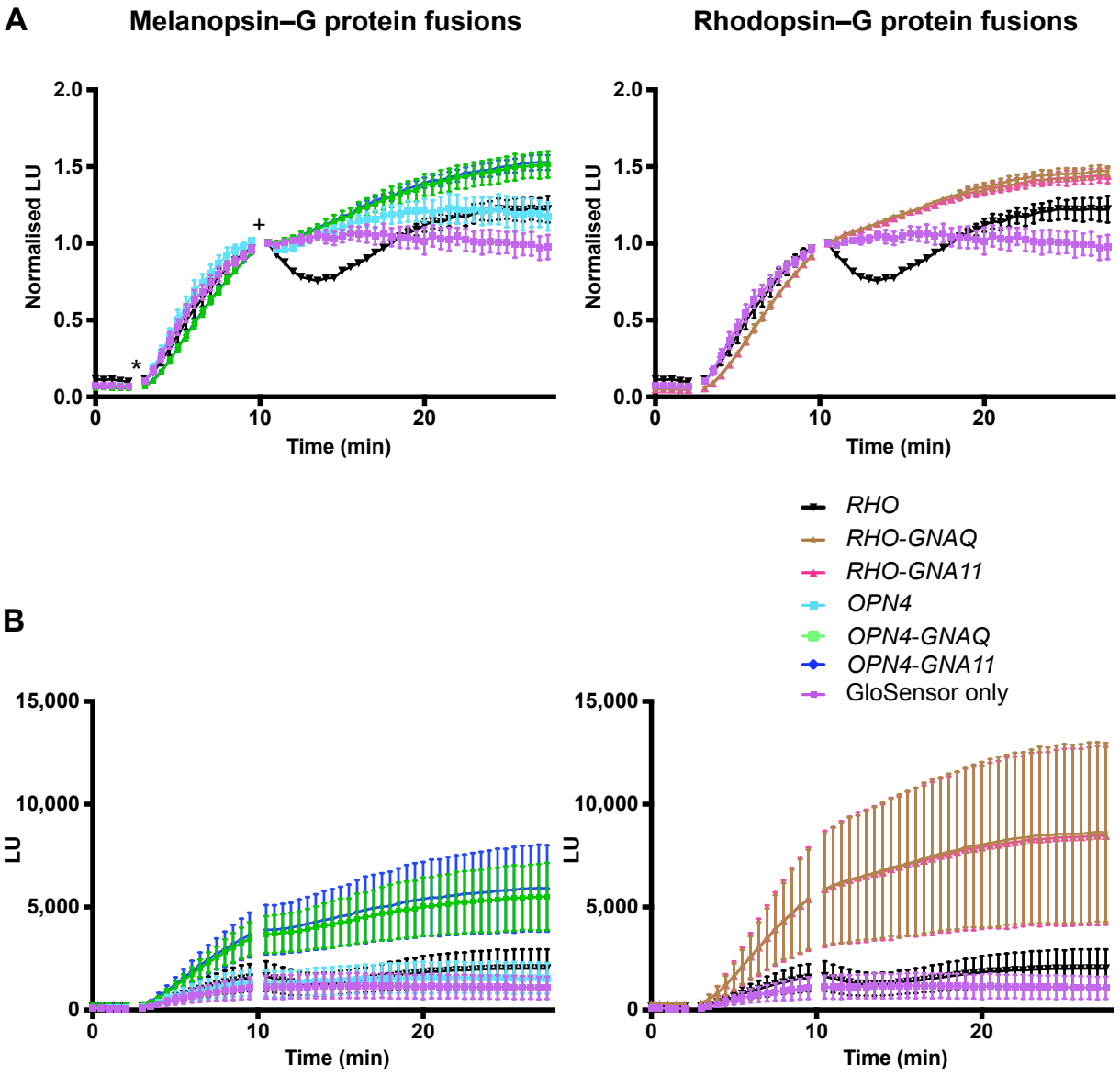


Figure 5.4. G_i activity of melanopsin– and rhodopsin–G protein fusion proteins in 293T cells
(**A**) The ability of melanopsin– and rhodopsin–G protein fusion proteins to couple to the G_i pathway was assayed using GloSensor, a cAMP biosensor. The baseline bioluminescence level was measured before forskolin was added (*) to raise the level of cAMP. The transfected 293T cells were illuminated with 485 nm light (+) and the response measured. The response was normalised to the first reading after the light stimulation (mean ± s.e.m.; n = 4). Neither of the four fusion proteins showed G_i activity resembling that of the unfused opsins. Wild type rhodopsin (*RHO*) produced a substantial decrease in GloSensor bioluminescence after light stimulation, but rhodopsin–G protein fusion proteins continuted to increase in their bioluminescence after the light stimulus. (**B**) Raw luminescence data showed the high luminescence values that the four opsin–G protein fusion proteins achieved. Following the application of forskolin the rate of luminescence increase was greater in opsin–G protein fusion transfected cells than in cells transfected with melanopsin (*OPN4*), rhodopsin or GloSensor only (no opsin) control cells. The rate of increase and maximum values was greatest in cells transfected with rhodopsin–G protein fusion constructs. LU, luminescence units.

peak luminescence of just over 2,000 luminescence units. The large increases in luminescence were independent of the light stimulus. Cells that received forskolin but no light stimulus still reached very high levels of luminescence signal (data not shown).

5.2.2 *In vivo* assessment of a melanopsin–G protein fusion AAV vector

Melanopsin–G protein fusion proteins demonstrated greater response rates and magnitudes of response in a G protein knockdown state *in vitro*, compared to wild type melanopsin. Given the similar *in vitro* performance of both melanopsin–*GNAQ* and melanopsin–*GNA11*, other factors were considered when selecting which fusion construct should be compared against wild type melanopsin in an *in vivo* study. The *GNA11* fusion construct was chosen as there is evidence that *GNA11* is expressed at higher levels in more cells of the retina (Siegert et al., 2012), suggesting that more transduced retinal cells may be primed to signal via G_{11} rather than G_q.

A vector with human melanopsin cloned in an inverse orientation, such that no protein should be produced, was used as an injection control vector (AAV-sham) (Figure 5.5 A). All three expression cassettes were driven by a ubiquitous CAG promoter and were packaged as single stranded DNA into AAV2/2(7m8).

5.2.2.a *In vitro* testing of AAV vectors

As a qualitative assessment to validate that AAV2/2(7m8)-CAG-*OPN4* and AAV2/2(7m8)-CAG-*OPN4*-*GNA11* (to be referred to as AAV-*OPN4* and AAV-*OPN4*-*GNA11*, respectively) were able to transduce cells and express functional protein, 293T cells were transduced with these two AAV vectors, as well as AAV2/2(7m8)-EF1α-F.*OPN4*, (to be referred to as AAV-sham). Cells that had been transduced with AAV-*OPN4* and AAV-*OPN4*-*GNA11* produced a strong calcium response following light exposure in a plate reader assay of $G_{q/11}$ function (Figure 5.5 B). The response was of

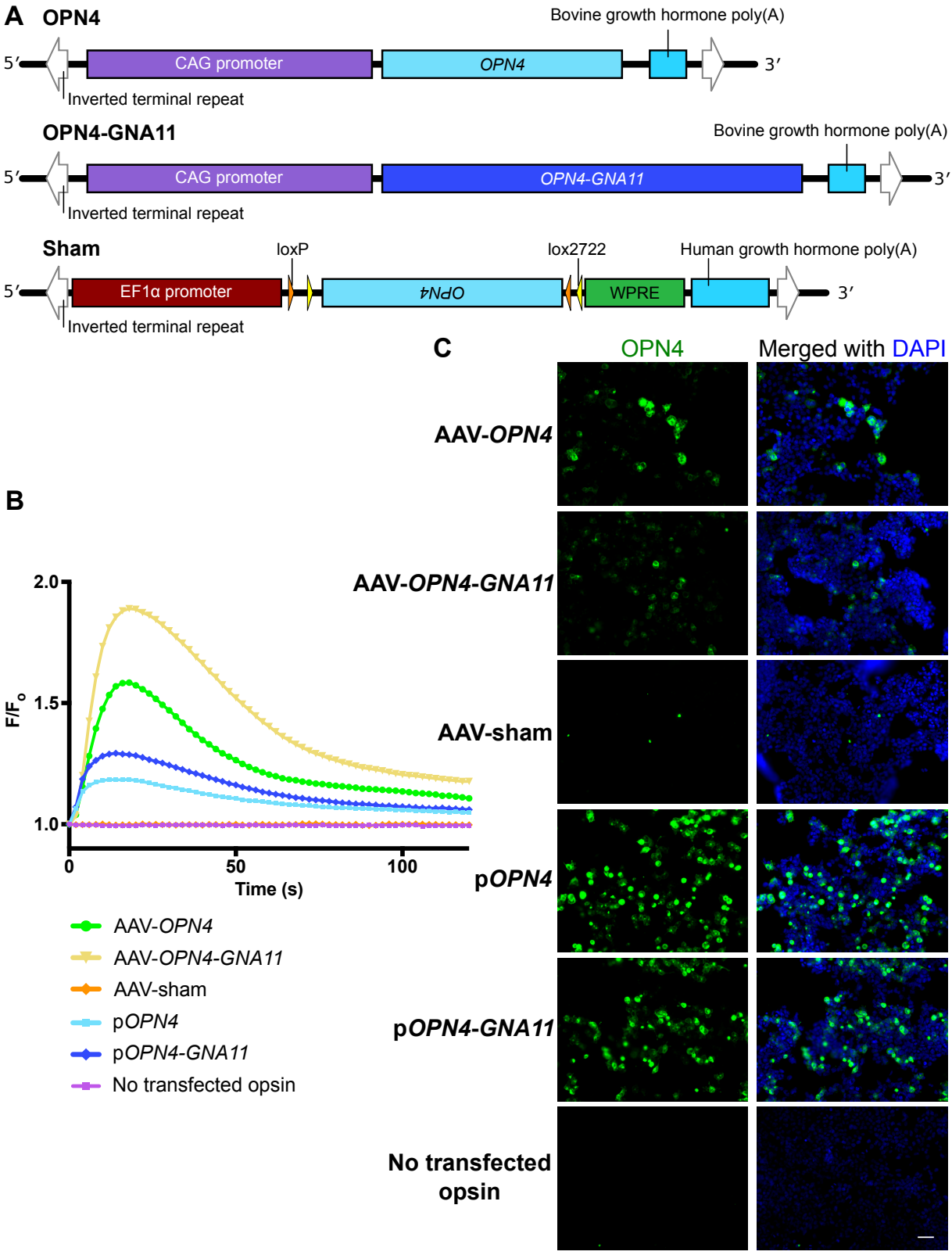


Figure 5.5. *In vitro* testing of AAV2/2(7m8)-*OPN4* and AAV2/2(7m8)-*OPN4-GNA11*
(**A**) Schematics of the DNA expression cassettes used to produce AAV2/2(7m8) vectors. (**B**) 293T cells were transduced with AAV2/2(7m8)-*OPN4*, AAV2/2(7m8)-*OPN4-GNA11*, a floxed, inverted melanopsin control AAV vector (AAV-sham) and control plasmids. Three days post-transfection, a plate reader-based assay of $G_{q/11}$ activity using Fluo-4 fluorescent calcium dye showed that cells transduced with *OPN4* and *OPN4-GNA11* AAV vectors responded to a light stimulus with a rise in fluorescence. The magnitude of the response was greater than that from cells transfected with *OPN4* and *OPN4-GNA11* plasmids. (**C**) Following the assay, the cells were fixed and stained using an anti-human melanopsin (OPN4) antibody. Immunolabelling was clearly present in cells transduced or transfected with *OPN4* and *OPN4-GNA11* AAV vectors and plasmids. Scale bar represents 50 µm. EF1α, elongation factor-1 alpha; WPRE, woodchuck hepatitis virus posttranscriptional regulatory element; F/F_o, fluorescence intensity relative to baseline fluorescence.

greater magnitude than that induced by melanopsin and melanopsin–*GNA11* plasmids. AAV-sham did not produce a calcium response following light stimulation.

Three days after transducing 293T cells with AAV-*OPN4*, AAV-*OPN4*-*GNA11* and AAV-sham, cells were fixed and immunolabelled. Both AAV-*OPN4* and AAV-*OPN4*-*GNA11* showed widespread signal from anti-human melanopsin immunolabelling, while no cells transduced with AAV-sham showed melanopsin expression (Figure 5.5 C). Signal from transduced cells was lower than that from plasmid transfected cells.

Mice with rod-cone dystrophy due to the *rd1* mutation ($Pde6b^{rd1/rd1}$) were chosen as the model of retinal degeneration for the *in vivo* study. This mutation causes a severe and rapid loss of rods, followed by cones (Carter-Dawson et al., 1978); *rd1* mice have been extensively utilised in previous optogenetics for vision studies (Bi et al., 2006; Lagali et al., 2008; Zhang et al., 2009; Doroudchi et al., 2011; Macé et al., 2014; Cehajic-Kapetanovic et al., 2015; Gaub et al., 2015; van Wyk et al., 2015). A number of strains of mice that have the *rd1* mutation are also homozygous for the $Gpr179^{nob5}$ mutation that causes a no b-wave (nob) electroretinogram phenotype (Balmer et al., 2013; Chang, 2015). GPR179 has a role in modifying the sensitivity of the signalling cascade in ON bipolar cells (Ray et al., 2014). Mutations in *GPR179* are known to cause night blindness in humans (Audo et al., 2012). C3H/HeH mice from Medical Research Council Harwell were genotyped for *rd1* and *Gpr179* mutations and were found to be homozygous for the *rd1* mutation and homozygous for the wild type allele of *Gpr179* (Figure 5.6 A). As sighted controls, mice from a strain of C3H/HeN $Pde6b^{+/+}$ without the *rd1* mutation were a gift from Professor Russell Foster. They were also genotyped for *rd1* and *Gpr179* mutations and found to be homozygous wild type for both (data not shown).

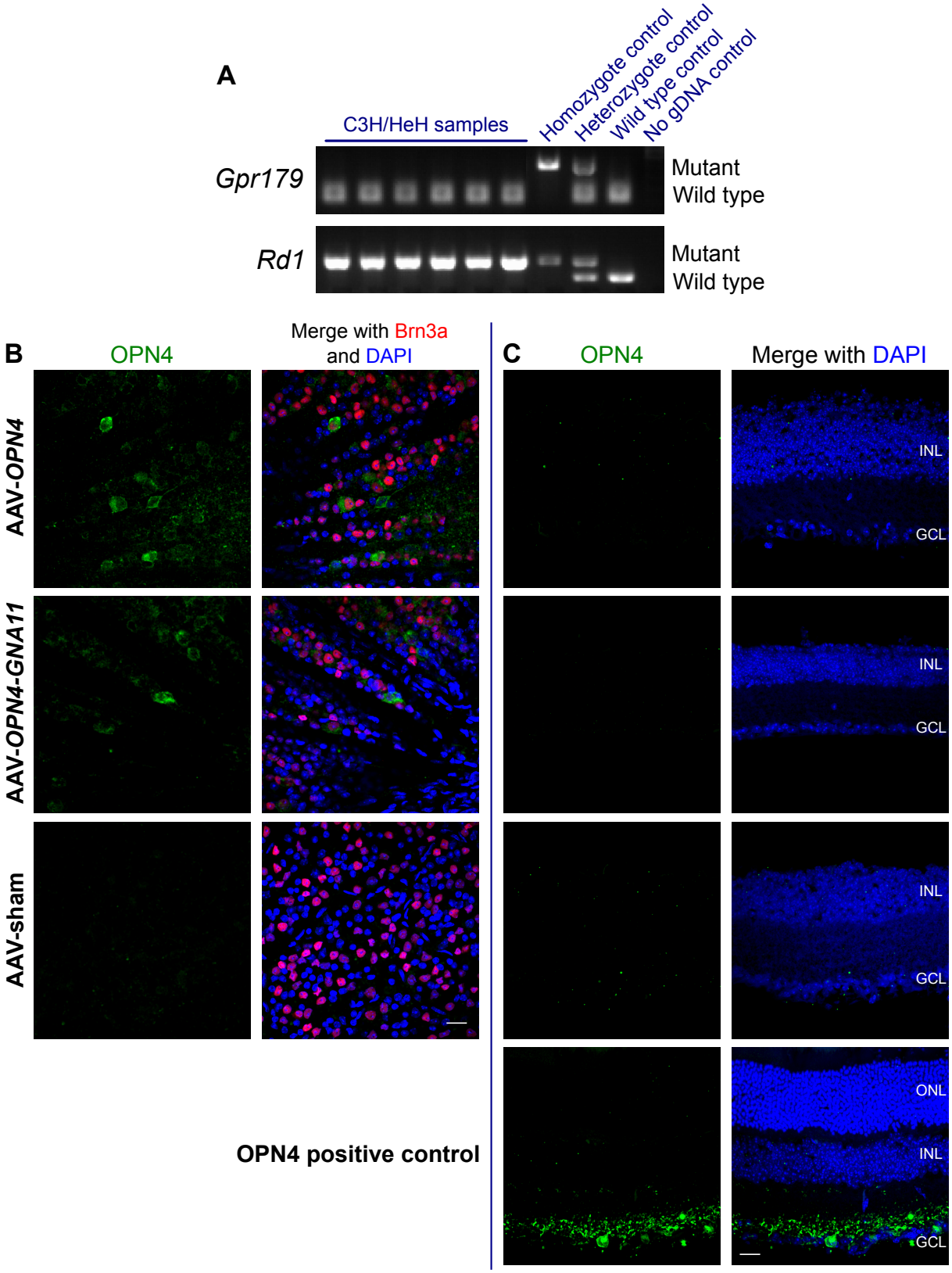


Figure 5.6. Melanopsin–G protein and melanopsin AAV vectors injected into C3H/HeH mice
(**A**) C3H/HeH female mice were genotyped for *rd1* and *Gpr179* mutations. All mice were homozygote for both the *rd1* mutation and the wild type *Gpr179* allele (six representative samples shown). (**B**) C3H/HeH mice were injected intravitreally with AAV2/2(7m8)-*OPN4*, AAV2/2(7m8)-*OPN4-GNA11* or a negative control injection of AAV2/2(7m8)-F.*OPN4* (floxed melanopsin). A small number of weakly immunloabelled retinal ganglion cells were identified as expressing human melanopsin (OPN4) in flat mount preparations. (**C**) In vertical sections of injected eyes human melanopsin expression was not identified in six eyes from each group. Image acquisition settings for the melanopsin channel were the same as those for the positive control (injection of AAV2/2(quad Y-F)-F.*OPN4* into an *Opn4*-Cre mouse). Scale bar represents 20 µm. Brn3a, brain-specific homeobox/POU domain protein 3A; GCL, ganglion cell layer; INL, inner nuclear layer; ONL, outer nuclear layer.

5.2.2.b Transgene expression following AAV vector intravitreal injections

Thirteen six to eight-week-old female C3H/HeH mice received bilateral intravitreal injections of either AAV-*OPN4*, AAV-*OPN4*-*GNA11* or AAV-sham. The AAV titre was diluted, where necessary, so that 2×10^9 vg were injected into each eye. The investigator was masked to the AAV vector delivered. Eight age-matched, uninjected C3H/HeH mice and ten age-matched C3H/HeN *Pde6b*$^{+/+}$ mice served as natural history and sighted controls, respectively.

Tissue was taken approximately ten weeks post-injection, when the mice were 16 to 18 weeks old. Injected retinas were prepared as flat mounts and vertical sections and immunolabelled with anti-human melanopsin antibody. Immunofluorescence was only evident on flat mount preparations. Immunolabelled cells were only seen in the ganglion cell layer around the optic disc in AAV-*OPN4* and AAV-*OPN4*-*GNA11* injected retinas (Figure 5.6 B). The intensity of immunolabelling was relatively weak. Immunolabelled vertical sections failed to show any clear evidence of immunolabelled cells in any layer of the retina. A positive control sample clearly demonstrated the efficacy and specificity of the anti-human melanopsin antibody (Figure 5.6 C). All retinas from C3H/HeH mice showed an absence of the outer nuclear layer, as expected for *rd1* mice.

5.2.2.c Functional assessment of optogenetically treated retinally degenerate mice

A series of functional tests were performed on injected mice to examine whether melanopsin or melanopsin–*GNA11* gene therapy mediated a functional benefit to the visual system. The tests were conducted six to nine weeks post-injection and included pupillometry, optomotor response and visually-guided behavioural tests.

5.2.2.c.i Pupillometry

Six to seven weeks post-injection, pupillometry at four different light intensities was conducted (Figure 5.7 A). Full-spectrum light from a xenon arc light source was varied in intensity by the use of neutral density filters. An irradiance response curve derived

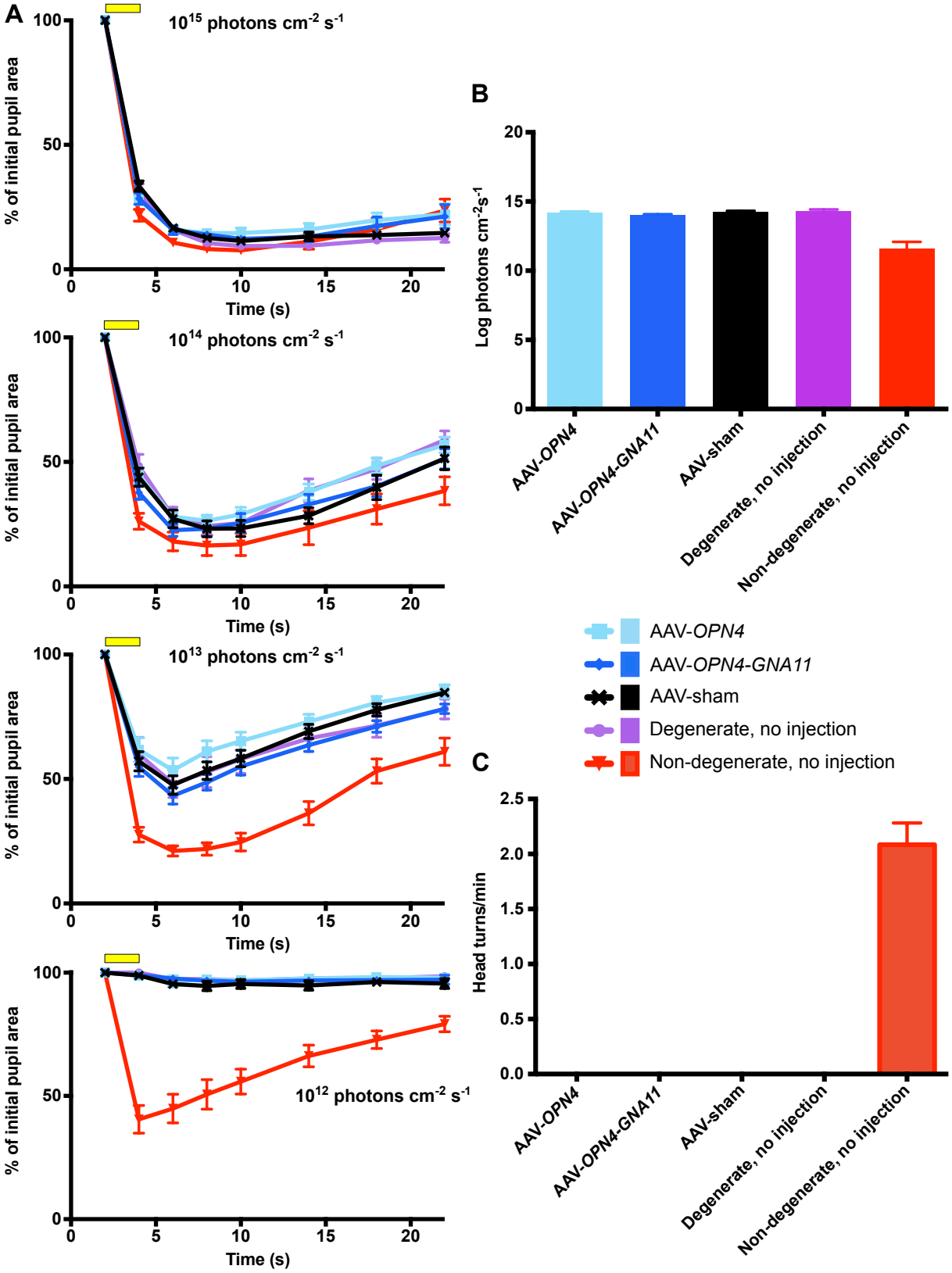


Figure 5.7. Pupillometry and optomotor response of retinally degenerate mice injected with AAV-*OPN4* and AAV-*OPN4-GNA11*

(**A**) Six to seven weeks post-injection with AAV-*OPN4*, AAV-*OPN4-GNA11* and AAV-sham, C3H/HeH mice underwent pupillometry at four different light intensities (10^{12} – 10^{15} photons cm^{-2} s^{-1}). Baseline pupil area was recorded before a two second white light pulse was applied (yellow bar; mean ± s.e.m.; n = 13, AAV groups; n = 8, degenerate, no injection; n = 10, non-degenerate, no injection). (**B**) The light intensity for half maximal response was calculated. The differences between injected groups was not statistically significant ($P = 0.17$, ordinary one-way ANOVA; n = 13, AAV groups; n = 8, degenerate, no injection; n = 7, non-degenerate, no injection). (**C**) Mice were assessed for an optomotor response with a spatial frequency of 0.1 cycles/degree. Only non-degenerate mice showed any head turning responses (n = 13, AAV groups; n = 8, degenerate, no injection; n = 10, non-degenerate, no injection).

from data on pupil area at the end of the two second light pulse enabled the calculation of a value representing the light intensity required for half maximal response (EC_{50} value). The differences between the EC_{50} values of the injected C3H/HeH groups were not statistically significant (F (2, 36) = 1.89; P = 0.17, ordinary one-way ANOVA; n = 13; Figure 5.7 B). As expected, the sighted control group had a lower EC_{50} value, representing greater light sensitivity, compared to the four other degenerate groups (F (4, 49) = 33.17; $P < 0.0001$, ordinary one-way ANOVA; $P < 0.0001$ post hoc tests with Bonferroni's correction, between non-degenerate and each degenerate group). The kinetics of the light responses were similar between the C3H/HeH groups at all four light intensities (Figure 5.7 A).

5.2.2.c.ii Optomotor response and visually-guided behavioural tests

An optomotor response test was conducted approximately nine weeks post-injection. By placing each mouse in the centre of a rotating drum that was lined with alternating black and white vertical stripes, the frequency of reflexive head tracking of the stripes was quantified. Characteristic head turns were reliably seen in all of the sighted control mice at a rate of 2.1 ± 0.20 turns/minute. However, no head turns were identified in any of the C3H/HeH mice, irrespective of any gene therapy treatment (Figure 5.7 C).

Three different visually-guided behavioural tests were conducted but did not provide interpretable results. A novel object recognition test that compared the time spent with novel and familiar objects following a change in the visual scene within a test arena, was conducted using both novel objects and novel odours. A third test compared the time spent with an object that moved relative to a visual scene, to the time spent with an object that was stationary relative to the visual scene. In all three behavioural tests the sighted control group of C3H/HeN *Pde6b*$^{+/+}$ mice did not consistently show a statistically significant preference for the novel object/odour or the displaced object

(data not shown). Without a positive control group, the degenerate C3H/HeH mice were not tested.

5.2.2.c.iii Light-induced Fos expression

As a terminal experiment studying retinal light sensitivity, FBJ osteosarcoma oncogene (*c-fos*) expression in response to a light pulse was examined. *C-fos* is an immediate early gene, meaning that it has rapid and transient increased expression in response to a variety of external stimuli. Light is a well characterised stimulus for Fos (the protein encoded by *c-fos*) expression in amacrine cells (Koistinaho and Sagar, 1995) and cells of the ganglion cell layer, including photosensitive retinal ganglion cells (Earnest et al., 1990; Sagar and Sharp, 1990; Pickard et al., 2009; Hughes et al., 2013). Thus Fos expression can act as a marker of recent neuronal activity (Dragunow and Faull, 1989).

Ten weeks post-injection three animals from each experimental group were subjected to a 30 minute white light pulse four hours into their dark phase and three animals were handled in a similar manner, but not exposed to any light. Vertical sections showed strong Fos expression in the ganglion cell layer and inner part of the inner nuclear layer of sighted control mice exposed to the light pulse, and minimal expression in sighted controls that were not exposed to light (Figure 5.8 A). The area above the background fluorescence was higher in the light pulse mice compared to the no light pulse mice from the sighted control group (1.5 ± 0.34% compared to 0.079 ± 0.025%; Figure 5.8 B).

In the four *rd1* degenerate groups, there was no clear difference between the Fos expression in the light pulse and no light pulse groups (Figure 5.8 A). An ordinary two-way ANOVA examining the effects of light pulse and AAV injection on the Fos-positive area above the background fluorescence showed non-significant interactions ($F(2, 12) = 1.03$; $P = 0.39$; n = 3). The cells that were immunopositive for Fos were nearly

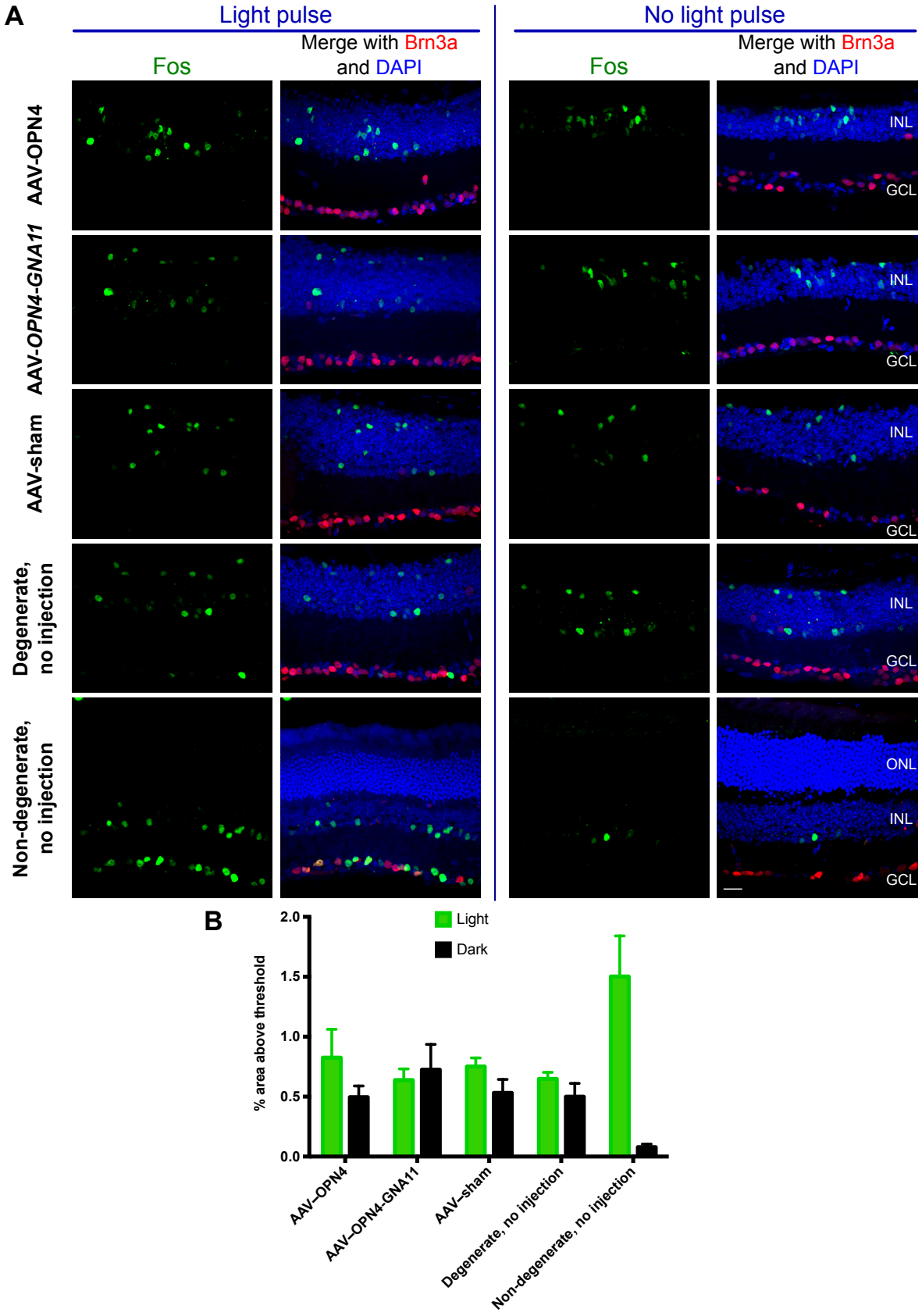


Figure 5.8. Light-induced Fos expression in AAV-melanopsin and AAV-melanopsin-*GNA11* injected degenerate murine retina

(**A**) Ten weeks after injection with AAV-*OPN4*, AAV-*OPN4-GNA11* or AAV-sham, retinally degenerate *rd1* mice and non-degenerate control mice were light pulsed to induce Fos expression. In non-degenerate control eyes, strong Fos expression was seen in the light pulsed group, but very little was evident in the no light pulse eyes. In the four retinally degenerate groups similar levels of Fos immunolabelling was present in both light pulse and no light pulse groups. (**B**) The area of Fos immunolabelling above the background fluorescence was quantified. The differences between the three injected groups were not statistically signficant ($P > 0.05$, ordinary two-way ANOVA; n = 3). Scale bar represents 20 μm. GCL, ganglion cell layer; INL, inner nuclear layer; ONL, outer nuclear layer.

all in the inner nuclear layer, with very few in the ganglion cell layer, in contrast to the sighted controls eyes that received the light pulse.

5.3 Discussion

This set of experiments aimed to test the hypothesis that fusing G proteins to human opsins could modify their signalling properties in a way that enhanced their use as optogenetic tools for restoring vision. The *in vitro* data from these experiments suggests that opsin–G protein fusion proteins are a viable strategy that can offer some potential benefits. However, the *in vivo* experiments were unable to provide significant evidence to support or negate the original hypothesis.

5.3.1 Opsin–G protein fusion proteins are able to utilise the fused Gα subunit

The results of testing both the melanopsin–G protein and rhodopsin–G protein fusion proteins suggests that the fused Gα subunit is able to interact with a covalently fused opsin.

By using siRNA to knockdown endogenous *GNAQ* and *GNA11* gene expression, 293T cells were used to model cells that had relatively reduced levels of $G_{q/11}$ proteins. It is currently unknown as to whether the efficient delivery and expression of melanopsin in cells of the degenerate retina would make the availability of G_q and G_{11}, the first effector protein of the melanopsin signalling cascade, become the rate limiting component in restoring functional vision. Having GNAQ or GNA11 fused to melanopsin provided some insurance against low Gα subunit concentration being a limiting factor. In 293T cells with lowered levels of *GNAQ* and *GNA11*, the frequency and magnitude of the light-induced calcium response was maintained when either of the melanopsin–G protein constructs were expressed, while cells transfected with wild type melanopsin responded at a lower frequency and with a lower magnitude of response. The maintenance of $G_{q/11}$ signalling by melanopsin–G protein transfected cells in a state

of endogenous G protein depletion is evidence that the fused G protein is mediating the cells' calcium responses.

Further evidence that the fused G protein was having a functional impact came from the cAMP assay, which was used to interrogate G_i signalling. In this bioluminescence assay all four fusion constructs showed large increases in bioluminescence in response to the application of forskolin. The large elevations in bioluminescence signal were dependent on forskolin, but not light. The rate of signal increase accelerated after the application of forskolin but before the light stimulus; withholding the light stimulus did not change the magnitude of the bioluminescence signal increase. A possible explanation for this effect of opsin–G protein fusion proteins is that GDP and GTP, which are known to potentiate the forskolin-induced cAMP increase (Seamon and Daly, 1981), may be in greater abundance in the cell due to their binding to fused Gα subunits. Because the effect appears to be forskolin-dependent, it is not thought that opsin–G protein fusion proteins would induce aberrant cAMP levels in normal physiological conditions.

The large increase in bioluminescence signal following forskolin application made it difficult to interpret whether the rhodopsin in rhodopsin–G protein fusion proteins was still able to activate the G_i pathway; the much greater cAMP-increasing effects of forskolin may have masked G_i activation.

Although 80 – 90% of *GNAQ* and *GNA11* mRNA was knocked down by the application of siRNA, it was not uncommon to see light responsive 293T cells transfected with wild type melanopsin. There are several possible reasons for why melanopsin transfected cells still show light-induced calcium responses in a GNAQ and GNA11 depleted state. Firstly, 293T cells are known to express *GNA14*, another member of the $G_{q/11}$ family of Gα subunits (Atwood et al., 2011). Melanopsin may therefore be inducing calcium responses via G_{14} activation in cells transfected with anti-*GNAQ* and anti-*GNA11*

siRNA. *In vitro* and *in vivo* evidence has suggested that greater functional knockdown of melanopsin signalling can be achieved by knocking down *GNA14* in addition to *GNAQ* and *GNA11* (Hughes et al., 2014). Cotransfection with anti-*GNA14* siRNA effectively knocked down *GNA14* levels in 293T cells (data not shown), but it was also found to target the coding region of *GNA11*, meaning that it could not be used in this present study where *GNA11* fusion constructs were used. Secondly, as qPCR measures the levels of mRNA rather than protein expression it is possible that the substantial knockdown of mRNA does not equate to a corresponding decrease in protein levels, for example due to high mRNA stability and/or low protein turnover. Thirdly, it is possible that siRNA transfection and opsin transfection were not equally distributed. Therefore cells that were poorly transfected with siRNA may have been well transfected with opsin, leaving such cells with normal levels of G proteins to mediate a melanopsin calcium response.

There was a theoretical risk that the fused G protein may impair the accessibility of G protein dependent kinases to the C-terminal phosphorylation sites of melanopsin (Blasic et al., 2014). However, the onset and offset kinetics of the calcium response in light-stimulated 293T cells transfected with wild type melanopsin or melanopsin–G protein fusion plasmids were indistinguishable, suggesting the offset of the melanopsin response was not impaired by the presence of a fused G protein subunit.

5.3.2 *In vivo* assessment of melanopsin–G protein fusion protein efficacy was impaired by inefficient gene delivery

Retinally degenerate *rd1* mice were injected with either AAV-*OPN4*, AAV-*OPN4-GNA11* or AAV-sham (floxed and inverted melanopsin) and assayed for whether melanopsin or melanopsin–*GNA11* was more effective at restoring light sensitivity. Fos immunostaining of light-pulsed retinas examined light-induced activity at the cellular level, while pupillometry assessed the light detecting capabilities of the entire retina and

the optomotor response tested pattern vision. Unfortunately, none of the lines of investigation demonstrated convincing evidence that either melanopsin or melanopsin–*GNA11* were superior when compared to each other or to a sham AAV injection.

The poor functional results are thought to be due to low levels of transgene expression. At least six eyes from each group were immunolabelled for human melanopsin. Of these, only the samples flat mounted showed faint signs of positive immunolabelling identified in a small number of cells in the retinal ganglion cell layer near the optic disc. Tissue from mouse retina that had been successfully transduced with human melanopsin in another experiment (Ms Jessica Rodgers, University of Oxford, unpublished data) served as a positive control and showed effective labelling by the antibody.

Such a low level of transgene expression was unexpected as earlier studies using a GFP-expressing AAV vector had produced far greater levels of expression (Figures 3.2 and 3.5). Using an AAV vector of the same serotype and a very similar promoter, AAV2/2(7m8)-GFP injections in to *rd1* mice led to widespread GFP expression across the retina (but most concentrated around the optic disc) and in all layers of the retina, including the retinal pigment epithelium. This serotype was selected because of its superior performance to two other serotypes (see chapter three). The number of vector genomes injected in both GFP and opsin studies was very similar.

A factor that may have contributed to the discrepancy in results between objectively similar AAV-GFP and AAV-opsin (AAV-*OPN4* and AAV-*OPN4*-*GNA11*) vectors was a difference in the biophysical properties of the virions. Making AAV-*OPN4* and AAV-*OPN4*-*GNA11* to a titre appropriate for *in vivo* studies was challenging due to the low yields from a given AAV production run. The reason for low yields is not known. The lead author of the paper describing the AAV2/2(7m8) capsid was not aware of any issues unique to this serotype that reduced the AAV yield (Dalkara, 2015). To achieve

the desired concentrations multiple batches were combined and underwent a secondary concentration process. This further step in processing the AAV-*OPN4* and AAV-*OPN4-GNA11* vectors required an additional freeze/thaw cycle and additional handling that the AAV-GFP vectors did not undergo. Repeated freeze/thaw cycles are known to cause vector aggregation, which leads to inconsistencies in the performance of AAV vectors (Wright et al., 2005). Without a means of quantifying the aggregation and viability of AAV virions, the qPCR titre was the only technique available to compare AAV vectors. Improved consistency of AAV vector performance would be expected if further quality control measures were made on every batch of AAV vector produced (see §8.5.3 for further discussion).

Another possible explanation for relatively low levels of detectable melanopsin in AAV-*OPN4* and AAV-*OPN4-GNA11* injected eyes could be that the delivered transgenes are less efficiently processed into episomes, transcribed and translated by the transduced cells. If this is the case then even though the AAV transduction and unpackaging rate may have been the same between the AAV-GFP and AAV-opsin vectors (due to sharing the same capsid), differential efficiency in the downstream processes involved the conversion of single- to double-stranded DNA, transcription and translation of the transgenes may have contributed to lower levels of opsin expression (Ferrari et al., 1996; Fisher et al., 1996).

A further inconsistency between the AAV-GFP and AAV-opsin *in vivo* experiments was the time between the injection and fixing of the eyes. After three weeks, eyes injected with AAV-GFP were fixed and immunostained with anti-GFP antibody, whereas eyes injected with AAV-opsin were not fixed until at least ten weeks post-injection. Given the long and stable transgene expression that AAV is known to induce (Lebherz et al., 2005; Rivera et al., 2005), the greater time post-injection might be expected to favour greater transgene expression, rather than be a reason for less

expression. Human melanopsin has been detected in the retina of *rd1* mice approximately one year post-injection by a colleague in the laboratory (Dr Samantha de Silva, unpublished data), suggesting transcriptional silencing of melanopsin transgenes is unlikely to be a significant issue reducing expression levels.

Ideally there would have been more time between the date of injection and when the functional tests were performed. More time between treatment and assessment would have provided a greater opportunity for central brain circuits to develop and adapt to the new pattern of light-dependent action potentials (if present). Such plasticity would likely lead to improved function in tests such as the optomotor response, which relies on pattern vision. However, using *rd1* mice as a model may in fact limit the degree of neural plasticity that can be exploited by optogenetic gene therapy, even if a greater length of time was allowed (see §8.2 for further discussion).

5.3.3 Fused G_q and G_{11} Gα subunits are inefficient at changing the signalling pathway of an opsin

Rhodopsin–G protein fusion constructs were created to test the hypothesis that fusing a non-native G protein to the C-terminus of an opsin could modify the G protein pathway activated by the opsin. Light-stimulated rhodopsin normally activates transducin, G_t, but can also activate the G_i pathway (Li et al., 2005; Gutierrez et al., 2011b; Bailes and Lucas, 2013).

Light-activated rhodopsin does not stimulate the $G_{q/11}$ intracellular pathway (see chapter four for data and discussion) and fusing either G_q or G_{11} to the C-terminus of human rhodopsin did not increase its $G_{q/11}$ signalling abilities, despite the close proximity of the Gα subunit. Calcium concentrations, as quantified by calcium-sensitive fluorescent dyes, increased in response to light stimulation in only a very small number of cells transfected with rhodopsin–G protein fusion plasmids. While the responses were slightly greater than the few seen in rhodopsin transfected cells, they were not

consistent enough to suggest the fused G protein was enabling rhodopsin to signal via the $G_{q/11}$ pathway in an efficient manner.

The lack of $G_{q/11}$ activation by rhodopsin–G protein fusion proteins is likely to reflect the low specificity of activated rhodopsin for G_q and G_{11}. The shorter C-terminus of rhodopsin (27 amino acid residues) compared to melanopsin (112 residues) is unlikely to be a limiting factor, as other GPCR–Gα subunit fusion studies using a GPCR with an even shorter C-terminus showed that the fused Gα subunit was still able to couple efficiently to the GPCR (Wenzel-Seifert et al., 1998).

In summary, this experimental work successfully achieved the aim of cloning and testing human opsin–G protein fusion proteins as potential candidates for optogenetic gene therapy for vision restoration and developing an understanding of the structure/function relationship of human opsin–Gα subunit fusions proteins. Success was limited to *in vitro* work as *in vivo* studies were inconclusive and require further investigation.

In vitro studies demonstrated that human melanopsin–Gα subunit fusion proteins are able to activate melanopsin's native $G_{q/11}$ intracellular signaling pathway and in conditions of reduced endogenous G proteins have an advantage over non-fused wild type melanopsin. These data suggested that the fused Gα subunit was able to interact with its activated melanopsin partner and transduce the signal to the second messenger system. Data from rhodopsin–G protein fusion proteins indicated that fusing a non-native Gα subunit partner to an opsin cannot force the opsin to activate the non-native G protein pathway.

Based on the encouraging *in vitro* results, AAV vectors expressing wild type melanopsin and melanopsin fused to GNA11 were created and tested in the *rd1* model of retinal degeneration. Unfortunately, the aim of comparing these proteins as

optogenetic tools *in vivo* was not achieved due to low expression levels of both proteins being observed in the injected mice. Functional tests of the mice confirmed that there was no improvement in functional outcomes, relative to mice that received a sham AAV vector injection. Further studies using more efficacious AAV vectors should be conducted to determine if the opsin–G protein fusion approach could have potential benefits as a translational therapy for inherited retinal degeneration.

Floxing

The sandwiching of a DNA sequence (which is then said to be floxed) between two lox sites.

Abbreviation: **F**lanked by **lox**P

6

Bipolar Cell-Targeted and Non-Targeted Opsin Expression

6.1 Introduction

Choosing a light-sensitive molecule is only one aspect of designing an optogenetic gene therapy strategy to restore vision. The other critical aspect is deciding which cells in the degenerate retina should express the light-sensitive molecule.

Early studies of optogenetics for vision restoration used ubiquitous expression systems to achieve maximal transgene expression across the retina. This strategy partly relies on the retina and brain's plasticity to relearn what component of the visual stimulus each pathway is conveying. Plasticity of the visual pathways has been described following retinal gene supplementation gene therapy (Ashtari et al., 2015). In the first vision optogenetics publication Bi and colleagues (2006) used a ubiquitous promoter and AAV2/2 serotype to express channelrhodopsin-2 in a wide range of cells, including ON and OFF ganglion cells and amacrine cells. Multielectrode array recordings and visually evoked potentials demonstrated improved light sensitivity of the retina, but no visually-guided behavioural outcomes were reported. Lin and colleagues (2008) also used a ubiquitous promoter to express melanopsin in any cell transduced by their AAV2/2

vector. Retinally degenerate *rd1* mice treated with this gene therapy show improvements in pupillary response and greater light avoidance.

As AAV vectors and transcriptional regulatory tools have developed, more groups have used these tools to engineer targeted gene expression. Most studies have utilised an enhancer element from the metabotropic glutamate receptor 6 gene (*Grm6*) to limit transgene expression to rod bipolar and ON cone bipolar cells (Lagali et al., 2008; Doroudchi et al., 2011; Cronin et al., 2014; Macé et al., 2014; Cehajic-Kapetanovic et al., 2015; Gaub et al., 2015; van Wyk et al., 2015). Others have used photoreceptor-specific promoters to limit expression to residual rods and cones (Busskamp et al., 2010).

There is a paucity of comparisons between targeted and non-targeted strategies. One study compared human rhodopsin expression driven by either a ubiquitous (CAG) promoter or a cell-specific *Grm6* enhancer (Cehajic-Kapetanovic et al., 2015). In a customised visually-guided behavioural test there was some evidence that the group of *rd1* mice that received the cell-specific gene therapy performed better than the group that received ubiquitously-expressing rhodopsin gene therapy.

The two methods commonly used to target a particular cell type are cell-specific transcriptional regulatory elements and the Cre-lox system. Cell-specific transcriptional regulatory elements, such as the *Grm6* enhancer mentioned above, work by only enabling transcription to occur in the presence of transcription factors that are expressed in a limited subset of cells. However, as reported by van Wyk and colleagues (2015), the *Grm6* enhancer element is not always cell-specific and the transduction efficiency can be low. To improve expression of their transgene in ON bipolar cells, van Wyk and colleagues created a transgenic mouse line to achieve widespread transgene expression. Others in our laboratory have tried a *Chx10* bipolar cell-specific promoter, but this did

not lead to an appreciable level of transgene expression (Dr Samantha de Silva, unpublished data).

An alternative genetic tool to achieve cell-specific transgene expression is the Cre-lox system. The Cre-lox system utilises Cre recombinase and short sequences of DNA known as lox sequences/sites from bacteriophage P1 to manipulate DNA at specific locations. Cre recombinase acts like a key that locates lox sequences and 'unlocks' the sequence flanked by lox sequences by causing recombination between the pair of lox sequences. Depending on the orientation and location of lox sites, Cre expression can switch on or off gene expression (Zheng et al., 2000). By using transgenic mice that express Cre under the control of a cell-specific promoter, the effects of Cre can be limited to particular cell types (Figure 6.1 A – D). A cell-specific promoter may only drive a relatively low level of transgene expression, but by placing lox sites at either end of an inverted transgene coding sequence (creating a so-called 'floxed' gene) a strong ubiquitous promoter can be used in the expression cassette. Only in the presence of Cre will the lox sequences be recombined resulting in the transgene being placed in the correct orientation, thereby allowing expression to be driven by the ubiquitous promoter.

Given the limitations of cell-specific promoters, it was decided that the Cre-lox mechanism would be utilised to achieve cell-specific gene expression. The requirement for transgenic animals to achieve cell-specific expression using the Cre-lox system makes these results less directly translatable to a clinical study. However, the means of cell-specific delivery was considered less critical for these early stage studies with the key objective being a comparison of which opsin is more appropriate and whether a cell-specific approach is superior to a non-targeted strategy. Once these preclinical studies have answered these strategic questions then optimised cell-specific

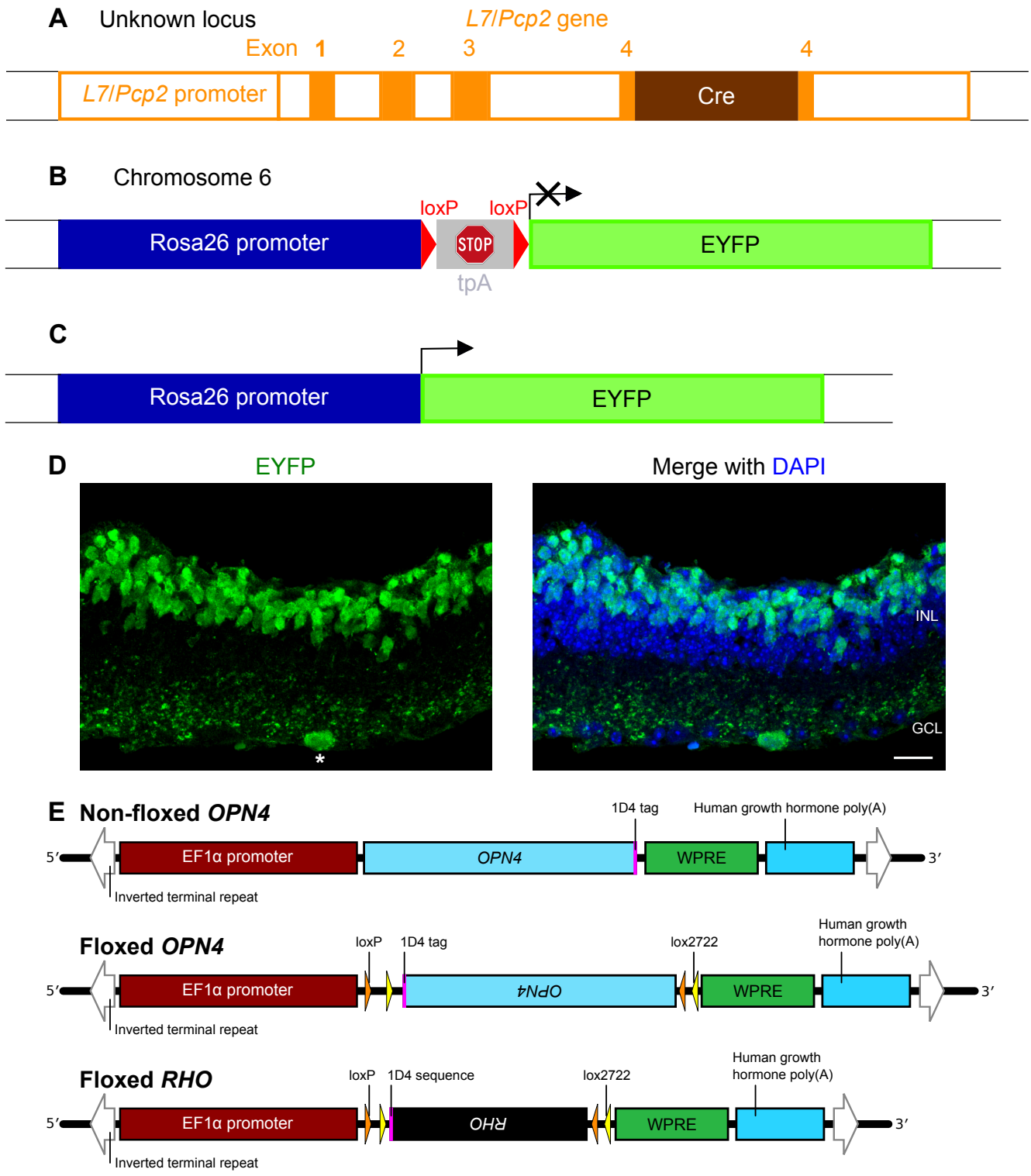


Figure 6.1. *L7*-Cre EYFP transgenic mice and floxed and non-floxed opsin AAV vectors
(**A** – **C**) Schematics of the salient genomic loci in *L7*-Cre EYFP mice. (**A**) At an unknown locus *L7*-Cre mice have a transgene consisting of a Cre DNA sequence cloned into exon 4 of the *L7/Pcp2* gene and promoter. (**B**) R26-stop-EYFP mice have a targeted mutation to the Rosa26 locus in chromosome 6. By placing a transcriptional roadblock (a triple polyadenylation sequence, tpA) flanked by lox sequences upstream of enhanced yellow fluorescent protein (EYFP) cDNA, the Rosa26 promoter does not drive expression of EYFP in the absence of Cre. (**C**) In the presence of Cre the transcriptional roadblock is removed by recombination and the Rosa26 promoter is able to drive EYFP expression. (**D**) Mice from *L7*-Cre, R26-stop-EYFP and *rd1* lines were crossed to produce mice with retinal degeneration that expressed EYFP in rod bipolar cells, types 2 and 6 cone bipolar cells of the inner nuclear layer (INL) and approximately 1,700 bistratified retinal ganglion cells (*) in the ganglion cell layer (GCL). Scale bar represents 20 µm. (**E**) Schematics of the DNA expression cassettes used to produce AAV2/2(7m8) vectors. Inverted cDNA sequences are shown upside down and flanked by lox sequences. Melanopsin cDNA sequences were tagged with a 1D4 sequence tag. EF1α, elongation factor-1 alpha; WPRE, woodchuck hepatitis virus posttranscriptional regulatory element.

transcriptional regulatory elements that have been developed in parallel can replace the Cre-lox system.

This series of experiments set about to compare the opsin expression efficiency and functional outcomes of expressing non-floxed and floxed melanopsin and floxed rhodopsin in retinally degenerate *rd1* mice expressing Cre in a subset of retinal bipolar cells. To restrict opsin expression primarily to retinal bipolar cells, a line of *L7*-Cre transgenic mice was utilised. *L7*-Cre express Cre recombinase under the control of a Purkinje cell protein 2 (*Pcp2*, also known as *L7*) promoter. This transgenic model has been found to express Cre in Purkinje cells of the cerebellum (Marino et al., 2002), rod bipolar cells, types 2 and 6 cone bipolar cells (Lu et al., 2013) and a subset of bistratified retinal ganglion cells (Ivanova et al., 2013). When crossed with a mouse strain featuring a floxed fluorescent reporter gene, Cre expressing cells unlock the fluorescent reporter (see Figure 6.1 A – D for the results of crossing *L7*-Cre and floxed EYFP strains).

Melanopsin was the first mammalian opsin to be used for optogenetic gene therapy to restore vision (Lin et al., 2008). Since then other groups have utilised rhodopsin (Cehajic-Kapetanovic et al., 2015; Gaub et al., 2015) and a melanopsin/mGluR6 chimeric construct (van Wyk et al., 2015). No published study has directly compared melanopsin and rhodopsin as optogenetic gene therapy tools, therefore one of the arms of this study included a floxed rhodopsin AAV vector to generate preliminary data comparing these two human opsins.

Aims

- To compare the relative efficacy of human opsins expressed in a targeted versus non-targeted manner as alternative optogenetic approaches to vision restoration in a mouse model of retinal degeneration.

- To compare the relative efficacy of AAV vectors expressing human opsins at different concentrations in a mouse model of retinal degeneration.

- To compare human rhodopsin and human melanopsin as alternative optogenetic tools for vision restoration in a mouse model of retinal degeneration.

6.2 Results

6.2.1 *In vitro* testing of floxed and non-floxed human opsins

Floxed and non-floxed versions of human melanopsin (*OPN4*) were cloned into a eukaryotic expression cassette for AAV2/2(7m8) production. Using the same strategy human rhodopsin (*RHO*) was ligated into the same plasmid backbone in inverse orientation (Figure 6.1 E). Melanopsin coding sequences included a 3′ 1D4 tag from bovine rhodopsin for immunodetection. Expression was driven by a ubiquitous elongation factor-1 alpha (EF1α) promoter when in the correct orientation (that is, once inverted by the action of Cre recombinase in the case of floxed constructs). A woodchuck hepatitis virus posttranscriptional regulatory element (WPRE) sequence was included to increase transgene expression (Loeb et al., 1999).

A test transduction of 293T cells demonstrated that the floxed melanopsin plasmid was dependent on the presence of cotransfected Cre for positive melanopsin and 1D4 immunolabelling. As expected, the non-floxed melanopsin plasmid did not require Cre cotransfection to induce positive immunolabelling (Figure 6.2).

The *in vitro* function of the floxed and non-floxed opsins were tested using assays for $G_{q/11}$ and G_i activity. 293T cells transfected with floxed melanopsin and loaded with Rhod-2 fluorescent calcium dye, showed a light-dependent increase in intracellular calcium, a sign of $G_{q/11}$ activity, only when cotransfected with a Cre plasmid. In the absence of Cre, floxed melanopsin-transfected cells showed minimal changes in fluorescence, indistinguishable from negative control cells (Figure 6.3 A).

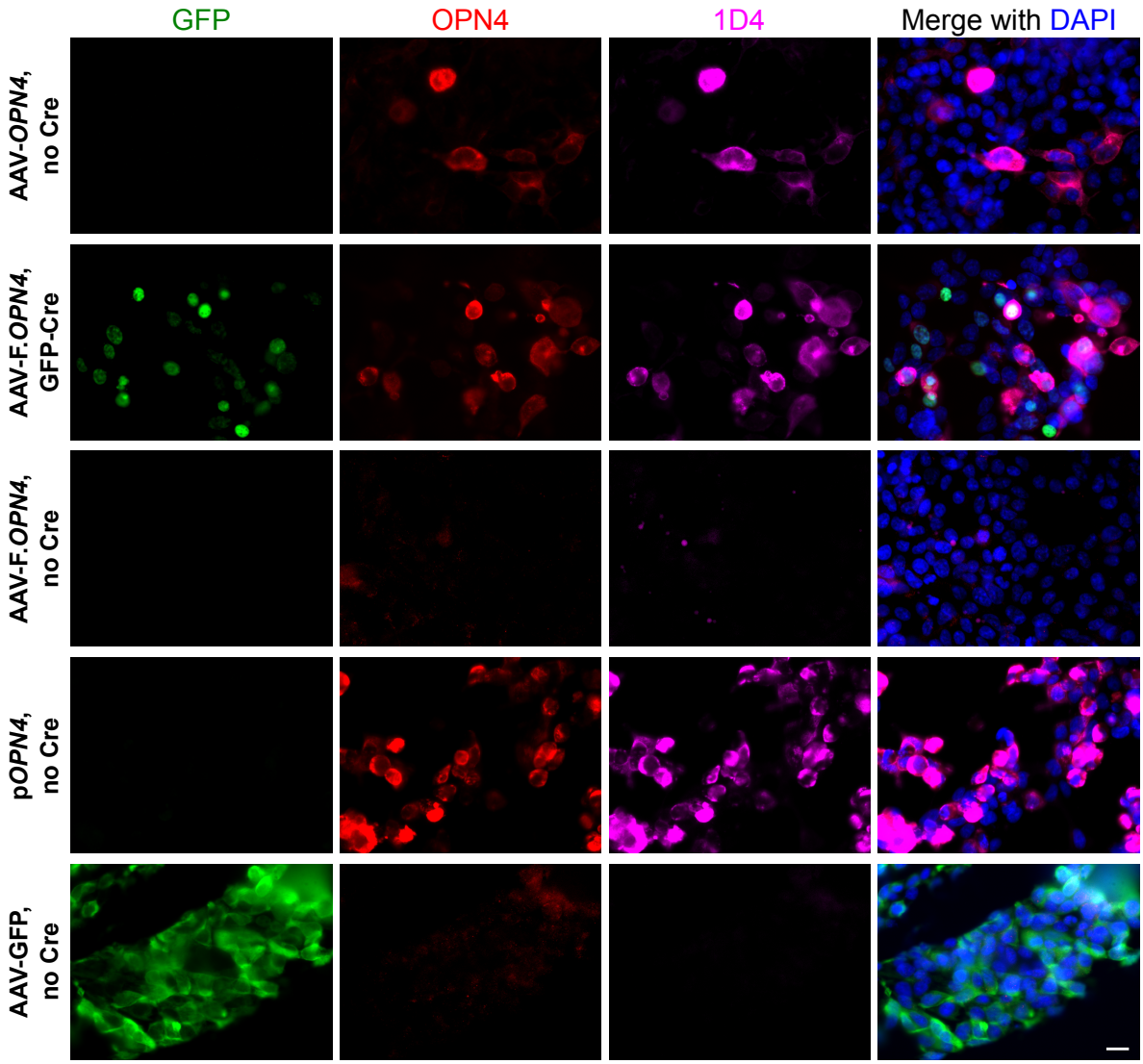


Figure 6.2. *In vitro* expression of floxed and non-floxed melanopsin AAV vectors
293T cells were transduced with a non-floxed melanopsin AAV vector (AAV-*OPN4*); a floxed melanopsin AAV vector (AAV-F.*OPN4*), with and without transfected GFP-Cre; or a GFP-expressing AAV vector. Cells were also transfected with a melanopsin plasmid (p*OPN4*) as an immunocytochemistry control. Three days later the cells were fixed and stained using anti-GFP, anti-human melanopsin (OPN4) and anti-1D4 antibodies. Melanopsin and 1D4 immunolabelling was present in cells transduced with non-floxed melanopsin in the absence of Cre, but only in the presence of Cre was such immunolabelling present in floxed melanopsin transduced cells. Scale bar represents 20 µm.

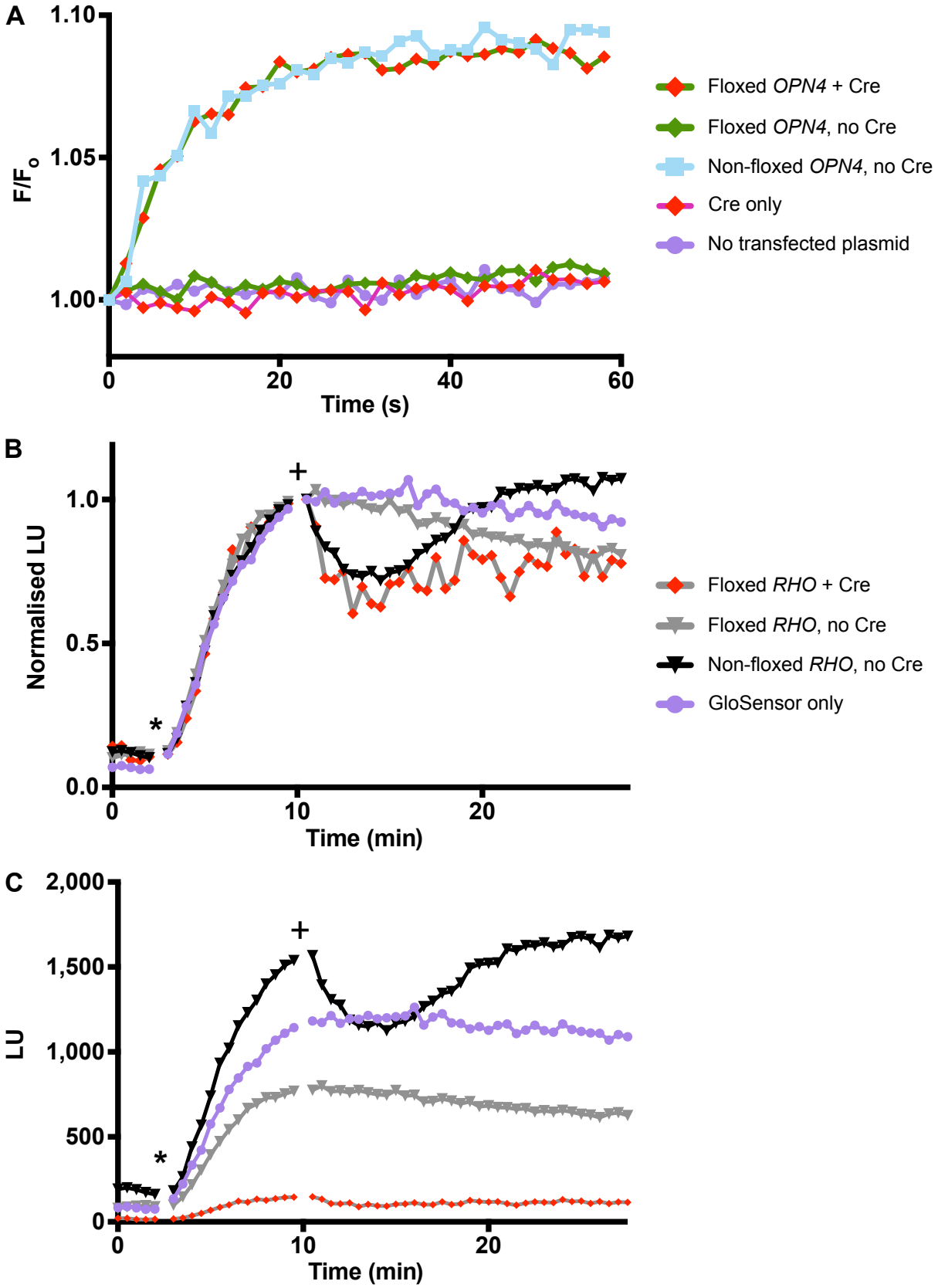


Figure 6.3. *In vitro* function of floxed and non-floxed melanopsin and rhodopsin constructs
(**A**) 293T cells transfected with floxed or non-floxed melanopsin (*OPN4*) plasmids were assayed for $G_{q/11}$ function. Only when Cre was cotransfected with floxed melanopsin did the cells respond with a light-dependent rise in fluorescence, similar to that of non-floxed melanopsin without Cre. In the absence of Cre, cells transfected with floxed melanopsin showed no rise in fluorescence following a light stimulus (n = 1). (**B**) Similarly, only in the presence of cotransfected Cre did cells transfected with floxed rhodopsin (*RHO*) show a light-dependent (+) bioluminescence decrease in an assay of G_i function (n = 1). (**C**) The noise of the normalised floxed rhodopsin with Cre trace was relatively high due to the low absolute luminescence unit (LU) values at baseline and in response to forskolin (added at time denoted by *). F/F_o, fluorescence intensity relative to baseline fluorescence.

The *in vitro* function of floxed rhodopsin was qualitatively assessed using a plate reader-based assay of G_i function by cotransfection with GloSensor plasmid, a bioluminescent marker of intracellular cAMP concentration. After raising the cAMP concentration using forskolin, illuminating the cells with 485 nm light led to a reduction in bioluminescence signal from cells transfected with non-floxed rhodopsin and floxed rhodopsin cotransfected with a Cre plasmid (Figure 6.3 B). In the absence of Cre, the signal of floxed rhodopsin transfected cells followed a similar trend to that of cells only transfected with GloSensor plasmid. The raw levels of bioluminescence from cells cotransfected with Cre, floxed rhodopsin and GloSensor were significantly lower compared to that of all other cells. While the other samples reached peak luminescence unit values of approximately 800 – 1,700, Cre-transfected cells only reached a peak value of 147 luminescence units (Figure 6.3 C). This low level of cAMP-dependent bioluminescence may be due to Cre up-regulating protein kinase A inhibitor, which controls the levels of cAMP and protein kinase A activity (Gangoda et al., 2012).

6.2.2 A pilot *in vivo* study of floxed and non-floxed opsins in a mouse model of retinal degeneration

To compare the efficacy of a targeted versus a non-targeted optogenetic gene therapy approach to vision restoration, floxed and non-floxed opsins were injected bilaterally and subretinally into *L7*-Cre *rd1* mice. These mice were homozygous for the retinal degeneration allele (*rd1*) of phosphodiesterase 6B ($Pde6b^{rd1/rd1}$), causing a rapid loss of the outer nuclear layer. *L7*-Cre *rd1* mice were bred to exclude the *Gpr179* mutation that causes a no b-wave phenotype (Balmer et al., 2013).

Six male and 12 female *L7*-Cre *rd1* mice aged between 6.4 and 16.7 weeks old (mean age: 8 weeks) received bilateral subretinal injections of one of five different AAV vectors (Table 6.1). To compare the effects of a targeted versus non-targeted delivery strategy, 1.0×10^9 vg of either non-floxed or floxed melanopsin were delivered to each

	Opsin	Floxed?	Number of vector genomes injected per eye	Number of mice injected
AAV2/2(7m8)	Melanopsin	No	1.0×10^9	4
		Yes	1.0×10^9	4
		Yes	2.0×10^{10}	4
	Rhodopsin	Yes	2.0×10^{10}	3
	(Saline)	n/a	n/a	3

Table 6.1. Intraocular injections of floxed and non-floxed opsins into *L7*-Cre *rd1* mice
L7-Cre *rd1* mice were injected with floxed and non-floxed melanopsin and floxed rhodopsin packaged into AAV2/2(7m8). A sham control group received injections of BSS saline. All injections were bilateral and subretinal.

eye. To compare the difference between lower and higher dose melanopsin a third group received the same floxed melanopsin vector, but at a higher concentration: each eye received approximately 2.0×10^{10} vg. To compare melanopsin with rhodopsin, a fourth group received 2.0×10^{10} vg of floxed rhodopsin in each eye. Finally, the fifth group received a sham injection of BSS, the same saline used in making the other four vectors. The investigator was masked to the AAV vector used in the injections until after all the data had been collected and analysed.

Transgene expression was detected in the retina by co-immunolabelling with anti-human melanopsin and anti-1D4, which targeted the C-terminal 1D4 tag of each of the opsins (Figure 6.4). Expression was assessed 9 to 12 weeks post-injection. Vertical sections showed that the injection of 1.0×10^{9} vg of non-floxed melanopsin led to immunopositive cells mostly in the outer part of the inner nuclear layer and the occasional immunolabelled cell in the ganglion cell layer (Figure 6.5). Co-labelling with calbindin demonstrated that some of the melanopsin-expressing cells were also calbindin-positive. However, melanopsin-positive cells in the outer part of the inner nuclear layer were also calbindin-negative (Figure 6.6 A).

Only eyes injected with a higher dose of AAV vector containing floxed melanopsin (2.0×10^{10} vg per eye compared with 1.0×10^{9} vg) showed detectable levels of melanopsin using anti-melanopsin or anti-1D4 antibodies (Figures 6.4 and 6.5). Despite the AAV vector being delivered subretinally, the strongest levels of immunofluorescence came from cells in the ganglion cell layer. Weak immunofluorescence signal was detected in the inner nuclear layer when labelled with anti-1D4 monoclonal antibody but not with an anti-human melanopsin polyclonal antibody.

Subretinal injection of 2.0×10^{10} vg of floxed rhodopsin AAV vector per eye resulted in strong immunofluorescence from cells in the inner nuclear layer (Figure 6.4 and 6.5).

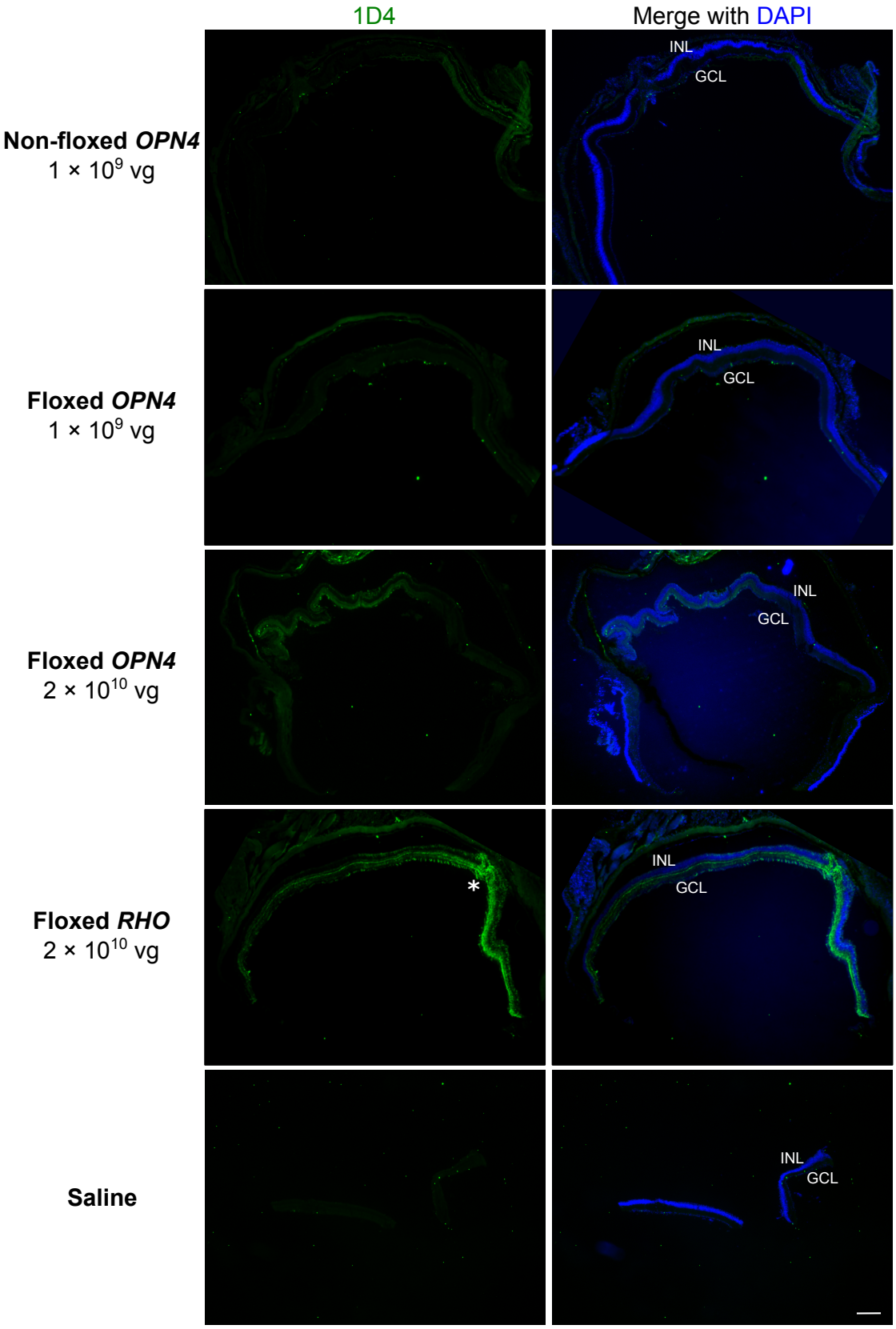


Figure 6.4. Immunolabelling of floxed and non-floxed melanopsin and floxed rhodopsin injections into *L7*-Cre retinally degenerate mice

L7-Cre mice were injected subretinally with non-floxed melanopsin (*OPN4*), floxed melanopsin at two different concentrations (1 × 10^9 or 2 × 10^{10} vg per eye), floxed rhodsopsin (*RHO*) or saline. All were in AAV2/2(7m8) vectors. Nine to 12 weeks post-injection, transgene expression was examined by imunolabelling vertical retinal sections with an anti-1D4 antibody (all transgenes included a 1D4 sequence). Floxed rhodopsin injections resulted in relatively high levels of expression across approximately one third of the retina around the probable injection site (*). Non-floxed melanopsin and high-dose floxed melanopsin injections resulted in lower levels of immunolabelling across less retinal area. Minimal immunolabelling was detected in low-dose floxed melanopsin and saline injected eyes. Scale bar represented 200 µm. GCL, ganglion cell layer; INL, inner nuclear layer; vg, vector genomes.

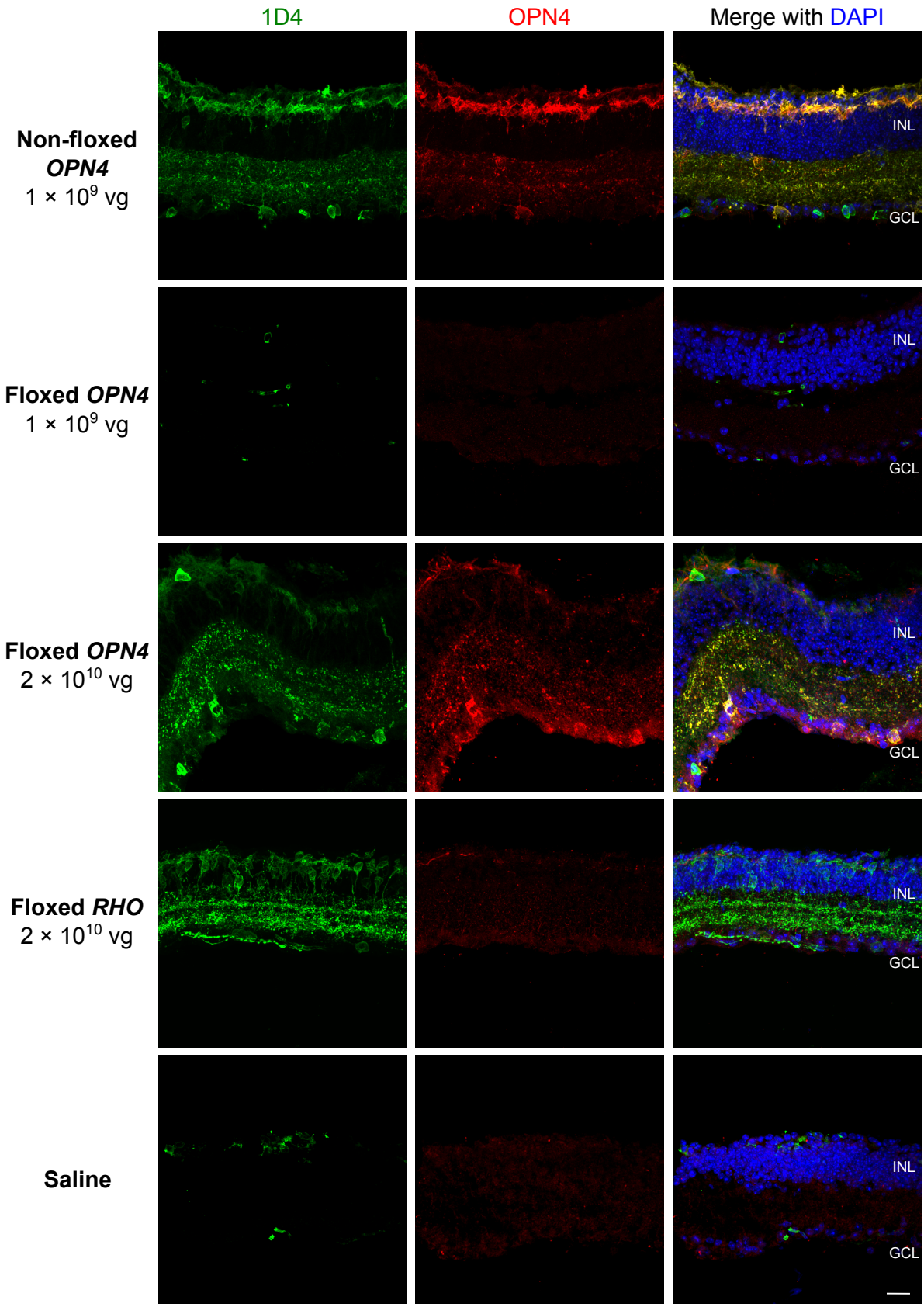


Figure 6.5. Immunolabelling of floxed and non-floxed melanopsin and floxed rhodopsin AAV injections into *L7*-Cre retinally degenerate mice

Nine to 12 weeks after subretinal injection with either non-floxed melanopsin (*OPN4*), floxed melanopsin at two concentrations (1 × 10^9 or 2 × 10^{10} vg per eye), floxed rhodsopsin (*RHO*) or saline, vertical sections were immunolabelled for transgene expression using anti-1D4 and anti-melanopsin antibodies (all transgenes included a 1D4 sequence). Melanopsin injected eyes had 1D4 and melanopsin immunopositive cells in the ganglion cell layer (GCL) and outer inner nuclear layer (INL) in non-floxed melanopsin eyes, while in floxed melanopsin injected eyes the immunopositive cells were predominantly in the ganglion cell layer. Floxed rhodopsin injected eyes featured areas of cells that were strongly 1D4-positive, but melanopsin-negative. Scale bar represented 20 µm.

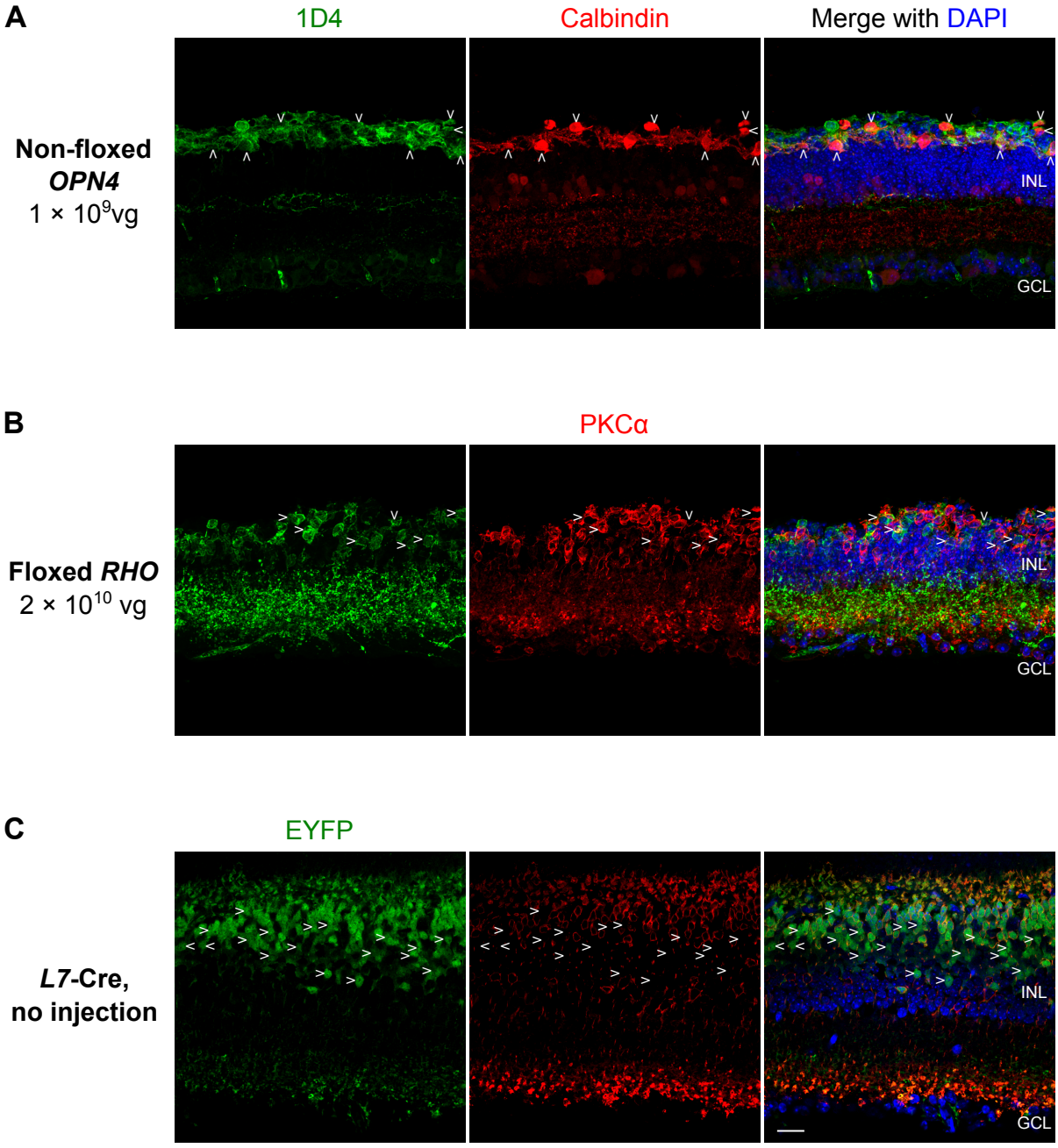


Figure 6.6. Immunolabelling of non-floxed melanopsin and floxed rhodopsin AAV injections into *L7*-Cre retinally degenerate mice
(**A**) Eyes injected subretinally with non-floxed melanopsin (*OPN4*) AAV vector were colabelled with antibodies against the 1D4 C-terminal tag of the transgene and against calbindin. A number of calbindin-positive cells were also 1D4-positive (<) indicating transgene expression in horizontal cells. (**B**) Eyes injected subretinally with floxed rhodopsin (*RHO*) AAV vector were colabelled with anti-1D4 and anti-protein kinase C, alpha (PKCα). A minority of 1D4-positive cells were also PKCα-positive (<), with most being PKCα-negative. (**C**) EYFP-positive, PKCα-negative cells (<) are relatively common in *L7*-Cre EYFP mice and represent cone bipolar cells. Scale bar represented 20 µm. GCL, ganglion cell layer; INL, inner nuclear layer; vg, viral genomes.

Occasional cells in the ganglion cell layer were also noted to be immunopositive. As expected, these cells did not immunolabel with anti-melanopsin antibody. Co-labelling with anti-PKCα antibody resulted in some cells of the inner nuclear layer that were positive for both anti-1D4 and anti-PKCα, but a significant number of 1D4-positive cells appeared to be PKCα-negative (Figure 6.6 B). *L7*-Cre positive, PKCα-negative cells were frequently identified in uninjected eyes (Figure 6.6 C) and are likely to represent cone bipolar cells (Lu et al., 2013).

L7-Cre *rd1* eyes injected with saline as a control for the trauma associated with a subretinal injection showed sparse 1D4 immunolabelling and no appreciable melanopsin labelling (Figures 6.4 and 6.5).

In those retinas with a detectable level of transgene expression the area transduced by subretinal injection ranged from approximately one third to half of the retina, as assessed by vertical sections (Figure 6.4). The site of injection could be identified as an area of tissue damage surrounded by an area with a high level of transduction.

6.2.2.a *In vivo* functional assessment of targeted and non-targeted opsin expression in a mouse model of retinal degeneration

Five to six weeks post-injection *L7*-Cre *rd1* mice were assessed for functional effects of the injected opsins by pupillometry and optomotor response. Pupillometry was performed at four different light intensities ranging from 10^{12} to 10^{15} photons cm^{-2} s^{-1} (Figure 6.7 A). As a positive control, non-degenerate mice of similar ages were also assessed (the same *Pde6b*$^{+/+}$ as used in chapter five). Data from the four light intensities was used to construct an irradiance response curve for each animal, from which the light intensity for half maximal response was calculated (EC_{50}; Figure 6.7 B). The study was underpowered (n = 3 – 4) to detect statistically significant differences between these groups (F (4, 13) = 0.86, P = 0.51, ordinary one-way ANOVA between injected groups), but some interesting trends were noted. At the higher two light intensities (10^{14}

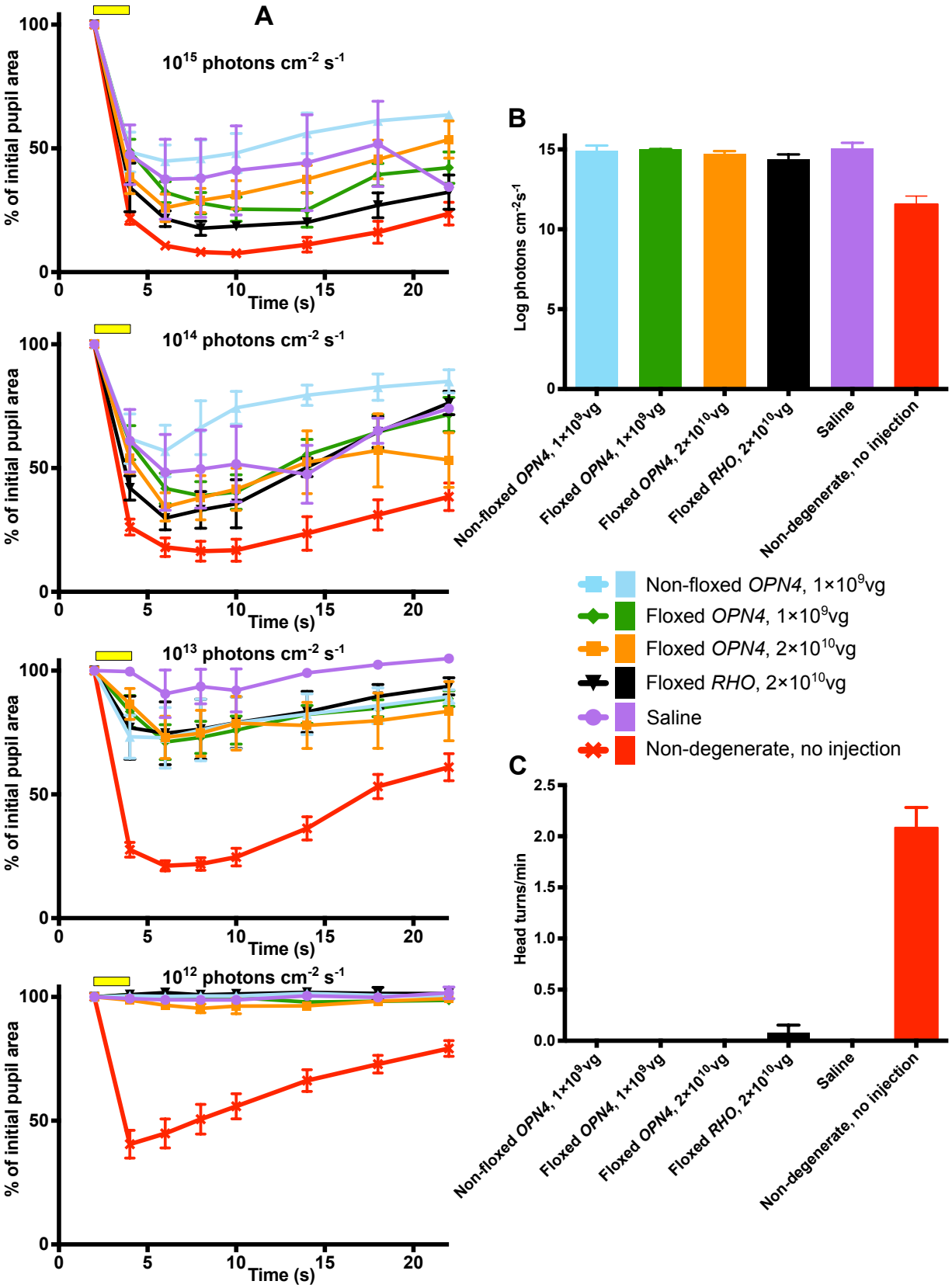


Figure 6.7. Pupillometry and optomotor response of retinally degenerate mice injected with floxed and non-floxed melanopsin and floxed rhodopsin AAV vectors

(**A**) Five to six weeks post-bilateral injections with non-floxed melanopsin (*OPN4*), floxed melanopsin at two concentrations (1 × 10^9 or 2 × 10^{10} vg per eye), floxed rhodopsin (*RHO*) or saline, *L7*-Cre *rd1* mice underwent pupillometry at four different light intensities. Baseline pupil area was recorded before a two second white light pulse (yellow bar; mean ± s.e.m.; n = 4, *OPN4* groups; n = 3, *RHO* and sham; n = 10, degenerate, no injection). (**B**) The light intensity for half maximal response was calculated (n = 4, *OPN4* groups; n = 3, *RHO* and sham; n = 7, non-degenerate, no injection). (**C**) Eight weeks post-injection, mice were assessed for an optomotor response. Apart from a single head turn in the floxed rhodopsin group, only non-degenerate mice showed any head turning responses (n = 4, *OPN4* groups; n = 3, *RHO* and sham; n = 10, degenerate, no injection).

and 10^{15} photons cm^{-2} s^{-1}), the group that was transduced with floxed rhodopsin and the group that was transduced with the higher dose of floxed melanopsin had greater pupil constrictions immediately following the two second light pulse than the other injected groups. These differences led to slightly lower EC_{50} values compared to the saline negative control group: floxed rhodopsin 14.4 ± 0.29 log photons cm^{-2} s^{-1}; floxed melanopsin, high dose, 14.7 ± 0.20 log photons cm^{-2} s^{-1} and saline, 15.0 ± 0.40 log photons cm^{-2} s^{-1}.

An optomotor response assay was applied to the *L7*-Cre *rd1* injected mice eight weeks post-injection as a test of pattern vision. The non-degenerate control mice had 2.1 ± 0.20 reflexive head turns per minute. Only one animal from the floxed rhodopsin group showed a characteristic head turn (Figure 6.7 C). This mouse had a single head turn in the more than four minutes of imaging, resulting in a low rate for the entire group: 0.076 ± 0.076 head turns per minute. The groups of injected mice did not show a statistically significant difference in their optomotor response (F (4, 13) = 1.35, P = 0.30, ordinary one-way ANOVA).

6.3 Discussion

By creating AAV2/2(7m8) vectors expressing either non-floxed or floxed human melanopsin or floxed rhodopsin a number of hypotheses were addressed. The small numbers of animals available for an *in vivo* experiment limits the strength of the conclusions that can be drawn, but this set of experiments provides useful information to guide further studies.

6.3.1 Targeted versus non-targeted expression of melanopsin in the degenerate retina

The relative efficacy of targeted and non-targeted optogenetic gene therapy strategies were compared by injecting *L7*-Cre *rd1* mice with AAV2/2(7m8) containing non-floxed melanopsin driven by the ubiquitous mammalian promoter EF1α and another group

with the same concentration of an identical AAV vector except for the melanopsin transgene being inverted and floxed.

As assessed by immunohistochemistry, the non-targeted approach using non-floxed melanopsin produced greater numbers of immunopositive cells. Melanopsin-positive cells were concentrated in the outer part of the inner nuclear layer; some co-labelled with calbindin, suggesting they were horizontal cells. Melanopsin-positive, calbindin-negative cells may represent residual cone cells. By contrast, the delivery of 1.0×10^9 vg per eye of floxed melanopsin was insufficient to lead to the expression of detectable levels of melanopsin by standard immunohistochemical techniques.

Despite the small number of biological replicates, it is worth noting that the non-floxed melanopsin group performed the poorest in pupillometry with high light intensities. Therefore, despite expressing an appreciable amount of melanopsin, the non-floxed melanopsin group did not show any functional gains, relative to mice that received a saline injection.

This small comparison suggests that a that a higher concentration of vector should be used for further studies.

6.3.2 Transduction efficiency improved with higher concentration AAV vectors

The transduction efficiency of *L7*-Cre-positive cells was compared by injecting the same AAV2/2(7m8) floxed melanopsin vector at two different concentrations. As already noted, the lower dose of 1.0×10^9 vg per eye did not lead to the detection of immunopositive cells following subretinal injection into *L7*-Cre-positive mice. In contrast, injections of 2.0×10^{10} vg per eye was sufficient to lead to strongly immunopositive cells in the ganglion cell layer and weakly positive bipolar cells. Such a pattern of expression has been reported by another group that injected a floxed

transgene into *L7*-Cre retinas (Lu et al., 2013). The *L7*-Cre-positive cells in the ganglion cells layer are most likely to be bistratified retinal ganglion cells (Ivanova et al., 2013).

The observation that the immunolabelling of bipolar cells in the inner nuclear layer was much lower than that of retinal ganglion cells following a subretinal injection suggests that despite a higher concentration of AAV virions surrounding the bipolar cells (due to the subretinal nature of the injection), the ganglion cells were more efficiently transduced. This provides further evidence of the relative difficulty of transducing retinal bipolar cells (see §3.3.3).

6.3.3 Comparison of floxed rhodopsin and floxed melanopsin AAV vectors

By injecting the same high concentration, 2.0×10^{10} vg per eye, of AAV2/2(7m8) containing floxed rhodopsin, the transduction efficiency and light sensitivity properties of melanopsin and rhodopsin were compared. Floxed rhodopsin injections resulted in relatively strong rhodopsin expression across approximately half of the retina. Unlike in eyes injected with floxed melanopsin, bipolar cells were strongly immunopositive in eyes injected subretinally with floxed rhodopsin. This difference in immunolabelling using the same 1D4 antibody suggests that bipolar cells may be more efficient at expressing rhodopsin, than they are at expressing melanopsin. (An alternative explanation is that the anti-1D4 antibody is more efficient at detecting the 1D4 epitope of rhodopsin than that of melanopsin. However, the strong immunopositivity of ganglion cells in floxed melanopsin injected eyes shows that the anti-1D4 antibody is effective at detecting tagged melanopsin, at least in this cell type.)

The high level of rhodopsin detected in bipolar cells was associated with the greatest functional improvements of the groups tested. The floxed rhodopsin group had the lowest light intensity required for half maximal pupil response and was the only group in which a head turn was identified in the optomotor response test. Although the small

numbers of animals make it difficult to draw strong conclusions, it is interesting to note the correlation between a high level of opsin expression and the greatest functional improvement. These signs of functional improvement are despite the fact that the expression of Cre has been found to inhibit the cAMP/protein kinase A pathway (Gangoda et al., 2012) that rhodopsin may be signalling through. Therefore, it can be hypothesised that if rhodopsin expression was limited to bipolar cells by the use of a bipolar cell-specific promoter, the functional improvements may be greater. There was no evidence from *in vitro* studies that Cre co-expression with melanopsin inhibited the calcium response of 293T to light stimulation (data not shown).

Of all the AAV vectors tested in this research project, floxed rhodopsin resulted in the highest frequency and intensity of transgene expression. This can be attributed to the high concentration of AAV vector, the subretinal delivery route and the use of rhodopsin. Only floxed melanopsin and floxed rhodopsin eyes received more than 10^{10} vg per eye, while most other injections involved injecting less than 5×10^{9} vg per eye. There appears to be a threshold that needs to be exceeded to achieve efficient bipolar cell transduction. Other published studies that have demonstrated good transgene expression in bipolar cells have injected at least 10^{10} vg per eye (Macé et al., 2014; Gaub et al., 2015). Studies that have used lower doses have reported poor transduction efficiency (van Wyk et al., 2015).

Given that very similar quantities of floxed melanopsin and floxed rhodopsin were injected with all other factors being equal, the greater expression of rhodopsin in bipolar cells suggest that there may be something specific to rhodopsin that makes it more efficient in the way it is unpackaged from the capsid, forms episomes and/or is transfected and translated into protein. Alternatively, these differences may be due to the different quality of the AAV vector preparations — for example, the floxed

rhodopsin AAV virions may have been less aggregated and therefore had greater infectivity (see §8.5.3 for further discussion).

The time available limited the scope of this study. The *in vivo* opsin expression and functional data suggest that there may be functional benefits from the use of some of these optogenetic gene therapy strategies. If further investment were to be made into these research questions, it would be most relevant to compare non-floxed and floxed melanopsin and rhodopsin at the higher concentrations tested — at least 10^{10} vg per injection. Cellular-level data from multielectrode array and/or patch clamp recordings will give valuable insights into the effects such treatments have on retinal cell physiology. As the efficiency of bipolar cell-specific promoters continues to improve, it would be advantageous to replace the Cre-lox system with cell-specific promoters to achieve targeted gene expression.

Floxed and non-floxed human melanopsin and floxed human rhodopsin AAV vectors were constructed and injected into a model of retinal degeneration in order to investigate: the relative efficacy of human rhodopsin and melanopsin as potential optogenetic tools for vision restoration, to determine differences in retinal transduction using two concentrations of viral vector and to compare visual outcomes following a targeted and non-targeted approach. All of these aims address important questions in the field of optogenetics for vision.

The data from this set of experiments suggest potential trends towards answering these important questions, but did not achieve these aims conclusively. Due to the time available for this project only a pilot experiment was possible, so more highly powered studies are required to properly address these research aims. Immunohistochemistry data from this pilot study suggested that there was notably greater expression of rhodopsin than melanopsin, when delivered at the same concentration. Pupillometry and

optokinetic response functional data also suggested rhodopsin therapy may lead to greater improvements. Comparing the same AAV vector delivered at two different concentrations, showed that transgene expression was greater with the higher concentration, but functional data was not conclusive in showing a benefit. Finally, using floxed and non-floxed versions of a melanopsin transgene-containing AAV vector injected into L7-Cre positive *rd1* mice enabled the comparison of a cell-specific approach to be compared with a non-specific transgene expression approach. Immunohistochemistry data suggested the non-targeted approach lead to greater overall levels of transgene expression, but pupillometry data suggested this non-targeted group performed worse than the targeted group. The differences between groups were not statistically significant. Therefore, further *in vivo* investigation in a larger cohort of animals is required to distinguish between these groups more definitively.

Bipolar

1. (of a nerve cell) having two axons, one either side of the cell body.
2. (of a person) suffering from bipolar disorder.

Bi- from Latin, **'doubly, having two'**; related to Greek *di-* **'two'**.

Polar mid 16th cent.: from medieval Latin *polaris* **'heavenly'**, from Latin *polus* **'end of an axis'**.

7

Bipolar Cell Gene Expression in Retinal Degeneration

7.1 Introduction

7.1.1 Bipolar cells as a target for optogenetic gene therapy for vision restoration

Of the more than 60 functionally distinct cell types in the mammalian retina (Masland, 2011), retinal bipolar cells are the highest priority target cell for optogenetic gene therapy to restore vision (Dalkara et al., 2015). Bipolar cells are second-order neurons that form synapses with photoreceptors in healthy retinas. In the absence of photoreceptors, bipolar cells become the most upstream cell type in the visual processing pathway. In such degenerate retinas, making bipolar cells light sensitive has the potential to enable visual processing in the retina.

The physiology of bipolar cells is relatively well understood (Euler et al., 2014) when compared to our understanding of the many other types of inner retinal cells, thus providing a theoretical framework on which to base an optogenetics for vision strategy.

The cell bodies of retinal bipolar cells reside in the outer part of the inner nuclear layer where they send dendrites into the outer plexiform layer to synapse with either rod or cone cells. A typical mouse retina has more than four million photoreceptors synapsing

with 600,000 bipolar cells, 200,000 of which are rod bipolar cells and 400,000 cone bipolar cells (Jeon et al., 1998; Strettoi and Pignatelli, 2000; Strettoi et al., 2003). Axons of bipolar cells pass through the inner nuclear layer to the inner plexiform layer where they synapse with amacrine cells and retinal ganglion cells.

The mouse retina features at least 13 subtypes of bipolar cell (Helmstaedter et al., 2013), which are identified by their photoreceptor connectivity, axonal stratification, morphology and immunohistochemical markers. These distinct functional classes of bipolar cells are essential to the centre-surround physiology of the retina. There is a single class of rod bipolar cell and 12 known subtypes of cone bipolar cells in the mouse retina. Types 1, 2, 3a, 3b and 4 are OFF bipolar cells and are sign-conserving. The release of glutamate from depolarised photoreceptors leads to the opening of AMPA/kainate class ionotropic glutamate cation channels (Sasaki and Kaneko, 1996; Lindstrom et al., 2014). OFF bipolar cells' axon terminals are found in the outer part of the inner plexiform layer. Types 5a, 5b, XBC, 6, 7, 8 and 9 are ON bipolar cells that are sign-inverting — light-induced hyperpolarisation of photoreceptors leads to depolarisation of ON bipolar cells through inactivation of metabotropic glutamate receptor, type 6 (mGluR6). Bipolar cells receive inhibitory or excitatory input from horizontal cells, depending on the functional class (Vardi et al., 2000; Puller et al., 2014). Bipolar cell responses can be graded potentials or spikes (Baden et al., 2013).

While one study has targeted halorhodopsin to residual cone cells (Busskamp et al., 2010) and another targeted channelrhodopsin-2 and halorhodopsin to ganglion cells (Greenberg et al., 2011), the majority of optogenetic gene therapy preclinical studies have targeted light-sensitive molecules to ON bipolar cells (Lagali et al., 2008; Doroudchi et al., 2011; Cronin et al., 2014; Cehajic-Kapetanovic et al., 2015; Gaub et al., 2015; van Wyk et al., 2015). ON bipolar cells have the practical advantages of having cell-specific transcriptional regulatory elements available to restrict expression

to these cells (Cronin et al., 2014) and a relatively well understood GPCR signalling pathway, which can be utilised for GPCR-based optogenetic strategies (Morgans et al., 2010; Cehajic-Kapetanovic et al., 2015; Gaub et al., 2015; van Wyk et al., 2015).

To successfully light-sensitise a cell for many years and not cause long-term damage, it is necessary to understand the physiology of the cell. More particularly, if ON bipolar cells are to be light sensitised by optogenetic gene therapy, then a greater understanding of their physiology in the diseased state is required. This is because it is bipolar cells of the degenerate retina, rather than the better studied non-degenerate retina, that will be the target tissue for optogenetic gene therapy.

7.1.2 Pathophysiology of retinal bipolar cells in retinal degeneration

The loss of photoreceptors caused by inherited retinal dystrophies causes significant secondary changes in the retina. At the gross anatomical level the human retina develops an attenuation in the calibre of retinal vessels, the optic disc appears pale and the migration of retinal pigment epithelial cells into the retina creates so-called bone spicules (Jones and Marc, 2005), but the inner retinal layer remains present and grossly intact for decades following the onset of symptoms. More detailed investigation has found that the primary loss of photoreceptors is associated with a secondary loss of cells in the inner nuclear and ganglion cell layers in humans (Santos et al., 1997; Humayun et al., 1999) and mice (Strettoi and Pignatelli, 2000).

At the microscopic level more significant changes in retinal bipolar cells have been found following the degeneration of photoreceptors. Following the loss of photoreceptor input, bipolar cells and horizontal cells undergo significant anatomical reorganisation including retraction of dendritic arbours (Strettoi and Pignatelli, 2000; Chen et al., 2012). Late-stage sprouting of bipolar cell dendrites has also been documented in some models of retinal degeneration (Cuenca et al., 2005). By

approximately 60 days old, rod bipolar cell density in the *rd1* mouse has been documented to be more than 30% lower in the central area of degenerate retinas compared to non-degenerate retinas (Strettoi and Pignatelli, 2000). Proteins, such as mGluR6, that are normally restricted to the dendrites are aberrantly localised (Strettoi and Pignatelli, 2000; Cuenca et al., 2005). Anatomical changes have been correlated with functional changes, including a demonstration that bipolar cells from a *rd1* degenerate retina are much less sensitive to glutamate but more sensitive to GABA compared to bipolar cells from a non-degenerate retina (Varela et al., 2003). A subset of cone bipolar cells have also been found to be a source of low amplitude oscillatory activity that is evident in degenerate retinas (Borowska et al., 2011).

Cone bipolar cells also show a loss of dendritic arborisation, but the rate of loss is delayed relative to rod bipolar cells and appears to occur at a uniform rate across the retina, rather than following the central to peripheral pattern seen in rod bipolar cell loss (Strettoi et al., 2003; Chen et al., 2012).

In addition to changes in retinal bipolar cell dendrites, there are late-stage changes in the synapses between bipolar cells and amacrine and ganglion cells (Strettoi et al., 2002; Chen et al., 2012). Rod bipolar cell endings were found to be smaller and disorganised in the *rd1* mouse by P30 (Strettoi et al., 2002). Levels of synaptophysin, a synaptic vesicle protein, have been found to be elevated in bipolar cells of *rd1* degenerate retinas (Dagar et al., 2014). Based on their findings, Chen and colleagues suggested that optogenetic gene therapy targeting bipolar cells should occur relatively early in degeneration, before such synaptic changes occur.

A number of studies have investigated gene expression changes in the degenerate retina. Hackam and colleagues (2004) compared gene expression of *rd1* and non-degenerate control retinas at three ages: postnatal days (P) 14, 35 and 50. Not surprisingly, given

the dramatic early loss of photoreceptors in the *rd1* mouse, most of the genes with reduced expression were photoreceptor-specific genes. G protein signalling-related genes that were noted to be decreased in expression were all genes known to be expressed in photoreceptors, including rhodopsin; the guanine nucleotide binding proteins, alpha transducing 1 (*Gnat1*) and beta polypeptide 1 (*Gnb1*); and S-antigen (*Sag*). Other genes showing differential expression were those involved in oxidative stress, cell structure (both upregulated), metabolism, signalling and transport (downregulated).

A more detailed study of multiple models of retinal degeneration by Holt and colleagues (2015) confirmed some of the gene expression changes previously documented in *rd1* retinas. This study used Affymetrix microarrays to confirm the downregulation of known photoreceptor genes, such as *Grk1*, *Pdc*, *Pde6a*, *Pde6b*, *Pde6g* and *Sag*, in P80 *rd1* mice. Pathway analysis revealed the over-representation of genes associated with metabolism and the cytoskeleton. This study also highlighted the differential expression of known retinal dystrophy-causing genes in the process of retinal degeneration and identified 30 poorly characterised genes that are candidate human disease genes.

Studies that utilise whole retina tissue sampling do not provide information on the direction and magnitude of gene expression changes in specific cell types. Upregulation of gene expression in one cell type may be masked due to the small contribution that cell type makes to the total pool of RNA, or because its effects may be countered by a downregulation of the same gene in another cell type. Perhaps as a consequence of these experimental limitations, none of the studies that utilised whole retina samples reported significant changes in the expression of bipolar-specific genes.

A study by Armata and colleagues (2006) investigated the differential expression of *Grm6*, a bipolar cell-specific gene that encodes mGluR6, in a rat model of retinal

degeneration. Using *in situ* hybridisation contrasting changes in *Grm6* expression were demonstrated at different ages, relative to the expression in non-degenerate retinas in the Royal College of Surgeons rat, which contains a recessive mutation in the *Mertk* gene (D'Cruz et al., 2000). At P17 *Grm6* expression was decreased in the degenerate retina, while at P60 and P120 higher levels of expression were present relative to control retinas. This variation reinforces how retinal degeneration is a dynamic process and how results are dependent on the time of sampling.

Punzo and Cepko (2007) used a whole-retina microarray as an initial screening tool of candidate genes and followed this with an *in situ* hybridisation study to gain cell-specific data. *In situ* hybridisation performed on P35 *rd1* retinas showed that at this relatively early phase of retinal remodelling, bipolar cells and Müller cells have greater induction of gene expression compared to other cell types. The value of cell-specific data was demonstrated by the finding that, relative to the non-degenerate control, 10 per cent of the genes screened were upregulated in one cell type and down regulated in another cell type.

7.1.3 A study of bipolar cell-specific gene expression changes in a mouse model of retinal degeneration

To gain information about the retinal bipolar cell-specific gene expression changes in retinal degeneration and to avoid the limitations associated with sourcing RNA from whole retina samples, a fluorescence-activated cell sorting (FACS)-based method of isolating retinal bipolar cells was developed. It was hoped that the cell-specific data would provide both insights into the pathophysiological response of bipolar cells to the loss of contact with photoreceptors as well as useful data to optimise an optogenetic gene therapy strategy to restore vision. Specifically of interest were changes in the relative expression of genes associated with G protein signalling cascades; significant

changes in these genes could have important implications for the development of optogenetic tools for vision restoration.

A transgenic line of mice was used for the isolation of bipolar cells. *L7*-Cre mice express Cre recombinase under the control of a Purkinje cell protein 2 (*Pcp2* also known as *L7*) promoter. This transgenic model has been found to express Cre in Purkinje cells of the cerebellum (Marino et al., 2002), rod bipolar cells, types 2 and 6 cone bipolar cells (Lu et al., 2013) and a subset of bistratified retinal ganglion cells (Ivanova et al., 2013). By crossing this line with a strain of mice that had a targeted mutation inserting enhanced yellow fluorescent protein (EYFP) with an upstream floxed transcriptional road block into the Rosa26 locus, a line of mice that expressed EYFP in a high fraction of bipolar cells was created (Figure 6.1).

Mating the progeny of this cross with mice carrying the *rd1* retinal degeneration mutation allowed the breeding of retinally degenerate and non-degenerate siblings on which FACS was performed (Figure 7.1). The advantages of this model is that there is an established body of literature around the anatomical and molecular responses of the bipolar cells to the loss of photoreceptors (Strettoi and Pignatelli, 2000; Hackam et al., 2004; Punzo and Cepko, 2007; Holt et al., 2015).

Aim

- To study the gene expression changes in retinal bipolar cells in a mouse model of retinal degeneration to better understand their potential as target cells for optogenetic gene therapy or alternative strategies for vision preservation or restoration.

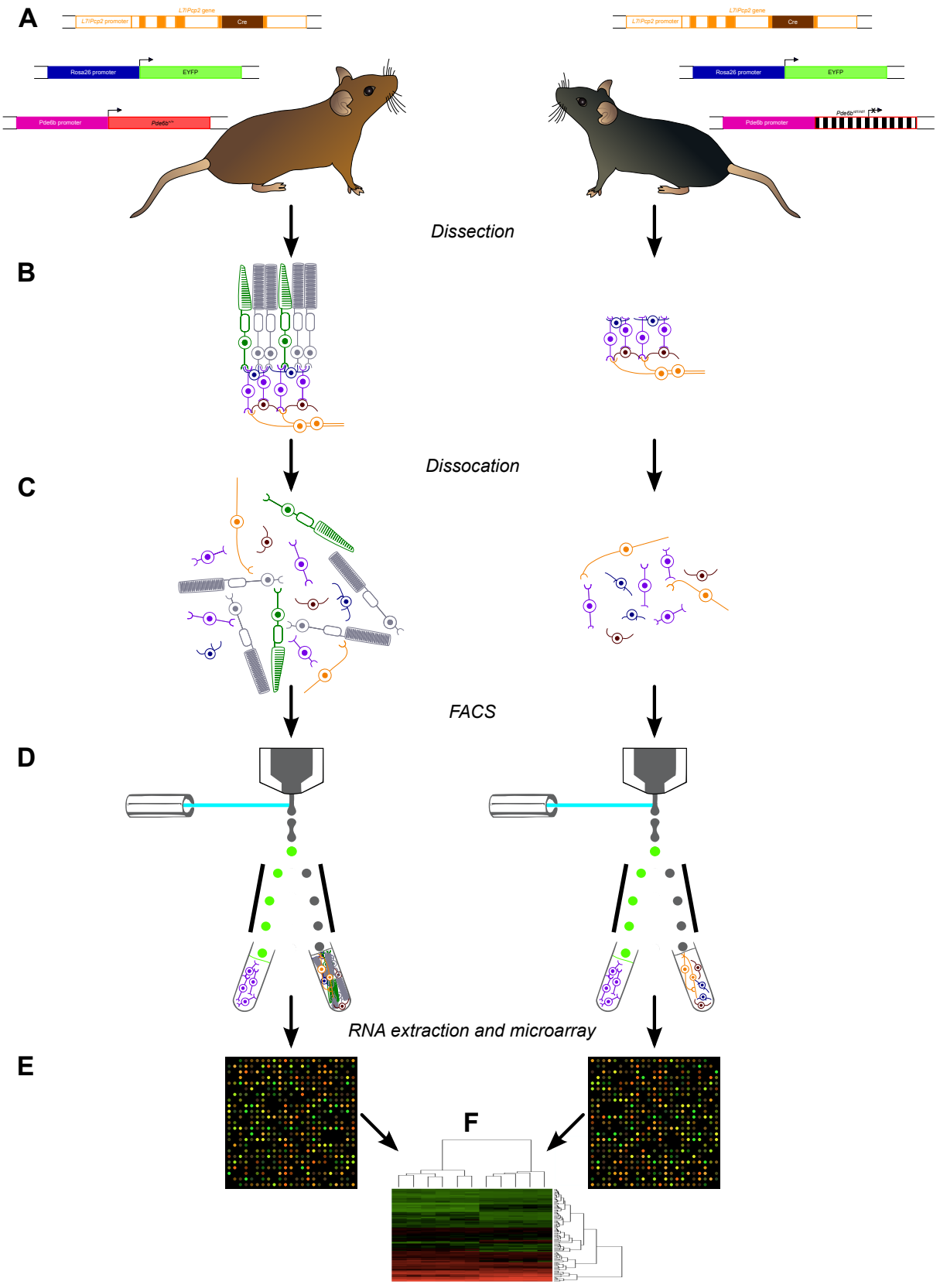


Figure 7.1. Fluorescence-activated cell sorting for a microarray study of retinal bipolar cells from degenerate retinas
(**A**) *L7*-Cre EYFP non-degenerate (*Pde6b*$^{+/+}$) and degenerate (*Pde6b*$^{rd1/rd1}$) mice were culled and (**B**) the retinas removed and (**C**) dissociated. (**D**) FACS was used to isolate YFP-positive cells (predominantly rod bipolar cells). (**E**) RNA was extracted from YFP-positive cells and used for a microarray study. (**F**) Microarray results compared the expression of genes in non-degenerate and degenerate samples.

7.2 Results

7.2.1 FACS isolation of retinal bipolar cells from *L7*-Cre-positive retinas

Mice from three lines were crossed to produce siblings that were positive for the *L7*-Cre allele (Tg(Pcp2-cre)756Mro/0), homozygous for an EYFP targeted mutation to the Rosa26 locus (Gt(ROSA)26Sor$^{tm1(EYFP)Cos}$) and either homozygous for the *rd1* mutation (*Pde6b*$^{rd1/rd1}$) or homozygous for the wild type allele (*Pde6b*$^{+/+}$). All mice used in these experiments were homozygous for the wild type *Gpr179* allele (*Gpr179*$^{+/+}$; data not shown).

Dissected retinas were dissociated and sorted by FACS (Figure 7.1). As anticipated, a YFP-positive cell population was isolated from *L7*-Cre-positive EYFP mice and not from *L7*-Cre-negative EYFP mice (Figure 7.2 C). FACS settings were optimised to avoid contamination with dead cells, which were readily identified by propidium iodide staining (Figure 7.2 A and B).

To confirm the identity of the sorted cells, cells from YFP-positive and YFP-negative fractions were seeded onto cell culture dishes. On the day of seeding the YFP-positive fraction was highly enriched with YFP-positive cells, while no YFP-positive cells were identified in the YFP-negative cell fraction (Figure 7.3 A). Within one day of seeding, the endogenous EYFP fluorescence had diminished significantly (data not shown). Immunolabelling with anti-GFP and anti-PKCα antibodies one day post-FACS revealed that the YFP-positive cell fraction was highly enriched with YFP-positive and PKCα-positive cells (Figure 7.3 B).

Quantitative PCR provided further evidence of enrichment of retinal bipolar cells following FACS of *L7*-Cre-positive, EYFP retinas. RNA from YFP-positive and YFP-negative sorted cell fractions from both *rd1* degenerate mice and non-degenerate mice were analysed for their expression of bipolar cell-specific genes and rod-specific genes.

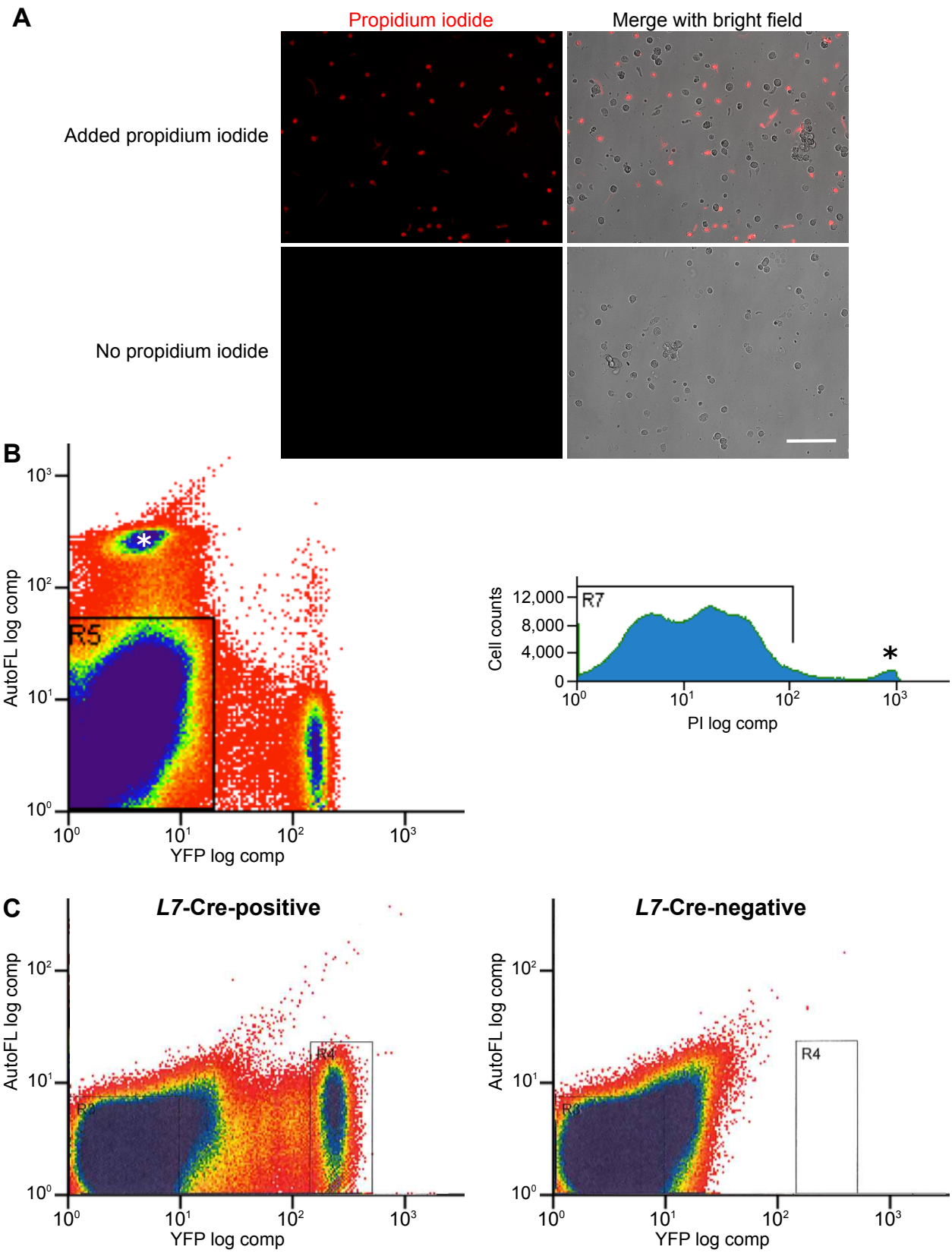


Figure 7.2. Validation of FACS techniques to isolate live YFP-positive cells from *L7*-Cre-positive mouse retinas

(**A**) Propidium iodide (PI) was added to dissociated cells to identify dead and dying cells. Here PI was added at a concentration of 1 µg/ml to 293T cells to demonstrate its effective fluorescence when bound to dead cells. (**B**) The PI-positive population was evident on FACS dot plots (left) and histograms (right) as a distinct population (*) that was excluded from the sorted cell populations. (**C**) The YFP-positive cell population was identified by sorting cells from *L7*-Cre-positive (left) and *L7*-Cre negative (right) retinas. A distinct population in and around the 'R4' gated area was present when cells from a *L7*-Cre-positive were sorted, but absent when cells from a *L7*-Cre-negative retina were sorted. Fluorescence signal was compensated ('comp') for the presence of a second fluorophore. Scale bar represents 50 µm.

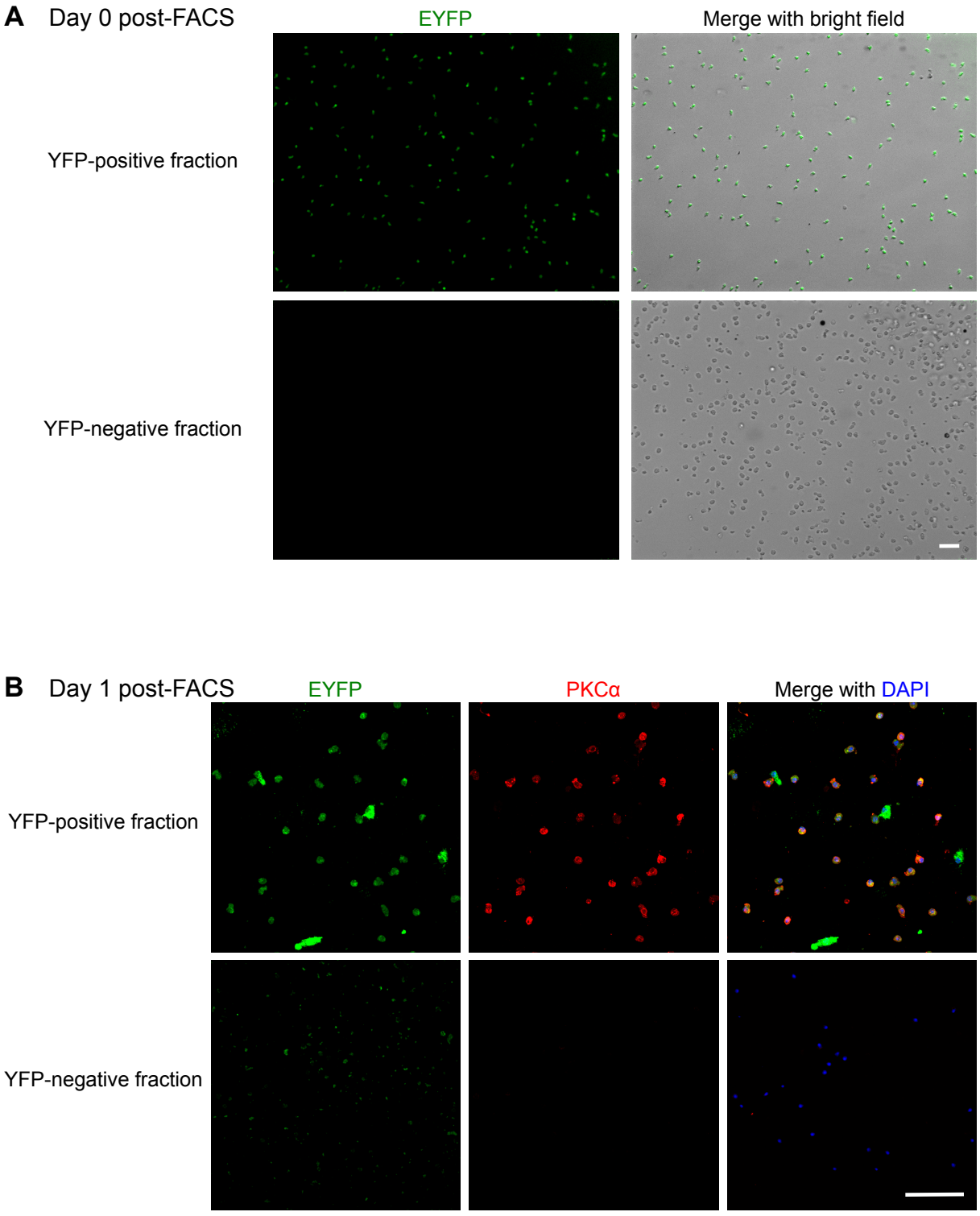


Figure 7.3. Identification of fluorescence-activated cell sorted cell populations
(**A**) Cells sorted by FACS into YFP-positive and YFP-negative cell populations were seeded and imaged by fluorescence microscopy. The vast majority of cells in the YFP-positive cell fraction were clearly fluorescent in the YFP channel. (**B**) FAC-sorted cells that were left overnight to adhere to a glass coverslip were fixed and immunolabelled with antibodies binding EYFP and protein kinase C alpha (PKCα). Cells in the YFP-positive fraction were positive for EYFP and the vast majority were also positive for PKCα. In the YFP-negative fraction cells were negative for both EYFP and PKCα. Scale bar represents 50 µm.

The YFP-positive cell fractions from degenerate and non-degenerate retinas both had high levels of bipolar-specific genes and low levels of rod-specific genes, relative to the YFP-negative population and normalised to housekeeper genes (Figure 7.4 A). Bipolar-specific genes (*Cabp5*, *Grm6*, *Pcp2* and *Prkca*) were on average 15-fold higher in the YFP-positive fraction relative to the YFP-negative fraction. In the non-degenerate YFP-positive samples, rod-specific genes were approximately 4% of the gene expression levels detected in the YFP-negative sample. (Due to the unmeasurable levels of rod-specific genes in the degenerate samples, a relative expression level could not be determined from these samples.)

As a preliminary investigation into the relative expression levels of genes in the bipolar cells of degenerate versus non-degenerate retinas, the levels of expression of bipolar-specific genes in the YFP-positive cell populations from degenerate and non-degenerate samples were compared, normalised to housekeeper gene expression (Figure 7.4 B). Bipolar-specific genes were found to be four to seven fold higher in bipolar cells from degenerate retina compared to the levels in non-degenerate retina. The level of rhodopsin in the degenerate retina sample was less than 1% of the expression level in the non-degenerate sample. The relative expression level of the other rod-specific gene, *Cnga1*, could not be determined.

7.2.2 Microarray study of bipolar cell gene expression changes in retinal degeneration

YFP-positive cells were isolated by FACS from six non-degenerate (*Pde6b*$^{+/+}$) and six degenerate (*Pde6b*$^{rd1/rd1}$) mice for a microarray study of bipolar cell gene expression changes in retinal degeneration (Figure 7.5). Both non-degenerate and degenerate groups each consisted of three males and three females. Two sibling pairs of the same gender were used, with one of the siblings being retinally degenerate and the other non-degenerate. The 12 mice were sourced from five breeding pairs. Mice were 89 to 91

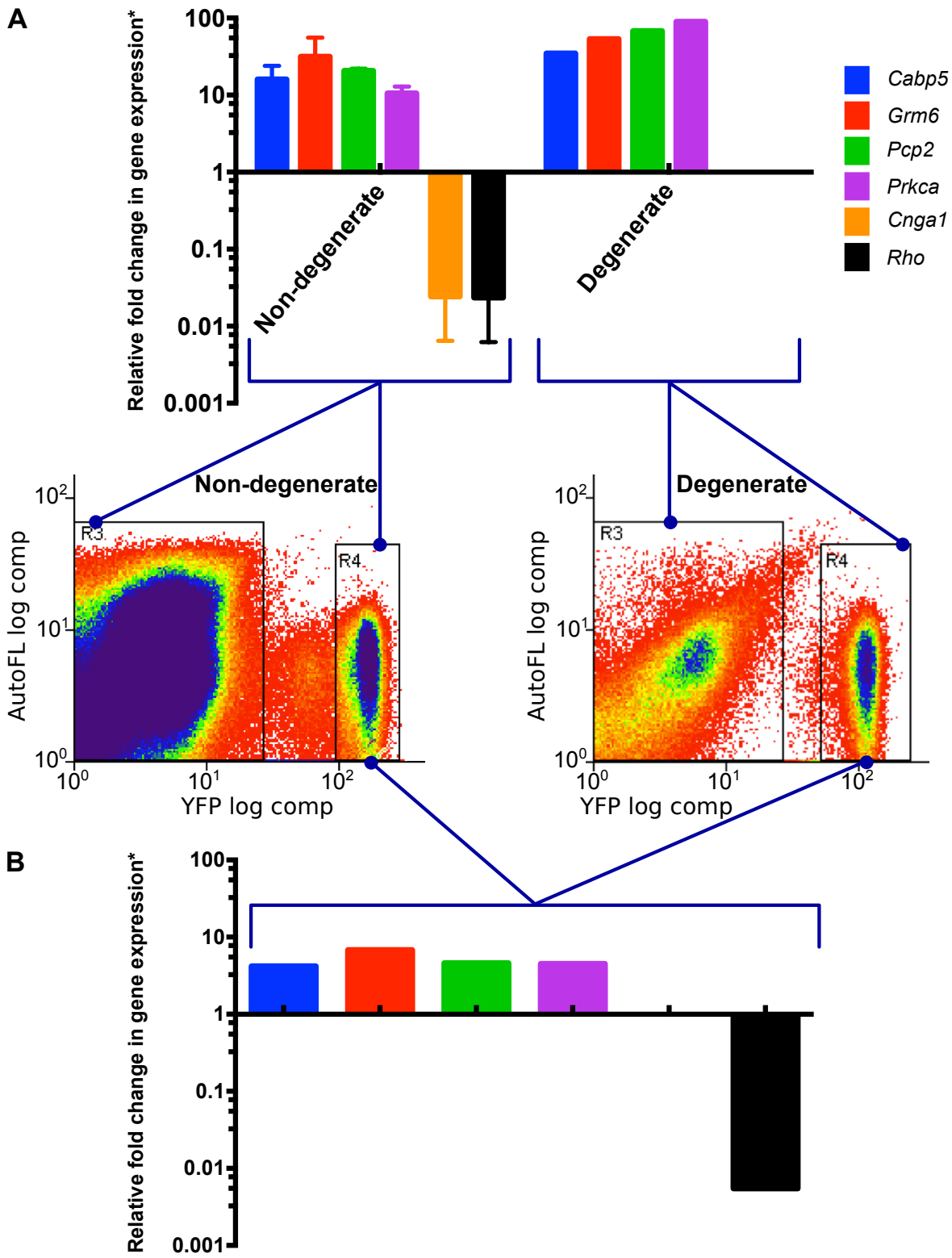


Figure 7.4. Quantitative PCR of retinal bipolar cell-specific and rod cell-specific genes in isolated cell populations from degenerate and non-degenerate mouse retinas

(**A**) The relative fold change in the expression of retinal bipolar cell-specific genes (*Cabp5*, *Grm6*, *Pcp2* and *Prkca*) and rod cell-specific genes (*Cnga1* and *Rho*) were compared in the YFP-positive cell population, relative to the YFP-negative cell population in samples from non-degenerate (left) and degenerate (right) *L7*-Cre EYFP retinas following FACS. The YFP-positive cell fraction had higher expression of bipolar-specific and lower expression of rod-specific genes, indicating that the YFP-positive population was enriched in bipolar cells (mean ± s.e.m.; n = 2, non-degenerate, n = 1, degenerate). (**B**) The relative fold change in the expression of the same genes were compared between the YFP-positive cell populations from non-degenerate and degenerate FAC-sorted retinas (n = 1). *Gene expression normalised to *Gapdh* and *Rplp0* housekeeper genes and negative control sample(s). *Cabp5*, calcium binding protein 5; *Grm6*, glutamate receptor, metabotropic 6; *Pcp2*, Purkinje cell protein 2 (L7); *Prkca*, protein kinase C, alpha; *Cnga1*, cyclic nucleotide gated channel alpha 1; *Rho*, rhodopsin; *Gapdh*, glyceraldehyde-3-phosphate dehydrogenase; *Rplp0*, ribosomal protein, large, P0.

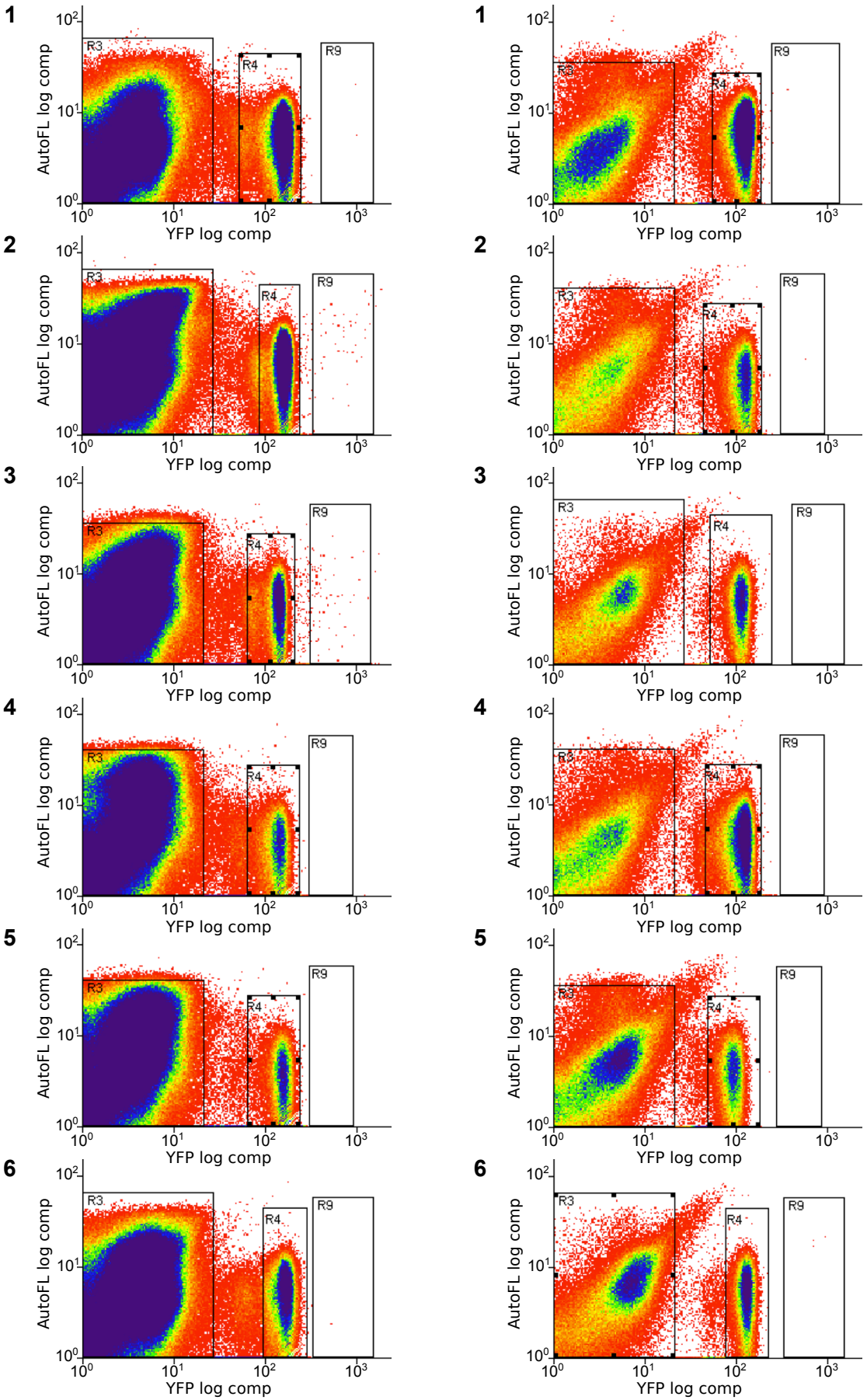


Figure 7.5. FACS dot plots of non-degenerate and degenerate *L7*-Cre EYFP retinas utilised for a microarray study
Retinas from six non-degenerate (left column) and six degenerate (right column) *L7*-Cre EYFP mice were dissociated and underwent fluorescence-activated cell sorting (FACS). The YFP-negative (R3) and YFP-positive (R4) cell populations from each were isolated, the RNA extracted and RNA from the YFP-positive population utilised for a microarray study comparing gene expression between non-degenerate and degenerate samples.

days old on the day of FACS (Table 7.1). Non-degenerate retinas yielded 95,300 ± 10,900 YFP-positive cells and degenerate retinas yielded 73,200 ± 13,900 YFP-positive cells.

When visualised as a heat map, clusters of genes were noted to differ in their expression levels between the two groups (Figure 7.6 A). Sixty-six probes representing 64 genes had differences between the two groups that had an adjusted *P* value less than 0.05 (Figure 7.6 B). Of those, 19 probes from 19 genes had an adjusted *P* value less than 0.01. A list of probes that had a statistically significant ($P < 0.05$) difference in expression level between degenerate and non-degenerate groups is provided in Table 7.2.

To investigate whether the genes that had a statistically significant change in expression between degenerate and non-degenerate retinas were interrelated by a common function or process, the genes were inputted to protein-protein interaction prediction software. Known photoreceptor genes were excluded from the analysis. A group of six genes (*Atox1*, *Car2*, *Clip1*, *Msrb2*, *Mt1* and *Mt2*) shared the function of transition metal ion binding (Figure 7.7). Previous microarray studies of different tissues had found a number of these genes to have been co-expressed (Gallardo et al., 2007; Andrechek et al., 2009).

To more closely examine the gene expression changes of genes that might be utilised in an optogenetics gene therapy for vision strategy, expression level changes and adjusted *P* values of selected genes are presented in Table 7.3. Genes that are associated with photoreceptors were excluded. Of the selected genes involved in G protein signalling, only three intracellular effector genes were found to be differentially expressed to a statistically significant extent.

A **Non-degenerate**

Sample	Gender	Age (days)	YFP-positive cells	Concentration (pg/µl)	RIN
1	F	90	141,000	190	9.8
2	F	90	112,000	275	9.0
3	F	91	71,000	159	8.8
4	M	89	89,000	1,414	9.9
5	M	90	85,000	1,460	9.4
6	M	89	74,000	150	9.2
Mean		89.8	95,333	608	9.4

B **Degenerate**

Sample	Gender	Age (days)	YFP-positive cells	Concentration (pg/µl)	RIN
1	F	90	98,000	743	9.4
2	F	90	73,000	470	9.7
3	F	90	41,000	61	9.1
4	M	90	128,000	790	9.5
5	M	89	54,000	42	9.2
6	M	89	45,000	77	9.8
Mean		89.7	73,167	364	9.5

Table 7.1. Summary of YFP-positive FACS samples from *L7*-Cre mice used for a microarray study of retinal degeneration
Male and female *L7*-Cre EYFP (**A**) non-degenerate and (**B**) degenerate mice aged 89 – 91 days were used for FACS to isolate YFP-positive cells. The number of YFP-positive cells isolated by FACS is provided. RNA extracted from YFP-positive cells was assessed by Bioanalyzer for its quantity and quality (RNA Integrity Number, RIN). Sample numbers correspond to Figure 7.5.

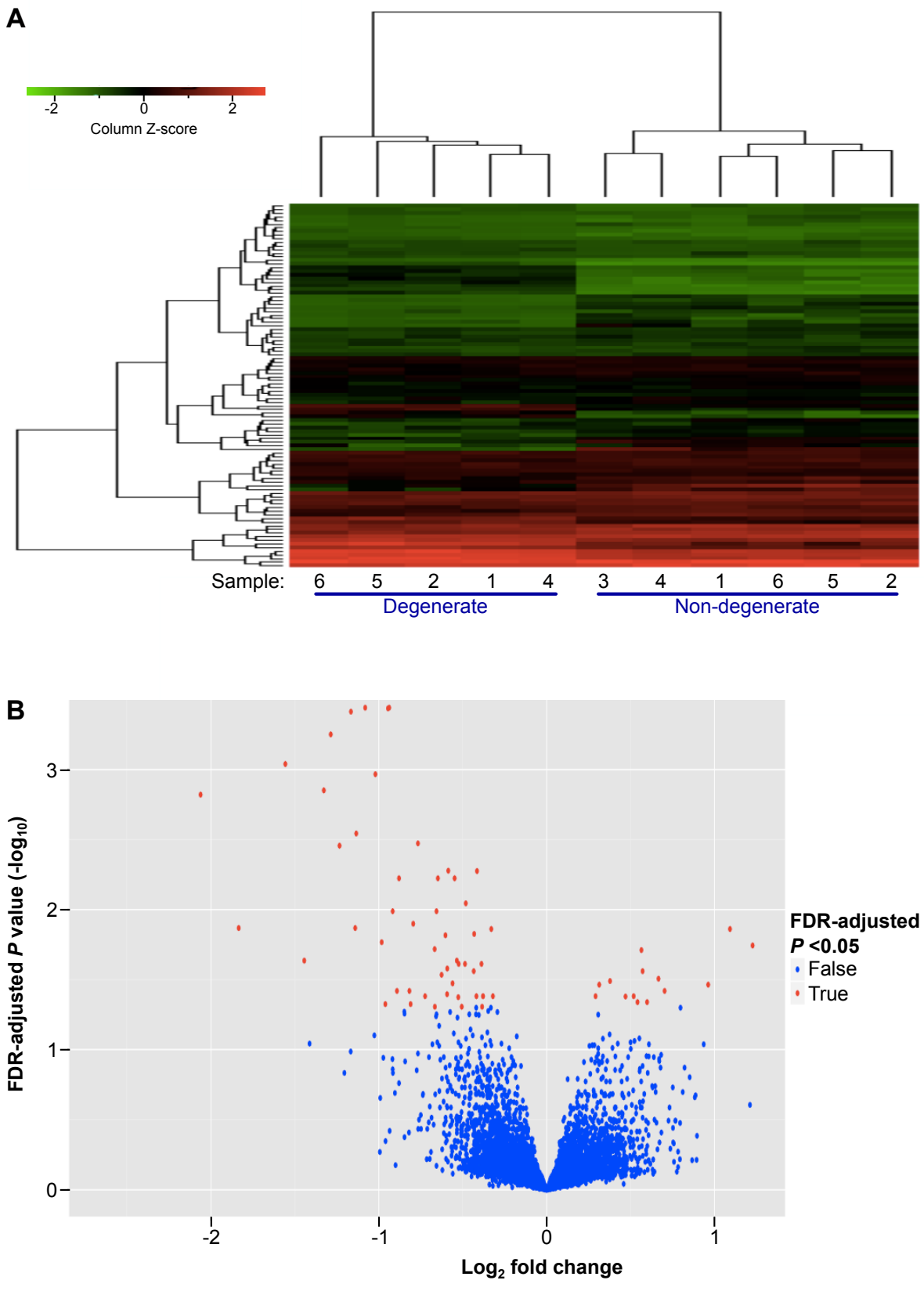


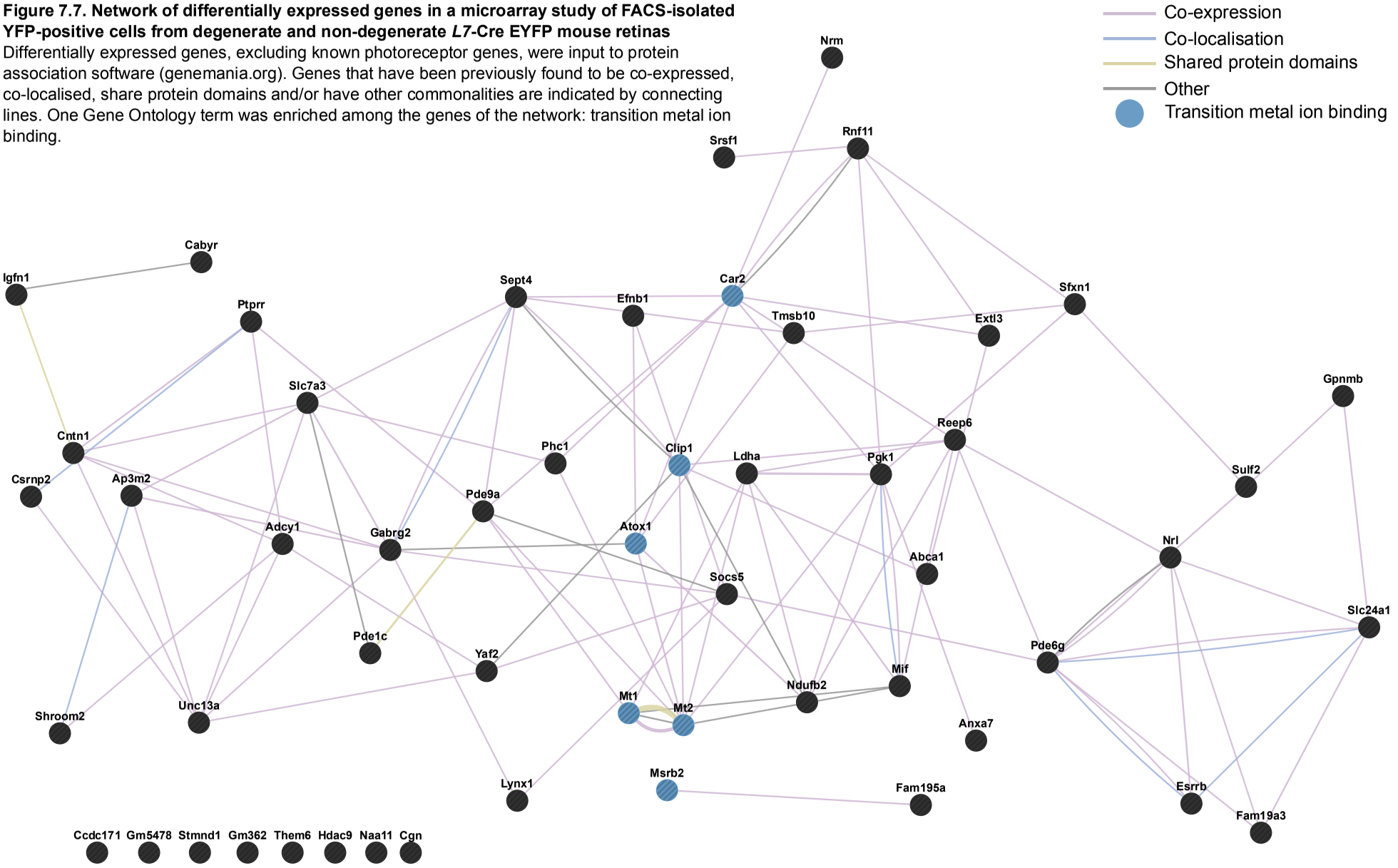
Figure 7.6. Overview of results of a microarray study comparing the gene expression of FACS-isolated YFP-positive cells from *L7*-Cre EYFP degenerate and non-degenerate mouse retinas
(**A**) Heat map of gene expression levels, coloured by sample/column *Z*-score, showing clustering of samples into degenerate and non-degenerate groups. (**B**) Volcano plot of the adjusted *P* value against fold change for each of the probes in an Illumina MouseWG-6 microarray study. Red dots represent probes that demonstrated a statistically significant change in expression level between degenerate and non-degenerate samples. A positive fold change represents higher expression in the degenerate samples, on average, than in the non-degenerate samples. FDR, false discovery rate.

Symbol	Full name	Log_{10} fold change	Adjusted *P* value	Chromosome
Igfn1	Immunoglobulin-like and fibronectin type III domain containing 1	1.2	0.018	1
Cgn	Cingulin	1.1	0.014	3
Msrb2	Methionine sulfoxide reductase B2.	0.96	0.034	2
Cabyr	Calcium binding tyrosine-(Y)-phosporylation regulated	0.70	0.038	18
Efnb1	Ephrin-B1	0.67	0.031	X
Ccdc171	Coiled-coil domain containing 171	0.60	0.046	4
Phc1	Polyhomeotic homolog 1 (Drosophila)	0.57	0.028	6
Sfxn1	Sideroflexin 1	0.56	0.020	13
Fam19a3	Family with sequence similarity 19 (chemokine (C-C motif)-like), member A3	0.54	0.046	3
Shroom2	Shroom family member 2	0.52	0.042	X
Sfrs1	Serine/arginine-rich splicing factor 1	0.47	0.042	11
Sept4	Septin 4	0.38	0.032	11
Sulf2	Sulfatase 2	0.31	0.034	2
Nrm	Nurim (nuclear envelope membrane protein)	0.29	0.042	17
LOC385699	*Withdrawn by NCBI. Similar to Ab2-162*	-0.32	0.042	-
Gm362	Predicted gene 362	-0.33	0.014	X
Pde9a	Phosphodiesterase 9A	-0.38	0.042	17
Ndufb2	NADH dehydrogenase (ubiquinone) 1 beta subcomplex, 2	-0.38	0.041	6
Gabrg2	Gamma-aminobutyric acid (GABA) A receptor, gamma 2	-0.38	0.049	11
Anxa7	Annexin A7	-0.39	0.024	14
Fam195a	Family with sequence similarity 195, member A	-0.41	0.0053	17
Atox1	Antioxidant 1 copper chaperone	-0.42	0.041	11
Socs5	Suppressor of cytokine signaling 5	-0.43	0.015	17
Csrnp2	Cysteine-serine-rich nuclear protein 2	-0.43	0.028	15
D730001G18Rik	Riken cDNA D730001G18 gene	-0.48	0.0090	15
Rnf11	Ring finger protein 11	-0.49	0.024	4
Cntn1	Contactin 1	-0.51	0.049	15
mtDNA_COXIII	Mitochondrial cytochrome oxidase II subunit	-0.52	0.024	Mitochondrial
Pdc*	Phosducin	-0.53	0.042	1
Ap3m2	Adapter-related protein complex 3, mu 2 subunit	-0.53	0.023	8
Rnf11	Ring finger protein 11	-0.55	0.0060	4
Mif	Macrophage migration inhibitory factor	-0.56	0.034	10
Pde1c	Phosphodiesterase 1C, calmodulin-depdendent 70kDa	-0.59	0.0053	6
Pcdha7	Protocadherin alpha 7	-0.59	0.026	18
LOC676420	*Withdrawn by NCBI. Similar to ceramide kinase (mCERK)*	-0.59	0.040	-
Esrrb	Estrogen-related receptor beta	-0.60	0.015	12
Extl3	Exostosin-like glycosyltransferase 3	-0.63	0.029	14
Unc13a	Unc-13 homolog A	-0.65	0.0060	8
Gm5478	Predicted pseudogene 5478	-0.66	0.010	15
Tmsb10	Thymosin beta 10	-0.67	0.049	6
Pdc*	Phosducin	-0.67	0.019	1
Pgk1	Phosphoglycerate kinase 1	-0.72	0.041	X
Stmnd1	Stathmin domain containing 1	-0.77	0.0034	13
Mt2	Metallothionein 2	-0.80	0.013	8
Yaf2	YY1 associated factor 2	-0.81	0.047	15
Reep6	Receptor accessory protein 6	-0.82	0.038	10
Clip1	CAP-GLY domain containing linker protein 1	-0.88	0.0060	5
Nrl	Neural retina leucine zipper	-0.89	0.038	14
Slc7a3	Solute carrier family 7 (cationic amino acid transporter, Y+ system), member 3	-0.92	0.010	X
Car2	Carbonic anhydrase II	-0.94	0.00036	3
Adcy1	Adenylate cyclase 1	-0.95	0.00037	11
Pde6g	Phosphodiesterase 6G	-0.96	0.047	11
Abca1	ATP-binding cassette, sub-family A (ABC1), member 1	-0.98	0.017	4
Them6	Thioesterase superfamily member 6	-1.0	0.0011	15
Pde6b*	Phosphodiesterase 6B	-1.1	0.00036	5
Hdac9	Histone deacetylase 9	-1.1	0.0029	12
Ptprr	Protein tyrosine phosphatase, receptor type, R	-1.1	0.014	10
Naa11	N(alpha)-acetyltransferase 11, NatA catalytic subunit	-1.2	0.00039	5
Gpnmb	Glycoprotein (transmembrane) Nmb	-1.2	0.0035	6
LOC100047936	*Withdrawn by NCBI. Similar to sortilin-related receptor, LDLR class A repeats-containing*	-1.3	0.00056	-
Ldha	Lactate dehydrogenase A	-1.3	0.0014	7
Slc24a1	Solute carrier family 24 (sodium/potassium/calcium exchanger), member 1	-1.4	0.023	9
Sag*	S-antigen, retina and pineal gland (arrestin)	-1.6	0.00092	1
Lynx1	Ly6/neurotoxin 1	-1.8	0.014	15
Mt1	Metallothionein 1	-2.1	0.0015	8
Gnat1*	Guanine nucleotide binding protein (G Protein), alpha transducing activity polypeptide 1	-2.7	0.00015	9

Table 7.2. Differentially expressed genes in a microarray study comparing FACS-isolated YFP-positive cells from degenerate and non-degenerate *L7*-Cre EYFP mouse retinas

Statistically significantly differentially expressed probes are listed, according to log fold change. A positive log fold change represents upregulation in the degenerate samples. Genes that are known photoreceptor genes from a Gene Ontology Consortium list are indicated (*). The adjusted *P* value is colour-coded for the signficance level. The chromosomal location of each gene is indicated. Genes located in chromosome 5, the chromosome containing Pde6b, are highlighted.

Figure 7.7. Network of differentially expressed genes in a microarray study of FACS-isolated YFP-positive cells from degenerate and non-degenerate *L7*-Cre EYFP mouse retinas
Differentially expressed genes, excluding known photoreceptor genes, were input to protein association software (genemania.org). Genes that have been previously found to be co-expressed, co-localised, share protein domains and/or have other commonalities are indicated by connecting lines. One Gene Ontology term was enriched among the genes of the network: transition metal ion binding.



Probe	Gene name	Log_2 fold change	Adjusted *P* value
Receptor			
Grm6	Glutamate receptor, metabotropic 6	0.046	0.86
Gα subunits			
Gna11	Guanine nucleotide binding protein, alpha 11	0.036	0.79
Gna11		-0.061	0.86
Gna14	Guanine nucleotide binding protein, alpha 14	-0.070	0.78
Gnai1	Guanine nucleotide binding protein, alpha inhibiting 1	-0.073	0.94
Gnai2	Guanine nucleotide binding protein, alpha inhibiting 2	-0.035	0.88
Gnai3	Guanine nucleotide binding protein, alpha inhibiting 3	0.0058	0.99
Gnao1	Guanine nucleotide binding protein, alpha O, transcript variant A	-0.18	0.79
Gnao1		0.017	0.98
Gnaq	Guanine nucleotide binding protein, alpha q polypeptide	-0.29	0.054
Gnaq		-0.024	0.88
Gβγ subunits			
Gnb3	Guanine nucleotide binding protein, beta 3	0.56	0.17
Gnb4	Guanine nucleotide binding protein, beta 4	-0.045	0.93
Gnb5	Guanine nucleotide binding protein, beta 5, transcript variant 1	-0.0082	0.97
Gng2	Guanine nucleotide binding protein, gamma 2, transcript variant 2	-0.085	0.80
Gng3	Guanine nucleotide binding protein, gamma 3	0.25	0.84
Gng5	Guanine nucleotide binding protein, gamma 5	0.031	0.82
Gng7	Guanine nucleotide binding protein, gamma 7, transcript variant 2	0.43	0.60
Gng7	Guanine nucleotide binding protein, gamma 7	0.057	0.77
Gng10	Guanine nucleotide binding protein, gamma 10	-0.068	0.78
Gng11	Guanine nucleotide binding protein, gamma 11	-0.043	0.80
Gng13	Guanine nucleotide binding protein, gamma 13	-0.10	0.71
Intracellular effectors			
Adcy1	Adenylate cyclase 1	-0.95	0.00037
Adcy1		0.038	0.80
Adcy2	Adenylate cyclase 2	0.50	0.57
Adcy3	Adenylate cyclase 3	0.012	0.95
Adcy8	Adenylate cyclase 8	0.048	0.81
Adcy9	Adenylate cyclase 9	0.041	0.80
Pde1b	Phosphodiesterase 1B, Ca^{2+}-calmodulin dependent	-0.27	0.58
Pde1b		-0.30	0.62
Pde1c	Phosphodiesterase 1C, transcript variant 2	-0.59	0.0053
Pde1c		-0.17	0.19
Pde1c		-0.072	0.76
Pde1c		0.15	0.79
Pde1c		-0.086	0.83
Pde1c		0.0019	1.0
Pde3a	Phosphodiesterase 3A, cGMP inhibited	-0.029	0.85
Pde3a		0.010	0.94
Pde3a		0.000079	1.0
Pde3b	Phosphodiesterase 3B, cGMP inhibited	-0.018	0.93
Pde4a	Phosphodiesterase 4A, cAMP specific, transcript variant 5	-0.10	0.57
Pde4b	Phosphodiesterase 4B, cAMP specific	-0.20	0.41
Pde4b		-0.16	0.77
Pde4b		0.21	0.83
Pde4b		-0.015	0.94
Pde4d	Phosphodiesterase 4D, cAMP specific	-0.62	0.52
Pde4d		-0.0019	0.99
Pde7a	Phosphodiesterase 7A	-0.052	0.79
Pde7b	Phosphodiesterase 7B	-0.13	0.62
Pde8b	Phosphodiesterase 8B	-0.021	0.89
Pde9a	Phosphodiesterase 9A	-0.38	0.042
Plcb3	Phospholipase C, beta 3	0.060	0.75
Plcb4	Phospholipase C, beta 4	0.19	0.80
TRP channels			
Trpc6	Transient receptor potential cation channel, subfamily C, member 6	-0.043	0.77
Trpc7	Transient receptor potential cation channel, subfamily C, member 7	-0.22	0.79
Trpm1	Transient receptor potential cation channel, subfamily M, member 1, transcript variant 1	0.15	0.78
Trpm1		-0.10	0.80
Trpm1		0.076	0.82
Trpm1		0.15	0.84
Arrestin			
Arrb2	Arrestin, beta 2	-0.093	0.87
Kinases			
Grk4	G protein-coupled receptor kinase 4, transcript variant 2	0.11	0.72
Grk4	G protein-coupled receptor kinase 4, transcript variant 1	-0.057	0.79
Grk5	G protein-coupled receptor kinase 5	0.075	0.79
Grk5		0.032	0.86
Bipolar cell-specific			
Cabp5	Calcium binding protein 5, transcript variant 2 (predicted)	0.34	0.54
Pcp2	Purkinje cell protein 2 (L7)	-0.10	0.80
Prkca	Protein kinase C, alpha	-0.074	0.75
Scgn	Secretagogin, EF-hand calcium binding protein	0.29	0.80
Scgn		-0.019	0.97
Vsx1	Visual system homeobox 1 homolog (zebrafish)	0.035	0.91
Vsx2	Visual system homeobox 2 (Vsx2)	0.17	0.81
Vsx2		0.079	0.90
Housekeeping genes			
Actb	Actin, beta	0.32	0.61
Actb		-0.24	0.71
Actb		-0.025	0.98
Actb		-0.023	0.98
Gapdh	Glyceraldehyde-3-phosphate dehydrogenase	-0.36	0.20
Rplp0	Ribosomal protein, large, P0	-0.12	0.80
Rplp0		0.013	0.99

Table 7.3. Differential expression of G protein signalling genes from a microarray study comparing FACS-isolated YFP-positive cells from degenerate and non-degenerate *L7*-Cre EYFP mouse retinas
Numeric columns are colour coded from low (red) to high (green) values. Photoreceptor-specific genes are excluded.

Intracellular effector genes are a large group of genes that include adenylate cyclase, phosphodiesterase and phospholipase C genes. One probe for adenylate cyclase 1 had gene expression levels in the degenerate samples that were 52% of the levels in non-degenerate samples, on average ($P = 0.00037$). However, another probe for the same gene showed slightly higher expression levels (3%; $P = 0.80$). One of the probes for phosphodiesterase 1C, transcript variant 2 found the gene expression level in degenerate samples to be 66% of non-degenerate levels ($P = 0.0053$). Three of the other probes for the same gene also showed decreased expression levels, but two others showed an increase, none of which were statistically significant. Phosphodiesterase 9A was also found to be expressed at a lower level in degenerate samples relative to non-degenerate (77% of non-degenerate levels, $P = 0.042$).

To gain what information was available on the comparative expression levels of the different genes, the average expression level of select probes associated with genes relating to G protein-coupled signalling were examined (Figure 7.8). While most probes had expression levels of 6 to 7 (arbitrary units), a number of probes had notably elevated expression levels. Genes involved in the mGluR6 signalling pathway were among those significantly elevated. *Grm6* had one of the highest expression levels of all the 20,002 probes (12.7). The Gα subunit that couples to mGluR6, *Gnao1* (Dhingra et al., 2002), was also elevated with probe expression levels of 7.9 and 9.5 (two different probes). Of the two Gβ subunits that are known to be required for normal ON bipolar cell function, *Gnb3* (Dhingra et al., 2012) and *Gnb5* (Rao et al., 2007), *Gnb3* was not elevated (7.3) but *Gnb5* was detected at elevated expression levels (10.6 and 6.8 values for two probes). The Gγ subunit thought to interact with G_o and Gβ3 to form a heterotrimeric G protein, *Gng13* (Huang et al., 2003), was also highly elevated, with an average expression value of 12.3. The end effector channel of mGluR6 activation, TRPM1, showed strong evidence of being highly expressed, with four probes having

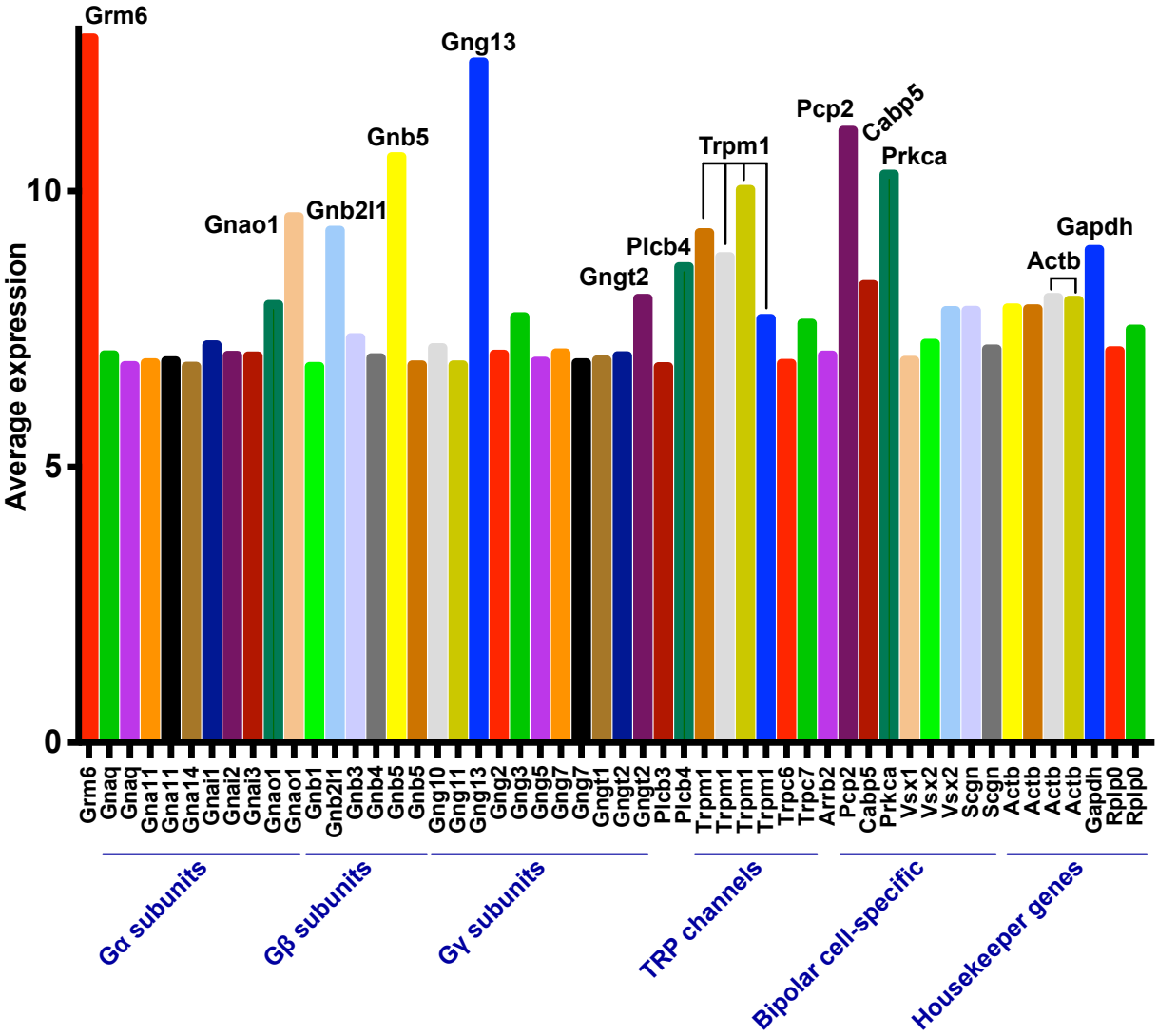


Figure 7.8. Average gene expression of select G protein signalling genes from a microarray study comparing FACS-isolated YFP-positive cells from degenerate and non-degenerate *L7*-Cre EYFP mouse retinas
The average expression levels across all samples of probes targeting selected genes involved in G protein signalling, bipolar cell-specific genes and housekeeper genes. Gene probes with values over 8 (arbitrary units) are labelled adjacent the top of their bar. See Table 7.3 for gene names.

elevated expression values: 10.0, 9.2, 8.8 and 7.7. Other bipolar-specific genes, including *Cabp5*, *Pcp2* and *Prkca*, were also detected at high expression levels.

7.3 Discussion

Retinal bipolar cells, particularly of the ON class, are of great interest for optogenetic gene therapy to restore vision. A greater understanding of their molecular functions in health and disease will better inform the choice of light-sensitive molecule and gene delivery mechanism for an optogenetic vision restoration strategy. This set of experiments investigated the gene expression changes in a subset of bipolar cells in the degenerate mouse retina relative to non-degenerate control retinas. This dataset provides valuable information on the transcriptional profile of retinal bipolar cells from non-degenerate retina and the expression changes of bipolar cells from degenerate retina. A deeper appreciation of the normal and pathological state of bipolar cells will inform not only our fundamental understanding of the pathophysiology of retinal degeneration, but also the field of optogenetics for vision restoration and, potentially, the discovery of candidate disease-causing genes.

7.3.1 Analysis of G protein signalling-related genes in the degenerate retina informs the choice of optogenetic gene therapy

Although the signal transduction pathways of visual opsins and melanopsin are generally well understood when these opsins are expressed in their native cell types, it is less well understood which signalling partners will be required for effective signalling when expressed ectopically for an optogenetic purpose.

Overall, the data from this microarray study suggests that the level of expression of most genes important for $G_{q/11}$ and $G_{i/o}$ intracellular signalling do not show statistically significant changes in the retinal bipolar cells of degenerate retinas, relative to bipolar cells from age-matched non-degenerate retinas and may, therefore, be suitable for

melanopsin- or rhodopsin-based gene therapy (Table 7.3). The general trend was for a modest decrease in expression levels, with some intracellular effector genes showing statistically significant decreases.

The G_o signalling mGluR6 (encoded by the *Grm6* gene), which is natively expressed in ON bipolar cells, was not differentially expressed to a statistically significant degree. Compared to a non-degenerate control, an increase in *Grm6* mRNA was found in the late stages of retinal degeneration in rat model (Armata et al., 2006). At the protein level, the amount of mGluR6 immunoreactivity detectable in the outer plexiform layer is diminished in the *rd1* mouse, but it is also detected in the cell body and along axons — locations that are devoid of mGluR6 immunoreactivity in non-degenerate retinas (Strettoi and Pignatelli, 2000). Therefore it is not clear whether the overall protein level differs in the degenerate retina. The expression levels of Gα, Gβ and Gγ subunits important for mGluR6 signalling (Dhingra et al., 2002, 2012) were not statistically significantly different between degenerate and non-degenerate groups.

Although the molecular effector molecules linking the activation of G_o and the inactivation of TRPM1 channels are not well understood, adenylate cyclase and phosphodiesterases are involved in signalling via the $G_{i/o}$ pathway. Probes for adenylate cyclase sequences were generally slightly increased in the degenerate samples, but the only sample to have a statistically significant result was an adenylate cyclase 1 probe showing a decrease in expression in the degenerate samples. The expression levels of genes encoding phosphodiesterase proteins not expressed in photoreceptors showed a trend for levels to be generally lower in the degenerate retinas. Phosphodiesterases 1C and 9A both showed statistically significant decreases in expression in the degenerate state.

An interesting perspective of the data was gained by analysing the average expression levels of some of the probes targeting genes involved in G protein-coupled signalling. Although microarrays are not optimal for determining absolute levels of genes expression (Held et al., 2006; Fu et al., 2009), there were some standout differences in this dataset that are worth discussing. Most significantly was that most of the genes known to be critical for normal ON bipolar cell functioning, *Grm6*, *Gnao1*, *Gnb5*, *Gng13* and *Trpm1*, were all highly elevated, relative to genes encoding proteins not known to be critical to ON bipolar cell function. These findings have two important implications. Firstly, this provides further evidence that the samples were highly enriched for ON bipolar cell genes, giving confidence in the methodology and results. Secondly, despite any changes in response to retinal degeneration, the levels of expression of the genes associated with the native G protein pathway of mGluR6 are clearly the most abundant in ON bipolar cells. An optogenetic strategy that utilises this pathway would be expected to have the greater success over coupling to other pathways with less abundant components.

7.3.2 Non-G protein signalling related gene expression changes in the degenerate retina

In addition to investigating changes in the expression of genes that would be utilised by the ectopic expression of opsins, a secondary goal of this study was to investigate any patterns of gene expression changes that may provide insights into the cellular response of bipolar cells in the degenerate retina. A better understanding could provide useful insights to inform an optogenetic gene therapy, or to develop alternative approaches to slow or reverse retinal degeneration. Some observations of note from the 64 genes that showed statistically significant changes in gene expression will be discussed.

Using protein-protein interaction prediction software, six of the genes that showed statistically significant differential expression between degenerate and normal retina

have a function in transition metal ion binding. Methionine sulfoxide reductase B2 (*Msrb2*) was found at higher levels in the degenerate samples, while antioxidant 1 copper chaperone (*Atox1*), carbonic anhydrase II (*Car2*), CAP-GLY domain containing linker protein 1 (*Clip1*) and two metallothionein genes, *Mt1* and *Mt2*, were decreased. This grouping, combined with decreases seen in the levels of other genes involved in metabolism, such as NADH dehydrogenase (ubiquinone) 1 beta subcomplex, 2 (*Ndufb2*), mitochondrial cytochrome oxidase III subunit (mtDNA_COXIII) and lactate dehydrogenase A (*Ldha*) suggests the retinal bipolar cells of the degenerate retina are under reduced metabolic stress than bipolar cells in the non-degenerate retina. Metallothioneins, for example, are important for metal ion homeostasis and provide zinc ions as cofactors. Metallothioneins have been found to scavenge free radicals in tissue under oxidative stress (Vasák, 2005; Suemori et al., 2006). The lack of photoreceptors in the degenerate retina means that the metabolic activity of bipolar cells would be expected to decrease (Bramall et al., 2010). Therefore, the demand for energy would reduce, leading to lower production of antioxidants and lower demand for the proteins involved in these processes.

Hackam and colleagues (2004) also found a statistically significant downregulation of genes involved in metabolism at P35 and P50 ages. In this same study comparing the gene expression changes of whole degenerate and non-degenerate retinas, it was also found that genes involved in oxidative stress were upregulated. The discrepancy between the Hackam data and the data from the current study could be explained by the fact that photoreceptors, which were collected in the Hackam methodology, would be expected to have highly upregulated oxidative stress-related genes, while bipolar cells, which were targeted in the current study do not have the same oxidative stressors, and so downregulate their expression. These differences show the utility of isolating a particular cell type to gain cell type-specific data.

There are suggestions from the data that the degenerate retina may undergo epigenetic changes, which will have downstream consequences for the expression of multiple genes. Polyhomeotic homolog 1 (Drosophila) (*Phc1*) was found to be upregulated (P = 0.028) and histone deacetylase 9 (*Hdac9*) was downregulated (P = 0.0029) in degenerate retina samples. *Phc1* is a member of the polycomb group of genes, which are known to remodel chromatin and therefore repress gene expression (Simon and Kingston, 2009; Margueron and Reinberg, 2011). Histone deacetylases remove acetyl groups from histones, enabling tighter DNA packing (Yang and Seto, 2007). Interestingly, *in vivo* knockdown of a related histone deacetylase, *Hdac4*, in the developing mouse retina leads to apoptosis of rods and bipolar cells (Chen and Cepko, 2009). Chromatin immunoprecipitation could be used to assay the histone modification profile of degenerate retinas to better understand the implications of this finding (Carey et al., 2009).

Some genes that were found to show statistically significant differential expression in this study have also been found to demonstrate similar changes in expression levels in other microarray studies of retinal degeneration. By extracting RNA from whole retinas from 50-day-old *rd1* mice Hackam and colleagues (2004) found phosducin (*Pdc*), *Sag* and *Gnat1* to be highly downregulated in the degenerate retina, relative to non-degenerate controls. Neural retinal leucine zipper (*Nrl*), one of the genes downregulated in the current study, was also found to be downregulated by Hackam and colleagues, but only at the P14 time point. By extracting RNA from whole retina Holt and colleagues (2015) found *Pde6b*, *Pdc* and *Gnat1* were statistically significantly downregulated in *rd1* and *Pde6b*, *Pdc*, *Gnat1* and *Sag* downregulated in *rd/rd cl* mice. As these genes are photoreceptor-specific genes, these overlapping findings do not have significant consequences for our understanding of bipolar cell adaptations to degeneration.

The expression changes in some genes may have implications for the choice of AAV vector for an optogenetic gene therapy strategy. Sulfatase 2 (*Sulf2*) encodes a protein that removes sulphate groups from heparan sulphate (Morimoto-Tomita et al., 2002). As the primary receptor for AAV2 cell binding are heparan sulphate proteoglycans, the upregulation of *Sulf2* ($P = 0.034$) may have implications for the binding ability of AAV2. Exostatin-like glycosyltransferase 3 (*Extl3*) is a gene that was downregulated ($P = 0.029$) in the degenerate retina samples. The protein encoded by this gene plays an important role in the synthesis of heparin and heparan sulphate (Kim et al., 2001). This combination of statistically significant changes in expression of *Sulf2* and *Extl3* suggest that AAV2 vectors may function more poorly in the degenerate retina relative to their results in a non-degenerate retina.

The results obtained from this microarray are preliminary and require additional validation by qPCR and histological studies. To confirm the gene expression changes, qPCR needs to be completed (Yuen et al., 2002). *In situ* hybridisation could also provide a semi-quantitative read out of gene expression change (Armata et al., 2006; Punzo and Cepko, 2007). Due to the effects of post-transcriptional regulation, including mRNA stability and small RNA mediated regulation, changes in the levels of mRNA may not directly correlate with changes in the protein levels of the corresponding translated protein (Greenbaum et al., 2003; Cox et al., 2005). Therefore, ideally, quantitative or semi-quantitative protein techniques, such as immunohistochemistry, two-dimensional electrophoresis or quantitative mass spectrometry, could be applied to tissue from degenerate and non-degenerate mouse eyes from a similar age to assay for the relationship between gene expression changes and protein level changes (Delahunty and Yates, 2005). All but two of the 64 statistically significantly differentially expressed genes are located on a chromosome different to that of *Pde6b* (located on chromosome 5), the gene that was systematically different between the degenerate ($Pde6b^{rd1/rd1}$) and

the non-degenerate (*Pde6b*$^{+/+}$) groups (Table 7.2). *Clip1* and *Naa11* are the two differentially expressed genes that are also located on chromosome 5. This suggests that the vast majority of the observed gene expression changes are unlikely to be due to a congenic footprint effect (where genes flanking *Pde6b* show differences in their expression not because of biological differences, but due to their proximity to the gene critical to defining the different experimental groups (Schalkwyk et al., 2007)). All mice used in these experiments were positive for L7-Cre (unknown genomic locus) and homozygous for floxed YFP (Rosa26 locus on chromosome 6), so degenerate and non-degenerate groups did not differ in these genes and their flanking chromosomal regions.

A very useful and valuable application of this data would be as baseline data to investigate the gene expression changes that occur in response to optogenetic gene therapy. By introducing a light-sensitive molecule to the degenerate retina, especially if targeted to bipolar cells, it is hypothesised that the greater metabolic demands and the greater activity in the pathway that the light-sensitive molecule signals through, would lead to further changes in gene expression. Such a study would further inform our understanding of how cells respond to the ectopic expression of a light-sensitive molecule and could refine the choice of light-sensitive molecule to optimise cellular response.

7.3.3 Quality of data from a microarray study of retinal bipolar cell adaptation to retinal degeneration

FACS was used to create RNA samples that were highly enriched in RNA from *L7*-Cre-positive bipolar cells. Lu and colleagues (2013) have shown that *L7*-Cre-positive cells are predominantly rod bipolar cells. Many type 6 ON cone bipolar cells were also found to be *L7*-Cre-positive, as was the occasional type 2 OFF cone bipolar cell (Lu et al., 2013). Approximately 1,000 – 2,500 retinal ganglion cells per eye are also known to express *L7*-Cre (Ivanova et al., 2013). Therefore, a limitation of this animal model is

that even with optimal retinal dissociation and FACS settings, the YFP-positive population will not represent a single subtype of bipolar cells. However, given the relative abundance of ON bipolar cells, particularly rod bipolar cells, it was thought that FACS would give a resolution of data from bipolar cells that was not possible using RNA extracted from whole retinas. FACS isolation was selected over laser-capture microdissection (Espina et al., 2006) due to the greater ease with which large numbers of cells could be isolated in a timely manner.

The microarray results indicate that the non-degenerate samples contained RNA from rods. Five of the genes that had a statistically significant decrease in expression in degenerate compared to non-degenerate samples, were rod-specific (*Gnat1*, *Pde6b* and *Pde6g*) or photoreceptor-specific (*Pdc* and *Sag*) genes. The rod cell RNA could have contaminated the non-degenerate YFP-positive RNA samples in a number of possible ways. Firstly, close examination of anti-YFP immunolabelled sections from *L7*-Cre-positive non-degenerate retina showed that a small number of photoreceptors were weakly YFP-positive (Figure 7.9 A). These weakly YFP-positive photoreceptors could have been included in the YFP-positive sorted fraction, despite the use of FACS settings that were optimised for isolation of more highly fluorescent cells. Secondly, the dissociation may not have been complete, allowing some YFP-positive bipolar cells to maintain their connection with rods. Sort criteria were set to exclude droplets with multiple cells, so this possibility is unlikely. Finally, it is possible that RNA from lysed rods was present in the solution that also contained YFP-positive bipolar cells. As the droplet containing a YFP-positive bipolar cell was sorted it would have taken with it RNA from lysed rods. Although the RNA would have been significantly diluted, the

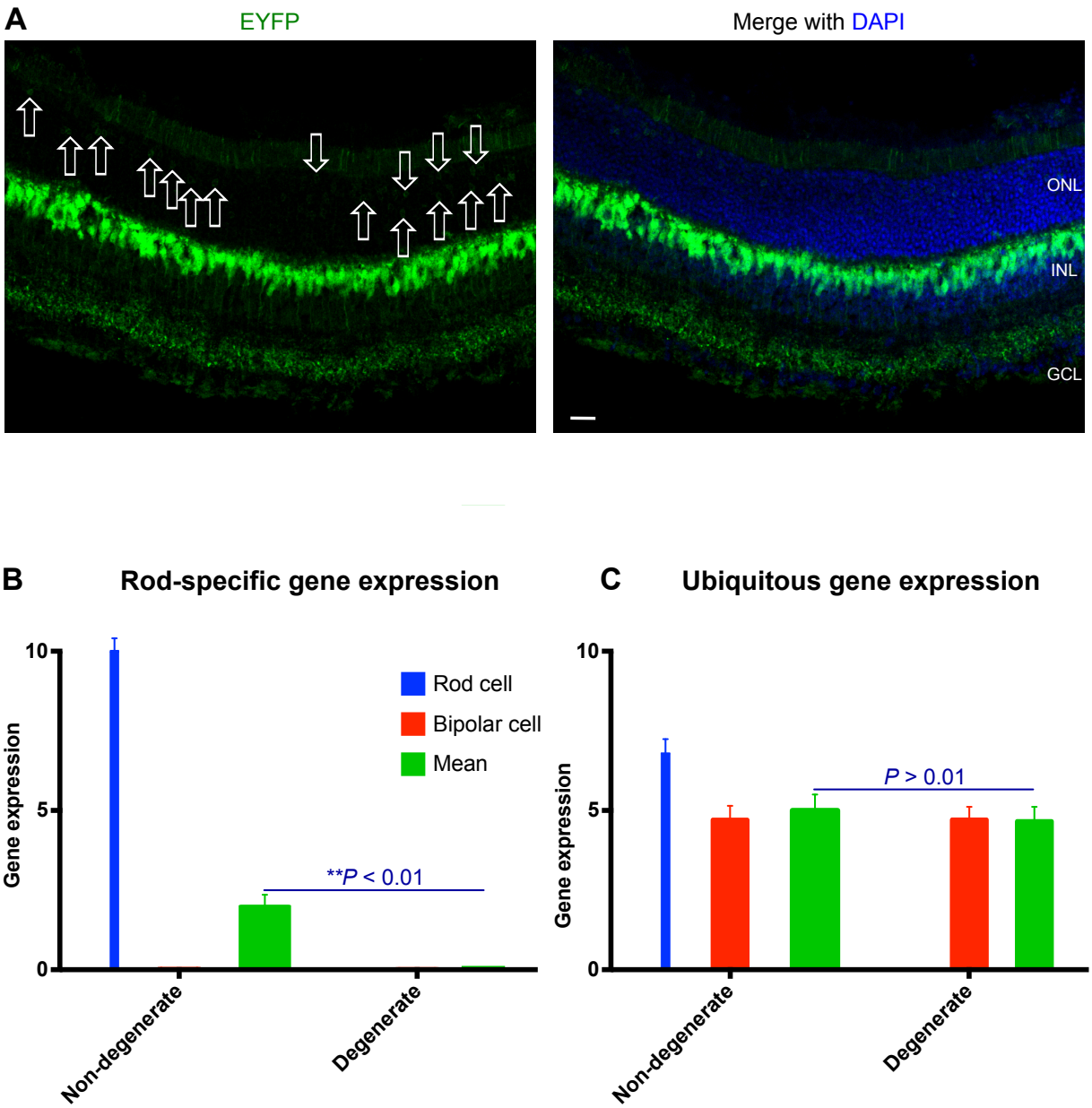


Figure 7.9. Potential sources of statistically significant differential expression results of rod cell-specific genes in a microarray study

(**A**) A potential source of rod RNA contamination of a YFP-positive cell population was YFP-positive rod cells. Weakly YFP-positive rod cells were occasionally identified in *L7*-Cre-positive non-degenerate retinas (arrows). (**B** and **C**) The effect of rod cell RNA contamination would be greater for rod-specific genes than for ubiquitously expressed genes, as shown by these bar graphs where bar width represents the prevalence of the cells in the sample and bar height represents gene expression level. (**B**) If a gene is highly expressed exclusively in rod cells, the mean expression level in the whole sample is moderate in the non-degenerate sample. However, in the degenerate sample rod cells are absent, so the level is negligible and a statistically significant decrease is detected. (**C**) Genes that are expressed in both rods and bipolar cells are less likely to produce statistically significant differential expression results as rods are estimated to make a relatively small contribution to the total pool of RNA, so rod expression levels are averaged out by the larger contribution from bipolar cells. Scale bar respresents 20 µm. GCL, ganglion cell layer; INL, inner nuclear layer; ONL, outer nuclear layer.

high abundance of rods in the non-degenerate retina means that RNA may still have been at a detectable level.

A relatively small contamination of the non-degenerate samples with RNA from rod cells could have been enough to produce the microarray results seen for photoreceptor-specific genes. If the non-degenerate RNA samples were contaminated with a small amount of RNA from rods, then the average expression level of photoreceptor-specific genes would be expected to decrease significantly, as the *rd1* mutation of the rod-specific gene *Pde6b* ensured that there would be a very low level of rod RNA available to contaminate the degenerate samples (Figure 7.9 B). It is worth noting that four of the five photoreceptor-specific genes (*Gnat1*, *Pdc, Pde6g* and *Sag*) were found to be in the top ten highly expressed genes in an RNA-seq study of the transcriptome of the whole retina (Gamsiz et al., 2012). Therefore, these genes are highly abundant in the retina and only a small contamination could lead to a statistically significant decrease in gene expression in the degenerate samples. However, for genes that are not specific to rods, the effect that this contamination would have on the microarray results would be much less pronounced, due to the rod contamination of the total RNA pool being small, relative to the contribution from bipolar cells (Figure 7.9 C).

The absolute numbers of YFP-positive cells sorted represent approximately 20% and 23% of the numbers of rod bipolar cells documented by Strettoi and colleagues (2000) to be present in *rd1* degenerate and non-degenerate retinas, respectively. However, these cell counts were done by Strettoi and colleagues at two months of age, so the cell numbers expected at three months of age, the time point used for this experiment, would be lower, equating to a higher percentage yield. Approximately 22,000 more YFP-positive cells were collected, on average, from each non-degenerate retina compared to each degenerate retina. These differences may have been due to random variation (P = 0.24, unpaired two-tail t test) or contamination with rods may have increased the

number in the non-degenerate samples. The loss of both rod and cone bipolar cells in the process of retinal degeneration in the *rd1* mouse is also likely to have contributed significantly to these differences (Strettoi and Pignatelli, 2000; Chen et al., 2012).

Caution should be applied when analysing the RNA concentrations and RNA integrity number (RIN) values of the microarray samples. Bioanalyzer results provided by the contract research organisation that ran the tests varied significantly between repeat runs. One sample had a concentration of 109 pg/µl and a RIN of 9.1 on the first run and increased to 743 pg/µl and 9.4 on the second run. The poor repeatability makes it difficult to accurately state the concentrations of each of the samples and therefore the mass of RNA per cell.

The requirement for all samples to undergo amplification in the preparation of a cDNA library may have reduced the signal to noise ratio of the final data. The low concentrations of RNA made amplification necessary for this microarray study. Unfortunately, this introduced a potential source of error and bias and therefore potentially led to type I and type II errors for some probes (Boelens et al., 2007; Croner et al., 2009).

This set of experiments aimed to better understand the gene expression changes that retinal bipolar cells undergo during the process of retinal degeneration with the greater objective of using this data to inform a strategy for optogenetic gene therapy for vision restoration and/or alternative approaches to minimising vision loss in patients with inherited retinal degeneration. This work succeeded in acquiring a substantial database of gene expression changes in retinal bipolar cells from degenerate retinas, compared to bipolar cells from non-degenerate retinas. Although the results from this microarray study need validation, there is potential for this data to be used to understand normal bipolar cell gene expression, the perturbations that occur when photoreceptor inputs are

lost in retinal degeneration and, therefore, what therapeutic approaches may yield the greatest benefits. For example, comparing degenerate to non-degenerate samples, there does not appear to be a significant change in expression for most of the genes involved in the G protein second messenger systems that melanopsin and rhodopsin would be likely to utilise if ectopically expressed in bipolar cells as part of an optogenetic therapy. Therefore, it is hypothesised that such opsins would be similarly effective in bipolar cells from a degenerate or non-degenerate retina. Absolute expression levels of genes important for G protein signaling also provide valuable information suggesting that signaling via the native G_o pathway may yield the optimal outcome. Therefore, the aim of better understanding gene expression changes in retinal bipolar cells during retinal degeneration has been achieved and has provided initial insights that can be used to guide further research into utilising these cells as targets for optogenetic gene therapy for vision restoration.

8

General Discussion

By delivering light-sensitising molecules to the degenerate retina, optogenetic gene therapy for vision aims to light-sensitise remaining neurons and enable them to take over the light-sensing role from the photoreceptors that have undergone apoptosis. The objective of this research project was to investigate a number of the challenges that must be met in order to restore vision using an optogenetics approach. Specifically, the experiments in this research project aimed to provide data on a) the choice of light-sensitive optogenetic tool, b) the choice of target cell/s for gene therapy, c) the optimal way in which the light-sensitive molecule should be delivered to the eye, and d) the gene expression changes seen in one particular target cell type, the retinal bipolar cell, during retinal degeneration (Figure 8.1).

8.1 Selecting a light-sensitive molecule for optogenetic gene therapy

The selection of a light-sensitive molecule has many important implications for optogenetic gene therapy to restore vision. The light-sensitive molecule will determine not only the spectral sensitivity of the retina, but has important implications in determining the retina's light sensitivity, the onset and offset response characteristics of transduced cells and whether such therapy has the potential for toxicity or causing an immune response.

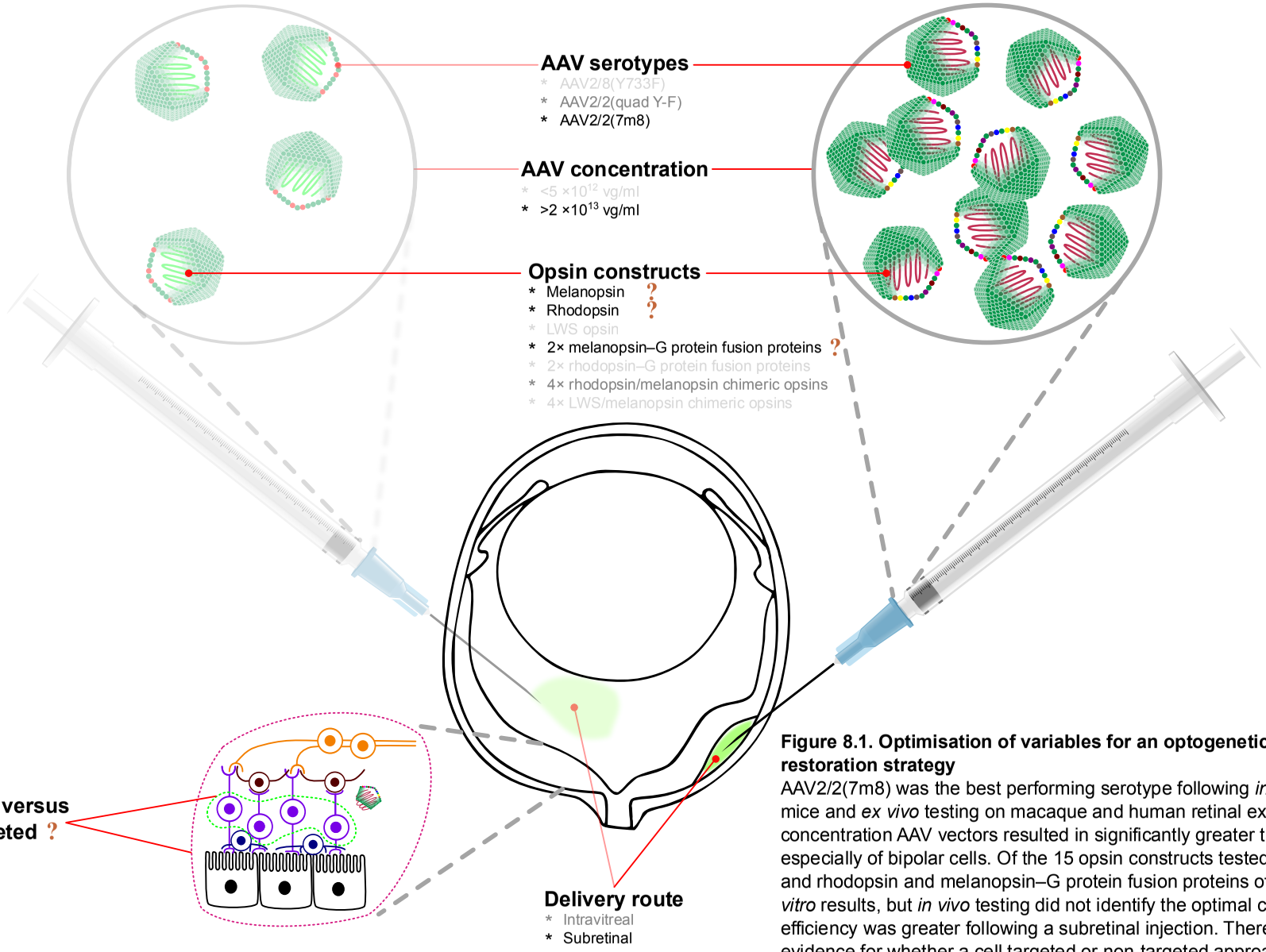


Figure 8.1. Optimisation of variables for an optogenetics for vision restoration strategy
AAV2/2(7m8) was the best performing serotype following *in vivo* testing in *rd1* mice and *ex vivo* testing on macaque and human retinal explants. Higher concentration AAV vectors resulted in significantly greater transduction efficiency, especially of bipolar cells. Of the 15 opsin constructs tested, wild type melanopsin and rhodopsin and melanopsin–G protein fusion proteins offered promising *in vitro* results, but *in vivo* testing did not identify the optimal construct. Transduction efficiency was greater following a subretinal injection. There was no clear evidence for whether a cell targeted or non-targeted approach was superior.

This research project has focussed on human opsin proteins as light-sensitisers due to their perceived advantages in terms of greater light sensitivity and low risk of inducing an immune response, compared to microbial opsins. The selected opsin must also work effectively in the biochemical environment of those cells transduced by the AAV vector to activate the available intracellular signalling pathways. The ability of melanopsin to signal via the ubiquitous $G_{q/11}$ pathway therefore made it an attractive candidate for optogenetic gene therapy (Bailes and Lucas, 2013). Rhodopsin, which activates $G_{t\text{-}r}$ in rod cells, is also known to activate $G_{i/o}$ pathways *in vitro* (Kanaho et al., 1984; Terakita et al., 2002) and *in vivo* (Li et al., 2005; Gutierrez et al., 2011b; Cao et al., 2012) and so it is a good candidate opsin to activate the native G_o pathway in ON bipolar cells.

The comparative efficacy of wild type melanopsin and rhodopsin as optogenetic gene therapies were examined in a pilot *in vivo* study in a mouse model of retinal degeneration. Both transgenes were floxed, thereby restricting expression to Cre-expressing cells. The mice that received these subretinal injections expressed Cre under the control of an *L7*/*Pcp2* promoter, which is active in rod bipolar cells, types 2 and 6 cone bipolar cells (Lu et al., 2013) and some bistratified ganglion cells (Ivanova et al., 2013). Despite injecting very similar quantities of vector genomes into each eye, greater levels of rhodopsin than melanopsin were detected by immunohistochemistry (Figure 6.5). Pupillometry showed floxed rhodopsin treated mice to have a slightly lower light intensity required for half maximal response, than floxed melanopsin treated mice, but the result was not statistically significant (Figure 6.7 A and B). Interestingly, only a mouse from the floxed rhodopsin treated group showed any reflexive head turns in an optomotor response assay, while all other treated groups failed to demonstrate any such turns (Figure 6.7 C). Therefore, there are some indications that the higher level of opsin expression found in the rhodopsin group may have had greater functional outcomes, but higher powered studies are needed to clarify these differences.

Wild type human melanopsin was also compared as an optogenetic tool for vision restoration to chimeric opsins and opsin–G protein fusion constructs. Chimeric opsins were made by replacing the intracellular surface of rhodopsin and LWS opsin with the corresponding sequences from melanopsin. The intention was to maintain the spectral and kinetic properties of rhodopsin and LWS opsin, but for them to signal via the $G_{q/11}$ pathway, rather than their native G_t pathways. Melanopsin–G protein fusion proteins were created to test whether fusing melanopsin to its native Gα subunits, G_q or G_{11}, changed its light-sensitising properties in a way that demonstrated benefits over wild type melanopsin. Rhodopsin–G protein fusion proteins were created to test the different question as to whether fusion to non-native Gα subunits, G_q or G_{11}, could force rhodopsin to signal via the $G_{q/11}$ pathway.

Melanopsin–G protein fusion constructs provided the greatest evidence of a potential benefit over wild type opsins as optogenetic tools for vision. Using siRNA directed against *GNAQ* and *GNA11*, the genes encoding the Gα proteins that melanopsin normally activates, 293T cells were used to model cells with relatively low levels of these endogenous Gα subunits. In this situation, melanopsin–G protein fusion transfected cells responded more frequently and with greater magnitudes of response compared to wild type melanopsin. Gene expression data from the microarray study, suggested *Gnaq* and *Gna11* are expressed in mouse ON bipolar cells, but not to the same level as *Gnao1*. Therefore, melanopsin signalling in these cells may be rate-limited by the availability of G_q and G_{11} Gα subunits. An *in vivo* study to test for any functional differences between melanopsin and melanopsin–*GNA11* was conducted in *rd1* retinally degenerate mice. Unfortunately, the level of transgene expression was unexpectedly low following an intravitreal injection (Figure 5.6). Consequently, no statistically significant differences in pupillometry, optomotor response or Fos induction assays were detected between treatment and sham groups (Figures 5.7 and 5.8). Low

transgene expression is attributed to the relatively low concentration of melanopsin AAV vector that was achieved (see §8.5.2 below) and potentially due to factors relating to the quality of the AAV vector, which were not quantified (see §8.5.3 below).

Creating four rhodopsin/melanopsin chimeric opsins and four LWS opsin/melanopsin chimeric opsins facilitated exploration of the structure–function relationships of these proteins. The replacement of just the third intracellular loop of rhodopsin with the corresponding sequence from melanopsin significantly diminished the response of transfected cells in a bioluminescence cAMP assay, while conferring some ability to couple to melanopsin's native $G_{q/11}$ pathway. However, by replacing both the second and third intracellular loops of rhodopsin with the corresponding sequence from melanopsin, the $G_{q/11}$ coupling ability was greatly increased, while the G_i coupling ability was further reduced. Modifying the intracellular surface to a greater extent did not increase the $G_{q/11}$ coupling any further, while G_i activity decreased. These data therefore confirmed the importance of the second and third loops for defining G protein coupling (Wess, 1997; Yamashita et al., 2000; Terakita et al., 2002). None of the chimeric opsins were able to match either of their derivative wild type opsins for the magnitude and speed of light-induced response in the $G_{q/11}$ and G_i assays. Although offering no benefit for optogenetic vision restoration studies, these experiments did create exogenous retinal-dependent chimeric opsins that can couple to both $G_{q/11}$ and G_i pathways with moderate effectiveness. Direct comparison with a bovine rhodopsin-based chimeric opsin developed by another group (Airan et al., 2009) showed that the chimeric opsins developed in this project have faster onset and offset kinetics and greater magnitudes of calcium responses. The properties of these rhodopsin/melanopsin chimeric opsins may be of value as optogenetic tools for basic research.

Unfortunately, the cAMP assay was not able to measure a light-dependent effect in 293T cells expressing LWS opsin, so it was not possible to determine any loss of

function with increased modifications to the intracellular surface. The calcium assay of $G_{q/11}$ function also did not show a gain of function as more of LWS opsin was replaced with the intracellular surface from human melanopsin. Ultraviolet–visible absorbance spectroscopy of regenerated wild type LWS opsin demonstrated a photopigment with maximal absorbance similar to the expected wavelength, suggesting functional opsin was being produced following plasmid transfection. The failure to produce a functional photopigment from LWS opsin with the complete intracellular surface of melanopsin and the appearance of potential aggresomes on immunocytochemistry suggested the LWS-based chimeric opsins might have misfolded.

Based on the data from this research project it is possible to eliminate some opsins as candidates for optogenetic gene therapy for vision, but the results are not clear enough to recommend a single opsin construct from the 15 tested. None of the rhodopsin/melanopsin chimeric opsins and rhodopsin–G protein fusion proteins displayed light response characteristics that were in any way superior to wild type human proteins. The assays used were not able to assess the *in vitro* function of LWS opsin or LWS/melanopsin chimeric opsins, so it is not possible to say if they functioned efficiently. This leaves wild type melanopsin and rhodopsin and melanopsin–G protein fusions as light-sensitive proteins that displayed maximal responses in their respective *in vitro* assays. While statistically significant functional differences could not be detected in *in vivo* studies using these three proteins, they are recommended for further investigation.

8.1.1 Potential benefits of G_o-coupled opsins for vision restoration

In addition to these three proteins, the results from this project's microarray study (chapter seven) suggest that it could be beneficial to utilise the mGluR6 signalling pathway as components of this pathway have higher levels of expression than

components of other G protein signalling pathways in degenerate retina. In fact, a chimeric opsin of mouse melanopsin and mouse mGluR6 has been created and successfully tested *in vivo* (van Wyk et al., 2015). Such a construct needs to be compared directly with wild type human rhodopsin and perhaps other opsins that may signal more efficiently through the native G_o pathway of ON bipolar cells.

It would also be worthwhile testing wild type opsins from other species that are known, or are predicted, to couple to the G_o pathway (Koyanagi and Terakita, 2014). It has been shown that a chimeric opsin of bovine rhodopsin with the third intracellular loop from the G_o-coupled scallop rhodopsin enhanced G_o activity by a factor of four (Terakita et al., 2002). Perhaps such a chimeric opsin may offer functional improvements, as could a fusion of human rhodopsin and G_o proteins. Although the use of human opsins is advantageous to limit the potential for an immune response, opsins from other species are worth testing in case they are tolerated and have far greater efficacy as optogenetic tools for vision. The approval of channelrhodopsin-2 for a clinical trial (NCT02556736, clinicaltrials.gov) demonstrates that non-human proteins can be approved by regulators for an optogenetics clinical study.

8.1.2 Challenges of melanopsin AAV vectors

It is worth noting that in the course of this project melanopsin was found to be a relatively difficult sequence to handle for generating high titre AAV vectors and achieving high levels of expression in the retina. While floxed rhodopsin and GFP-expressing AAV vectors were made to a titre of more than 10^{13} vg/ml using a standard 293T triple transfection and iodixanol gradient protocol, melanopsin and melanopsin–*GNA11* vector production often resulted in titres of 10^{11} vg/ml and occasionally 10^{10} vg/ml. To produce AAV vectors $>10^{12}$ vg/ml suitable for *in vivo* use, multiple production batches were combined in a secondary concentration process. When equal

quantities of vector genomes of floxed melanopsin and floxed rhodopsin were injected into *L7*-Cre *rd1* eyes, floxed rhodopsin was expressed at higher levels over a wider area. Other published studies that utilised melanopsin-expressing AAV vectors also used low to moderate AAV titres: Lin and colleagues (2008) used a 2×10^{12} vg/ml mouse melanopsin AAV vector, while van Wyk and colleagues (2015) used a 8×10^{12} vg/ml mouse melanopsin/mouse mGluR6 chimeric opsin vector and only achieved low transduction efficiency. It can be speculated that these difficulties may be attributed to the secondary structure of melanopsin cDNA being less efficient to package into and/or unpackage out of AAV or due to the expression of melanopsin protein in transfected 293T cells causing light-dependent calcium fluxes that perturb normal function, leading to reduced AAV synthesis. These challenges with the use of melanopsin contributed to the difficulty in achieving sufficient expression to potentially demonstrate a functional difference between melanopsin and rhodopsin and between wild type melanopsin and melanopsin–*GNA11*.

8.2 Appropriate choice of animal model of retinal degeneration

More accurate and meaningful *in vivo* data on optogenetic gene therapies will also be facilitated by selecting an appropriate animal model. Currently, in preclinical gene therapy studies that provide a wild type copy of a defective or deficient gene, demonstrating safe expression of the wild type protein in the appropriate cellular location is often considered more important than evidence of significant vision gains if the genetic defect does not cause a vision loss phenotype in the model animal. However, with many competing optogenetic strategies to restore light-sensitivity to the degenerate retina, proof of vision restoration is paramount — this is the critical factor that should decide which safe treatments undergo clinical investigation.

Although the rate of vision loss in humans with inherited retinal dystrophy can vary widely (Hayward et al., 2003; Sharon et al., 2003; Hartong et al., 2006; Berger et al., 2010), very few experience a loss of photoreceptors as rapid and as early in development as *rd1* mice (Carter-Dawson et al., 1978). It has been posited that the rate of neurodegeneration negatively correlates with maximum lifespan potential and positively correlates with the rate of formation of mitochondrial reactive oxygen and nitrogen species (Wright et al., 2004). Therefore, any mutation is expected to lead to a more rapid rate of degeneration in mice, compared to humans. The rapid rate of photoreceptor loss in mice means that synapses between photoreceptors and bipolar cells never properly form (Blanks et al., 1974; Chen et al., 2012). Rod-mediated electroretinograms show no response at all ages of *rd1* mice and the cone-mediated photopic electroretinogram is greatly affected as early as postnatal day 14 (Strettoi et al., 2003). These data indicate that the brain of *rd1* mice is unlikely to develop normal visual centres. It is therefore unlikely that, even with the most effective optogenetic gene therapy, *rd1* mice have the potential to perform as well as non-degenerate mice.

These factors suggest that a more appropriate mouse model for optogenetic gene therapy studies would be one with a slower form of retinal degeneration to allow cortical circuits to develop before retinal degeneration causes vision loss. Strains carrying the $Prph2^{Rd2}$ naturally occurring mutation is one potential choice that could offer greater functional vision restoration (Chang et al., 2002). However, such a model comes with the greater resource costs of housing the mice for up to a year until they are sufficiently degenerate (Sanyal and Hawkins, 1986). This more prolonged period of degeneration could be exploited to test the effects of delivering an optogenetic gene therapy vector at different stages in the degeneration process, potentially identifying an optimal window for treatment.

8.3 Appropriate vision tests for optogenetic vision restoration

A further aspect of experimental design that needs optimisation for optogenetic gene therapy is the functional tests used to assess vision. Because light-sensitive proteins are being expressed outside of the cells that they would normally be expressed in, the other molecular components that regulate the activation and deactivation of the protein will not be present in the usual quantities (if they are present at all). It is therefore expected that the onset and offset characteristics of cells expressing ectopic opsins will be suboptimal, relative to the characteristics of photoreceptors.

For a patient that has been treated with optogenetic gene therapy for vision, it is likely that their visual experience will be very different to a normally sighted person. Therefore, tests of vision that were designed for people with a photoreceptor-based visual system may not be suitable for assessing optogenetic-based vision. For example, the optomotor response was found to be useful for detecting vision in the sighted control mice, but only a single reflexive head turn was detected in all of the *rd1* degenerate mice. It may be that even if high levels of melanopsin were detected in the retinas of treated mice, their visual experience may not have led to reflexive head turns due to the low refresh rate of light-sensitive cells causing the turning black and white stripes to be indistinguishable.

8.4 Selecting target cells for optogenetic gene therapy

The selection of target cells in the degenerate retina is of critical importance for a successful optogenetics gene therapy strategy. With more than 60 functionally distinct cell types in the retina (Masland, 2011), light-sensitising an inappropriate cell type or an incompatible combination of cells may limit the visual improvement from such a therapy. For example, if ON and OFF bipolar cells both expressed an opsin that leads to depolarisation in response to a light stimulus then the simultaneous activation of both

pathways in the same location may limit the conscious light perception at that location in visual space. Although neural plasticity may enable the brain to relearn the information encoded in the signals (Ashtari et al., 2015), the optimal outcome is expected to come from stimulating an isolated channel of the visual pathway.

A logical cell type to initially target for optogenetic gene therapy for vision is the ON bipolar pathway. The are a number of advantages to targeting this cell type: ON bipolar cells are numerous in the retina (approximately 400,000 in the mouse retina (Strettoi et al., 2003)); they are regulated by a G protein pathway that is relatively well understood (Morgans et al., 2010); their upstream position in the visual pathway means that some visual processing could still occur in the retina; and cell-specific transcriptional regulatory elements are available to limit expression to ON bipolar cells (Lagali et al., 2008; Doroudchi et al., 2011; Cronin et al., 2014; Macé et al., 2014; Cehajic-Kapetanovic et al., 2015; Gaub et al., 2015; van Wyk et al., 2015).

The use of ON bipolar cells to produce the optimal optogenetic outcome was investigated in this research project by comparing a non-targeted and targeted gene expression approach and by studying the gene expression changes in ON bipolar cells in the degenerate retina.

A bipolar cell-targeted expression approach was compared to a non-targeted approach by using a transgenic line of *L7*-Cre mice that expressed Cre in rod bipolar cells, types 2 and 6 cone bipolar cells and a subset of bistratified retinal ganglion cells (chapter six). By injecting these retinally degenerate mice with a floxed melanopsin AAV vector the expression of melanopsin could be limited to Cre-positive cells. These mice were compared to mice that received a non-floxed melanopsin construct. In this pilot study only four mice were available for each arm of the study, prohibiting the detection of any statistically significant functional changes, but the immunohistochemistry results were

informative. At the concentration of AAV vector injected (1×10^9 vg/eye) very little melanopsin was detected in eyes that received the floxed melanopsin vector, while a moderate level of melanopsin was detected in eyes that received non-floxed melanopsin (Figure 6.5). Horizontal cells and cells of the ganglion cell layer were the predominant melanopsin-expressing cell types. The pupillometry and optomotor response results of both of these groups were not statistically significantly different from AAV-sham treated mice (Figure 6.7). Further experiments using higher concentration vectors (see §8.5.2 below) and with more statistical power should be completed to elucidate the functional differences between the targeted and non-targeted optogenetic approaches.

The selection of a target cell for optogenetic gene therapy is also informed by the microarray study, which sheds light on the gene expression profile of retinal bipolar cells from a mouse model of rod-cone dystrophy. (For a discussion of limitations of this study and required validation, see §7.3.) Using six retinally degenerate and six non-degenerate *L7*-Cre EYFP mice aged 89 to 91 days old, samples highly enriched in retinal bipolar cells were obtained using FACS. With the exception of three genes encoding intracellular effector enzymes (adenylate cyclase 1 and phosphodiesterases 1C and 9A), other genes that could be considered to be important for G protein signalling in bipolar cells were not differentially expressed to a statistically significant degree in the samples from degenerate retina, compared to non-degenerate. This suggests that the G protein signalling physiology of bipolar cells in the degenerate retina is not highly modified relative to the non-degenerate state and so should be receptive to ectopically expressed opsin.

While the above discussion indicates that bipolar cells are suitable targets for optogenetic gene therapy, it is important to consider how bipolar cells are affected as retinal degeneration progresses. Indeed, the lower number of YFP-positive cells isolated from degenerate retinas compared to non-degenerate retinas through the process of

FACS lends support to the body of data showing that bipolar cell numbers decline with retinal degeneration (Humayun et al., 1999; Strettoi and Pignatelli, 2000). While, this argues for earlier intervention in human patients to maximise the number of light-sensitised inner retinal cells, ultimately, whether optogenetic gene therapy will slow or halt the loss of bipolar cells is unknown. Data from *RPE65* gene therapy studies in humans and dogs suggests gene supplementation gene therapy may not change the rate of retinal degeneration (Cideciyan et al., 2013).

8.5 Variables to maximise transduction efficiency in the degenerate retina

Once a light-sensitive molecule and target cell type have been selected, there are a number of variables that can be modified to maximise transgene expression in those target cells. These include the selection of the AAV vector, its delivery route, vector concentration and transcriptional regulatory elements (as to the latter see §8.1 above).

8.5.1 Choice of AAV vector

AAV was chosen as the viral vector due to its proven ability to safely transduce non-dividing cells of the retina (Bennett, 2003; Bennett et al., 2012; Jacobson et al., 2012). The challenge of an optogenetics gene therapy is to find an AAV vector that effectively transduces a wide range of cell types for a non-targeted approach, or transduces a specific cell type highly effectively if a targeted approach is taken. Because this research project tested both a non-targeted therapy and targeted expression to bipolar cells, an AAV vector with high overall transduction efficiency, and especially bipolar cell transduction efficiency, was desired. Three AAV serotypes that had been shown to be effective at transducing a wide range of retinal cells, including bipolar cells, were compared to test which best suited these criteria (Petrs-Silva et al., 2009, 2011; Dalkara et al., 2013).

In initial experiments using GFP-expressing vectors, AAV2/2(7m8) showed superior performance compared to AAV2/2(quad Y-F) and AAV2/8(Y733F) in both *in vivo* studies in a mouse model of retinal degeneration and *ex vivo* studies using macaque and human retinal explants (chapter three). The transduction efficiencies of AAV2/2(7m8) and AAV2/2(quad Y-F) were similar following intravitreal and subretinal injections in degenerate mice, but the results from macaque and human transductions suggested AAV2/2(7m8) performed better in these species. As the ultimate goal is to translate this treatment to humans, it was reasoned that AAV2/2(7m8) should be used for subsequent *in vivo* experiments in mouse models because of its superior performance in primates.

Melanopsin and melanopsin–*GNA11* AAV2/2(7m8) vectors performed poorly following an intravitreal injection, with little transgene expression detected. This result is thought to be due to other factors (see below §8.5.2 and §8.5.3) and not attributable solely to the use of the AAV2/2(7m8) serotype. Although transduced bipolar cells were only sparsely identified in retinas injected with AAV2/2(7m8)-GFP at a concentration of 2×10^{12} vg/ml, transduced bipolar cells were much more common when AAV2/2(7m8) was injected at the higher concentration of 2×10^{13} vg/ml, emphasising the importance of vector concentration (see below).

Data from the microarray study of retinal degeneration also offers insights that could inform the choice of AAV vector for optogenetic gene therapy. Some AAV serotypes, including AAV2, bind to heparan sulphate proteoglycan receptors to enable entry to the cell (Summerford and Samulski, 1998). The differential expression of *Sulf2* and *Extl3* genes, which are known to be involved in heparan sulphate synthesis and maintenance (Kim et al., 2001; Morimoto-Tomita et al., 2002), indicates that AAV2 may not function as efficiently in the degenerate retina as in the non-degenerate retina. Whether these differences are in fact functionally important needs to be determined empirically.

8.5.2 Vector concentration

A factor that is arguably as important as the AAV serotype at determining the pattern of transduction is the concentration of the injected vector. This was highlighted in this research project, which demonstrated the challenge of transducing retinal bipolar cells.

Consistent across three AAV serotypes applied to mouse, macaque and human retinas, a moderate concentration of AAV vector (up to 5×10^{12} vg/ml) results in poor bipolar cell transduction. Only using a higher titre vector (2×10^{13} vg/ml) expressing floxed rhodopsin can relatively high rates of bipolar cell transduction be achieved. Injecting floxed melanopsin AAV vectors at two different concentrations (1×10^{12} and 2×10^{13} vg/ml) also demonstrated concentration-dependent transduction differences. There was no appreciable transgene expression in eyes that received the low concentration, while low levels of expression in Cre-positive cells were identified in eyes that received the high dose. Other studies using moderate AAV vector concentrations have also found limited expression. A recent study by van Wyk and colleagues (2015) showed poor bipolar cell transduction efficiency with 8×10^{12} vg/ml AAV vector. Studies that have achieved good bipolar cell transduction efficiencies have used high titre viruses: 1.8×10^{14} vg/ml (Macé et al., 2014), 1×10^{13} vg/ml (Cehajic-Kapetanovic et al., 2015), $1 \times 10^{13} – 1 \times 10^{14}$ vg/ml (Gaub et al., 2015).

Virion access to bipolar cells did not seem to be a limiting factor. GFP-expressing AAV vectors that were delivered intravitreally led to transgene expression in retinal pigment epithelium and horizontal cells and vectors injected subretinally led to expression in retinal ganglion cells. Yet via both delivery routes bipolar cell transduction was minimal. In the case of these injections the AAV concentration gradients established across the depth of the retina produced high enough concentrations at either end to transduce ganglion and horizontal cells, but the concentration at the level of the bipolar cells was insufficient for appreciable levels of transgene expression to result.

In summary, to achieve effective bipolar cell transduction in *rd1* degenerate retinas using the current generation of AAV serotypes at least 1×10^{13} vg/ml of vector should be used. Using lower concentrations risks having such low levels of transgene expression that functional experiments are unlikely to demonstrate any differences. If, however, retinal ganglion cells, horizontal cells or retinal pigment epithelium are the target cells then concentrations as low as 1×10^{12} vg/ml would be expected to be effective. This is consistent with different cell types in the retina having different concentration thresholds that need to be exceeded for efficient transgene expression to occur (Ivanova and Pan, 2009; Petrs-Silva et al., 2009). The development of bipolar cell-specific AAV vectors (Scalabrino et al., 2015) will allow lower doses to achieve the same rate of bipolar cell transduction with a lower risk of off-target effects.

8.5.3 Quality control of AAV vectors

A variable that is also important to the transduction efficiency, but which was only tested to a very limited degree in the current research project, is the quality of the AAV vector. This is indeed a broader problem in the field and one that needs to be addressed in order to aid study comparability and reproducibility. In the vast majority of publications there are no metrics to assess the quality of the AAV vectors. Instead, the only way a vector is assessed is by concentration. Even the concentration is not reported in a consistent manner, with come publications reporting “particles of AAV” (Macé et al., 2014) (presumed to be the number of virions, rather than vector genomes), and others reporting “genomic counts” or “vector genomes” (Lin et al., 2008; Cronin et al., 2014; Cehajic-Kapetanovic et al., 2015; van Wyk et al., 2015). Depending on the size and sequence of the expression cassette, and the method of AAV production and purification, up to 98% of AAV capsids can be empty (Sommer et al., 2003). This means that reporting the number of AAV particles says little about how many transgene copies are being delivered. Also, the physical properties of AAV virions, such as their

rates of aggregation, are known to have a significant effect on their transduction efficiency (Wright et al., 2005). However, these properties are an unknown for most AAV vectors.

It is speculated that one of the reasons that the melanopsin and melanopsin–*GNA11* AAV vectors performed poorly *in vivo*, compared to a GFP-expressing vector of equivalent concentration, was due to differences in the physical properties of the vectors, such as a higher rate of virion aggregation or vector-related impurities. Without measuring such properties it is difficult to know what factors most contributed to the low level of transgene expression.

Quantifying the properties of the vectors more thoroughly will also enable greater study reproducibility. A basic approach could be to assess the ratio of full to empty vectors and the degree of uniformity of particle size and shape to assess aggregation. Electron microscopy can assess these properties, but other technologies, such as tunable resistive pulse sensing (Billinge et al., 2013), are becoming available.

8.5.4 Injection delivery route

The site of viral vector injection influences the distribution of virions and their localised concentration. The choice of delivery route can therefore have an important effect on the distribution and efficiency of transgene delivery to the degenerate retina for optogenetic gene therapy. An intravitreal injection is expected to spread over a large area of retina but, in doing so, virions are diluted. Virions delivered by intravitreal injection must pass through the inner limiting membrane to transduce retinal cells, a barrier which is greater in the non-degenerate retina than in the degenerate (Kolstad et al., 2010). Due to their greater access to the anterior segment of the eye, an intravitreal injection has greater potential for inducing an inflammatory response (Bennett, 2003; Dalkara et al., 2013). In contrast, the subretinal route delivers virions to the subretinal

space between the retinal pigment epithelium and inner nuclear layer (or photoreceptors in a non-degenerate retina), where it is more contained and focally concentrated. It also generates a hydrostatic force that hydrates the neurosensory retina with vector solution. Although the risk of inflammation is lower with a subretinal injection, the resulting detachment of the retina can have negative implications (Jacobson et al., 2006, 2012; Bainbridge et al., 2015).

Both the intravitreal and subretinal routes of delivery were utilised for different experiments within this research project. A direct comparison of the two routes was completed as part of an experiment comparing the tropism of three AAV serotypes (chapter three). AAV2/2(7m8) and AAV2/2(quad Y-F) both transduced a similar area of the retina regardless of their route of delivery. In contrast, AAV2/8(Y733F) transduced only a very small area when delivered by the intravitreal route, but transduced an area similar to the other two serotypes when injected subretinally (Figures 3.2 and 3.3).

In vivo testing of candidate optogenetic opsin constructs used both intraocular delivery routes to achieve different objectives. The experiment comparing wild type melanopsin with melanopsin–*GNA11* and a sham injection used intravitreal injections because transgene expression was driven by a ubiquitous promoter and the maximal retinal coverage was desired. By contrast, floxed and non-floxed melanopsin and floxed rhodopsin were delivered subretinally to put the highest possible concentration of virions in closest proximity to the bipolar cells, the predominant Cre-positive cell population. Subretinal injections resulted in higher levels of transgene expression, as assessed by immunohistochemistry. The melanopsin intravitreal injection results were discordant with intravitreal injections of AAV-GFP vectors of a similar concentration, suggesting the results may have been partly due to the specific vector, rather than just the route of delivery.

An important consideration when deciding on a delivery route is that these results will be used to inform the approach taken to treating human patients. The human eye has a vitreous cavity of much greater volume relative to the retinal area, compared to that of a mouse eye. Therefore, the potential for dilution throughout the vitreous cavity following an intravitreal injection is much greater in the human eye. In contrast, a subretinal injection controls the volume through which virions are distributed in both the mouse and human eye. Other studies that have injected the same AAV serotype intravitreally into mouse and primate eyes have observed a much lower rate of transduction in the primate eye (Dalkara et al., 2013). Therefore, given the more encouraging transduction results from subretinal injections of opsin-expressing AAV vectors in this research project and the easier translation of these results into other species, the results of the present study suggests the subretinal approach as being advantageous for optogenetic gene therapy strategies.

8.6 Heading towards the optogenetically sensed light

A highly effective optogenetic gene therapy for vision strategy will be achieved through the coordination of multiple factors. An exquisitely light-sensitive molecule that seamlessly coordinates its signalling with the endogenous pathways of the transduced cells needs to be highly expressed in the target cell type(s) without having toxic effects or inducing a clinically significant immune response. Developments in AAV vectors, transcriptional regulatory elements and AAV production techniques will all assist in achieving this objective.

Placing these results into the context of the field of optogenetic gene therapy for vision restoration, this work has excluded some potential light-sensitising molecules and highlighted the potential benefits of the melanopsin—G protein fusion protein approach as well as wild type melanopsin and rhodopsin. Data from *in vitro* functional testing of

rhodopsin/melanopsin and LWS opsin/melanopsin chimeric opsins did not suggested that these constructs have advantages as optogenetic tools and so are not worth further investigation. The most encouraging *in vitro* data were from wild type melanopsin and rhodopsin as well as melanopsin covalently fused to either GNAQ or GNA11. These three light-sensitising molecules should be further studied in animal models of retinal degeneration to determine which has the greatest potential benefit for vision restoration. In parallel, these animal opsins should be compared directly in a range of *in vivo* functional tests with the best candidate microbial opsin, channelrhodopsin-2. Such direct comparisons are essential to evaluating which light-sensitising molecule is most worthy of clinical trials. Proceeding to a clinical trial using a suboptimal light-sensitising molecule may lead to disappointing clinical outcomes that set the field of optogenetics for vision restoration back as researchers, funding bodies and/or investors lose confidence in the technology.

Beyond studying the light-sensitising molecule best suited for optogenetic gene therapy, this series of experiments also investigated other critical aspects that need to be considered to maximise the potential benefits of this approach. Whether to inject gene therapy vectors through the intravitreal or subretinal route is an ongoing question in the retinal gene therapy field (Jacobson et al., 2006, 2012; Bainbridge et al., 2015, MacLaren et al., 2014). This series of experiments suggested that similar coverage of transgene expression may be achievable through intravitreal injection, without the potentially damaging effects of retinal detachment required for subretinal injection. However, this comparison was completed in mice, so anatomical differences with humans need to be considered before final conclusions can be made. Additionally, different surgical routes may be more appropriate for therapies designed to target different retinal cell types, so one approach may not be suitable for all retinal gene therapy strategies.

Previous optogenetic for vision studies have utilised both cell-targeted (Lagali et al., 2008; Doroudchi et al., 2011; Cronin et al., 2014; Macé et al., 2014; Cehajic-Kapetanovic et al., 2015; Gaub et al., 2015; van Wyk et al., 2015) and non-targeted approaches (Bi et al., 2006; Tomita et al., 2007; Lin et al., 2008), but data directly comparing these is lacking. In this research project a Cre-lox system was used to directly compare the outcomes of ubiquitous opsin expression compared to limiting the expression to retinal bipolar cells. As assessed by immunohistochemistry, more opsin was expressed in retinas that received the non-targeted expression AAV vector, but functionally this group appeared to perform worse than the group that received bipolar cell-targeted therapy. The study was not adequately powered to detect statistically significant differences between these groups, but the trends suggest there may be functional benefits to targeting retinal bipolar cells. Further studies need to be conducted to more definitively confirm that optogenetic approaches should aim to target a particular subset of retinal cells, rather than light-sensitising all transduced cells.

Finally, the microarray study of retinal bipolar gene expression changes in retinal degeneration provides a potentially valuable database for further studies into normal and pathological bipolar cell function. Previous studies have either looked at bipolar cell-specific gene expression in the normal, non-degenerate state (Rao et al., 2007; Morgans et al., 2009; Siegert et al., 2009), or at gene expression changes in the degenerate retina as a whole, rather than focusing on a particular class of retinal cell (Livesey et al., 2000; Hackam et al., 2004; Corbo and Cepko, 2005). As bipolar cells are a particular cell of interest for optogenetics for vision restoration studies (Dalkara et al., 2015), having this dataset of gene expression changes in bipolar cells from degenerate retina could potentially provide valuable insights that inform (a) whether bipolar cells are a suitable target for light-sensitising in the degenerate retina (this data suggests the gene expression changes are not so extensive that the underlying health and function of the

cells would prevent them from being a suitable target cell); (b) what light-sensitising molecules may work most effectively (the data suggests G_o-coupled opsins may be most effective, due to the relatively high expression levels of genes involved in this pathway); and (c) other potential factors that may influence functional outcomes to an optogenetic gene therapy (for example, changes in the expression of genes related to synthesising the receptors that the AAV vectors are likely to use for cell attachment). Therefore, this unique dataset of gene expression changes from retinal bipolar cells from degenerate *rd1* retina could make significant contribution to the optogenetics for vision field by providing insights into the biology of the cells that are best suited to taking over the light detecting role from degenerate photoreceptors.

Translating the data into a therapeutic recommendation, this research project supports injecting a relatively high concentration ($> 2 \times 10^{13}$ vg/ml) of AAV2/2(7m8) expressing human rhodopsin, melanopsin or melanopsin–Gα subunit fusion into the subretinal space as the most efficacious approach to restoring vision using an optogenetic gene therapy strategy (Figure 8.1). However, further *in vivo* studies comparing these with microbial opsins and other mammalian opsins need to be completed to confirm a lead optogenetic product for human testing.

This is an exciting time in the field of optogenetics for vision. Not only are a diverse range of optogenetic tools being tested, but the first clinical study of an optogenetic therapy will soon see a microbial opsin, channelrhodopsin-2, being expressed in a human retina. The subjective and objective data gathered from this study will inform and inspire further development in the field. Developments which will hopefully enable everyone's world to extend beyond their fingertips.

Appendices

Appendix I – Reagents

Reagent	Catalogue number	Company	Headquarters
10% Criterion Tris-HCl gel	3450010	Bio-Rad	Hercules, CA
2-mercaptoethanol	M3148	Sigma-Aldrich	St. Louis, MO
9-*cis* retinal	R5754	Sigma-Aldrich	St. Louis, MO
Agarose – high resolution	A4-0700	Geneflow	Lichfield, UK
AnalaR water	102927G	VWR International	Radnor, PA
Antisedan (atipamezole, 5 mg/ml)	107237US-5	Orion Corporation	Espoo, Finland
B-27 supplement	12587-010	Gibco*	Waltham, MA
Benzonase, 250 U/µl	1016950001	Merck Millipore	Billerica, MA
CO2-independent medium	18045-054	Gibco*	Waltham, MA
DNase I (RNase-free)	M0303	New England Biolabs	Ipswich, MA
DNAZap PCR DNA degradation solutions	AM9890	Ambion*	Waltham, MA
Donkey serum	D9663	Sigma-Aldrich	St. Louis, MO
Dulbecco's Modified Eagle's Medium (DMEM) - high glucose	D6546	Sigma-Aldrich	St. Louis, MO
Dulbecco's Modified Eagle's Medium (DMEM) - phenol red-free	D5921	Sigma-Aldrich	St. Louis, MO
Ethanol, 200 proof	E7023	Sigma-Aldrich	St. Louis, MO
Ethidium bromide	E1510	Sigma-Aldrich	St. Louis, MO
EZBlue Gel Staining Reagent	G1041	Sigma-Aldrich	St. Louis, MO
Fetal bovine serum	F7524	Sigma-Aldrich	St. Louis, MO
Fluo-4, AM	F-14201	Invitrogen*	Waltham, MA
Forskolin	F6886	Sigma-Aldrich	St. Louis, MO
GCaMP6f plasmid	40755	Addgene	Cambridge, MA
GeneJuice	70967	Merck Millipore	Billerica, MA
HBSS	14175	Gibco*	Waltham, MA
HBSS, Cell Dissociation Buffer, enzyme-free	13150-016	Gibco*	Waltham, MA
Hoechst 33342	H3570	Molecular Probes*	Waltham, MA
Hypromellose BPC 0.3% (w/v)	105-7686	Martindale Pharma	Romford, UK
Immomix Red	BIO-25022	Bioline	London, UK
L-glutamine, 200 mM	G7513	Sigma-Aldrich	St. Louis, MO
Laemmli buffer, 2×	S3401	Sigma-Aldrich	St. Louis, MO
Laemmli buffer, 5×	EC-887	National Diagnostics	Atlanta, GA
Lipofectamine RNAiMAX transfection reagent	13778	Invitrogen*	Waltham, MA
Luciferin, bettle. Potassium salt	E1602	Promega	Fitchburg, WI
Luminata Forte Western HRP substrate	WBLUF0100	Merck Millipore	Billerica, MA
Magnesium chloride	M8266	Sigma-Aldrich	St. Louis, MO
N-2 supplement	17502-048	Gibco*	Waltham, MA
Negative control siRNA, med GC	12935300	Ambion*	Waltham, MA
Neurobasal A	10888-022	Gibco*	Waltham, MA
Optimum cutting temperature (OCT) compound	361603E	Tissue-Tek, Sakura Finetek	Tokyo, Japan

Reagent	Catalogue number	Company	Headquarters
OptiPrep density gradient medium, iodixanol (60% w/v in water)	D1556	Sigma-Aldrich	St. Louis, MO
Papain dissociation system	LK003153	Worthington Biochemical Corporation	Lakewood, NJ
Paraformaldehyde, 16%	28906, 28908	Thermo Fisher Scientific	Waltham, MA
PBS solution, 1×	10010-015	Gibco*	Waltham, MA
PBS tablets	18912-014	Gibco*	Waltham, MA
Penicillin (10,000 units/ml)-streptomicin (10 mg/ml) solution	P4333	Sigma-Aldrich	St. Louis, MO
pGloSensor-22F cAMP plasmid	E2301	Promega	Fitchberg, WI
Phenol red solution	P0290	Sigma-Aldrich	St. Louis, MO
Pluronic F-127, 20% in DMSO	P-3000MP	Invitrogen*	Waltham, MA
Pluronic F-68, 10% solution	24040-032	Gibco*	Waltham, MA
Poly(ethylene glycol)	P5413	Sigma-Aldrich	St. Louis, MO
Polyethylenimine, linear, MW ~25,000	23966	Polysciences	Warrington, PA
Potassium chloride	P9333	Sigma-Aldrich	St. Louis, MO
Probenecid	P36400	Invitrogen*	Waltham, MA
ProLong Gold with DAPI	P36934	Invitrogen*	Waltham, MA
Propidium iodide	ENZ-52403	Enzo Life Sciences	Farmingdale, NY
Protease inhibitor cocktail tablets, cOmplete	4693116001	F. Hoffman-La Roche	Basel, Switzerland
Protein ladder	S6-0024	Geneflow	Lichfield, UK
Restriction enzymes - multiple	–	New England Biolabs	Ipswich, MA
Rhod-2, AM	R-1245MP	Invitrogen*	Waltham, MA
RiboLock RNase Inhibitor	11581505	Fisher Scientific*	Waltham, MA
RNase H	M0297	New England Biolabs	Ipswich, MA
RNaseOUT Recombinant Ribonuclease Inhibitor	10777-019	Invitrogen*	Waltham, MA
RNaseZap wipes	AM9786	Ambion*	Waltham, MA
Rompun (xylazine, 20 mg/ml)	–	Bayer AG	Leverkusen, Germany
RPMI-1640 medium	R0883	Sigma-Aldrich	St. Louis, MO
S.O.C Medium	15544-034	Invitrogen*	Waltham, MA
Sodium chloride	S3014	Sigma-Aldrich	St. Louis, MO
Sucrose	84097	Sigma-Aldrich	St. Louis, MO
Trans-Blot Turbo Midi PVDF Transfer Pack	1704157	Bio-Rad	Hercules, CA
Tris(hydroxymethyl)aminomethane	103156X	VWR International	Radnor, PA
Tris/glycine/SDS PAGE buffer (10×)	EC-870	National Diagnostics	Atlanta, GA
Triton X-100	X100	Sigma-Aldrich	St. Louis, MO
Trypsin-EDTA solution, 10×	T4174	Sigma-Aldrich	St. Louis, MO
Tween 20	P1379	Sigma-Aldrich	St. Louis, MO
Vetalar (ketamine, 100 mg/ml)	–	Zoetis	Florham Park, NJ
Virkon	330003 (Anachem)	DuPont	Wilmington, DE
Viscotears Liquid gel (polyacrylic acid, 2 mg/g)	–	Alcon (Novartis)	Hünenberg, Switzerland
Water, molecular grade	95284	Sigma-Aldrich	St. Louis, MO
XL10-Gold ultra compentent cells	200315	Agilent Technologies	Santa Clara, CA

* A Thermo Fisher Scientific owned company

Appendix II – Primers and small interfering RNA

Application	Name	F/R	Sequence (5′ – 3′)	Annealing temperature
Cloning - chimeric opsins	ICL1	F	AGAGCAGAAGCCTCCGGACACCGCTGAACTGGATC	60
		R	GGTGTCCGGAGGCTTCTGCTCTTCATGGTGGCCGC	
	ICL2_1	F	AGGTGGCTGGTGGTGACACGCCCGCTGGCC	60
		R	GGCCAGCGGGCGTGTCACCACCAGCCACCT	
	ICL2_2	F	TTTGGTGTGGCGTCCAAGCTGGCCATCGTG	60
		R	CACGATGGCCAGCTTGGACGCCACACCAAAG	
	ICL3_1	F	CTCTGCTACCTCCAAATCTTCAGGGCCATC	60
		R	GATGGCCCTGAAGATTTGGAGGTAGCAGAG	
	ICL3_2	F	CAGCGGCTGCAGAGCGAGAAGGAAGTGACG	60
		R	CGTCACTTCCTTCTCGCTCTGCAGCCGCTG	
	C-terminus	F	AACCCCGTTATCTATGCCATCACCCACCCC	60
		R	GGGGTGGGTGATGGCATAGATAACGGGGTTG	
Cloning - fusions	Opn4-Not-GNAQ_F		CAGGACCCCAGGATGGCGGCCGCAACTCTGGAGTCCATC	55
	Opn4-Not-GNAQ_R		GATGGACTCCAGAGTTGCGGCCGCCATCCTGGGGTCCTG	
	Opn4-Not-GNA11_F		CAGGACCCCAGGATGGCGGCCGCAACTCTGGAGTCCATG	55
	Opn4-Not-GNA11_R		CATGGACTCCAGAGTTGCGGCCGCCATCCTGGGGTCCTG	
	RH1-Not-GNAQ_F		CAGGTGGCCCCGGCCGCGGCCGCAACTCTGGAGTCCATC	55
	RH1-Not-GNAQ_R		GATGGACTCCAGAGTTGCGGCCGCGGCCGGGGCCACCTG	
	RH1-Not-GNA11_F		CAGGTGGCCCCGGCCGCGGCCGCAACTCTGGAGTCCATG	55
	RH1-Not-GNA11_R		CATGGACTCCAGAGTTGCGGCCGCGGCCGGGGCCACCTG	
	PE_GNAQ_Sal_R		CGGCGTCGACTAGCTAGTTAGACCAGATTGTACTCCTTC	55
	PE_GNA11_Sal_R		CGGCGTCGACTAGCTAGTCAGACCAGGTTGTACTCCTTG	
	PE_hRH1_R		CGGCTCGAGAATTCTAGGCTAGTTAGGCCGGGGCCACCTG	55
	PE_hOpn4		CGGCTCGAGAATTCTAGGCTAGCTACATCCTGGGGTCCTG	
Cloning – fusions – silent mutations of EcoRI and SalI sites in GNAQ	GNA_mutSalI_F		GTATTCCCATCTAGTGGATTACTTCCCAGAATATG	55
	GNA_mutSalI_R		CATATTCTGGGAAGTAATCCACTAGATGGGAATAC	
	GNA_mutEcoRI_F		CCAGGCAGCCCGAGAGTTTATTCTGAAGATGTTC	55
	GNA_mutEcoRI_R		GAACATCTTCAGAATAAACTCTCGGGCTGCCTGG	
Subcloning *OPN4* and *OPN4-GNA11* into ITR-containing plasmid	PE_OPN4_HindIII_F		CGCGAAGCTTCACCATGAACCCTCC	60
	PE_OPN4_AvrII_R		CGCTCCTAGGCTAGCTAGCTACATC	
	PE_GNAQ_AvrII_R		CGCTCCTAGGCTAGCTAGTTAGACC	
	PE_GNA11_AvrII_R		CGCTCCTAGGCTAGCTAGTCAGACC	
Floxed and non-floxed opsins				
Floxed melanopsin	Flox_hOPN4_NheI_HT		CGCCGCTAGCCACCATGAACCCTCCTTCG	60
	Flox_AscI_hOPN4		TAATGGCGCGCCCTACTAGGCAGGCGCCACTT	
Non-floxed melanopsin	XbaI_hOPN4		GCTATCTAGAGCCACCATGAACCCTCCTTCG	60
	OPN4 w 1D4_EcoRI		GACGAATTCTAGGCAGGCGCCACTTGGC	
Floxed rhodopsin	Flox_hRHO_NheI		CGCCGCTAGCCACCATGAATGGCACAGAAG	60
	Flox_AscI_hRHO		TAATGGCGCGCCCTATTAGGCCGGGGCC	

Application	Name	F/R	Sequence (5′ – 3′)	Annealing temperature	Expected amplicon
Genotyping	Cre_transgene_F		GCGGTCTGGCAGTAAAAACTATC	51.7	101
	Cre_transgene_R		GTGAAACAGCATTGCTGTCACTT		
	Cre_control_F		CTAGGCCACAGAATTGAAAGATCT		324
	Cre_control_R		GTAGGTGGAAATTCTAGCATCATCC		
	Gpr179_1		TGTGCCTGGGTATCTGTTGA	56	113 (WT) and 400 (mutant)
	Gpr179_2		GCATGTGCCAAGGGTATCTT		
	Gpr179_3		GCTTACACACTTACACACAGATAGATG		
	RD3		TGACAATTACTCCTTTTCCCTCAGTCT	60	400 (WT) and 550 (mutant)
	RD4		GTAAACAGCAAGAGGCTTTATTGGGAA		
	RD6		GCATTAATTCTGGGGCGCATGG		
	EYFP_WT		GGAGCGGGAGAAATGGATATG	65, reduce by 1.5 every cycle for 10 cycles. 50 for 28 cycles.	603 (WT) and 320 (mutant)
	EYFP_transgene		AAGACCGCGAAGAGTTTGTC		
	EYFP_common		AAAGTCGCTCTGAGTTGTTAT		
qPCR – viral titering	*OPN4*	F	GTTGCTGACATCCTGCTCCT	60	144
		R	TCCCGGATGGCCCTGAAGAT		
	RHO	F	CCTCTCTGCATGGATACTTCGTC	60	139
		R	ATGGGCTTACACACCACCAC		
qPCR - siRNA efficacy	*ACTB*	F	GCATCGTCACCAACTG	60	222
		R	TACGGCCAGAGGCGT		
	GNAQ	F	CCTACCTGCCTACGCAACAA	60	129
		R	TCTTCTCTCTGACCTTTGGCC		
	GNA11	F	GCACCTGGTGGACTACTTCC	60	255
		R	TGTCTCCATCCCGTCTCCCT		
	RPLP0	F	CGACCTGGAAGTCCAACTAC	60	109
		R	ATCTGCTGCATCTGCTTG		
qPCR – bipolar, rod and housekeeper genes	*Cabp5*	F	GACTTTGTGGAACTGATGACCC	60	125
		R	TCTGCCAGTGTGATCTCCC		
	Cnga1	F	CTGACGATGACAATGGCTCTCT	60	120
		R	CCATAGTACCTGGCAAGTGCT		
	Gapdh	F	TGCACCACCAACTGCTTAG	60	176
		R	GATGCAGGGATGATGTTC		
	Grm6	F	TCACCATGTACACCACCTGT	60	120
		R	TCAGGCTCAGGGACACAGT		
	Pcp2	F	TATGCTGGTCAACACCCAGG	60	120
		R	CTGAGGGTCCCAGGTCGTTT		
	Prkca	F	CGAGGGAGAGAGGGATGTCA	60	119
		R	TTTCTGCTCCTTTGCCACAC		
	Rho	F	ACTCTGCCAGCTTTCTTTGC	60	120
		R	CAGTGGATTCTTGCCGCAG		
	Rplp0	F	CGACCTGGAAGTCCAACTAC	60	109
		R	ATCTGCTGCATCTGCTTG		

Appendix III – Kits

Kit	Company	Catalogue code	Headquarters
BiotinIL kit	NuGEN Technologies	4210	San Carlos, CA
DNase I, Amplification Grade kit	Invitrogen*	18068	Waltham, MA
EndoFree Plasmid Megaprep kit	Qiagen	12381	Hilden, Germany
GenElute Plasmid Miniprep kit	Sigma-Aldrich	PLN350	St. Louis, MO
iTaq Universal SYBR Green Supermix kit	Bio-Rad	172-5121	Hercules, CA
KOD Hot Start DNA polymerase kit	Toyobo	71086	Osaka, Japan
Ovation Pico WTA v2 kit	NuGEN Technologies	3302	San Carlos, CA
Papain dissociation kit	Worthington Biochemical Corporation	LK003153	Lakewood, NJ
PureLink HiPure Plamid Maxiprep kit	Invitrogen*	K2100	Waltham, MA
PureLink RNA Mini kit	Ambion*	12183018A	Waltham, MA
QIAfilter Plasmid Mega kit	Qiagen	12281	Hilden, Germany
QIAquick Gel Extraction kit	Qiagen	28704	Hilden, Germany
QIAquick PCR purification kit	Qiagen	28104	Hilden, Germany
RNA 6000 Pico kit	Agilent Technologies	5067-1513	Santa Clara, CA
RNase-Free DNase Set	Qiagen	79254	Hilden, Germany
RNeasy Micro kit	Qiagen	74004	Hilden, Germany
SuperScript III Reverse Transcriptase kit	Invitrogen*	18080-044	Waltham, MA

Appendix IV – Hardware

Generic name	Model	Catalogue code	Company	Headquarters
0.22 µm filter	Millex-GV Syringe Filter Unit, 0.22 µm	SLGV033RB	Merck Millipore	Billerica, MA
1 ml syringe	1 ml 100 IU without needle	5010.A00V0	Henke-Sass, Wolf GmbH	Tuttlingen, Germany
6 mm coverslip	Cover glasses, round	631-0168	VWR International	Radnor, PA
96 well plate	TC plate 96 well	83.3924.500	Sarstedt	Nümbrecht, Germany
AAV filter - 15 ml	Amicon Ultra-15 centrifugal filter unit	UFC910024	Merck Millipore	Billerica, MA
AAV filter - 2 ml	Amicon Ultra-2 centrifugal filter unit	UFC210024	Merck Millipore	Billerica, MA
Barrier pen	ImmEdge Hydrophobic Barrier Pen	H-4000	Vector Laboratories	Burlingame, CA
Bioanalyzer	2100 (Firmware: C.01.069)	G2938C	Agilent Technologies	Santa Clara, CA
Camera (pupillometry)	Prosilica NIR sensitive CCD video camera	–	BRSL	Newbury, UK
Cell filter	BD Falcon 12 x 75 mm Tube with Cell Strainer Cap	352235)	Becton, Dickinson and Company	Franklin Lakes, NJ
Centrifuge - benchtop	Biofuge Pico	#	Heraeus*	Waltham, MA
Centrifuge - large volume	Heraeus Megafuge 16R	75004270	Thermo Scientific*	Waltham, MA
Centrifuge - ultracentrifuge	Optima XE-90K	A94471	Beckman Coulter	Brea, CA
Centrifuge - ultracentrifuge rotor	Type 70 Ti	337922	Beckman Coulter	Brea, CA
Centrifuge - ultracentrifuge tubes	Optiseal polyallomer centrifuge tube	361625	Beckman Coulter	Brea, CA
Centrifuge bottle	400 ml centrifugation polypropylene bio-bottles	75-007-585	Thermo Scientific*	Waltham, MA
Centrifuge bottle	500 ml PPCO centrifuge bottles	3120	Thermo Scientific*	Waltham, MA
Cryostat	LM1850	–	Leica Biosystems	Wetzlar, Germany
FACS	MoFlo Legacy	#	Beckman Coulter	Brea, CA
Ganzfeld dome	2" integrating sphere	–	Pro-Lite Technology	Cranfield, UK
Glass slides	Polysine slides	J2800AMNZ	Menzel-Gläser*	Braunschweig, Germany
Hemocytometer	Bright-Line Hemocytometer	–	Hausser Scientific	Horsham, PA
Hybridisation incubator	HB-1D	FHB1DE	Techne	Stone, UK
Hyperflask	Corning CellBIND Surface HYPERflask vessel	CLS10030	Sigma-Aldrich	St. Louis, MO
Incubator	HERA Cell 150	–	Thermo Electon*	Waltham, MA
Insulin syringe with needle	1 ml insulin syringe (29 G)	BS-N1H2913	Terumo	Tokyo, Japan
Intraocular injection - needle	34 G, 100 mm long, point style 2	207434	Hamilton Company	Reno, NV
Intraocular injection - syringe	65 RN	7633-01	Hamilton Company	Reno, NV
Microbiological safety cabinet	Scanlaf, Mars	–	LaboGene	Lynge, Denmark
Microscope - confocal	LSM 710	#	Carl Zeiss AG	Oberkochen, Germany
Microscope - dissecting	EZ4	–	Leica Microsystems	Wetzlar, Germany
Microscope - epifluorescence	DM IL LED Fluo	–	Leica Microsystems	Wetzlar, Germany
Microscope - live cell fluorescent	IX71	IX71	Olympus	Tokyo, Japan
Monochromator	–	–	Cairn Research	Faversham, UK
ND filters (pupillometry)	Log 1 - 4 neutral density	–	L.O.T.-Oriel GmbH and Co. KG	Darmstadt, Germany
Needles	BD Microlance 3, 18 G, 21 G, 30 G	–	Becton, Dickinson and Company	Franklin Lakes, NJ
PCR machine	T100	1861096	Bio-Rad	Hercules, CA
PCR tubes	0.2ml 8-Strip PCR Tubes	I1402-3700	STARLAB	Hamburg, Germany
Pipettes	P2, P20, P200 and P1000 PIPETMAN Classic	–	Gilson	Middleton, WI
Plate reader	FLUOStar Omega	–	BMG Labtech	Ortenberg, Germany
Protein transfer machine	Trans-Blot Turbo Transfer System	1704155	Bio-Rad	Hercules, CA
qPCR machine	CFX Connect Real-Time PCR Detection System	–	Bio-Rad	Hercules, CA
Scanning laser ophthalmoscope	Spectralis HRA	HRA	Heidelberg Enginering	Heidelberg, Germany
Shutter	LSZ160 shutter	–	L.O.T.-Oriel GmbH and Co. KG	Darmstadt, Germany
Spectrometer	USB2000+ series	–	Ocean Optics	Dunedin, FL
Spectrophotometer (1)	Nanodrop 1000	#	Thermo Scientific*	Waltham, MA
Spectrophotometer (2)	UV-2550	–	Shimadzu	Kyoto, Japan
Syringe	BD Plastipak	302188	Becton, Dickinson and Company	Franklin Lakes, NJ
Tissue culture flask	T75	83.3911.002	Sarstedt	Nümbrecht, Germany
Tissue culture flask	T175	660 175	Greiner Bio-One	Kremsmünster, Austria
Tissue culture insert	Falcon 24 well, 0.4 µm pore size	734-0036	VWR International	Radnor, PA
Transfer pipette	3.5 ml	86.1173	Sarstedt	Nümbrecht, Germany
Ultra low temperature freezer	U570 Premium	–	New Brunswick Scientific	Hamburg, Germany
UV steriliser	CL-1000	–	UVP	Upland, CA
Water bath	–	FB60305	Fisherbrand*	Waltham, MA
Webcam	–	–	Logitech	Romanel-sur-Morges, Switzerland
Western blotting system	Snap i.d. Protein Detection System	#	Merck Millipore	Billerica, MA
Xenon arc lamp (calcium imaging)	–	–	Cairn Research	Faversham, UK
Xenon arc lamp (pupillometry)	150 W solar simulator	–	L.O.T.-Oriel GmbH and Co. KG	Darmstadt, Germany

No longer sold * Part of Thermo Fisher Scientific

Appendix V – Software

Software	Version	Company	Headquarters/URL
2100 Expert	B.02.07.SI532	Agilent Technologies	Santa Clara, CA
CFX Manager	3.1	Bio-Rad	Hercules, CA
Excel	15.16	Microsoft	Redmond, WA
Eye Explorer		Heidelberg	Heidelberg, Germany
Geneious	6.1.8	Biomatters	Auckland, New Zealand
GeneMANIA	3.1.2	n/a (open source)	genemania.org
ImageJ	1.42q	n/a (open source)	imagej.nih.gov/ij/
Inkscape	0.48	n/a (open source)	inkscape.org
MARS	3.00 R2	BMG Labtech	Ortenberg, Germany
Omega	3.00 R2	BMG Labtech	Ortenberg, Germany
Prism	6.0h	GraphPad	San Diego, CA
Summit	4.3	Beckman Coulter	Brea, CA
Time Series Analyzer plugin	2	n/a (open source)	http://rsb.info.nih.gov/ij/plugins/time-series.html

Appendix VI – AAV vectors

Vector	Transgene	Serotype	Concentration (vg/ml)	Chapter
AAV2/8(Y733F)-GFP	CAG-GFP	AAV2/8(Y733F)	2.0×10^{12}	3
AAV2/2(quad Y-F)-GFP	CAG-GFP	AAV2/2(quad Y-F)	2.0×10^{12}	3
AAV2/2(7m8)-GFP	CAG-GFP	AAV2/2(7m8)	2.0×10^{12}	3
AAV-*OPN4*	CAG-*OPN4*	AAV2/2(7m8)	1.3×10^{12}	5
AAV-*OPN4-GNA11*	CAG-*OPN4-GNA11*	AAV2/2(7m8)	1.3×10^{12}	5
AAV-sham	EF1α-F.OPN4	AAV2/2(7m8)	1.3×10^{12}	5
AAV-*OPN4*	EF1α-*OPN4*	AAV2/2(7m8)	1.0×10^{12}	6
AAV-F.*OPN4*	EF1α-F.*OPN4*	AAV2/2(7m8)	1.0×10^{12} and 2.0×10^{13}	6
AAV-F.*RHO*	EF1α-F.*RHO*	AAV2/2(7m8)	2.0×10^{13}	6

F. denotes a floxed gene

1 Material and Methods

Appendix VII - Microarray report

1.1 Array processing

RNA was assessed for concentration and quality using a SpectroStar (BMG Labtech, Aylesbury, UK) and a Bioanalyser (Agilent Technologies, Cheadle, UK). Microarray experiments were performed at Cambridge Genomic Services, University of Cambridge, using the MouseWG-6 v2 Expression BeadChip (Illumina, Chesterford, UK) according to the manufacturer's instructions. Briefly, total RNA was amplified using the Ovation Pico WTA v2 kit (NuGEN Technologies, Leek, Netherlands) and subsequently labelled using the BiotinIL kit (NuGEN Technologies) following the manufacturer's instructions. The concentration, purity and integrity of the resulting cDNA was measured using the Nanodrop ND-1000 (Thermo Scientific, Paisely, UK) and by Bioanalyser. Finally cDNA was hybridised to the MouseWG-6 v2 BeadChip overnight followed by washing, staining and scanning using the Bead Array Reader (Illumina).

1.2 Bioinformatics

After scanning the data are load in Illumina proprietary software, GenomeStudio. No background correction or normalisation is applied at this stage. A "final report" is generated, generating a text file containing the sample probe profile and the control probe information. The report is then processed in R using the lumi package [1] and the limma package [2]. The data are loaded and divided into subsets according to the groups being compared; only the samples involved in a given comparison are used. Subsets were then filtered to remove any non-expressed probes using the detection p-value from Illumina. Across all samples probes for which the intensity values were not significantly different ($p>0.01$) from the negative controls were removed from the analysis. Following filtering the data was transformed using the Variance Stabilization Transformation (VST [1]) from lumi and then normalised to remove technical variation between arrays using quantile normalisation. Comparisons were performed using the limma package with results corrected for multiple testing using False Discovery Rate (FDR) testing. Finally the quality of the data was assed and the correlation of the samples in the groups compared. In the interest of reproducibility the packages version and R session information [3] are provided in the reference.

2 Technical QC report

This section focuses on the technical aspect of the array, using the Illumina controls integrated to the array to check if the data generated is of good quality

2.1 Hybridsation control

The hybridisation controls are spiked in the hybridisation buffer at 3 different concentrations, low, medium and high. If the hybridisation steps as performed optimally the controls should display an increasing signal intensity from low to high.

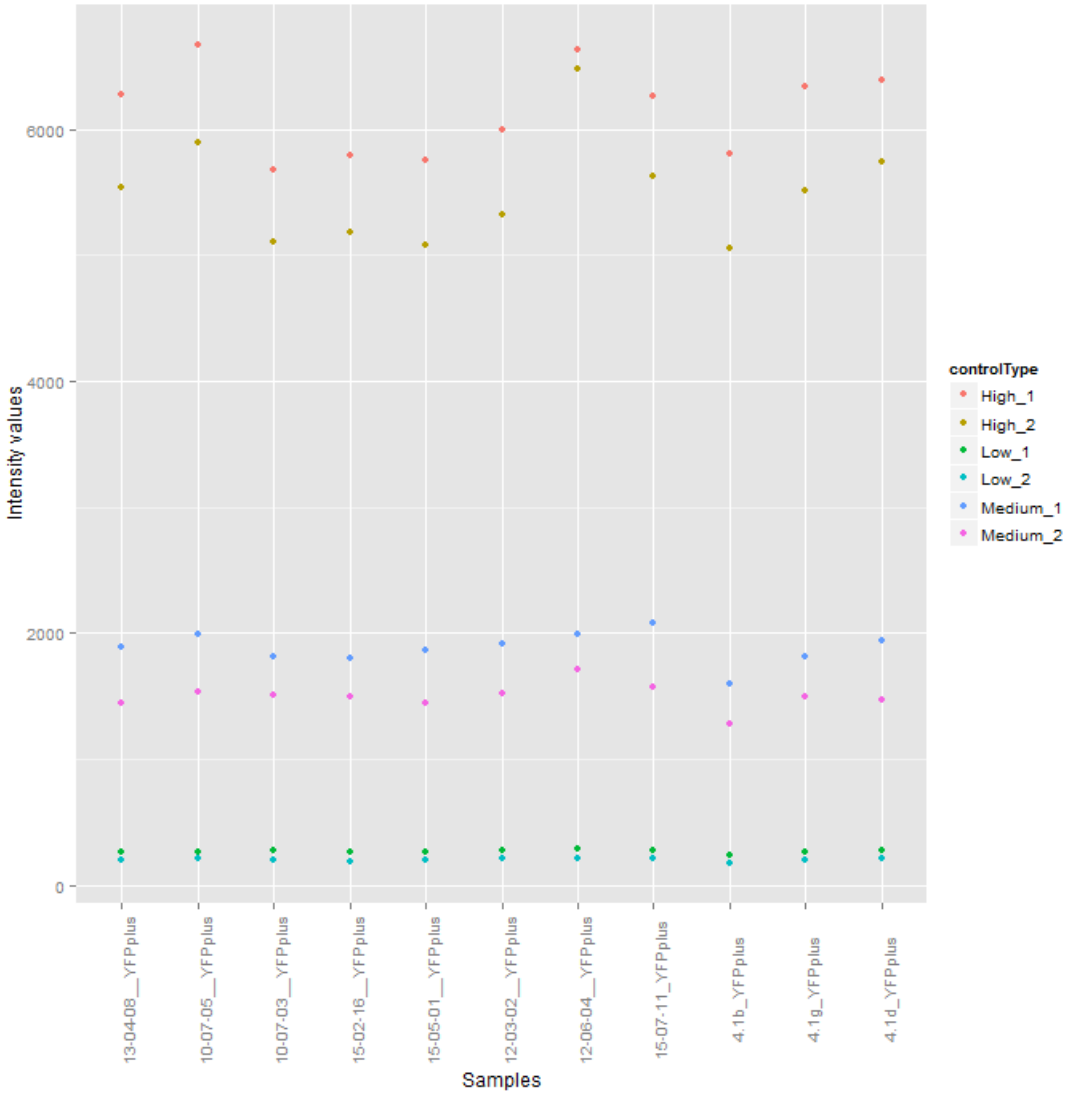


Figure 1: Hybridisation controls

2.2 Stringency controls

Stringency controls are design to assess the likelyhood of cross hybridisation during the assay. Two types of probes are present on the array:

- Mismatch probes, with 2 mismatches
- Perfect match probes with no mismatches

Ideally the perfect match probes should have a signal at least three times higher than the mismatch ones.

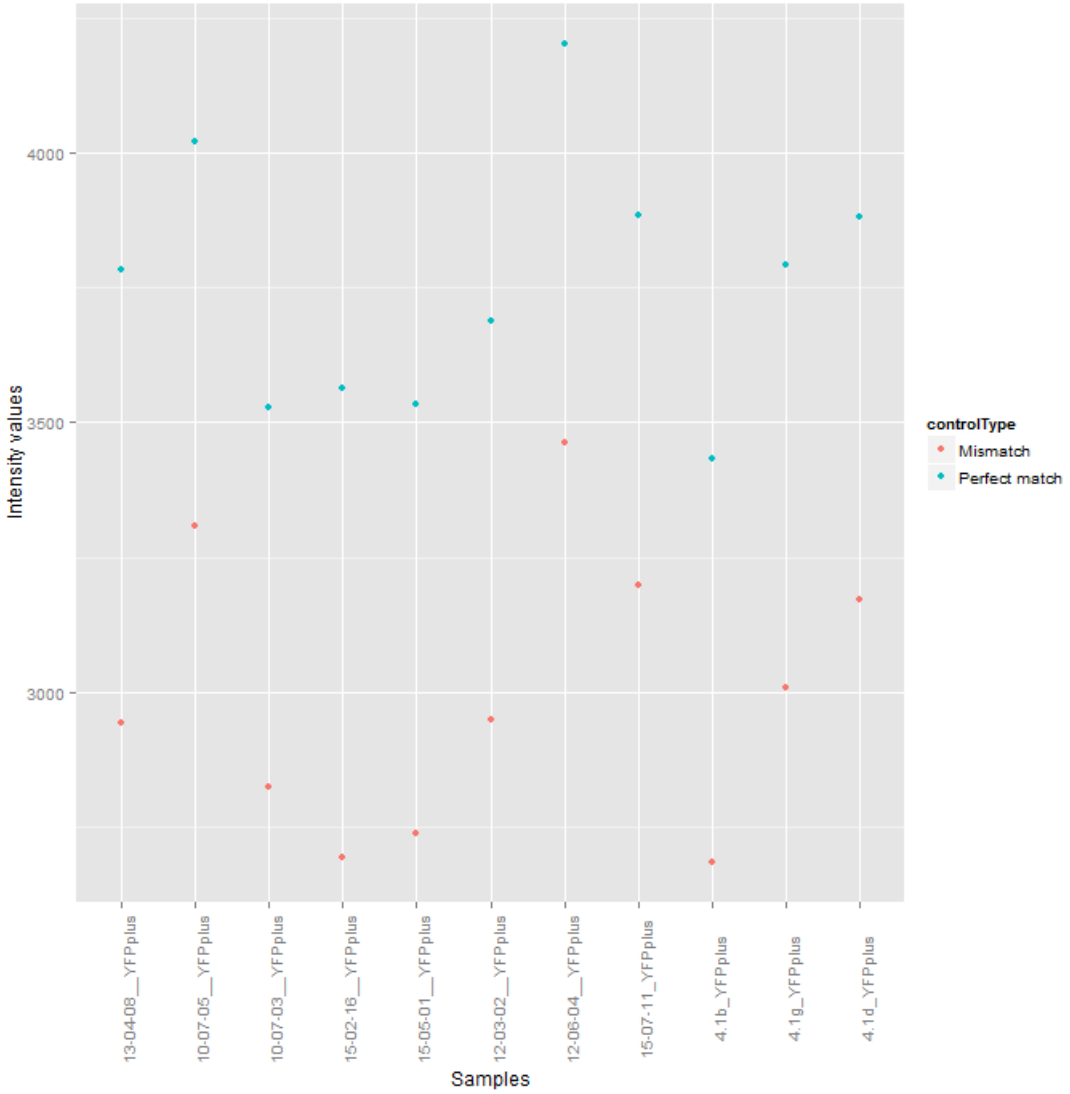


Figure 2: Stringency controls

2.3 Labelling controls

This controls are design to look at the efficiency of labelling, if the biotin has been well integrated it should give a high signal compare to background.

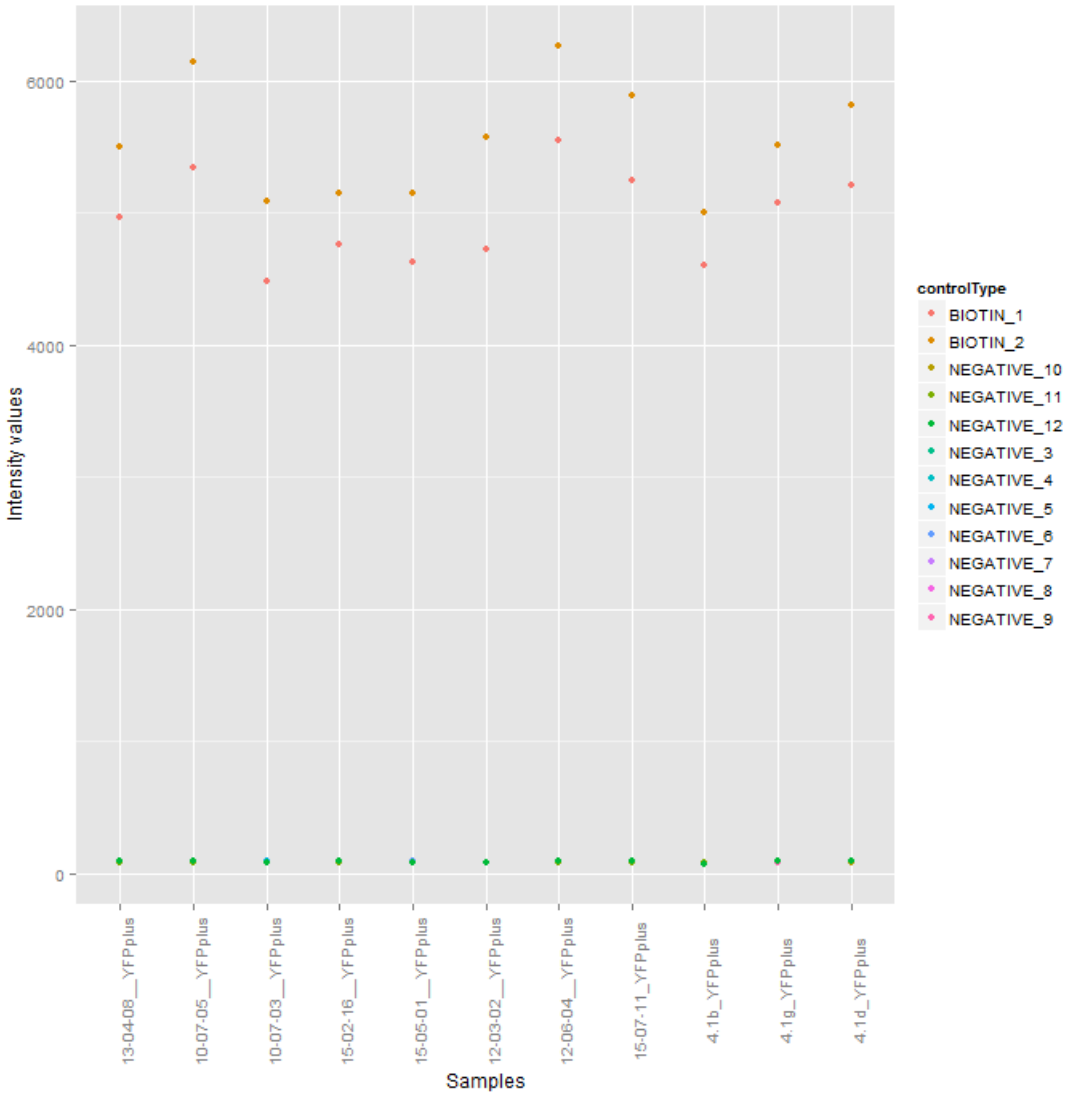


Figure 3: Labelling controls

2.4 Negative controls

Negative controls are empty beads on the array, they are a measure of the level of background on the array(s). Ideally the background should not vary too much between sections of the arrays. Increase in background signal could indicate issues with the array processing.

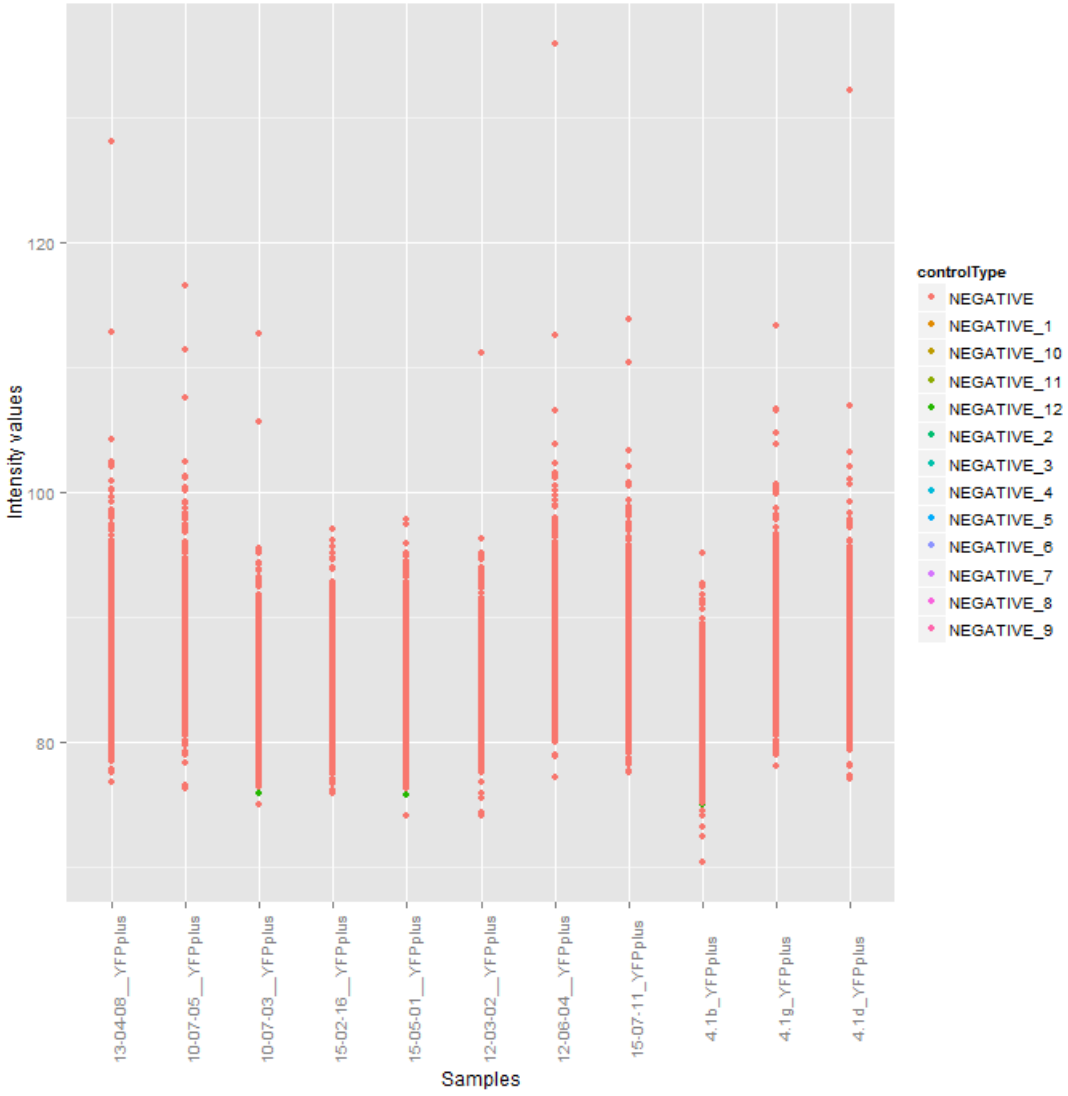


Figure 4: Labelling controls

3 Biological samples QC

Biological samples QC assess the relationship between samples within groups and between groups.

3.1 Hierarchical clustering

Hierarchical clustering plots the distance between samples as a tree, the longer the branches and the more nodes between the samples, the more distant they are. It is expected that sample should cluster according to their biological group.

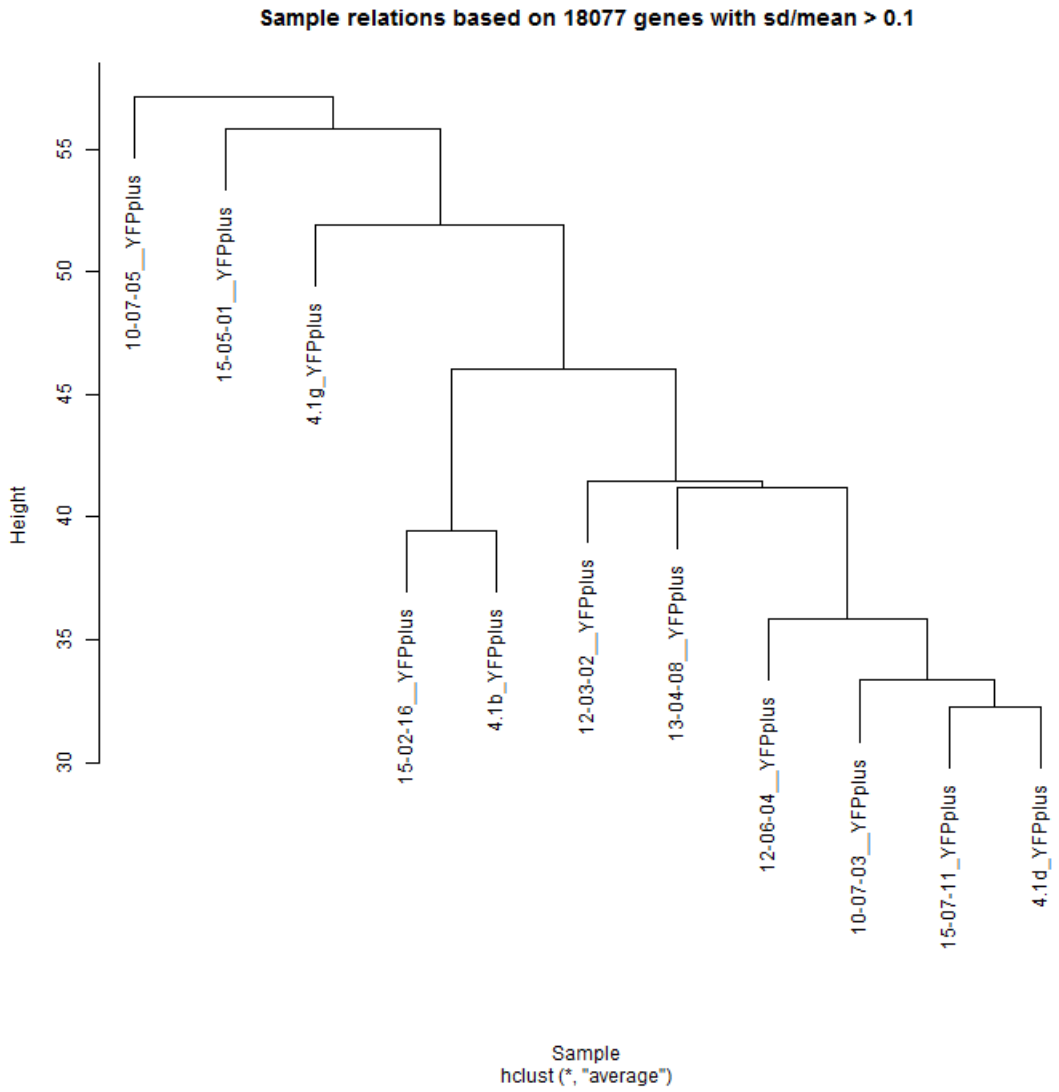


Figure 5: Hierarchical Clustering

3.2 MultiDimensional Scaling (MDS) clustering

MDS clustering clusters the samples in two dimensions (or more) instead of one, decomposing the variance into several components. Below are plotted the samples in relation to the two largest sources of potential variations. MDS can identify sources of variation potentially missed by relying on hierachical clustering alone.

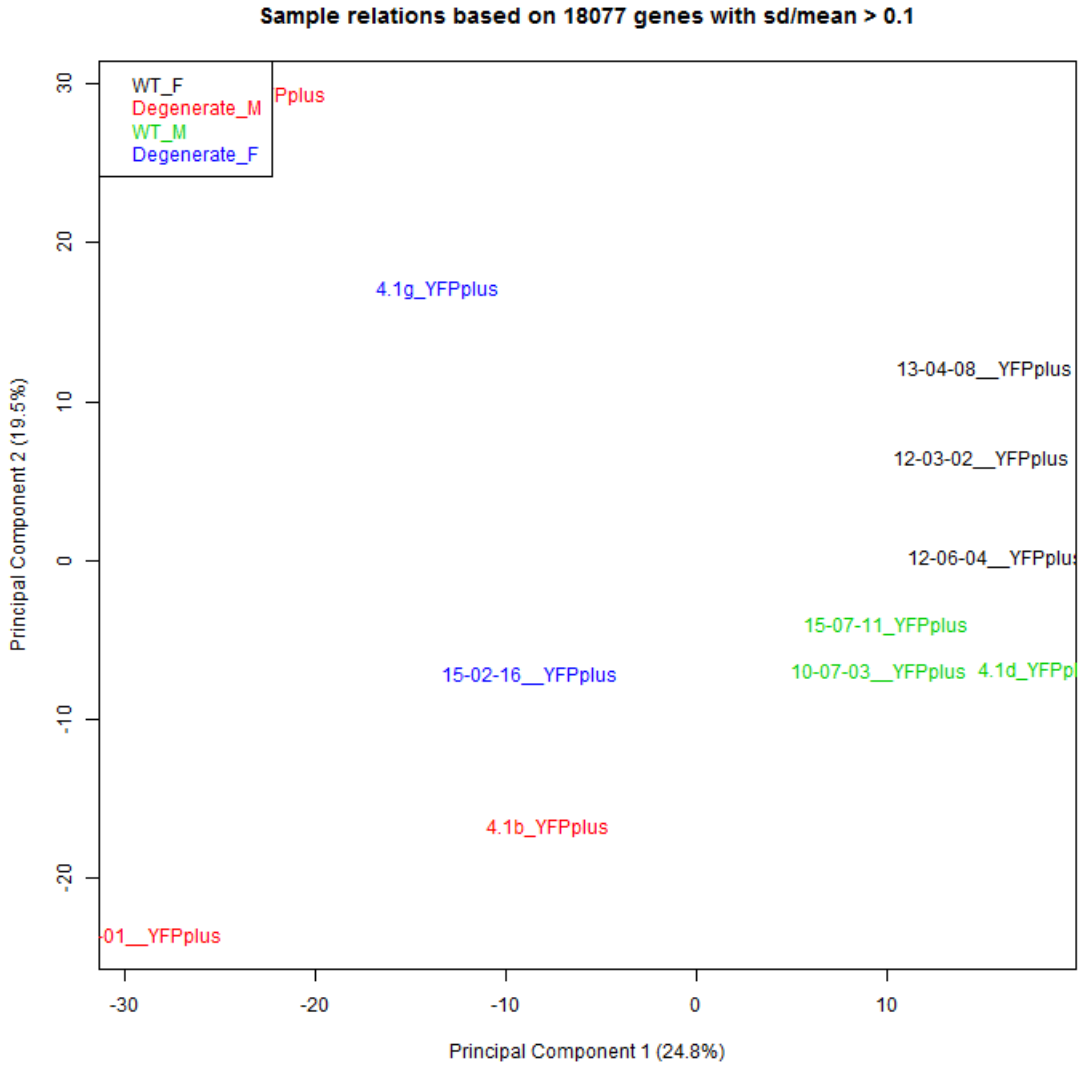


Figure 6: MDS clustering

3.3 Boxplots

Boxplots show the distribution of the intensity as a box with whiskers, the bottom of the box delimits the 25th percentile, the middle of the box the median, the top of the box the 75th percentile. Samples should have similar distribution of intensity. The intensity scale is log base 2.

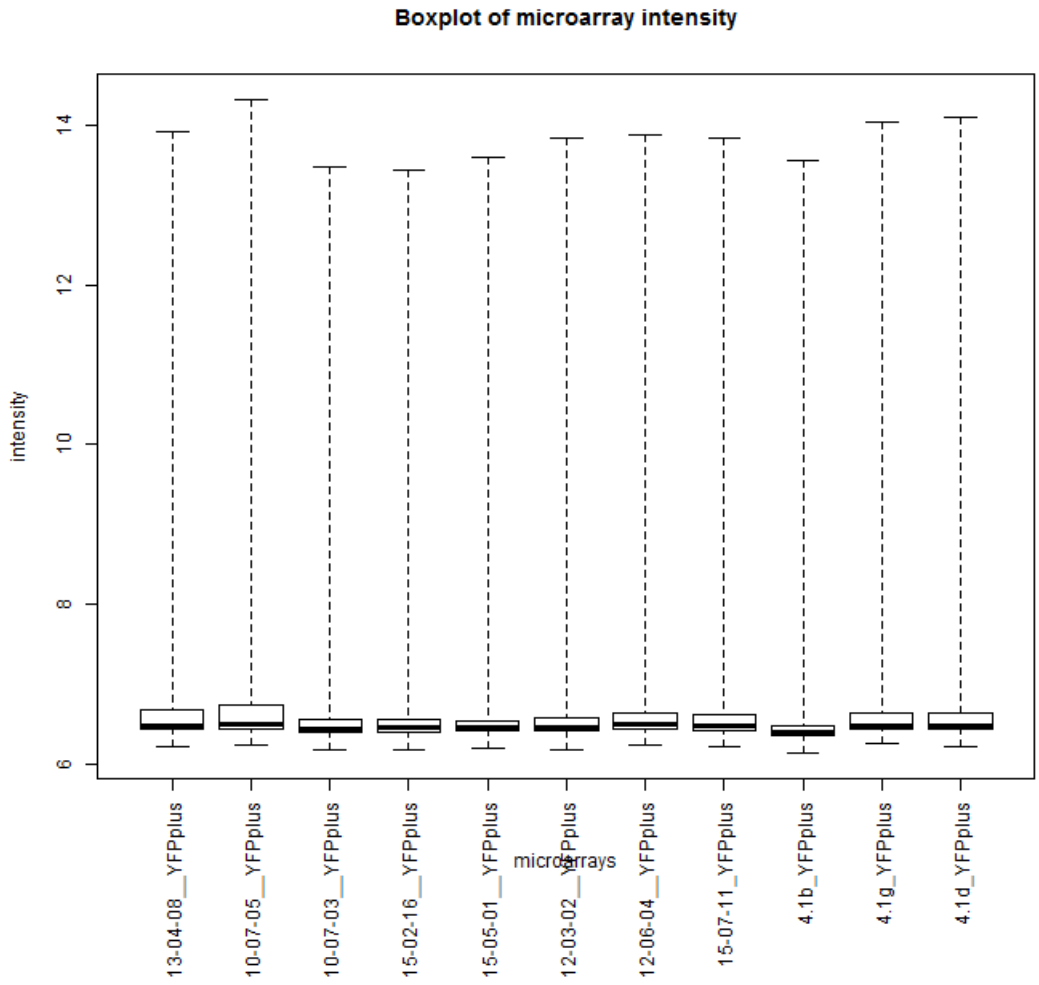


Figure 7: Boxplot

3.4 Density

The density plot represents the distribution of the intensity by plotting the intensities on the x axis against the frequency on the y axis, it is a less schematic representation of the distribution of the intensities.

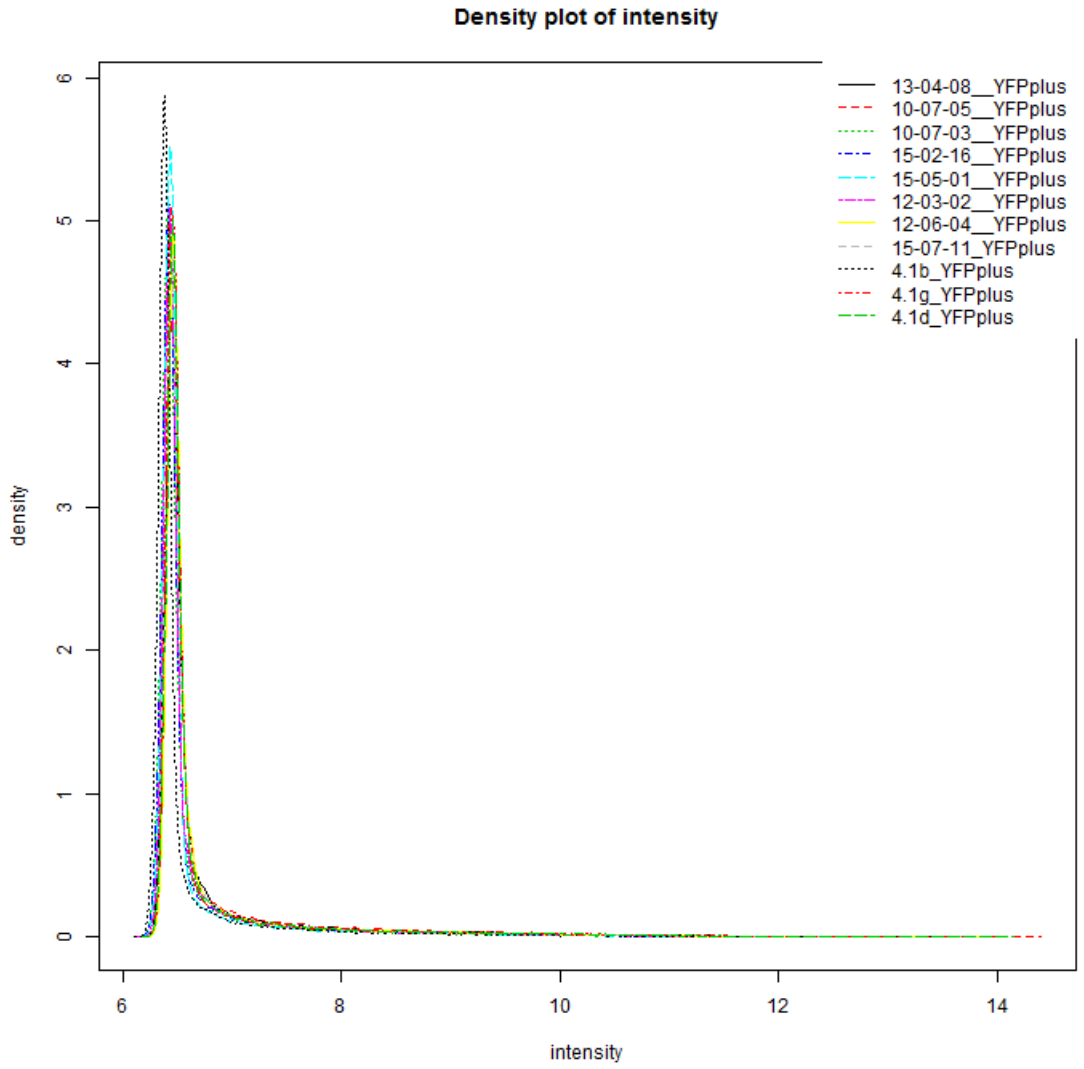


Figure 8: Boxplot

4.3 Scatter plots between groups

Scatter plots between two groups, theses type of plots allow a closer inspection of the correlation within and between groups. These graphs are also important when assessing potential outliers, their profiles should be markedly different from the other samples within their group.

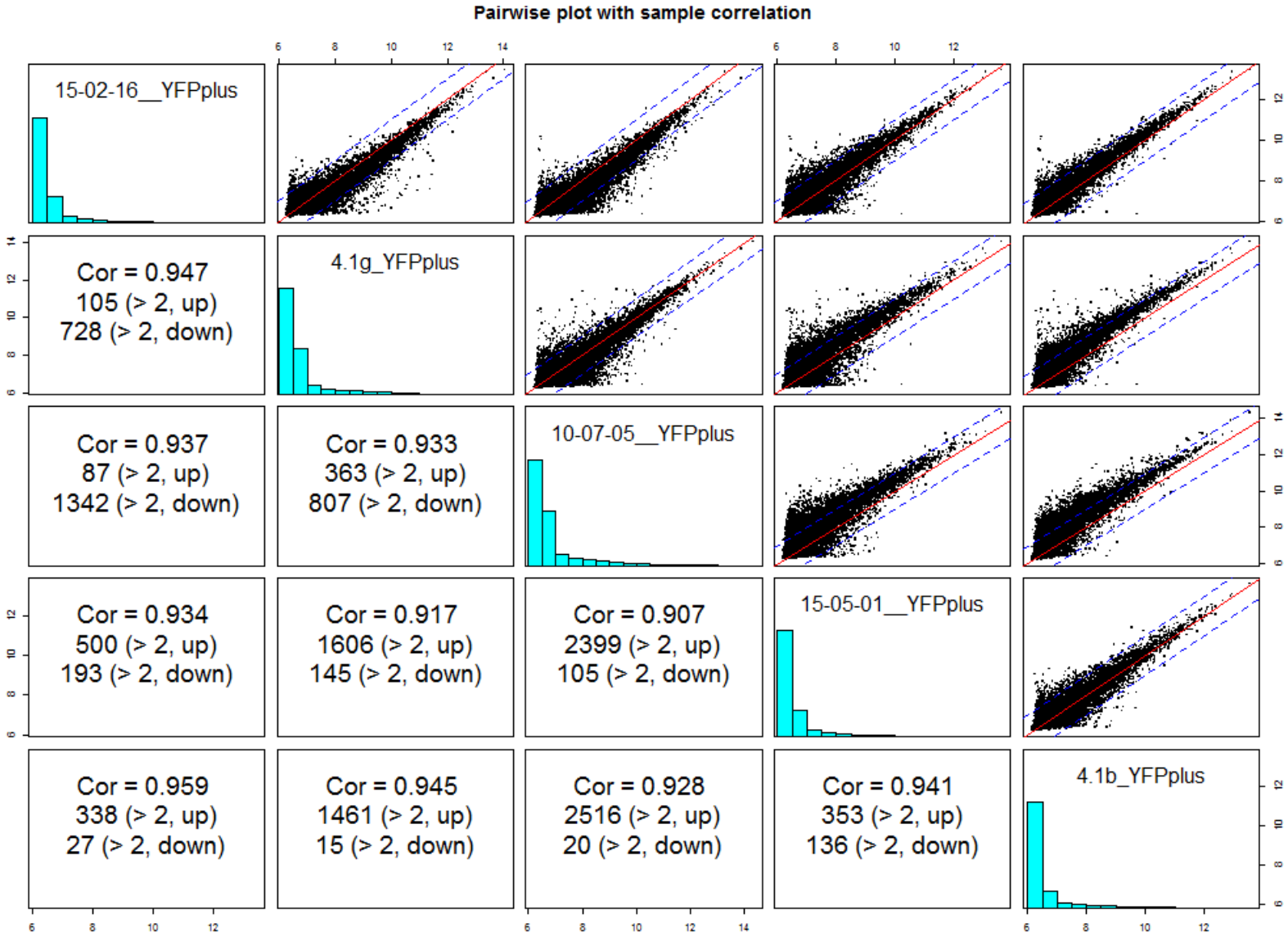


Figure 11: Scatter plots between two groups
Click here to access the other graphs

5 Normalisation

5.1 Normalisation Method

The normalisation method use by default is Quantile normalisation. Briefly, a reference distribution is constructed using the sample data. Then the intensity value of each sample and the reference distribution are ranked from highest to lowest. The sample values are fitted to the reference distribution, hence all the samples now share the same distribution of intensity. Sharing the same distribution of intensity allows for more powerful comparisons as the samples only differ by the change in gene expression and not change due to the intensity measurment, the asumption of the sample originating from the same population is validated. It is important to remove any source of noise (eg. outlier samples) before normalisation as otherwise their values will be used to construct the reference distribution. This is also why when performing a comparison between two groups, the rest of the data is removed.

5.2 Normalisation QC

All the QC graphs that were generated for the raw data are also regenerated for the normalisation data in order to check if there are any issue caused by the procedure. The expected results is that all the samples share the same distribution of intensities. Click here to access the normalised graphs

6 Comparisons

6.1 How to interpret your results

This section contains information about the comparisons performed. The datasets to compare are processed on a per comparison basis to make sure only the relevant samples are used for the analysis, therefore avoiding adding noise to the datasets when processing them which could be detrimental to the analysis. The steps used in the analysis are:

- Subset the data to include only the sample to be compared (usually from 2 groups)
- Perform pre-processing on the subset of data (filter, transformation and normalisation)
- Comparisons between the groups is performed using limma [2]

This is done for all the possible comparisons.

A summary table is generated (see below) to give an overview of the results. For each comparison a table with the top 10 genes is displayed along with a volcano plot and a heatmap. The volcano plot is useful to get an overview of the level of change and the level of significance, the x axis shows the level of change, the fold change (log2 scale), while the y axis represent the significance, -log10(pvalue). The heatmap displays the levels of expression for both groups as a color map for the top 50 genes. A direct link to the table is provided for each comparison.

To work on the results there are 2 important columns to use, logFC and adj.pvalue. The adj.pvalue contains the p-value corrected for multiple testing using False Dicovery Rate. The p.value column should **not** be used as it is not corrected for multiple testing, resulting in a large number of false positives. The adjusted p-value should be used as a primary filtering column. If there are still too many results after filtering using "classic" levels (0.05 or 0.01) consider lowering it further or using the logFC column as a secondary fiter to look at the higher rates of change in your data. The logFC represents the log in base 2 of the fold change. A value of 1 is equivalent to a change of 2 folds, 2 is 4 folds, 3 is 8, etc... Using the value as a power of 2 gives you the real fold change.

If there are still a large number of probes to study, it is recommended to take a functional approach to analyse the results. The aim of a functional analysis is to group genes according to function/pathways in order to reduce the complexity of the set. For this Gene Ontology tools or pathway finder can be used.

A note on the p-value: in some case the adjusted p-value will have the same value for several probes, which might look like an error has occured during the correction. This can happen as a results of how the correction is performed. The steps are as follow:

- Sort the p-value from low (rank 1) to high (rank N, with N the number of comparisons performed)
- Multiply the p-value by N
- Divide the p-value by its rank
- Check that the rank is kept

The last point is the reason why the adjusted p-value can share the same value, if the ranks are not kept and a higher ranked probe ends up with a lower adjusted p-value than a lower rank probe, the lower value of the higher ranked probe will be used for the lower ranked p-value.

6.3.6 Degenerate vs WT

PROBE_ID	SYMBOL	logFC	adj.P.Val	B
ILMN_2765547	Gnat1	-2.65	0.00	8.85
ILMN_2595543	Pde6b	-1.08	0.00	7.84
ILMN_2603504	Car2	-0.94	0.00	7.66
ILMN_2859960	Adcy1	-0.95	0.00	7.47
ILMN_2944168	C80008	-1.17	0.00	7.28
ILMN_2512149	LOC100047936	-1.29	0.00	6.90
ILMN_2730436	Sag	-1.56	0.00	6.44
ILMN_3065373	4930572J05Rik	-1.02	0.00	6.22
ILMN_1257965	Ldha	-1.33	0.00	5.93
ILMN_2596522	Mt1	-2.06	0.00	5.80

Click here to open the comparison table

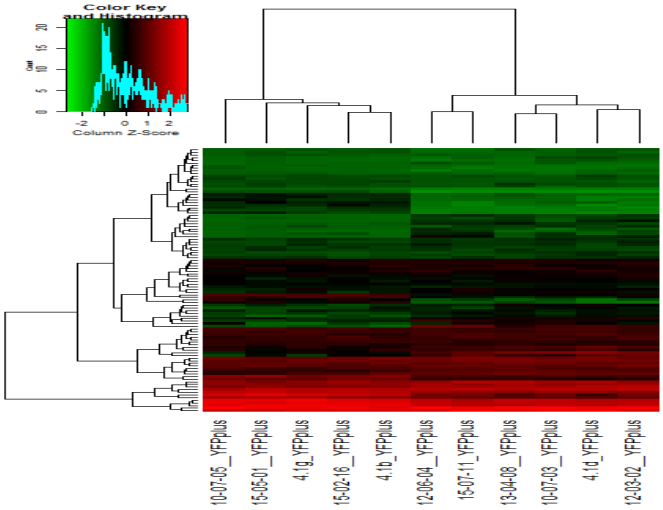


Figure 22: Heatmap

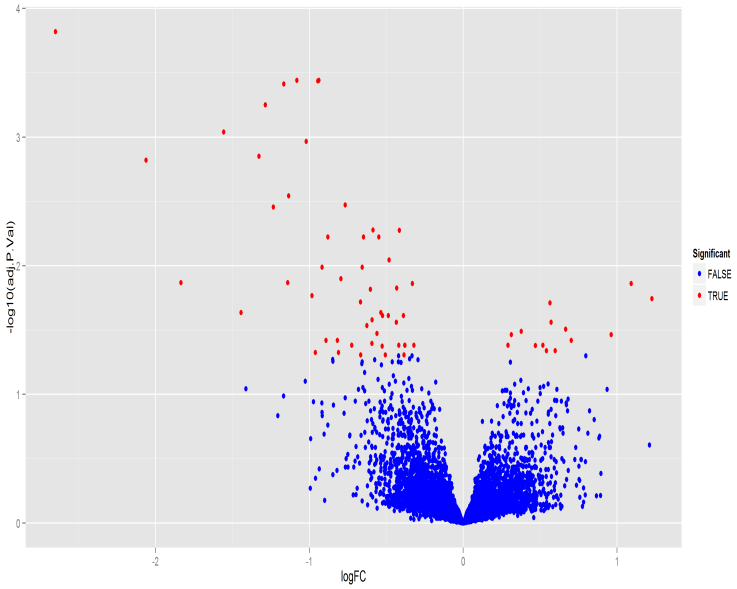


Figure 23: Volcano Plot

References

[1] Du, P., Kibbe, W.A. and Lin, S.M., (2008) 'lumi: a pipeline for processing Illumina microarray', Bioinformatics 24(13):1547-1548

Lin, S.M., Du, P., Kibbe, W.A., (2008) 'Model-based Variance-stabilizing Transformation for Illumina Microarray Data', Nucleic Acids Res. 36, e11

Package version: 2.22.0

[2] Ritchie, M.E., Phipson, B., Wu, D., Hu, Y., Law, C.W., Shi, W., and Smyth, G.K. (2015). limma powers differential expression analyses for RNA-sequencing and microarray studies. Nucleic Acids Research 43(7), e47.

A BibTeX entry for LaTeX users is

@Article, author = Matthew E Ritchie and Belinda Phipson and Di Wu and Yifang Hu and Charity W Law and Wei Shi and Gordon K Smyth, title = limma powers differential expression analyses for RNA-sequencing and microarray studies, journal = Nucleic Acids Research, year = 2015, volume = 43, number = 7, pages = e47,

Package version: 3.26.3

[3]
```
R version 3.2.2 (2015-08-14)
Platform: x86_64-w64-mingw32/x64 (64-bit)
Running under: Windows 7 x64 (build 7601) Service Pack 1

locale:
[1] LC_COLLATE=English_United Kingdom.1252
[2] LC_CTYPE=English_United Kingdom.1252
[3] LC_MONETARY=English_United Kingdom.1252
[4] LC_NUMERIC=C
[5] LC_TIME=English_United Kingdom.1252

attached base packages:
[1] parallel  stats     graphics  grDevices utils     datasets  methods
[8] base

other attached packages:
[1] xtable_1.8-0        lumi_2.22.0         Biobase_2.30.0
[4] BiocGenerics_0.16.1 limma_3.26.3        knitr_1.11

loaded via a namespace (and not attached):
 [1] nor1mix_1.2-1              splines_3.2.2
 [3] foreach_1.4.3              ellipse_0.3-8
 [5] bumphunter_1.10.0          affy_1.48.0
 [7] stats4_3.2.2               doRNG_1.6
 [9] Rsamtools_1.22.0           methylumi_2.16.0
[11] minfi_1.16.0               RSQLite_1.0.0
[13] lattice_0.20-33            quadprog_1.5-5
[15] digest_0.6.8               GenomicRanges_1.22.1
[17] RColorBrewer_1.1-2         XVector_0.10.0
[19] colorspace_1.2-6           Matrix_1.2-3
[21] preprocessCore_1.32.0      plyr_1.8.3
[23] GEOquery_2.36.0            siggenes_1.44.0
[25] XML_3.98-1.3               mixOmics_5.2.0
[27] biomaRt_2.26.1             genefilter_1.52.0
[29] zlibbioc_1.16.0            corpcor_1.6.8
[31] scales_0.3.0               affyio_1.40.0
[33] BiocParallel_1.4.0         nleqslv_2.9.1
[35] annotate_1.48.0            mgcv_1.8-9
[37] beanplot_1.2               pkgmaker_0.22
[39] IRanges_2.4.4              ggplot2_1.0.1
```

Appendix VIII – Solutions

Solution	Components
Complete DMEM	High glucose DMEM 10% fetal bovine serum 1% penicillin-steptomycin (final concentrations: 100 units/ml and 100 µg/ml, respectively) 2 mM L-glutamine
Complete CO_2-independent media	CO2 independent medium 10% fetal bovine serum 1% penicillin-steptomycin 2 mM L-glutamine
Complete neurobasal A	Neurobasal A 1% penicillin-steptomycin 800 µM L-glutamine 2% B-27 supplement 1% N-2 supplement
Lysis buffer	1 M Tris(hydroxymethyl)aminomethane 150 mM NaCl *Autoclave*
PBS-MK, 5×	5× PBS tablets 5 mM magnesium chloride 12.5mM potassium chloride *Autoclave 5× PBS before adding 0.22 µm filtered solutions of $MgCl_2$ and KCl*

References

Abdeljalil J, Hamid M, Abdel-Mouttalib O, Stéphane R, Raymond R, Johan A, José S, Pierre C, Serge P (2005) The optomotor response: A robust first-line visual screening method for mice. Vision Res 45:1439–1446.

Adamantidis AR, Zhang F, Aravanis AM, Deisseroth K, de Lecea L (2007) Neural substrates of awakening probed with optogenetic control of hypocretin neurons. Nature 450:420–424.

Airan R, Thompson K, Fenno L, Bernstein H, Deisseroth K (2009) Temporally precise in vivo control of intracellular signalling. Nature 458:1025–1029.

Ala-Laurila P, Cornwall MC, Crouch RK, Kono M (2009) The action of 11-cis-retinol on cone opsins and intact cone photoreceptors. J Biol Chem 284:16492–16500.

Allen AE, Storchi R, Martial FP, Petersen RS, Montemurro M a, Brown TM, Lucas RJ (2014) Melanopsin-Driven Light Adaptation in Mouse Vision. Curr Biol 24:2481–2490.

Amado D, Mingozzi F, Hui D, Bennicelli JL, Wei Z, Chen Y, Bote E, Grant RL, Golden J a, Narfstrom K, Syed N a, Orlin SE, High K a, Maguire AM, Bennett J (2010) Safety and efficacy of subretinal readministration of a viral vector in large animals to treat congenital blindness. Sci Transl Med 2:21ra16.

Andrechek ER, Cardiff RD, Chang JT, Gatza ML, Acharya CR, Potti A, Nevins JR (2009) Genetic heterogeneity of Myc-induced mammary tumors reflecting diverse phenotypes including metastatic potential. Proc Natl Acad Sci U S A 106:16387–16392.

Andrieu-Soler C, Bejjani R-A, de Bizemont T, Normand N, BenEzra D, Behar-Cohen F (2006) Ocular gene therapy: a review of nonviral strategies. Mol Vis 12:1334–1347.

Armata I a., Giompres P, Smith A, Stasi K, Kouvelas ED, Mitsacos A (2006) Genetically induced retinal degeneration leads to changes in metabotropic glutamate receptor expression. Neurosci Lett 393:12–17.

Arrenberg AB, Stainier DYR, Baier H, Huisken J (2010) Optogenetic Control of Cardiac Function. Science (80-) 330:971–974.

Arshavsky VY, Lamb TD, Pugh EN (2002) G proteins and phototransduction. Annu Rev Physiol 64:153–187.

Ashtari M, Zhang H, Cook PA, Cyckowski LL, Shindler KS, Marshall KA, Aravand P, Vossough A, Gee JC, Maguire AM, Baker CI, Bennett J (2015) Plasticity of the human visual system after retinal gene therapy in patients with Leber ' s congenital amaurosis. 7:1–14.

Atchison RW, Casto BC, Hammon WM (1965) Adeno-associated defective virus particles. Science (80-) 149:754–756.

Atwood BK, Lopez J, Wager-Miller J, Mackie K, Straiker A (2011) Expression of G protein-coupled receptors and related proteins in HEK293, AtT20, BV2, and N18 cell lines as revealed by microarray analysis. BMC Genomics 12:14.

Audo I et al. (2012) Whole-exome sequencing identifies mutations in GPR179 leading to autosomal-recessive complete congenital stationary night blindness. Am J Hum Genet 90:321–330.

Auricchio A (2003) Pseudotyped AAV vectors for constitutive and regulated gene expression in the eye. Vision Res 43:913–918.

Baden T, Berens P, Bethge M, Euler T (2013) Spikes in mammalian bipolar cells support temporal layering of the inner retina. Curr Biol 23:48–52.

Bailes H, Lucas R (2013) Human melanopsin forms a pigment maximally sensitive to blue light (λmax ≈ 479 nm) supporting activation of G(q/11) and G(i/o) signalling cascades. Proc Biol Sci 280:20122987.

Bailes H, Zhuang L-Y, Lucas R (2012) Reproducible and sustained regulation of Gαs signalling using a metazoan opsin as an optogenetic tool. PLoS One 7.
Bainbridge JWB et al. (2015) Long-Term Effect of Gene Therapy on Leber's Congenital Amaurosis. N Engl J Med:150504083137004.
Bainbridge JWB, Smith AJ, Barker SS, Robbie S, Henderson R, Balaggan K, Viswanathan A, Holder GE, Stockman A, Tyler N, Petersen-Jones S, Bhattacharya SS, Thrasher AJ, Fitzke FW, Carter BJ, Rubin GS, Moore AT, Ali RR (2008) Effect of gene therapy on visual function in Leber's congenital amaurosis. N Engl J Med 358:2231–2239.
Balaggan KS, Ali RR (2012) Ocular gene delivery using lentiviral vectors. Gene Ther 19:145–153.
Balmer J, Ji R, Ray TA, Selber F, Gassmann M, Peachey NS, Ronald G, Enzmann V (2013) Presence of the Gpr179 nob5 allele in a C3H-derived transgenic mouse. :2615–2625.
Barker SE, Broderick CA, Robbie SJ, Duran Y, Natkunarajah M, Buch P, Balaggan KS, MacLaren RE, Bainbridge JWB, Smith AJ, Ali RR (2009) Subretinal delivery of adeno-associated virus serotype 2 results in minimal immune responses that allow repeat vector administration in immunocompetent mice. J Gene Med 11:486–497.
Bayes M, Giordano M, Balcells S, Grinberg D, Vilageliu L, Martinez I, Ayuso C, Benitez J, Ramos-Arroyo MA, Chivelet P, et al. (1995) Homozygous tandem duplication within the gene encoding the beta-subunit of rod phosphodiesterase as a cause for autosomal recessive retinitis pigmentosa. Hum Mutat 5:228–234.
Baylor BYDA, Lamb TD, Yau K (1979) Responses of retinal rods to single photons. J Phsiology 288:613–634.
Becerra SP, Koczot F, Fabisch P, Rose J a (1988) Synthesis of adeno-associated virus structural proteins requires both alternative mRNA splicing and alternative initiations from a single transcript. J Virol 62:2745–2754.
Beiert T, Bruegmann T, Sasse P (2014) Optogenetic activation of Gq signalling modulates pacemaker activity of cardiomyocytes. Cardiovasc Res 102:507–516.
Benjamini Y, Hochberg Y (1995) Controlling the False Discovery Rate: A Practical and Powerful Approach to Multiple Testing. J R Stat Soc Ser B 57:289–300.
Bennett J (2003) Immune response following intraocular delivery of recombinant viral vectors. Gene Ther 10:977–982.
Bennett J et al. (2012) AAV2 Gene Therapy Readministration in Three Adults with Congenital Blindness. Sci Transl Med 4:120ra15–ra120ra15.
Berger W, Kloeckener-Gruissem B, Neidhardt J (2010) The molecular basis of human retinal and vitreoretinal diseases. Prog Retin Eye Res 29:335–375.
Berndt A, Yizhar O, Gunaydin LA, Hegemann P, Deisseroth K (2009) Bi-stable neural state switches. Nat Neurosci 12:229–234.
Berson EL, Rosner B, Sandberg M a, Hayes KC, Nicholson BW, Weigel-DiFranco C, Willett W (1993) A randomized trial of vitamin A and vitamin E supplementation for retinitis pigmentosa. Arch Ophthalmol 111:761–772.
Bertin B, Freissmuth M, Jockers R, Strosberg A, Marullo S (1994) Cellular signaling by an agonist-activated receptor/Gs alpha fusion protein. Proc Natl Acad Sci U S A 91:8827–8831.
Bi A, Cui J, Ma Y-P, Olshevskaya E, Pu M, Dizhoor A, Pan Z-H (2006) Ectopic expression of a microbial-type rhodopsin restores visual responses in mice with photoreceptor degeneration. Neuron 50:23–33.
Billinge ER, Muzard J, Platt M (2013) Tunable resistive pulse sensing as a tool to monitor analyte induced particle aggregation. Nanomater Nanosci 1:11.
Binkowski B, Fan F, Wood K (2009) Engineered luciferases for molecular sensing in living cells. Curr Opin Biotechnol 20:14–18.

Blanks JC, Adinolfi AM, Lolley RN (1974) Photoreceptor degeneration and synaptogenesis in retinal degenerative (rd) mice. J Comp Neurol 156:95–106.
Blasic JR, Matos-Cruz V, Ujla D, Cameron EG, Hattar S, Halpern ME, Robinson PR (2014) Identification of critical phosphorylation sites on the carboxy tail of melanopsin. Biochemistry 53:2644–2649.
Boelens MC, te Meerman GJ, Gibcus JH, Blokzijl T, Boezen HM, Timens W, Postma DS, Groen HJM, van Den Berg A (2007) Microarray amplification bias: loss of 30% differentially expressed genes due to long probe - poly(A)-tail distances. BMC Genomics 8:277.
Borowska J, Trenholm S, Awatramani GB (2011) An intrinsic neural oscillator in the degenerating mouse retina. J Neurosci 31:5000–5012.
Boughman JA, Conneally PM, Nance WE (1980) Population genetic studies of retinitis pigmentosa. Am J Hum Genet 32:223–235.
Bourges J-LL, Gautier SE, Delie F, Bejjani R a., Jeanny J-CC, Gurny R, BenEzra D, Behar-Cohen FF (2003) Ocular drug delivery targeting the retina and retinal pigment epithelium using polylactide nanoparticles. Invest Ophthalmol Vis Sci 44:3562–3569.
Bowes C, Li T, Danciger M, Baxter LC, Applebury ML, Farber DB (1990) Retinal degeneration in the rd mouse is caused by a defect in the beta subunit of rod cGMP-phosphodiesterase. Nature 347:677–680.
Boye SE, Boye SL, Lewin AS, Hauswirth WW (2013) A comprehensive review of retinal gene therapy. Mol Ther 21:509–519.
Boztug K, Schmidt M, Schwarzer A, Banerjee PP, Díez IA, Dewey RA, Böhm M, Nowrouzi A, Ball CR, Glimm H, Naundorf S, Kühlcke K, Blasczyk R, Kondratenko I, Maródi L, Orange JS, von Kalle C, Klein C (2010) Stem-cell gene therapy for the Wiskott-Aldrich syndrome. N Engl J Med 363:1918–1927.
Bramall AN, Wright AF, Jacobson SG, McInnes RR (2010) The genomic, biochemical, and cellular responses of the retina in inherited photoreceptor degenerations and prospects for the treatment of these disorders. Annu Rev Neurosci 33:441–472.
Bruegmann T, Malan D, Hesse M, Beiert T, Fuegemann CJ, Fleischmann BK, Sasse P (2010) Optogenetic control of heart muscle in vitro and in vivo. Nat Methods 7:897–900.
Buch PK, MacLaren RE, Durán Y, Balaggan KS, MacNeil A, Schlichtenbrede FC, Smith AJ, Ali RR (2006) In Contrast to AAV-Mediated Cntf Expression, AAV-Mediated Gdnf Expression Enhances Gene Replacement Therapy in Rodent Models of Retinal Degeneration. Mol Ther 14:700–709.
Burnight ER, Wiley L a, Drack a V, Braun T a, Anfinson KR, Kaalberg EE, Halder J a, Affatigato LM, Mullins RF, Stone EM, Tucker B a (2014) CEP290 gene transfer rescues Leber congenital amaurosis cellular phenotype. Gene Ther 21:662–672.
Burt AR, Sautel M, Wilson MA, Rees S, Wise A, Milligan G (1998) Agonist Occupation of an α2A-Adrenoreceptor-Gi11α Fusion Protein Results in Activation of Both Receptor-linked and Endogenous Gi proteins. J Biol Chem 273:10367–10375.
Busskamp V, Duebel J, Balya D, Fradot M, Viney TJ, Siegert S, Groner AC, Cabuy E, Forster V, Seeliger M, Biel M, Humphries P, Paques M, Mohand-Said S, Trono D, Deisseroth K, Sahel J a, Picaud S, Roska B (2010) Genetic reactivation of cone photoreceptors restores visual responses in retinitis pigmentosa. Science (80-) 329:413–417.
Byrne LC, Dalkara D, Luna G, Fisher SK, Clérin E, Sahel J, Léveillard T, Flannery JG (2015) Viral-mediated RdCVF and RdCVFL expression protects cone and rod photoreceptors in retinal degeneration. J Clin Invest 125:105–116.
Byrne LC, Oztürk BE, Lee T, Fortuny C, Visel M, Dalkara D, Schaffer D V, Flannery

JG (2014) Retinoschisin gene therapy in photoreceptors, Müller glia or all retinal cells in the Rs1h-/- mouse. Gene Ther:1–8.

Cahill H, Nathans J (2008) The optokinetic reflex as a tool for quantitative analyses of nervous system function in mice: application to genetic and drug-induced variation. PLoS One 3:e2055.

Cai X, Conley SM, Nash Z, Fliesler SJ, Cooper MJ, Naash MI (2010) Gene delivery to mitotic and postmitotic photoreceptors via compacted DNA nanoparticles results in improved phenotype in a mouse model of retinitis pigmentosa. FASEB J 24:1178–1191.

Calvert PD, Govardovskii VI, Krasnoperova N, Anderson RE, Lem J, Makino CL (2001) Membrane protein diffusion sets the speed of rod phototransduction. Nature 411:90–94.

Calvert PD, Krasnoperova N V, Lyubarsky a L, Isayama T, Nicoló M, Kosaras B, Wong G, Gannon KS, Margolskee RF, Sidman RL, Pugh EN, Makino CL, Lem J (2000) Phototransduction in transgenic mice after targeted deletion of the rod transducin alpha -subunit. Proc Natl Acad Sci U S A 97:13913–13918.

Cao P, Sun W, Kramp K, Zheng M, Salom D, Jastrzebska B, Jin H, Palczewski K, Feng Z (2012) Light-sensitive coupling of rhodopsin and melanopsin to Gi/o and Gq signal transduction in Caenorhabditis elegans. FASEB J 26:480–491.

Caporale N, Kolstad KD, Lee T, Tochitsky I, Dalkara D, Trauner D, Kramer R, Dan Y, Isacoff EY, Flannery JG (2011) LiGluR restores visual responses in rodent models of inherited blindness. Mol Ther 19:1212–1219.

Carey MF, Peterson CL, Smale ST (2009) Chromatin Immunoprecipitation (ChIP). Cold Spring Harb Protoc 2009:pdb.prot5279 – pdb.prot5279.

Carter-Dawson LD, LaVail MM, Sidman RL (1978) Differential effect of the rd mutation on rods and cones in the mouse retina. Invest Ophthalmol Vis Sci 17:489–498.

Cehajic-Kapetanovic J, Eleftheriou C, Allen AE, Milosavljevic N, Pienaar A, Bedford R, Davis KE, Bishop PN, Lucas RJ (2015) Restoration of Vision with Ectopic Expression of Human Rod Opsin. Curr Biol:1–12.

Chang B (2015) Survey of the nob5 mutation in C3H substrains. :1101–1105.

Chang B, Hawes NL, Hurd RE, Davisson MT, Nusinowitz S, Heckenlively JR (2002) Retinal degeneration mutants in the mouse. Vision Res 42:517–525.

Charbel Issa P, Barnard AR, Herrmann P, Washington I, MacLaren RE (2015) Rescue of the Stargardt phenotype in *Abca4* knockout mice through inhibition of vitamin A dimerization. Proc Natl Acad Sci U S A:201506960.

Chen B, Cepko CL (2009) HDAC4 regulates neuronal survival in normal and diseased retinas. Science (80-) 323:256–259.

Chen M, Wang K, Lin B (2012) Development and Degeneration of Cone Bipolar Cells Are Independent of Cone Photoreceptors in a Mouse Model of Retinitis Pigmentosa. PLoS One 7.

Chen T-W, Wardill TJ, Sun Y, Pulver SR, Renninger SL, Baohan A, Schreiter ER, Kerr R a, Orger MB, Jayaraman V, Looger LL, Svoboda K, Kim DS (2013) Ultrasensitive fluorescent proteins for imaging neuronal activity. Nature 499:295–300.

Chiang JP, Trzupek K (2015) The current status of molecular diagnosis of inherited retinal dystrophies. Curr Opin Ophthalmol 26:346–351.

Chiquet C, Dkhissi-Benyahya O, Chounlamountri N, Szel a., Degrip WJ, Cooper HM (2002) Characterization of calbindin-positive cones in primates. Neuroscience 115:1323–1333.

Cideciyan A V, Jacobson SG, Beltran W a, Sumaroka A, Swider M, Iwabe S, Roman AJ, Olivares MB, Schwartz SB, Komáromy AM, Hauswirth WW, Aguirre GD

(2013) Human retinal gene therapy for Leber congenital amaurosis shows advancing retinal degeneration despite enduring visual improvement. Proc Natl Acad Sci U S A 110:E517–E525.

Colella P, Sommella A, Marrocco E, Di Vicino U, Polishchuk E, Garrido MG, Seeliger MW, Polishchuk R, Auricchio A (2013) Myosin7a Deficiency Results in Reduced Retinal Activity Which Is Improved by Gene Therapy. PLoS One 8.

Collin RW, den Hollander AI, van der Velde-Visser SD, Bennicelli J, Bennett J, Cremers FP (2012) Antisense Oligonucleotide (AON)-based Therapy for Leber Congenital Amaurosis Caused by a Frequent Mutation in CEP290. Mol Ther — Nucleic Acids 1:e14.

Conklin BR, Farfel Z, Lustig KD, Julius D, Bourne HR (1993) Substitution of three amino acids switches receptor specificity of Gq alpha to that of Gi alpha. Nature 363:274–276.

Corbo JC, Cepko CL (2005) A hybrid photoreceptor expressing both rod and cone genes in a mouse model of enhanced S-cone syndrome. PLOS Genet 1:0140–0153.

Cox B, Kislinger T, Emili A (2005) Integrating gene and protein expression data: Pattern analysis and profile mining. Methods 35:303–314.

Cramer AO, MacLaren RE (2013) Translating induced pluripotent stem cells from bench to bedside: application to retinal diseases. Curr Gene Ther 13:139–151.

Crasto CJ (2010) Hydrophobicity profiles in G protein-coupled receptor transmembrane helical domains. J Receptor Ligand Channel Res 2010:123–133.

Croner RS, Lausen B, Schellerer V, Zeittraeger I, Wein A, Schildberg C, Papadopoulos T, Dimmler A, Hahn EG, Hohenberger W, Brueckl WM (2009) Comparability of microarray data between amplified and non amplified RNA in colorectal carcinoma. J Biomed Biotechnol 2009:837170.

Cronin T, Vandenberghe LH, Hantz P, Juttner J, Reimann A, Kacsó A-E, Huckfeldt RM, Busskamp V, Kohler H, Lagali PS, Roska B, Bennett J (2014) Efficient transduction and optogenetic stimulation of retinal bipolar cells by a synthetic adeno-associated virus capsid and promoter. EMBO Mol Med 6:1–16.

Cuenca N, Pinilla I, Sauvé Y, Lund R (2005) Early changes in synaptic connectivity following progressive photoreceptor degeneration in RCS rats. Eur J Neurosci 22:1057–1072.

D'Cruz PM, Yasumura D, Weir J, Matthes MT, Abderrahim H, LaVail MM, Vollrath D (2000) Mutation of the receptor tyrosine kinase gene Mertk in the retinal dystrophic RCS rat. Hum Mol Genet 9:645–651.

Dagar S, Nagar S, Goel M, Cherukuri P, Dhingra NK (2014) Loss of photoreceptors results in upregulation of synaptic proteins in bipolar cells and amacrine cells. PLoS One 9:40–43.

Daiger SP, Sullivan LS, Bowne SJ (2015) RetNet. Available at: https://sph.uth.edu/Retnet/ [Accessed December 20, 2015].

Dalkara D (2015) Personal communication on AAV2/2(7m8) production.

Dalkara D, Byrne LC, Klimczak RR, Visel M, Yin L, Merigan WH, Flannery JG, Schaffer D V (2013) In vivo-directed evolution of a new adeno-associated virus for therapeutic outer retinal gene delivery from the vitreous. Sci Transl Med 5:189ra76.

Dalkara D, Duebel J, Sahel J-A (2015) Gene therapy for the eye focus on mutation-independent approaches. Curr Opin Neurol 28:51–60.

Davies WIL, Downes SM, Fu JK, Shanks ME, Copley RR, Lise S, Ramsden SC, Black GCM, Gibson K, Foster RG, Hankins MW, Németh AH (2012) Next-generation sequencing in health-care delivery: lessons from the functional analysis of rhodopsin. Genet Med:1–9.

Davies WL, Carvalho LS, Hunt DM (2007a) SPLICE: A technique for generating in

vitro spliced coding sequences from genomic DNA. Biotechniques 43:785–789.
Davies WL, Cowing JA, Carvalho LS, Potter IC, Trezise AEO, Hunt DM, Collin SP (2007b) Functional characterization, tuning, and regulation of visual pigment gene expression in an anadromous lamprey. FASEB J 21:2713–2724.
de Silva SR, McClements ME, Hankins MW, MacLaren RE (2015) Adeno-Associated Viral Gene Therapy for Retinal Disorders. In: Gene Delivery and Therapy for Neurological Disorders, pp 203–228.
Delahunty C, Yates JR (2005) Protein identification using 2D-LC-MS/MS. Methods 35:248–255.
Dezawa M, Takano M, Negishi H, Mo X, Oshitari T, Sawada H (2002) Gene transfer into retinal ganglion cells by in vivo electroporation: a new approach. Micron 33:1–6.
Dhingra A, Jiang M, Wang T-L, Lyubarsky A, Savchenko A, Bar-Yehuda T, Sterling P, Birnbaumer L, Vardi N (2002) Light response of retinal ON bipolar cells requires a specific splice variant of Galpha(o). J Neurosci 22:4878–4884.
Dhingra A, Ramakrishnan H, Neinstein A, Fina ME, Xu Y, Li J, Chung DC, Lyubarsky A, Vardi N (2012) Gβ3 is required for normal light ON responses and synaptic maintenance. J Neurosci 32:11343–11355.
Do MTH, Kang SH, Xue T, Zhong H, Liao H-W, Bergles DE, Yau K-W (2009) Photon capture and signalling by melanopsin retinal ganglion cells. Nature 457:281–287.
Dong S, Rogan SC, Roth BL (2010) Directed molecular evolution of DREADDs: a generic approach to creating next-generation RASSLs. Nat Protoc 5:561–573.
Doroudchi MM, Greenberg KP, Liu J, Silka K a, Boyden ES, Lockridge J a, Arman a C, Janani R, Boye SE, Boye SL, Gordon GM, Matteo BC, Sampath AP, Hauswirth WW, Horsager A (2011) Virally delivered channelrhodopsin-2 safely and effectively restores visual function in multiple mouse models of blindness. Mol Ther 19:1220–1229.
Doshi M, Voaden MJ, Arden GB (1985) Cyclic GMP in the retinas of normal mice and those heterozygous for early-onset photoreceptor dystrophy. Exp Eye Res 41:61–65.
Dragunow M, Faull R (1989) The use of c-fos as a metabolic marker in neuronal pathway tracing. J Neurosci Methods 29:261–265.
Earnest DJ, Iadarola M, Yeh HH, Olschowka J a. (1990) Photic regulation of c-fos expression in neural components governing the entrainment of circadian rhythms. Exp Neurol 109:353–361.
Emanuel AJ, Do MTH (2015) Melanopsin tristability for sustained and broadband phototransduction. Neuron 85:1043–1055.
Espina V, Wulfkuhle JD, Calvert VS, VanMeter A, Zhou W, Coukos G, Geho DH, Petricoin EF, Liotta L a (2006) Laser-capture microdissection. Nat Protoc 1:586–603.
Euler T, Haverkamp S, Schubert T, Baden T (2014) Retinal bipolar cells: elementary building blocks of vision. Nat Rev Neurosci 15:507–519.
Evanko DS, Thiyagarajan MM, Siderovski DP, Wedegaertner PB (2001) Gbeta gamma isoforms selectively rescue plasma membrane localization and palmitoylation of mutant Galphas and Galphaq. J Biol Chem 276:23945–23953.
Fan F, Binkowski BF, Butler BL, Stecha PF, Lewis MK, Wood K V. (2008) Novel genetically encoded biosensors using firefly luciferase. ACS Chem Biol 3:346–351.
Farah N, Reutsky I, Shoham S (2007) Patterned optical activation of retinal ganglion cells. Annu Int Conf IEEE Eng Med Biol - Proc:6368–6370.
Fattal E, De Rosa G, Bochot A (2004) Gel and solid matrix systems for the controlled delivery of drug carrier-associated nucleic acids. Int J Pharm 277:25–30.

Fenno L, Yizhar O, Deisseroth K (2011) The development and application of optogenetics. Annu Rev Neurosci 34:389–412.
Ferguson KM, Higashijima T, Smigel MD, Gilman a. G (1986) The influence of bound GDP on the kinetics of guanine nucleotide binding to G proteins. J Biol Chem 261:7393–7399.
Ferrari FK, Samulski T, Shenk T, Samulski RJ (1996) Second-strand synthesis is a rate-limiting step for efficient transduction by recombinant adeno-associated virus vectors. J Virol 70:3227–3234.
Ferrendelli JA, Cohen AI (1974) The effects of light and dark adaptation on the levels of cyclic nucleotides in retinas of mice heterozygote for photorecepto dystrophy. Biochem Biophys Res Commun 73:421–427.
Fisher KJ, Gao GP, Weitzman MD, DeMatteo R, Burda JF, Wilson JM (1996) Transduction with recombinant adeno-associated virus for gene therapy is limited by leading-strand synthesis. J Virol 70:520–532.
Foster RG, Provencio I, Hudson D, Fiske S, De Grip W, Menaker M (1991) Circadian photoreception in the retinally degenerate mouse (rd/rd). J Comp Physiol A 169:39–50.
Fu X, Fu N, Guo S, Yan Z, Xu Y, Hu H, Menzel C, Chen W, Li Y, Zeng R, Khaitovich P (2009) Estimating accuracy of RNA-Seq and microarrays with proteomics. BMC Genomics 10:161.
Gal A, Orth U, Baehr W, Schwinger E, Rosenberg T (1994) Heterozygous missense mutation in the rod cGMP phosphodiesterase beta-subunit gene in autosomal dominant stationary night blindness. Nat Genet 7:64–68.
Gallardo TD, John GB, Shirley L, Contreras CM, Akbay E a., Haynie JM, Ward SE, Shidler MJ, Castrillon DH (2007) Genomewide discovery and classification of candidate ovarian fertility genes in the mouse. Genetics 177:179–194.
Gamsiz ED, Ouyang Q, Schmidt M, Nagpal S, Morrow EM (2012) Genome-wide transcriptome analysis in murine neural retina using high-throughput RNA sequencing. Genomics 99:44–51.
Gangoda L, Doerflinger M, Lee YY, Rahimi a, Etemadi N, Chau D, Milla L, O'Connor L, Puthalakath H (2012) Cre transgene results in global attenuation of the cAMP/PKA pathway. Cell Death Dis 3:e365.
Gao G-P, Alvira MR, Wang L, Calcedo R, Johnston J, Wilson JM (2002) Novel adeno-associated viruses from rhesus monkeys as vectors for human gene therapy. Proc Natl Acad Sci U S A 99:11854–11859.
Garcia PD, Onrust R, Bell SM, Sakmar TP, Bourne HR (1995) Transducin-alpha C-terminal mutations prevent activation by rhodopsin: a new assay using recombinant proteins expressed in cultured cells. EMBO J 14:4460–4469.
Garriga P, Liu X, Khorana HG (1996) Structure and function in rhodopsin: correct folding and misfolding in point mutants at and in proximity to the site of the retinitis pigmentosa mutation Leu-125-->Arg in the transmembrane helix C. Proc Natl Acad Sci U S A 93:4560–4564.
Gaub BM, Berry MH, Holt AE, Isacoff EY, Flannery JG (2015) Optogenetic Vision Restoration Using Rhodopsin for Enhanced Sensitivity. Mol Ther.
Gaub BM, Berry MH, Holt AE, Reiner A, Kienzler M a, Dolgova N, Nikonov S, Aguirre GD, Beltran W a, Flannery JG, Isacoff EY (2014) Restoration of visual function by expression of a light-gated mammalian ion channel in retinal ganglion cells or ON-bipolar cells.
Gérard X, Perrault I, Munnich A, Kaplan J, Rozet J-M (2015) Intravitreal Injection of Splice-switching Oligonucleotides to Manipulate Splicing in Retinal Cells. Mol Ther Acids 4:e250.
Gerry HW, Kelly TJ, Berns KI (1973) Arrangement of nucleotide sequences in Adeno-

associated virus DNA. J Mol Biol:207–225.
Goldmann T, Overlack N, Wolfrum U, Nagel-Wolfrum K (2011) PTC124-mediated translational readthrough of a nonsense mutation causing Usher syndrome type 1C. Hum Gene Ther 22:537–547.
Gomes dos Santos AL, Bochot A, Tsapis N, Artzner F, Bejjani RA, Thillaye-Goldenberg B, de Kozak Y, Fattal E, Behar-Cohen F (2006) Oligonucleotide-polyethylenimine complexes targeting retinal cells: structural analysis and application to anti-TGFbeta-2 therapy. Pharm Res 23:770–781.
Gonzalez-Cordero A, West EL, Pearson R a, Duran Y, Carvalho LS, Chu CJ, Naeem A, Blackford SJI, Georgiadis A, Lakowski J, Hubank M, Smith AJ, Bainbridge JWB, Sowden JC, Ali RR (2013) Photoreceptor precursors derived from three-dimensional embryonic stem cell cultures integrate and mature within adult degenerate retina. Nat Biotechnol 31:741–747.
Goshen I, Brodsky M, Prakash R, Wallace J, Gradinaru V, Ramakrishnan C, Deisseroth K (2011) Dynamics of retrieval strategies for remote memories. Cell 147:678–689.
Govardovskii VI, Fyhrquist N, Reuter T, Kuzmin DG, Donner K (2000) In search of the visual pigment template. Vis Neurosci 17:509–528.
Graham DM, Wong KY, Shapiro P, Frederick C, Pattabiraman K, Berson DM (2008) Melanopsin ganglion cells use a membrane-associated rhabdomeric phototransduction cascade. J Neurophysiol 99:2522–2532.
Granier S, Manglik A, Kruse AC, Kobilka TS, Thian FS, Weis WI, Kobilka BK (2012) Structure of the δ-opioid receptor bound to naltrindole. Nature 485:400–404.
Greenbaum D, Colangelo C, Williams K, Gerstein M (2003) Comparing protein abundance and mRNA expression levels on a genomic scale. Genome Biol 4:117.
Greenberg KP, Pham A, Werblin FS (2011) Differential Targeting of Optical Neuromodulators to Ganglion Cell Soma and Dendrites Allows Dynamic Control of Center-Surround Antagonism. Neuron 69:713–720.
Grimm C, Wenzel a., Williams TP, Rol PO, Hafezi F, Remé CE (2001) Rhodopsin-mediated blue-light damage to the rat retina: Effect of photoreversal of bleaching. Invest Ophthalmol Vis Sci 42:497–505.
Grisshammer R, Hermans E (2001) Functional coupling with Galpha(q) and Galpha(i1) protein subunits promotes high-affinity agonist binding to the neurotensin receptor NTS-1 expressed in Escherichia coli. FEBS Lett 493:101–105.
Guerin K, Gregory-Evans CY, Hodges MD, Moosajee M, Mackay DS, Gregory-Evans K, Flannery JG (2008) Systemic aminoglycoside treatment in rodent models of retinitis pigmentosa. Exp Eye Res 87:197–207.
Güler AD, Ecker JL, Lall GS, Haq S, Altimus CM, Liao H-W, Barnard AR, Cahill H, Badea TC, Zhao H, Hankins MW, Berson DM, Lucas RJ, Yau K-W, Hattar S (2008) Melanopsin cells are the principal conduits for rod-cone input to non-image-forming vision. Nature 453:102–105.
Gunaydin L a, Yizhar O, Berndt A, Sohal VS, Deisseroth K, Hegemann P (2010) Ultrafast optogenetic control. Nat Neurosci 13:387–392.
Gutierrez D V, Mark MD, Masseck O, Maejima T, Kuckelsberg D, Hyde R a, Krause M, Kruse W, Herlitze S (2011a) Optogenetic control of motor coordination by Gi/o protein-coupled vertebrate rhodopsin in cerebellar Purkinje cells. J Biol Chem 286:25848–25858.
Gutierrez D V, Mark MD, Masseck O, Maejima T, Kuckelsberg D, Hyde R a, Krause M, Kruse W, Herlitze S (2011b) Optogenetic control of motor coordination by Gi/o protein-coupled vertebrate rhodopsin in cerebellar Purkinje cells. J Biol Chem 286:25848–25858.
Guziewicz KE, Zangerl B, Komáromy AM, Iwabe S, Chiodo V a, Boye SL, Hauswirth WW, Beltran W a, Aguirre GD (2013) Recombinant AAV-mediated BEST1

transfer to the retinal pigment epithelium: analysis of serotype-dependent retinal effects. PLoS One 8:e75666.

Hacein-Bey-Abina S et al. (2003) LMO2-associated clonal T cell proliferation in two patients after gene therapy for SCID-X1. Science (80-) 302:415–419.

Hackam AS, Strom R, Liu D, Qian J, Wang C, Otteson D, Gunatilaka T, Farkas RH, Chowers I, Kageyama M, Leveillard T, Sahel J-A, Campochiaro P a, Parmigiani G, Zack DJ (2004) Identification of gene expression changes associated with the progression of retinal degeneration in the rd1 mouse. Invest Ophthalmol Vis Sci 45:2929–2942.

Haim M (2002) Epidemiology of retinitis pigmentosa in Denmark. Acta Ophthalmol:1–34.

Hangai M, Tanihara H, Honda Y, Kaneda Y (1998) In vivo delivery of phosphorothioate oligonucleotides into murine retina. Arch Ophthalmol 116:342–348.

Hanna J, Markoulaki, Cw S, a M, Jp C, Beard C, Brambrink T, Wu LC, Townes TM, Jaenisch R WM (2007) Treatment of Sickle Cell Anemia Mouse Model with iPS cells generated from Autoogous Skin. Science (80-) 318:1920–1923.

Harding TC, Dickinson PJ, Roberts BN, Yendluri S, Gonzalez-Edick M, Lecouteur RA, Jooss KU (2006) Enhanced gene transfer efficiency in the murine striatum and an orthotopic glioblastoma tumor model, using AAV-7- and AAV-8-pseudotyped vectors. Hum Gene Ther 17:807–820.

Hartong DT, Berson EL, Dryja TP (2006) Retinitis pigmentosa. Lancet 368:1795–1809.

Hatori M, Le H, Vollmers C, Keding SR, Tanaka N, Schmedt C, Jegla T, Panda S (2008) Inducible ablation of melanopsin-expressing retinal ganglion cells reveals their central role in non-image forming visual responses. PLoS One 3.

Hattar S, Liao HW, Takao M, Berson DM, Yau KW (2002) Melanopsin-containing retinal ganglion cells: architecture, projections, and intrinsic photosensitivity. Science (80-) 295:1065–1070.

Hattar S, Lucas RJ, Mrosovsky N, Thompson S, Douglas RH, Hankins MW, Lem J, Biel M, Hofmann F, Foster RG, Yau K-W (2003) Melanopsin and rod-cone photoreceptive systems account for all major accessory visual functions in mice. Nature 424:76–81.

Hauswirth WW, Aleman TS, Kaushal S, Cideciyan A V, Schwartz SB, Wang L, Conlon TJ, Boye SL, Flotte TR, Byrne BJ, Jacobson SG (2008) Treatment of leber congenital amaurosis due to RPE65 mutations by ocular subretinal injection of adeno-associated virus gene vector: short-term results of a phase I trial. Hum Gene Ther 19:979–990.

Hayward C, Shu X, Cideciyan A V, Lennon A, Barran P, Zareparsi S, Sawyer L, Hendry G, Dhillon B, Milam AH, Luthert PJ, Swaroop A, Hastie ND, Jacobson SG, Wright AF (2003) Mutation in a short-chain collagen gene, CTRP5, results in extracellular deposit formation in late-onset retinal degeneration: a genetic model for age-related macular degeneration. Hum Mol Genet 12:2657–2667.

Hedges SB, Marin J, Suleski M, Paymer M, Kumar S (2015) Tree of Life Reveals Clock-Like Speciation and Diversification. Mol Biol Evol 32:835–845.

Held G a., Grinstein G, Tu Y (2006) Relationship between gene expression and observed intensities in DNA microarrays - A modeling study. Nucleic Acids Res 34:1–15.

Helmstaedter M, Briggman KL, Turaga SC, Jain V, Seung HS, Denk W (2013) Connectomic reconstruction of the inner plexiform layer in the mouse retina. Nature 500:168–174.

Hoffman DR, Hughbanks-Wheaton DK, Pearson NS, Fish GE, Spencer R, Takacs A, Klein M, Locke KG, Birch DG (2014) Four-year placebo-controlled trial of

docosahexaenoic acid in X-linked retinitis pigmentosa (DHAX trial): a randomized clinical trial. JAMA Ophthalmol 132:866–873.
Hoffman LM, Maguire AM, Bennett J (1997) Cell-mediated immune response and stability of intraocular transgene expression after adenovirus-mediated delivery. Invest Ophthalmol Vis Sci 38:2224–2233.
Holt R, Brown L, Broadgate S, Butler R, Jagannath A, Downes SM, Peirson S, Halford S (2015) Identification of rod- and cone-specific expression signatures to identify candidate genes for retinal disease. Exp Eye Res 132:161–173.
Horowitz ED, Rahman KS, Bower BD, Dismuke DJ, Falvo MR, Griffith JD, Harvey SC, Asokan A (2013) Biophysical and ultrastructural characterization of adeno-associated virus capsid uncoating and genome release. J Virol 87:2994–3002.
Huang L, Max M, Margolskee RF, Su H, Masland RH, Euler T (2003) G protein subunit Gγ13 is coexpressed with Gαo, Gβ3, and Gβ4 in retinal ON bipolar cells. J Comp Neurol 455:1–10.
Hubbard KB, Hepler JR (2006) Cell signalling diversity of the Gqα family of heterotrimeric G proteins. Cell Signal 18:135–150.
Hughes S, Jagannath A, Hickey D, Gatti S, Wood M, Peirson SN, Foster RG, Hankins MW (2014) Using siRNA to define functional interactions between melanopsin and multiple G Protein partners. Cell Mol Life Sci:14–17.
Hughes S, Watson TS, Foster RG, Peirson SN, Hankins MW (2013) Nonuniform distribution and spectral tuning of photosensitive retinal ganglion cells of the mouse retina. Curr Biol 23:1696–1701.
Humayun MS, Dorn JD, Da Cruz L, Dagnelie G, Sahel JA, Stanga PE, Cideciyan A V., Duncan JL, Eliott D, Filley E, Ho AC, Santos A, Safran AB, Arditi A, Del Priore L V., Greenberg RJ (2012) Interim results from the international trial of second sight's visual prosthesis. Ophthalmology 119:779–788.
Humayun MS, Prince M, De Juan E, Barron Y, Moskowitz M, Klock IB, Milam AH (1999) Morphometric analysis of the extramacular retina from postmortem eyes with retinitis pigmentosa. Invest Ophthalmol Vis Sci 40:143–148.
Iiri T, Farfel Z, Bourne HR (1998) G-protein diseases furnish a model for the turn-on switch. Nature 394:35–38.
Imamoto Y, Seki I, Yamashita T, Shichida Y (2013) Efficiencies of activation of transducin by cone and rod visual pigments. Biochemistry 52:3010–3018.
Insinna C, Daniele LL, Davis J a., Larsen DD, Kuemmel C, Wang J, Nikonov SS, Knox BE, Pugh EN (2012) An S-Opsin Knock-In Mouse (F81Y) Reveals a Role for the Native Ligand 11-cis-Retinal in Cone Opsin Biosynthesis. J Neurosci 32:8094–8104.
Issa PC, Singh MS, Lipinski DM, Chong N V., Delori FC, Barnard AR, MacLaren RE (2012) Optimization of in vivo confocal autofluorescence imaging of the ocular fundus in mice and its application to models of human retinal degeneration. Invest Ophthalmol Vis Sci 53:1066–1075.
Ivanova E, Lee P, Pan ZH (2013) Characterization of multiple bistratified retinal ganglion cells in a purkinje cell protein 2-Cre transgenic mouse line. J Comp Neurol 521:2165–2180.
Ivanova E, Pan Z-H (2009) Evaluation of the adeno-associated virus mediated long-term expression of channelrhodopsin-2 in the mouse retina. Mol Vis 15:1680–1689.
Jacobs GH (1996) Primate photopigments and primate color vision. Proc Natl Acad Sci U S A 93:577–581.
Jacobson SG et al. (2006) Safety of Recombinant Adeno-Associated Virus Type 2-RPE65 Vector Delivered by Ocular Subretinal Injection. Mol Ther 13:1074–1084.
Jacobson SG et al. (2012) Gene Therapy for Leber Congenital Amaurosis Caused by

RPE65 Mutations: Safety and Efficacy in 15 Children and Adults Followed Up to 3 Years. Arch Ophthalmol 130:9–24.

Jacobson SG, Cideciyan A V., Roman AJ, Sumaroka A, Schwartz SB, Heon E, Hauswirth WW (2015) Improvement and Decline in Vision with Gene Therapy in Childhood Blindness. N Engl J Med:150503141523009.

Janz JM, Farrens DL (2004) Rhodopsin activation exposes a key hydrophobic binding site for the transducin ??-subunit C terminus. J Biol Chem 279:29767–29773.

Jazayeri M, Lindbloom-Brown Z, Horwitz GD (2012) Saccadic eye movements evoked by optogenetic activation of primate V1. Nat Neurosci 15:1368–1370.

Jeon CJ, Strettoi E, Masland RH (1998) The major cell populations of the mouse retina. J Neurosci 18:8936–8946.

Joly S, Francke M, Ulbricht E, Beck S, Seeliger M, Hirrlinger P, Hirrlinger J, Lang KS, Zinkernagel M, Odermatt B, Samardzija M, Reichenbach A, Grimm C, Remé CE (2009) Cooperative Phagocytes. Am J Pathol 174:2310–2323.

Jones BW, Marc RE (2005) Retinal remodeling during retinal degeneration. Exp Eye Res 81:123–137.

Kanaho Y, Tsai SC, Adamik R, Hewlett EL, Moss J, Vaughan M (1984) Rhodopsin-enhanced GTPase activity of the inhibitory GTP-binding protein of adenylate cyclase. J Biol Chem 259:7378–7381.

Kim BT, Kitagawa H, Tamura J, Saito T, Kusche-Gullberg M, Lindahl U, Sugahara K (2001) Human tumor suppressor EXT gene family members EXTL1 and EXTL3 encode alpha 1,4- N-acetylglucosaminyltransferases that likely are involved in heparan sulfate/ heparin biosynthesis. Proc Natl Acad Sci U S A 98:7176–7181.

Kim JM, Hwa J, Garriga P, Reeves PJ, RajBhandary UL, Khorana HG (2005) Light-driven activation of ß2-adrenergic receptor signaling by a chimeric rhodopsin containing the ß2-adrenergic receptor cytoplasmic loops. Biochemistry 44:2284–2292.

Klein RL, Dayton RD, Leidenheimer NJ, Jansen K, Golde TE, Zweig RM (2006) Efficient Neuronal Gene Transfer with AAV8 Leads to Neurotoxic Levels of Tau or Green Fluorescent Proteins. Mol Ther 13:517–527.

Klein RL, Dayton RD, Tatom JB, Henderson KM, Henning PP (2008) AAV8, 9, Rh10, Rh43 Vector Gene Transfer in the Rat Brain: Effects of Serotype, Promoter and Purification Method. Mol Ther 16:89–96.

Kleinlogel S, Feldbauer K, Dempski RE, Fotis H, Wood PG, Bamann C, Bamberg E (2011) Ultra light-sensitive and fast neuronal activation with the Ca^2+-permeable channelrhodopsin CatCh. Nat Neurosci 14:513–518.

Klevering BJ, Maugeri A, Wagner A, Go SL, Vink C, Cremers FPM, Hoyng CB (2004) Three families displaying the combination of Stargardt's disease with cone-rod dystrophy or retinitis pigmentosa. Ophthalmology 111:546–553.

Klimczak RR, Koerber JT, Dalkara D, Flannery JG, Schaffer D V (2009) A novel adeno-associated viral variant for efficient and selective intravitreal transduction of rat Müller cells. PLoS One 4:e7467.

Koenekoop RK, Sui R, Sallum J, van den Born LI, Ajlan R, Khan A, den Hollander AI, Cremers FPM, Mendola JD, Bittner AK, Dagnelie G, Schuchard R a., Saperstein D a. (2014) Oral 9-cis retinoid for childhood blindness due to Leber congenital amaurosis caused by RPE65 or LRAT mutations: An open-label phase 1b trial. Lancet 384:1513–1520.

Koistinaho J, Sagar SM (1995) Light-induced c-fos expression in amacrine cells in the rabbit retina. Brain Res Mol Brain Res 29:53–63.

Kolstad KD, Dalkara D, Guerin K, Visel M, Hoffmann N, Schaffer D V, Flannery JG (2010) Changes in adeno-associated virus-mediated gene delivery in retinal degeneration. Hum Gene Ther 21:571–578.

Komáromy AM, Rowlan JS, Corr ATP, Reinstein SL, Boye SL, Cooper AE, Gonzalez A, Levy B, Wen R, Hauswirth WW, Beltran W a, Aguirre GD (2013) Transient photoreceptor deconstruction by CNTF enhances rAAV-mediated cone functional rescue in late stage CNGB3-achromatopsia. Mol Ther 21:1131–1141.

Kong J, Kim S-R, Binley K, Pata I, Doi K, Mannik J, Zernant-Rajang J, Kan O, Iqball S, Naylor S, Sparrow JR, Gouras P, Allikmets R (2008) Correction of the disease phenotype in the mouse model of Stargardt disease by lentiviral gene therapy. Gene Ther 15:1311–1320.

Koyanagi M, Terakita A (2014) Diversity of animal opsin-based pigments and their optogenetic potential. Biochim Biophys Acta - Bioenerg 1837:710–716.

Lagali PS, Balya D, Awatramani GB, Münch T a, Kim DS, Busskamp V, Cepko CL, Roska B (2008) Light-activated channels targeted to ON bipolar cells restore visual function in retinal degeneration. Nat Neurosci 11:667–675.

Lamba D a, Gust J, Reh T a (2009) Transplantation of human embryonic stem cell-derived photoreceptors restores some visual function in Crx-deficient mice. Cell Stem Cell 4:73–79.

Landers GM, Olson JAC-E (1988) Rapid, simultaneous determination of isomers of retinal, retinal oxime and retinol by high-performance liquid chromatography. J Chromatogr A 438:383–392.

Lebherz C, Auricchio A, Maguire AM, Rivera VM, Tang W, Grant RL, Clackson T, Bennett J, Wilson JM (2005) Long-term inducible gene expression in the eye via adeno-associated virus gene transfer in nonhuman primates. Hum Gene Ther 16:178–186.

Lerea CL, Somers DE, Hurley JB, Klock IB, Bunt-Milam AH (1986) Identification of specific transducin alpha subunits in retinal rod and cone photoreceptors. Science (80-) 234:77–80.

Lhériteau E, Petit L, Weber M, Le Meur G, Deschamps J-Y, Libeau L, Mendes-Madeira A, Guihal C, François A, Guyon R, Provost N, Lemoine F, Papal S, El-Amraoui A, Colle M-A, Moullier P, Rolling F (2014) Successful gene therapy in the RPGRIP1-deficient dog: a large model of cone-rod dystrophy. Mol Ther 22:265–277.

Li X, Gutierrez D V, Hanson MG, Han J, Mark MD, Chiel H, Hegemann P, Landmesser LT, Herlitze S (2005) Fast noninvasive activation and inhibition of neural and network activity by vertebrate rhodopsin and green algae channelrhodopsin. Proc Natl Acad Sci U S A 102:17816–17821.

Liang P, Xu Y, Zhang X, Ding C, Huang R, Zhang Z, Lv J, Xie X, Chen Y, Li Y, Sun Y, Bai Y, Songyang Z, Ma W, Zhou C, Huang J (2015) CRISPR/Cas9-mediated gene editing in human tripronuclear zygotes. Protein Cell.

Liew G, Michaelides M, Bunce C (2014) A comparison of the causes of blindness certifications in England and Wales in working age adults (16-64 years), 1999-2000 with 2009-2010. Br Med J 4:e004015.

Lin B, Koizumi A, Tanaka N, Panda S, Masland RH (2008) Restoration of visual function in retinal degeneration mice by ectopic expression of melanopsin. Proc Natl Acad Sci U S A 105:16009–16014.

Lin JY, Lin MZ, Steinbach P, Tsien RY (2009) Characterization of engineered channelrhodopsin variants with improved properties and kinetics. Biophys J 96:1803–1814.

Lindstrom SH, Ryan DG, Shi J, DeVries SH (2014) Kainate receptor subunit diversity underlying response diversity in retinal off bipolar cells. J Physiol 592:1457–1477.

Lipinski DM, Barnard AR, Charbel Issa P, Singh MS, De Silva SR, Trabalza A, Eleftheriadou I, Ellison SM, Mazarakis ND, MacLaren RE (2014) Vesicular stomatitis virus glycoprotein- and Venezuelan equine encephalitis virus-derived glycoprotein-pseudotyped lentivirus vectors differentially transduce corneal

endothelium, trabecular meshwork, and human photoreceptors. Hum Gene Ther 25:50–62.
Lipinski DM, Barnard AR, Singh MS, Martin C, Lee EJ, Davies WIL, MacLaren RE (2015) CNTF Gene Therapy Confers Lifelong Neuroprotection in a Mouse Model of Human Retinitis Pigmentosa. Mol Ther 23:1308–1319.
Livesey FJ, Furukawa T, Steffen MA, Church GM, Cepko CL (2000) Microarray analysis of the transcriptional network controlled by the photoreceptor homeobox gene Crx. Curr Biol 10:301–310.
Loeb JE, Cordier WS, Harris ME, Weitzman MD, Hope TJ (1999) Enhanced expression of transgenes from adeno-associated virus vectors with the woodchuck hepatitis virus posttranscriptional regulatory element: implications for gene therapy. Hum Gene Ther 10:2295–2305.
Lolley RN, Rong H, Craft CM (1994) Linkage of photoreceptor degeneration by apoptosis with inherited defect in phototransduction. Invest Ophthalmol Vis Sci 35:358–362.
Long C, McAnally JR, Shelton JM, Mireault AA, Bassel-Duby R, Olson EN (2014) Prevention of muscular dystrophy in mice by CRISPR/Cas9-mediated editing of germline DNA. Science (80-) 345:1184–1188.
Lórenz-Fonfría V a., Heberle J (2014) Channelrhodopsin unchained: Structure and mechanism of a light-gated cation channel. Biochim Biophys Acta - Bioenerg 1837:626–642.
Low JC (1987) The corneal ERG of the heterozygous retinal degeneration mouse. Graefe's Arch Clin Exp Ophthalmol 225:413–417.
Lu Q, Ivanova E, Ganjawala TH, Pan Z-H (2013) Cre-mediated recombination efficiency and transgene expression patterns of three retinal bipolar cell-expressing Cre transgenic mouse lines. Mol Vis 19:1310–1320.
Luo D-G, Yue WWS, Ala-Laurila P, Yau K-W (2011) Activation of visual pigments by light and heat. Science 332:1307–1312.
Macé E, Caplette R, Marre O, Sengupta A, Chaffiol A, Barbe P, Desrosiers M, Bamberg E, Sahel J-A, Picaud S, Duebel J, Dalkara D (2014) Targeting channelrhodopsin-2 to ON-bipolar cells with vitreally administered AAV restores ON and OFF visual responses in blind mice. Mol Ther 23:7–16.
MacLaren RE, Groppe M, Barnard AR, Cottriall CL, Tolmachova T, Seymour L, Reed Clark K, During MJ, Cremers FPM, Black GCM, Lotery AJ, Downes SM, Webster AR, Seabra MC (2014) Retinal gene therapy in patients with choroideremia: initial findings from a phase 1/2 clinical trial. Lancet 383:1129–1137.
MacLaren RE, Pearson R a, MacNeil a, Douglas RH, Salt TE, Akimoto M, Swaroop a, Sowden JC, Ali RR (2006) Retinal repair by transplantation of photoreceptor precursors. Nature 444:203–207.
Maguire AM et al. (2008) Safety and efficacy of gene transfer for Leber's congenital amaurosis. N Engl J Med 358:2240–2248.
Maheshri N, Koerber JT, Kaspar BK, Schaffer D V (2006) Directed evolution of adeno-associated virus yields enhanced gene delivery vectors. Nat Biotechnol 24:198–204.
Manglik A, Kruse AC, Kobilka TS, Thian FS, Mathiesen JM, Sunahara RK, Pardo L, Weis WI, Kobilka BK, Granier S (2012) Crystal structure of the μ-opioid receptor bound to a morphinan antagonist. Nature 485:321–326.
Mao H, James T, Schwein A, Shabashvili AE, Hauswirth WW, Gorbatyuk MS, Lewin AS (2011) AAV delivery of wild-type rhodopsin preserves retinal function in a mouse model of autosomal dominant retinitis pigmentosa. Hum Gene Ther 22:567–575.
Margueron R, Reinberg D (2011) The Polycomb complex PRC2 and its mark in life.

Nature 469:343–349.
Marino S, Krimpenfort P, Leung C, van der Korput H a GM, Trapman J, Camenisch I, Berns A, Brandner S (2002) PTEN is essential for cell migration but not for fate determination and tumourigenesis in the cerebellum. Development 129:3513–3522.
Masland RH (2011) Cell populations of the retina: The proctor lecture. Invest Ophthalmol Vis Sci 52:4581–4591.
Matsuyama T, Yamashita T, Imamoto Y, Shichida Y (2012) Photochemical properties of mammalian melanopsin. Biochemistry 51:5454–5462.
McClements M, Davies WIL, Michaelides M, Young T, Neitz M, MacLaren RE, Moore AT, Hunt DM (2013) Variations in opsin coding sequences cause X-linked cone dysfunction syndrome with myopia and dichromacy. Invest Ophthalmol Vis Sci 54:1361–1369.
McLaughlin ME, Sandberg M a, Berson EL, Dryja TP (1993) Recessive mutations in the gene encoding the beta-subunit of rod phosphodiesterase in patients with retinitis pigmentosa. Nat Genet 4:130–134.
Melnick JL, Mayor HD, Smith KO, Rapp F (1965) Association of 20-Millimicron Particles with Adenoviruses. J Bacteriol 90:271–274.
Melyan Z, Tarttelin EE, Bellingham J, Lucas RJ, Hankins MW (2005) Addition of human melanopsin renders mammalian cells photoresponsive. Nature 433:741–745.
Merbs SL, Nathans J (1992) Absorption spectra of human cone pigments. Nature 356:433–435.
Merbs SL, Nathans J (1993) Role of hydroxyl-bearing amino acids in differentially tuning the absorption spectra of the human red and green cone pigments. Photochem Photobiol 58:706–710.
Michaelides M, Hardcastle AJ, Hunt DM, Moore AT (2006) Progressive Cone and Cone-Rod Dystrophies: Phenotypes and Underlying Molecular Genetic Basis. Surv Ophthalmol 51:232–258.
Michaelson D, Ahearn I, Bergo M, Young S, Philips M (2002) Membrane trafficking of heterotrimeric G proteins via the endoplasmic reticulum and Golgi. Mol Biol Cell 13:3294–3302.
Milam AH, Li ZY, Fariss RN (1998) Histopathology of the human retina in retinitis pigmentosa. Prog Retin Eye Res 17:175–205.
Millington-Ward S, Chadderton N, O'Reilly M, Palfi A, Goldmann T, Kilty C, Humphries M, Wolfrum U, Bennett J, Humphries P, Kenna PF, Farrar GJ (2011) Suppression and replacement gene therapy for autosomal dominant disease in a murine model of dominant retinitis pigmentosa. Mol Ther 19:642–649.
Molinari P, Ambrosio C, Riitano D, Sbraccia M, Gro MC, Costa T (2003) Promiscuous Coupling at Receptor-G Fusion Proteins: THE RECEPTOR OF ONE COVALENT COMPLEX INTERACTS WITH THE -SUBUNIT OF ANOTHER. J Biol Chem 278:15778–15788.
Moosajee M, Gregory-Evans K, Ellis CD, Seabra MC, Gregory-Evans CY (2008) Translational bypass of nonsense mutations in zebrafish rep1, pax2.1 and lamb1 highlights a viable therapeutic option for untreatable genetic eye disease. Hum Mol Genet 17:3987–4000.
Morgans CW, Brown RL, Duvoisin RM (2010) TRPM1: The endpoint of the mGluR6 signal transduction cascade in retinal ON-bipolar cells. BioEssays 32:609–614.
Morgans CW, Zhang J, Jeffrey BG, Nelson SM, Burke NS, Duvoisin RM, Brown RL (2009) TRPM1 is required for the depolarizing light response in retinal ON-bipolar cells. Proc Natl Acad Sci U S A 106:19174–19178.
Morimoto-Tomita M, Uchimura K, Werb Z, Hemmerich S, Rosen SD (2002) Cloning

and characterization of two extracellular heparin-degrading endosulfatases in mice and humans. J Biol Chem 277:49175–49185.

Murakami M, Kouyama T (2008) Crystal structure of squid rhodopsin. Nature 453:363–367.

Mure LS, Cornut P-L, Rieux C, Drouyer E, Denis P, Gronfier C, Cooper HM (2009) Melanopsin bistability: a fly's eye technology in the human retina. PLoS One 4:e5991.

Nagel G, Brauner M, Liewald JF, Adeishvili N, Bamberg E, Gottschalk A (2005) Light activation of Channelrhodopsin-2 in excitable cells of caenorhabditis elegans triggers rapid behavioral responses. Curr Biol 15:2279–2284.

Nagel G, Szellas T, Huhn W, Kateriya S, Adeishvili N, Berthold P, Ollig D, Hegemann P, Bamberg E (2003) Channelrhodopsin-2, a directly light-gated cation-selective membrane channel. Proc Natl Acad Sci U S A 100:13940–13945.

Natkunarajah M, Trittibach P, McIntosh J, Duran Y, Barker SE, Smith a J, Nathwani a C, Ali RR (2008) Assessment of ocular transduction using single-stranded and self-complementary recombinant adeno-associated virus serotype 2/8. Gene Ther 15:463–467.

Ni YQ, Gan DK, Xu HD, Xu GZ, Da C Di (2009) Neuroprotective effect of transcorneal electrical stimulation on light-induced photoreceptor degeneration. Exp Neurol 219:439–452.

Nikonov SS, Kholodenko R, Lem J, Pugh EN (2006) Physiological Features of the S- and M-cone Photoreceptors of Wild-type Mice from Single-cell Recordings. J Gen Physiol 127:191–204.

Nishiguchi KM, Carvalho LS, Rizzi M, Powell K, Holthaus S-MK, Azam S a., Duran Y, Ribeiro J, Luhmann UFO, Bainbridge JWB, Smith AJ, Ali RR (2015) Gene therapy restores vision in rd1 mice after removal of a confounding mutation in Gpr179. Nat Commun 6:6006.

Nöll GN (1996) High-performance liquid chromatographic analysis of retinal and retinol isomers. J Chromatogr A 721:247–259.

Noorwez SM, Malhotra R, McDowell JH, Smith KA, Krebs MP, Kaushal S (2004) Retinoids Assist the Cellular Folding of the Autosomal Dominant Retinitis Pigmentosa Opsin Mutant P23H. J Biol Chem 279:16278–16284.

Oldham WM, Hamm HE (2008) Heterotrimeric G protein activation by G-protein-coupled receptors. Nat Rev Mol Cell Biol 9:60–71.

Palczewski K (2000) Crystal Structure of Rhodopsin: A G Protein-Coupled Receptor. Science (80-) 289:739–745.

Pang JJ, Deng WT, Dai X, Lei B, Everhart D, Umino Y, Li J, Zhang K, Mao S, Boye SL, Liu L, Chiodo V a., Liu X, Shi W, Tao Y, Chang B, Hauswirth WW (2012) AAV-mediated cone rescue in a naturally occurring mouse model of CNGA3-achromatopsia. PLoS One 7:1–9.

Park JH, Scheerer P, Hofmann KP, Choe H-W, Ernst OP (2008) Crystal structure of the ligand-free G-protein-coupled receptor opsin. Nature 454:183–187.

Pascolini D, Mariotti SP (2012) Global estimates of visual impairment: 2010. Br J Ophthalmol 96:614–618.

Pearson R, Barber A, Rizzi M, Hippert C, Xue T, West E, Duran Y, Smith A, Chuang J, Azam S, Luhmann U, Benucci a, Sung C, Bainbridge J, Carandini M, Yau K, Sowden J, Ali R (2012) Restoration of vision after transplantation of photoreceptors. Nature:1–5.

Pei Y, Rogan SC, Yan F, Roth BL (2008) Engineered GPCRs as tools to modulate signal transduction. Physiology 23:313–321.

Pellissier LP, Quinn PM, Alves CH, Vos RM, Klooster J, Flannery JG, Heimel J a., Wijnholds J (2015) Gene therapy into photoreceptors and Muller glial cells

restores retinal structure and function in CRB1 retinitis pigmentosa mouse models. Hum Mol Genet:1–15.

Petrs-Silva H, Dinculescu A, Li Q, Deng W-T, Pang J-J, Min S-H, Chiodo V, Neeley AW, Govindasamy L, Bennett A, Agbandje-McKenna M, Zhong L, Li B, Jayandharan GR, Srivastava A, Lewin AS, Hauswirth WW (2011) Novel properties of tyrosine-mutant AAV2 vectors in the mouse retina. Mol Ther 19:293–301.

Petrs-Silva H, Dinculescu A, Li Q, Min S-H, Chiodo V, Pang J-J, Zhong L, Zolotukhin S, Srivastava A, Lewin AS, Hauswirth WW (2009) High-efficiency transduction of the mouse retina by tyrosine-mutant AAV serotype vectors. Mol Ther 17:463–471.

Pickard GE, Baver SB, Ogilvie MD, Sollars PJ (2009) Light-induced fos expression in intrinsically photosensitive retinal ganglion cells in melanopsin knockout (opn4) mice. PLoS One 4:e4984.

Pittler SJ, Baehr W (1991) Identification of a nonsense mutation in the rod photoreceptor cGMP phosphodiesterase beta-subunit gene of the rd mouse. Proc Natl Acad Sci U S A 88:8322–8326.

Polosukhina A, Litt J, Tochitsky I, Nemargut J, Sychev Y, De Kouchkovsky I, Huang T, Borges K, Trauner D, Van Gelder RN, Kramer RH (2012) Photochemical Restoration of Visual Responses in Blind Mice. Neuron 75:271–282.

Provencio I, Jiang G, de Grip WJ, Hayes WP, Rollag MD (1998) Melanopsin: An opsin in melanophores, brain, and eye. Proc Natl Acad Sci U S A 95:340–345.

Puller C, Haverkamp S, Neitz M, Neitz J (2014) Synaptic elements for GABAergic feed-forward signaling between HII horizontal cells and blue cone bipolar cells are enriched beneath primate S-cones. PLoS One 9:e88963.

Punzo C, Cepko C (2007) Cellular responses to photoreceptor death in the rd1 mouse model of retinal degeneration. Invest Ophthalmol Vis Sci 48:849–857.

Qiu X, Kumbalasiri T, Carlson SM, Wong KY, Krishna V, Provencio I, Berson DM (2005) Induction of photosensitivity by heterologous expression of melanopsin. Nature 433:745–749.

Rabinowitz JE, Samulski RJ (2000) Building a better vector: the manipulation of AAV virions. Virology 278:301–308.

Ran FA, Cong L, Yan WX, Scott D a., Gootenberg JS, Kriz AJ, Zetsche B, Shalem O, Wu X, Makarova KS, Koonin E V., Sharp P a., Zhang F (2015) In vivo genome editing using Staphylococcus aureus Cas9. Nature 520:186–190.

Rao A, Dallman R, Henderson S, Chen C-K (2007) Gbeta5 is required for normal light responses and morphology of retinal ON-bipolar cells. J Neurosci 27:14199–14204.

Raport CJ, Lem J, Makino C, Chen CK, Fitch CL, Hobson a., Baylor D, Simon MI, Hurley JB (1994) Downregulation of cGMP phosphodiesterase induced by expression of GTPase- deficient cone transducin in mouse rod photoreceptors. Investig Ophthalmol Vis Sci 35:2932–2947.

Rasmussen SGF, Choi H-J, Rosenbaum DM, Kobilka TS, Thian FS, Edwards PC, Burghammer M, Ratnala VRP, Sanishvili R, Fischetti RF, Schertler GFX, Weis WI, Kobilka BK (2007) Crystal structure of the human beta2 adrenergic G-protein-coupled receptor. Nature 450:383–387.

Ray T a, Heath KM, Hasan N, Noel JM, Samuels IS, Martemyanov K a, Peachey NS, McCall M a, Gregg RG (2014) GPR179 Is Required for High Sensitivity of the mGluR6 Signaling Cascade in Depolarizing Bipolar Cells. J Neurosci 34:6334–6343.

Reichel MB, Ali RR, Thrasher a J, Hunt DM, Bhattacharya SS, Baker D (1998) Immune responses limit adenovirally mediated gene expression in the adult mouse eye. Gene Ther 5:1038–1046.

Rivera VM, Gao GP, Grant RL, Schnell M a., Zoltick PW, Rozamus LW, Clackson T, Wilson JM (2005) Long-term pharmacologically regulated expression of erythropoietin in primates following AAV-mediated gene transfer. Blood 105:1424–1430.

Sagar SM, Sharp FR (1990) Light induces a Fos-like nuclear antigen in retinal neurons. Mol Brain Res 7:17–21.

Sagoo MS, Lagnado L (1997) G-protein deactivation is rate-limiting for shut-off of the phototransduction cascade. Nature 389:392–395.

Saliba RS, Munro PMG, Luthert PJ, Cheetham ME (2002) The cellular fate of mutant rhodopsin: quality control, degradation and aggresome formation. J Cell Sci 115:2907–2918.

Santos A, Humayun MS, Juan E De, Marsh MJ, Klock IB, Milam AH (1997) Preservation of the inner retina in retinitis pigmentosa. Arch Ophthalmol 115:511–515.

Sanyal S, Hawkins RK (1986) Development and degeneration of retina in rds mutant mice: effects of light on the rate of degeneration in albino and pigmented homozygous and heterozygous mutant and normal mice. Vision Res 26:1177–1185.

Sasaki T, Kaneko A (1996) L-glutamate-induced responses in OFF-type bipolar cells of the cat retina. Vision Res 36:787–795.

Sautel M, Milligan G (1998) Loss of activation of Gs but not Gi following expression of an alpha2A- adrenoceptor-Gi1alpha fusion protein. FEBS Lett 436:46–50.

Scalabrino ML, Boye SL, Fransen KMH, Noel JM, Dyka FM, Min SH, Ruan Q, De Leeuw CN, Simpson EM, Gregg RG, McCall MA, Peachey NS, Boye SE (2015) Intravitreal delivery of a novel AAV vector targets ON bipolar cells and restores visual function in a mouse model of complete congenital stationary night blindness. Hum Mol Genet 24:6229–6239.

Schalkwyk LC, Fernandes C, Nash MW, Kurrikoff K, Vasar E, K??ks S (2007) Interpretation of knockout experiments: The congenic footprint. Genes, Brain Behav 6:299–303.

Schatz A, Röck T, Naycheva L, Willmann G, Wilhelm B, Peters T, Bartz-Schmidt KU, Zrenner E, Messias A, Gekeler F (2011) Transcorneal electrical stimulation for patients with retinitis pigmentosa: a prospective, randomized, sham-controlled exploratory study. Invest Ophthalmol Vis Sci 52:4485–4496.

Scheerer P, Park JH, Hildebrand PW, Kim YJ, Krauss N, Choe H-W, Hofmann KP, Ernst OP (2008) Crystal structure of opsin in its G-protein-interacting conformation. Nature 455:497–502.

Schein SJ (1988) Anatomy of macaque fovea and spatial densities of neurons in foveal representation. J Comp Neurol 269:479–505.

Schmidt M, Voutetakis A, Afione S, Zheng C, Mandikian D, Chiorini J a (2008) Adeno-associated virus type 12 (AAV12): a novel AAV serotype with sialic acid- and heparan sulfate proteoglycan-independent transduction activity. J Virol 82:1399–1406.

Schneider C a, Rasband WS, Eliceiri KW (2012) NIH Image to ImageJ: 25 years of image analysis. Nat Methods 9:671–675.

Schwartz SD, Regillo CD, Lam BL, Eliott D, Rosenfeld PJ, Gregori NZ, Hubschman J-P, Davis JL, Heilwell G, Spirn M, Maguire J, Gay R, Bateman J, Ostrick RM, Morris D, Vincent M, Anglade E, Del Priore L V, Lanza R (2015) Human embryonic stem cell-derived retinal pigment epithelium in patients with age-related macular degeneration and Stargardt's macular dystrophy: follow-up of two open-label phase 1/2 studies. Lancet 385:509–516.

Seamon KB, Daly JW (1981) Forskolin: a unique diterpene activator of cyclic AMP-

generating systems. J Cyclic Nucleotide Res 7:201–224.
Seifert R, Lee TW, Lam VT, Kobilka BK (1998a) Reconstitution of beta2-adrenoceptor-GTP-binding-protein interaction in Sf9 cells--high coupling efficiency in a beta2-adrenoceptor-G(s alpha) fusion protein. Eur J Biochem 255:369–382.
Seifert R, Wenzel-Seifert K, Gether U, Lam VT, Kobilka BK (1999a) Examining the efficiency of receptor/G-protein coupling with a cleavable beta2-adrenoceptor-gsalpha fusion protein. Eur J Biochem 260:661–666.
Seifert R, Wenzel-Seifert K, Kobilka BK (1999b) GPCR-Galpha fusion proteins: molecular analysis of receptor-G-protein coupling. Trends Pharmacol Sci 20:383–389.
Seifert R, Wenzel-Seifert K, Lee TW, Gether U, Sanders-Bush E, Kobilka BK (1998b) Different effects of Gsalpha splice variants on beta2-adrenoreceptor-mediated signaling. The Beta2-adrenoreceptor coupled to the long splice variant of Gsalpha has properties of a constitutively active receptor. J Biol Chem 273:5109–5116 ST – Different effects of Gsalpha splice.
Seiler MP, Cerullo V, Lee B (2007) Immune response to helper dependent adenoviral mediated liver gene therapy: challenges and prospects. Curr Gene Ther 7:297–305.
Sharma AK, Spudich JL, Doolittle WF (2006) Microbial rhodopsins: functional versatility and genetic mobility. Trends Microbiol 14:463–469.
Sharon D, Sandberg MA, Rabe VW, Stillberger M, Dryja TP, Berson EL (2003) RP2 and RPGR mutations and clinical correlations in patients with X-linked retinitis pigmentosa. Am J Hum Genet 73:1131–1146.
Shukla AK, Manglik A, Kruse AC, Xiao K, Reis RI, Tseng W-C, Staus DP, Hilger D, Uysal S, Huang L-Y, Paduch M, Tripathi-Shukla P, Koide A, Koide S, Weis WI, Kossiakoff A a, Kobilka BK, Lefkowitz RJ (2013) Structure of active β-arrestin-1 bound to a G-protein-coupled receptor phosphopeptide. Nature 497:137–141.
Siegert S, Cabuy E, Scherf BG, Kohler H, Panda S, Le Y-Z, Fehling HJ, Gaidatzis D, Stadler MB, Roska B (2012) Transcriptional code and disease map for adult retinal cell types. Nat Neurosci 15:487–495.
Siegert S, Scherf BG, Del Punta K, Didkovsky N, Heintz N, Roska B (2009) Genetic address book for retinal cell types. Nat Neurosci 12:1197–1204.
Sieving PA, Caruso RC, Tao W, Coleman HR, Thompson DJS, Fullmer KR, Bush RA (2006) Ciliary neurotrophic factor (CNTF) for human retinal degeneration: phase I trial of CNTF delivered by encapsulated cell intraocular implants. Proc Natl Acad Sci U S A 103:3896–3901.
Simon J a, Kingston RE (2009) Mechanisms of polycomb gene silencing: knowns and unknowns. Nat Rev Mol Cell Biol 10:697–708.
Singh MS, Charbel Issa P, Butler R, Martin C, Lipinski DM, Sekaran S, Barnard AR, MacLaren RE (2013) Reversal of end-stage retinal degeneration and restoration of visual function by photoreceptor transplantation. Proc Natl Acad Sci U S A 110:1101–1106.
Sommer JM, Smith PH, Parthasarathy S, Isaacs J, Vijay S, Kieran J, Powell SK, McClelland A, Wright JF (2003) Quantification of adeno-associated virus particles and empty capsids by optical density measurement. Mol Ther 7:122–128.
Spudich JL, Yang CS, Jung KH, Spudich EN (2000) Retinylidene proteins: structures and functions from archaea to humans. Annu Rev Cell Dev Biol 16:365–392.
Srinivas S, Watanabe T, Lin CS, William CM, Tanabe Y, Jessell TM, Costantini F (2001) Cre reporter strains produced by targeted insertion of EYFP and ECFP into the ROSA26 locus. BMC Dev Biol 1:4.
Srivastava A, Lusby EW, Berns KI (1983) Nucleotide sequence and organization of the Nucleotide Sequence and Organization of the Adeno- Associated Virus 2 Genome.

Microbiology 45:555–564.
Steigert J (2010) Pico-Injector for the Discrete Chemical Stimulation of Individual Cells Featuring a High Temporal and Spatial Resolution.
Stevens G a., White R a., Flaxman SR, Price H, Jonas JB, Keeffe J, Leasher J, Naidoo K, Pesudovs K, Resnikoff S, Taylor H, Bourne RR a (2013) Global prevalence of vision impairment and blindness: Magnitude and temporal trends, 1990-2010. Ophthalmology 120:2377–2384.
Stingl K et al. (2015) Subretinal Visual Implant Alpha IMS – Clinical trial interim report. Vision Res 111:149–160.
Strathmann M, Simon MI (1990) G protein diversity: a distinct class of alpha subunits is present in vertebrates and invertebrates. Proc Natl Acad Sci U S A 87:9113–9117.
Strettoi E, Pignatelli V (2000) Modifications of retinal neurons in a mouse model of retinitis pigmentosa. Proc Natl Acad Sci U S A 97:11020–11025.
Strettoi E, Pignatelli V, Rossi C, Porciatti V, Falsini B (2003) Remodeling of second-order neurons in the retina of rd/rd mutant mice. Vision Res 43:867–877.
Strettoi E, Porciatti V, Falsini B, Pignatelli V, Rossi C (2002) Morphological and functional abnormalities in the inner retina of the rd/rd mouse. J Neurosci 22:5492–5504.
Suda K, Filipek S, Palczewski K, Engel A, Fotiadis D (2004) The supramolecular structure of the GPCR rhodopsin in solution and native disc membranes. Mol Membr Biol 21:435–446.
Suemori S, Shimazawa M, Kawase K, Satoh M, Nagase H, Yamamoto T, Hara H (2006) Metallothionein, an endogenous antioxidant, protects against retinal neuron damage in mice. Invest Ophthalmol Vis Sci 47:3975–3982.
Summerford C, Samulski RJ (1998) Membrane-associated heparan sulfate proteoglycan is a receptor for adeno-associated virus type 2 virions. J Virol 72:1438–1445.
Sung CH, Schneider BG, Agarwal N, Papermaster DS, Nathans J (1991) Functional heterogeneity of mutant rhodopsins responsible for autosomal dominant retinitis pigmentosa. Proc Natl Acad Sci U S A 88:8840–8844.
Tachibanaki S, Tsushima S, Kawamura S (2001) Low amplification and fast visual pigment phosphorylation as mechanisms characterizing cone photoresponses. Proc Natl Acad Sci U S A 98:14044–14049.
Takida S, Wedegaertner PB (2003) Heterotrimer Formation, Together with Isoprenylation, Is Required for Plasma Membrane Targeting of Gbeta gamma. J Biol Chem 278:17284–17290.
Tao W (2006) Application of encapsulated cell technology for retinal degenerative diseases. Expert Opin Biol Ther 6:717–726.
Terakita A (2005) Protein family review The opsins. Genome Biol:1–9.
Terakita A, Yamashita T, Nimbari N, Kojima D, Shichida Y (2002) Functional interaction between bovine rhodopsin and G protein transducin. J Biol Chem 277:40–46.
Terakita A, Yamashita T, Tachibanaki S, Shichida Y (1998) Selective activation of G-protein subtypes by vertebrate and invertebrate rhodopsins. FEBS Lett 439:110–114.
Thomas CE, Storm TA, Huang Z, Kay MA (2004) Rapid uncoating of vector genomes is the key to efficient liver transduction with pseudotyped adeno-associated virus vectors. J Virol 78:3110–3122.
Tighe S, Held MA (2010) Isolation of Total RNA from Transgenic Mouse Melanoma Subsets Using Fluorescence-Activated Cell Sorting. In: Microarray Methods for Drug Discovery, pp 27–44.
Tochitsky I, Polosukhina A, Degtyar VE, Gallerani N, Smith CM, Friedman A, Van

Gelder RN, Trauner D, Kaufer D, Kramer RH (2014) Restoring visual function to blind mice with a photoswitch that exploits electrophysiological remodeling of retinal ganglion cells. Neuron 81:800–813.

Tomita H, Sugano E, Yawo H, Ishizuka T, Isago H, Narikawa S, Kügler S, Tamai M (2007) Restoration of visual response in aged dystrophic RCS rats using AAV-mediated channelopsin-2 gene transfer. Invest Ophthalmol Vis Sci 48:3821–3826.

Trapani I, Toriello E, de Simone S, Colella P, Iodice C, Polishchuk E V., Sommella A, Colecchi L, Rossi S, Simonelli F, Giunti M, Bacci ML, Polishchuk RS, Auricchio A (2015) Improved dual AAV vectors with reduced expression of truncated proteins are safe and effective in the retina of a mouse model of Stargardt disease. Hum Mol Genet 24:ddv386.

Tschernutter M, Schlichtenbrede FC, Howe S, Balaggan KS, Munro PM, Bainbridge JWB, Thrasher AJ, Smith AJ, Ali RR (2005) Long-term preservation of retinal function in the RCS rat model of retinitis pigmentosa following lentivirus-mediated gene therapy. Gene Ther 12:694–701.

van Alphen B, Winkelman BHJ, Frens MA (2009) Age- and sex-related differences in contrast sensitivity in C57BL/6 mice. Invest Ophthalmol Vis Sci 50:2451–2458.

van Wyk M, Pielecka-Fortuna J, Löwel S, Kleinlogel S (2015) Restoring the ON Switch in Blind Retinas: Opto-mGluR6, a Next-Generation, Cell-Tailored Optogenetic Tool. PLOS Biol 13:e1002143.

Vardi N, Zhang LL, Payne J a, Sterling P (2000) Evidence that different cation chloride cotransporters in retinal neurons allow opposite responses to GABA. J Neurosci 20:7657–7663.

Varela C, Igartua I, De La Rosa EJ, De La Villa P (2003) Functional modifications in rod bipolar cells in a mouse model of retinitis pigmentosa. Vision Res 43:879–885.

Vasák M (2005) Advances in metallothionein structure and functions. J Trace Elem Med Biol 19:13–17.

Voaden MJ, Willmott NJ (1990) Evidence for reduced binding of cyclic GMP to cyclic GMP phosphodiesterase in photoreceptors of mice heterozygous for the rd gene. Curr Eye Res 9:643–651.

Vollrath D, Feng W, Duncan JL, Yasumura D, D'Cruz PM, Chappelow a, Matthes MT, Kay M a, LaVail MM (2001) Correction of the retinal dystrophy phenotype of the RCS rat by viral gene transfer of Mertk. Proc Natl Acad Sci U S A 98:12584–12589.

Wässle H (2004) Parallel processing in the mammalian retina. Nat Rev Neurosci 5:747–757.

Watanabe S, Sanuki R, Ueno S, Koyasu T, Hasegawa T, Furukawa T (2013) Tropisms of AAV for Subretinal Delivery to the Neonatal Mouse Retina and Its Application for In Vivo Rescue of Developmental Photoreceptor Disorders. PLoS One 8.

Wenzel-Seifert K, Lee TW, Seifert R, Kobilka BK (1998) Restricting mobility of Gsalpha relative to the beta2-adrenoceptor enhances adenylate cyclase activity by reducing Gsalpha GTPase activity. Biochem J 334:519–524.

Wert KJ, Davis RJ, Sancho-pelluz J, Nishina PM, Tsang SH (2013) Gene therapy provides long-term visual function in a pre-clinical model of retinitis pigmentosa. Hum Mol Genet 22:558–567.

Wess J (1997) G-protein-coupled receptors: molecular mechanisms involved in receptor activation and selectivity of G-protein recognition. FASEB J 11:346–354.

West EL, Pearson R a., Tschernutter M, Sowden JC, MacLaren RE, Ali RR (2008) Pharmacological disruption of the outer limiting membrane leads to increased retinal integration of transplanted photoreceptor precursors. Exp Eye Res 86:601–611.

Wettschureck N, Offermanns S (2005) Mammalian G Proteins and Their Cell Type

Specific Functions. Physilological Rev:1159–1204.
Wilkie TM, Gilbert DJ, Olsen a S, Chen XN, Amatruda TT, Korenberg JR, Trask BJ, de Jong P, Reed RR, Simon MI (1992) Evolution of the mammalian G protein alpha subunit multigene family. Nat Genet 1:85–91.
Wilkie TM, Scherle P a, Strathmann MP, Slepak VZ, Simon MI (1991) Characterization of G-protein alpha subunits in the Gq class: expression in murine tissues and in stromal and hematopoietic cell lines. Proc Natl Acad Sci U S A 88:10049–10053.
Willett K, Bennett J (2013) Immunology of AAV-mediated gene transfer in the eye. Front Immunol 4:1–8.
Winslow MM, Dayton TL, Verhaak RGW, Kim-Kiselak C, Snyder EL, Feldser DM, Hubbard DD, DuPage MJ, Whittaker C a, Hoersch S, Yoon S, Crowley D, Bronson RT, Chiang DY, Meyerson M, Jacks T (2011) Suppression of lung adenocarcinoma progression by Nkx2-1. Nature 473:101–104.
Witten IB, Lin S-C, Brodsky M, Prakash R, Diester I, Anikeeva P, Gradinaru V, Ramakrishnan C, Deisseroth K (2010) Cholinergic interneurons control local circuit activity and cocaine conditioning. Science (80-) 330:1677–1681.
Wright AF, Chakarova CF, Abd El-Aziz MM, Bhattacharya SS (2010) Photoreceptor degeneration: genetic and mechanistic dissection of a complex trait. Nat Rev Genet 11:273–284.
Wright AF, Jacobson SG, Cideciyan A V, Roman AJ, Shu X, Vlachantoni D, McInnes RR, Riemersma R a (2004) Lifespan and mitochondrial control of neurodegeneration. Nat Genet 36:1153–1158.
Wright JF, Le T, Prado J, Bahr-Davidson J, Smith PH, Zhen Z, Sommer JM, Pierce GF, Qu G (2005) Identification of factors that contribute to recombinant AAV2 particle aggregation and methods to prevent its occurrence during vector purification and formulation. Mol Ther 12:171–178.
Wu Y, Liang D, Wang Y, Bai M, Tang W, Bao S, Yan Z, Li D, Li J (2013) Correction of a genetic disease in mouse via use of CRISPR-Cas9. Cell Stem Cell 13:659–662.
Wu Z, Hiriyanna S, Qian H, Mookherjee S, Campos MM, Gao C, Fariss R, Sieving PA, Li T, Colosi P, Swaroop A (2015) A long-term efficacy study of gene replacement therapy for RPGR-associated retinal degeneration. Hum Mol Genet:ddv134 – .
Xiao W, Chirmule N, Berta SC, Cullough BMC, Gao G, Wilson JM (1999) Gene Therapy Vectors Based on Adeno-Associated Virus Type 1. 73:3994–4003.
Xiao X, Li J, Samulski RJ (1998) Production of high-titer recombinant adeno-associated virus vectors in the absence of helper adenovirus. J Virol 72:2224–2232.
Xie Q, Bu W, Bhatia S, Hare J, Somasundaram T, Azzi A, Chapman MS (2002) The atomic structure of adeno-associated virus (AAV-2), a vector for human gene therapy. Proc Natl Acad Sci U S A 99:10405–10410.
Yamashita T, Terakita A, Shichida Y (2000) Distinct roles of the second and third cytoplasmic loops of bovine rhodopsin in G protein activation. J Biol Chem 275:34272–34279.
Yáñez-Muñoz RJ, Balaggan KS, MacNeil A, Howe SJ, Schmidt M, Smith AJ, Buch P, MacLaren RE, Anderson PN, Barker SE, Duran Y, Bartholomae C, von Kalle C, Heckenlively JR, Kinnon C, Ali RR, Thrasher AJ (2006) Effective gene therapy with nonintegrating lentiviral vectors. Nat Med 12:348–353.
Yang X-J, Seto E (2007) HATs and HDACs: from structure, function and regulation to novel strategies for therapy and prevention. Oncogene 26:5310–5318.
Ye H, Daoud-El Baba M, Peng R-W, Fussenegger M (2011) A synthetic optogenetic transcription device enhances blood-glucose homeostasis in mice. Science (80-) 332:1565–1568.

Yin H, Xue W, Chen S, Bogorad RL, Benedetti E, Grompe M, Koteliansky V, Sharp P a, Jacks T, Anderson DG (2014) Genome editing with Cas9 in adult mice corrects a disease mutation and phenotype. Nat Biotechnol 32:551–553.

Yin L, Greenberg K, Hunter JJ, Dalkara D, Kolstad KD, Masella BD, Wolfe R, Visel M, Stone D, Libby RT, DiLoreto D, Schaffer D, Flannery J, Williams DR, Merigan WH (2011) Intravitreal injection of AAV2 transduces macaque inner retina. Invest Ophthalmol Vis Sci 52:2775–2783.

Yizhar O, Fenno LE, Davidson TJ, Mogri M, Deisseroth K (2011) Optogenetics in Neural Systems. Neuron 71:9–34.

Yuen T, Wurmbach E, Pfeffer RL, Ebersole BJ, Sealfon SC (2002) Accuracy and calibration of commercial oligonucleotide and custom cDNA microarrays. Nucleic Acids Res 30:e48.

Zallocchi M, Binley K, Lad Y, Ellis S, Widdowson P, Iqball S, Scripps V, Kelleher M, Loader J, Miskin J, Peng Y-W, Wang W-M, Cheung L, Delimont D, Mitrophanous K a, Cosgrove D (2014) EIAV-based retinal gene therapy in the shaker1 mouse model for usher syndrome type 1B: development of UshStat. PLoS One 9:e94272.

Zemelman B V., Lee G a., Ng M, Miesenböck G (2002) Selective photostimulation of genetically chARGed neurons. Neuron 33:15–22.

Zhang F, Prigge M, Beyrière F, Tsunoda SP, Mattis J, Yizhar O, Hegemann P, Deisseroth K (2008) Red-shifted optogenetic excitation: a tool for fast neural control derived from Volvox carteri. Nat Neurosci 11:631–633.

Zhang F, Wang L-P, Brauner M, Liewald JF, Kay K, Watzke N, Wood PG, Bamberg E, Nagel G, Gottschalk A, Deisseroth K (2007) Multimodal fast optical interrogation of neural circuitry. Nature 446:633–639.

Zhang K, Hopkins JJ, Heier JS, Birch DG, Halperin LS, Albini T a, Brown DM, Jaffe GJ, Tao W, Williams G a (2011) Ciliary neurotrophic factor delivered by encapsulated cell intraocular implants for treatment of geographic atrophy in age-related macular degeneration. Proc Natl Acad Sci U S A 108:6241–6245.

Zhang Y, Ivanova E, Bi A, Pan Z-H (2009) Ectopic expression of multiple microbial rhodopsins restores ON and OFF light responses in retinas with photoreceptor degeneration. J Neurosci 29:9186–9196.

Zheng B, Sage M, Sheppeard E a, Jurecic V, Bradley a (2000) Engineering mouse chromosomes with Cre-loxP: range, efficiency, and somatic applications. Mol Cell Biol 20:648–655.

Zhong L, Li B, Mah CS, Govindasamy L, Agbandje-McKenna M, Cooper M, Herzog RW, Zolotukhin I, Warrington KH, Weigel-Van Aken K a, Hobbs J a, Zolotukhin S, Muzyczka N, Srivastava A (2008) Next generation of adeno-associated virus 2 vectors: point mutations in tyrosines lead to high-efficiency transduction at lower doses. Proc Natl Acad Sci U S A 105:7827–7832.

Zhong L, Zhao W, Wu J, Li B, Zolotukhin S, Govindasamy L, Agbandje-McKenna M, Srivastava A (2007) A dual role of EGFR protein tyrosine kinase signaling in ubiquitination of AAV2 capsids and viral second-strand DNA synthesis. Mol Ther 15:1323–1330.

Zolotukhin S, Potter M, Hauswirth WW, Guy J, Muzyczka N (1996) A “humanized” green fluorescent protein cDNA adapted for high-level expression in mammalian cells. J Virol 70:4646–4654.

Zrenner E, Bartz-Schmidt KU, Benav H, Besch D, Bruckmann A, Gabel V-P, Gekeler F, Greppmaier U, Harscher A, Kibbel S, Koch J, Kusnyerik A, Peters T, Stingl K, Sachs H, Stett A, Szurman P, Wilhelm B, Wilke R (2011) Subretinal electronic chips allow blind patients to read letters and combine them to words. Proc Biol Sci 278:1489–1497.